NMR STUDIES OF THE MOTION OF MOLECULES RELATED IN STRUCTURE TO COMMERCIAL LUBRICANTS

STEFAN LUFF

A thesis submitted in candidature for the degree of
Doctor of Philosophy
in the Faculty of Science of the University of Surrey.

Joseph Kenyon Laboratory, and
Magnetic Resonance Centre,
Department of Chemistry,
University of Surrey,
Guildford,
Surrey.

August, 1995.

ProQuest LLC.
789 East Eisenhower Parkway
P.O. Box 1346
Ann Arbor, MI 48106 – 1346

ABSTRACT

A number of compounds were synthesized, including site specifically monodeuterated isotopomers, whose molecular structures parallel some of those found in commercial engineering lubricants. In the course of these syntheses, a new protocol was developed for the McMurry coupling of aliphatic ketones, involving toluene as the main reaction solvent, which gave greater economy and efficiency than those hitherto reported.

Variable temperature measurements at 41.405 MHz of deuterium relaxation rates of the pure liquids of monodeuterated isotopomers 9,10-di-*n*-octyl-*n*-octadecane-9d_1, 9-*n*-octyl-*n*-heptadecane-9d_1, and tricyclohexylmethane-d_1, gave accurate values of the rotational correlation times and activation energies for isotropic overall molecular reorientation, using an analysis which assumed quadrupolar relaxation. Measurements of silicon-29 relaxation rates for tri-*n*-octylsilane at 53.978 MHz determined an activation energy for isotropic overall molecular reorientation, using an analysis which included both dipolar and spin-rotational relaxation.

Extensive sequences of variable temperature carbon-13 NMR measurements of longitudinal relaxation rates and NOE factors were carried out at 67.83 and 100.53 MHz on the pure liquids of 9,10-di-*n*-octyl-*n*-octadecane, 9-*n*-octyl-*n*-heptadecane, tricyclohexylmethane and 1,1,2-tricyclohexylethane, and also on a sample of tri-*n*-octylsilane. The carbon-13 data were analyzed by assuming carbon-proton dipolar relaxation, within the theoretical picture of Lipari and Szabo, to determine correlation times, activation energies, and generalized order parameters related to their overall and internal molecular motions. The results obtained from the analyses of the deuterium relaxation measurements on 9,10-di-*n*-octyl-*n*-octadecane-9d_1, 9-*n*-octyl-*n*-heptadecane-9d_1, and tricyclohexylmethane-d_1, were used to describe the overall molecular motion in the corresponding carbon-13 analyses.

The differing examples of molecular motion enabled a careful examination of the appropriateness of the Lipari and Szabo picture in each case, and also its limitations. The relaxation data of the cyclohexyl derivatives were well described by the original Lipari and Szabo picture. A temperature dependent generalized order parameter was used to describe the relaxation data in the *n*-octyl compounds, and its likely significance discussed.

Estimates for the quadrupolar coupling constants in 9,10-di-*n*-octyl-*n*-octadecane-9d_1, 9-*n*-octyl-*n*-heptadecane-9d_1, and tricyclohexylmethane-d_1, emerged from a combination of the analyses of the deuterium and carbon-13 NMR data for these compounds.

(continued)

X-ray crystallographic structures were determined for tricyclohexylmethane and tricyclohexylmethylchloride, and the first spectroscopic and computational studies of the tricyclohexylmethyl radical were reported.

Attempts were made to devise a synthetic route to tricyclohexylmethylamine, an analogue of amantadine.

ACKNOWLEDGEMENTS

The Author thanks the SERC, and BP International plc., for financial support through a CASE studentship during most of this work. The Author also thanks Dr. R. Bolton and Dr. D. G. Gillies for their supervision, and kind interest in his research and future career, and particularly Prof. L. H. Sutcliffe, who provided many hours of stimulating scientific discussion on all aspects of this work, together with interesting stories from the history of Magnetic Resonance Spectroscopy, in which he has played a constant rôle. The Author was privileged to be involved by Dr. Gillies and Prof. Sutcliffe in all aspects of their current research interests.

The Author acknowledges the support and encouragement of the Head of the Chemistry Department, Prof. J. R. Jones, who was closely involved in the establishment of the Magnetic Resonance Centre at Surrey University.

The Author and his Supervisors are grateful to Dr. M. J. Taylor and Dr. Jane Boyle at B. P. Research, Sunbury-on-Thames, for allowing the Author considerable use of their Jeol GX400 spectrometer, which made possible the carbon-13 NMR work at 100.5 MHz, and for assisting him in its operation.

Invaluable technical support was given by staff of the Chemistry Department at the University of Surrey, and the Author thanks Mr. A. P. Hill, Mr. G. L. Wright, and especially Mr. V. H. Zettel, who provided excellent facilities for the Gas Chromatographic work. The Author also thanks Mr. R. D. G. Lane and Mr. B. F. Smethurst, of the Magnetic Resonance Centre, for technical assistance on many different occasions.

The Author and his Supervisors are indebted to Mr. G. W. Smith, who performed the X-ray structural analyses that are reported in this work, despite the constant demands of other work on his time.

The Author also records his gratitude to Miss M. E. Hall, a former postgraduate of the Chemistry Department at the University of Surrey, who introduced him to the practice of Organic Synthesis during his initial months of study.

CONTENTS

Chapter 4
SYNTHESES RELATED
TO TRICYCLOHEXYLMETHANE

NMR SPECTRA

Chapter 5
TRICYCLOHEXYLMETHANE,
TRICYCLOHEXYLMETHYLCHLORIDE, AND
TRICYCLOHEXYLMETHYL:
X-RAY CRYSTALLOGRAPHIC AND ESR STUDIES

Chapter 6
SAMPLE PREPARATION AND
NMR MEASUREMENT

Chapter 1

INTRODUCTION

1.1 ENGINEERING LUBRICANTS

The production of compounds suitable for use as engineering lubricants has been a major industry for many years now, its growth stimulated in particular by the discovery of naturally occurring mineral oil deposits and the development of the internal combustion engine around the turn of the last century. Previous to this, the lubrication requirements of steam engines and machinery were met largely by the use of animal fats and their by-products, together with vegetable oils, such as castor oil. In fact, for the earliest internal combustion engines castor oil was the preferred lubricant of highest performance.

All these products have in common the presence of long alkyl chains, in the form of esters of the relevant fatty acids and glycerol or other polyhydric alcohols. With the rapid development of the technique of fractional distillation of crude mineral oils, components could be isolated from these which showed the necessary properties required for lubrication of fast moving metal parts. Some of the earliest mineral lubricating oils were separated from the naphtha oils discovered in Pennsylvania, in the United States, and at the Russian oil fields at Baku, and these contained molecules of long alkyl chains linked to central aromatic systems, mixed with assorted large alkanes or waxes. With the growing need for lubricating oils, a whole industry was soon devoted to the isolation, analysis,and blending of such oils for specific purposes.

The simultaneous progress of organic chemistry led to attempts to produce completely synthetic lubricating oils, together with the synthesis of all manner of additives thought to improve performance. There are now many kinds of such synthetic lubricants available[1], among them various polyethers, polysiloxanes and alkyl and aromatic silanes, all produced for their specific physical chemical properties suited to particular applications.

1.2 LUBRICATING OILS OF INTEREST IN THIS WORK

Despite the wide range of products used as lubricants, this work has been conducted with interest focused on only two in particular: the poly-α-olefins, and the so-called traction fluids.

Polymerizations of α-olefins (such as α-decene) have been found to give lubricating oils of superior performance for internal combustion engines. Although these types of oils are mixtures of various homologous structures, the molecules produced consist mainly of a small number of long aliphatic side chains attached to a

short aliphatic backbone - the 'star oligomers'. The optimum performance is known to obtain for a large proportion of *n*-octyl side chains in the mixture. Analysis of mass spectral data has shown that the molecules typically have a median size containing some 6 octyl groups.

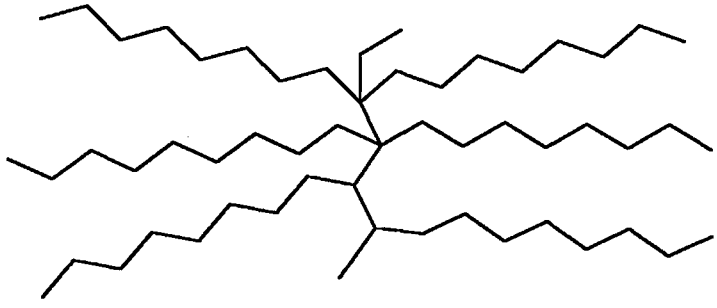

Fig 1.1: An oligomer of the type thought to be present in a poly-α-decene lubricant.

A different type of synthetic lubricant has been discovered for specialised use in continuously variable transmissions, or traction drives. Using these types of couplings power can be transmitted from one piece of machinery to another in a continuously variable way without the use of gearbox mechanisms, which leads to advantages of energy saving in many applications. The special lubricant provides protection for opposing machined metal surfaces (typically various cones or cylinders rolling on one another) as in the usual case; but the object is to provide this kind of mechanical protection together with the minimal possible amount of relative slippage of the surfaces, when they are forced into motion against each other. To everyday experience these would seem contradictory requirements, yet various synthetic fluids have been discovered which, by their inherent molecular properties, are able to accomplish this; they are called "traction fluids".

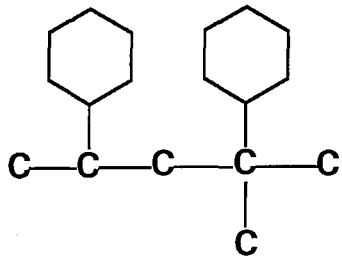

Fig 1.2: 2,4-dicyclohexyl-2-methylpentane, the main constituent of Santotrac, a traction fluid manufactured by Monsanto.

The compounds used at the present time usually contain several cyclohexyl groups attached to a short central backbone, either with an aliphatic linkage, as in Santotrac, or with ester type linkages in various experimental fluids. The

investigations carried out so far seem to indicate that the characteristic property of these is that their viscosity shows a strong increase with applied (extremely high) pressure, which is indicated by the traction coefficient in the engineering literature[2]. The more usual lubricants, of the type represented by poly-α-decene, do not have this property, and have correspondingly low traction coefficients[3].

1.3 LUBRICANTS, MOLECULAR MOTION, AND CARBON-13 NMR

One type of lubrication commonly involves separation of the moving parts where a lubricant layer of microscopic thickness is carefully maintained by suitable mechanical construction of the bearing and by limiting the operating conditions. However, the type of lubrication of interest as far as this work is concerned is boundary layer lubrication, where smoothly machined opposing surfaces are separated by a layer of lubricant only several molecules in thickness, and the most extreme conditions of temperature and pressure are present. It is believed that the special properties displayed by certain compounds as lubricating oils under these conditions are related not just to the overall shapes of their molecules, which are obviously important, but to their molecular motion. By this, one means both the overall motion of the molecules as units themselves, which takes place usually on the nanosecond time scale, and the internal motions of the different parts of the molecules. These internal motions take place on a much faster time scale, of the order of picoseconds.

A large amount of empirical data is available concerning the lubricating and other physical properties of oils, such as viscosities, viscosity/temperature dependence, viscosity/pressure dependence (especially important in this connection), pour points, and similar gross physical characteristics. However, these are all obtained on a rather ad hoc basis, from whatever particular samples are available, without probing the actual underlying molecular bases for such characteristics, so that the phenomenon of lubrication can be understood at a more fundamental level, and a unifying picture developed.

The use of NMR techniques can provide such information. As is well known, there are observables in NMR that depend not only on molecular structure, but also on orientation, conformation, and the rate of motional processes present in a sample. Coupling constants can provide information about the conformation of one part of a molecule relative to another, while relaxation times and NOE effects caused by complete proton decoupling in carbon-13 NMR depend on the time and spatial variation of overall and internal molecular motion. In order to interpret such NMR data in terms of these motions, it is necessary to assume a suitable theoretical basis, and one such interpretation for carbon-13 relaxation and NOE data is provided by the analysis of Lipari and Szabo.

1.4 THE THEORY OF LIPARI AND SZABO

This theory[4] was developed originally to analyze the carbon-13 relaxation and NOE data of the amino acid side chains present in protein molecules, and describes such a motion in a natural way for such a system, using three parameters. Starting from the assumption that the relaxation effects have their origin purely in the carbon-proton dipolar interaction energy, the equations which they obtained to describe them for a typical, isolated, carbon-proton fragment are

$$\frac{1}{T_1} = R_1 = \frac{(DCC)^2}{4}\left(J(\omega_H - \omega_C) + 3J(\omega_C) + 6J(\omega_H + \omega_C)\right) \tag{1}$$

$$\frac{1}{T_2} = R_2 = \frac{(DCC)^2}{8}\left(4J(0) + J(\omega_H - \omega_C) + 3J(\omega_C) + 6J(\omega_H) + 6J(\omega_H + \omega_C)\right) \tag{2}$$

$$\eta = \left(\frac{\gamma_H}{\gamma_C}\right)\frac{6J(\omega_H + \omega_C) - J(\omega_H - \omega_C)}{J(\omega_H - \omega_C) + 3J(\omega_C) + 6J(\omega_H + \omega_C)} \tag{3}$$

and $J(\omega)$ is the spectral density, which according to the theory of Lipari and Szabo can be written in the form

$$J(\omega) = \frac{2}{5}\left(\frac{S^2\tau_m}{1+\omega^2\tau_m^2} + \frac{(1-S^2)\tau}{1+\omega^2\tau^2}\right), \qquad \text{where} \qquad \frac{1}{\tau} = \frac{1}{\tau_m} + \frac{1}{\tau_i} \tag{4}$$

T_1, T_2, and η have their usual meanings and the angular frequencies, ω_C and ω_H ,, are the carbon and proton resonant frequencies in the given magnetic field. DCC is the dipolar coupling constant for such a carbon-proton fragment:

$$DCC = \left(\frac{\mu_0}{4\pi}\right)\frac{\gamma_C\gamma_H\hbar}{\langle r_{CH}^3\rangle} \tag{5}$$

Choosing the average carbon-proton bond length in a typical alkane fragment as 1.098 Å, (109.8 pm) gives DCC = 143.40 kHz, which was the value used in this work. In the case of methylene and methyl groups one assumes that the relevant relaxation rates, R_1 and R_2, should be given, respectively, by two, or three, times those of Eqs. (1) and (2).

The remaining three parameters, τ_m, τ_i and S^2 are related to the molecular motion itself, and are to be determined such that the values of T_1, T_2, and η predicted by Eqs. (1)-(3) agree with the measured NMR data. In the case of a large protein molecule, one might expect to be able describe the motion of a small attached side

chain with respect to a frame of reference fixed with respect to the main body of the protein, and in this way separate the motion into two parts; the slower, ponderous motion of the bulk of the molecule as a whole through surrounding solvent molecules, and the more rapid wiggling and rotation of the side chain atoms superimposed upon this. This is what the theory of Lipari and Szabo has done.

Taking firstly the simple case of a fragment with no internal motion, the molecule, and its attached C-H vectors, are imagined to undergo a rotational diffusion in a series of small steps, on account of the impact of neighbouring molecules. In this way the dipole-dipole interaction of the relaxing carbon atom with its attached proton has an induced time variation, dependent on some random function f(t). If this diffusion is isotropic and fast in some sense, the solutions for the relaxation rates in NMR experiments depend on the autocorrelation function derived from f(t),

$$G(\tau) = \underset{T \to \infty}{\text{LIM}} \frac{1}{T}\int_0^T f(t)f(t+\tau)dt \propto \exp\left(-|\tau|/\tau_m\right) \qquad (6)$$

Since this reorientation, and hence the time variation f(t), results from random molecular collisions, it is possible to make contact with the theory of Brownian motion. The assumption of an exponential form for G(t) in Eq. (6) then follows, and the introduction of the time constant of decay, τ_m, which indicates how quickly the random variations loose any short term coherence.

In the more general case, including internal motion of the C-H fragment, Lipari and Szabo were able to follow through a similar analysis, in which the extra motion was accounted for by introducing a second correlation time τ_i, and a parameter, S^2, which they called the generalised order factor. The correlation time τ_m is as before, while the internal correlation time τ_i appears from an appropriate convolution integral in a similar way to τ_m. However, the internal motion is allowed to be restricted within the molecular frame of reference and the generalised order parameter S^2 is a measure of this, although the exact detail of the internal motion can only be determined if other information is available. The theoretical derivation shows that $0 \leq S^2 \leq 1$ always.

Thus for $S = 1$, the carbon atom would be (theoretically) fixed rigidly to the macromolecule and the frame of reference moving with it, so that only a single correlation time, τ_m, would be needed to describe the overall isotropic rotational diffusion; while for $S = 0$, it would be effectively severed and its C-H vectors free to move at the fastest rate in all directions, and only the fast correlation time, τ_i, would be needed to describe the motion. This general rule has, however, to be treated with some caution, as certain types of motion can be proposed for which $S^2 = 0$, although the motion is still geometrically restricted. This depends on a "magic angle" effect, where a spatial average vanishes because of a special angular dependence of the

internal motion, and was discussed by Lipari and Szabo in their original paper. But in the absence of any obvious special factors, one can probably assume the simple link between S^2 and the degree of restriction of the internal motion. Obviously, each carbon position will have its own S^2 value, and a corresponding individual τ_i, appropriate to its particular kind of internal motion, while the value of τ_m should be common to all carbon positions in the molecule.

Although all these equations contain no explicit temperature dependence, this can be introduced through the correlation times τ_m and τ_i. The assumption is made that these parameters have an Arrhenius type dependence on the (absolute) temperature, involving an activation energy and a scaling parameter, often chosen as τ^{298}, and known from the context of reaction rates as the 'frequency factor' :

$$\tau_m = \tau_m^{298} \exp\left(\frac{E_m}{R}\left(\frac{1}{T} - \frac{1}{298}\right)\right) \tag{7}$$

$$\tau_i = \tau_i^{298} \exp\left(\frac{E_i}{R}\left(\frac{1}{T} - \frac{1}{298}\right)\right) \tag{8}$$

By extending the Lipari and Szabo formulae in this way, and making variable temperature measurements of NMR relaxation data, the values of these activation energies can be determined in favourable circumstances, and even more insight obtained into the behaviour of the molecular motion. As for S^2, it can often be assumed to be essentially constant, at least over a limited temperature range, although this is discussed further in Chapter 7, where it is suggested that a strong variation can be detected in some cases, and this may be significant for the properties of a lubricating oil.

Lipari and Szabo devoted considerable effort to verifying the correctness of their approach against various reported NMR data, and also simulated data generated from other more complicated theories which assume particular types of molecular motion a priori. They found that their approach was consistent with such data, as long as certain conditions were satisfied regarding the relative rates and nature of the molecular motions. Their papers go into these conditions at some length, but the only one of significance to the present work is that the theory can be expected to apply well if $\tau_i << \tau_m$, and the overall motion of the molecule as a whole is isotropic.

It is not easy to assess, from the mathematical point of view, the relative importance and interactions of the three parameters τ_m, τ_i,and S^2 in Eqs.(1)-(4). However, from Eq.(4) it is clear that almost always $\tau \approx \tau_i$ will be a valid approximation when $\tau_i << \tau_m$. If in the case in question, S^2 is suitably large and $\tau_i << 1/(\omega_C + \omega_H)$, then the second term in Eq.(4) for $J(\omega)$ will probably be negligible, and one can make the substitution

$$J(\omega) = \frac{2}{5}\left(\frac{S^2\tau_m}{1+\omega^2\tau_m^2}\right) \tag{9}$$

The reduced Lipari and Szabo equations so obtained correspond to the model in which the fast internal motions of the C-H fragment are accounted for as simply averaging out a certain proportion of the dipolar interaction, during a slower isotropic rotational diffusion of the molecule as a whole. The parameter S^2 becomes the appropriate scaling factor. Whether this is in fact a valid approximation depends on the experimental data; and each case requires careful examination using all available information.

Proceeding one stage further, in the case that even τ_m becomes sufficiently small, one enters the region of extreme narrowing where

$$J(\omega) = \frac{2S^2\tau_m}{5} \tag{10}$$

and Eqs.(1)-(3) become the classical formulae:

$$\frac{1}{T_1} = \frac{1}{T_2} = R_1 = R_2 = (DCC)^2 S^2\tau_m \tag{11}$$

$$\eta = \frac{1}{2}\left(\frac{\gamma_H}{\gamma_C}\right) \tag{12}$$

1.5 PREVIOUS NMR WORK USING THE THEORY OF LIPARI AND SZABO

The theory of Lipari and Szabo describing carbon-13 NMR relaxation and NOE effects has been used by several authors since it was proposed, to obtain information concerning molecular motion. As long as the conditions referred to above regarding the general nature of the molecular motion are satisfied, the theory has been found to be applicable not only to macromolecules such as proteins, but to molecules of smaller molecular weight. These conditions are not in fact very critical under normal conditions, since the overall rate of motion of molecule in solution at ordinary temperatures can be expected to be 10 to 100 times slower than the rates of internal gyration relative to the molecular frame, and can be assumed to be isotropic if the molecule has similar dimensions in all directions.

Gillies and Sutcliffe, together with co-workers, have undertaken studies of the molecular motion of lubricants of various kinds, related alkyl structures, and

surfactant molecules in solution[5], using carbon-13 NMR data. They analyzed numerous sets of available relaxation and NOE data related to various *n*-alkyl derivatives, and determined the parameters required in the equations of Lipari and Szabo to fit these data sets. In particular, they suggested that the correlation times, τ_i, for the internal motions of the last few carbon positions of the free ends of *n*-octyl chains were more or less invariant among different compounds. At 298 ^{0}C, the values which they obtained for the last four positions were; C5, 19 ps; C6, 14 ps; C7, 11 ps; C8, 4.9 ps.

In other work they have reported the results of their own NMR measurements made on various traction fluids and similar cyclohexyl derivatives[6], and also compounds containing several linked *n*-octyl chains - in particular the commercial lubricant poly-α-decene[7] and tetra-*n*-octyl tin[8]. Measurements of relaxation times and NOE factors on each compound were made at variable temperature using several different field strengths, and in some cases under pressures of several thousand atmospheres, using special equipment. The values predicted by the extended temperature dependent forms of the Lipari and Szabo equations were then fitted to the experimental values by minimization of least squares differences using standard numerical methods, executed by computer. In this way they were able to obtain values for the activation energies and frequency factors appearing in the equations for the temperature dependence of τ_m and τ_i, as well as the order parameters, S^2.

More recent papers to appear on molecular motion, using the Lipari and Szabo theory together with variable temperature and/or multifrequency carbon-13 measurements, have been those of Kowalevski and co-workers, who studied the molecular motions in solution of a tetrasaccharide[9], and two cyclodextrins[10], with some success.

1.6 THE PRESENT WORK

The intention was to continue the investigations of the molecular motion of lubricant molecules by NMR methods begun by Gillies and Sutcliffe, and mentioned above, with particular interest in those molecules containing clustered *n*-octyl groups, such as poly-α-decene, and cyclohexyl derivatives related to traction fluids.

However, there are certain problems associated with the use of actual commercial lubricants for such investigations. They are usually complicated mixtures of homologous structures of varying molecular sizes, and also intentional additives. Their carbon-13 spectra may thus contain a multiplicity of overlapping resonances, which cannot be assigned precisely to any one part of any component of the mixture. Not only does this obstruct any attempt at numerical measurement from the spectra, it also makes it impossible to try to identify the motional parameters of particular parts of the lubricant molecules. Ideally, one would prefer to have clear single resonances

present in the spectra, corresponding to dynamically equivalent parts of the molecular structure. By the later, one means those parts (usually single carbon atom positions, in this work) whose dynamics can be expected to be equivalent under all conditions, by simple considerations of molecular symmetry.

Therefore it was decided not to use actual commercial products for these measurements, but rather to synthesize chemically pure samples of compounds whose structures would be close analogues, or models, of the molecular species known to be present in such commercial lubricants. In fact, even more simplification was achieved by choosing particularly symmetrical structures, so that in the resulting carbon-13 spectra the chemical and dynamic equivalencies coincided as much as possible. In this way, accurate data could be expected from numerical measurements, referring to precisely identified dynamic groupings within the given molecule. And of course, data referring to pure compounds might offer more hope of a systematic understanding of the behaviours observed in a series of related molecular species.

The choice of highly symmetric molecules was also important for the application of the theories used to analyze the NMR relaxation data in this work, since it made it possible to assume that, to a good approximation, the overall molecular motion would be isotropic. Generally speaking, the results that were obtained pointed to this being a reasonable assumption.

The following three compounds were chosen as models for the kinds of lubricants represented by poly-α-decene, whose star-like clusters of *n*-octyl chains they imitate:

1. 9,10-Di-*n*-octyl-*n*-octadecane
2. 9-*n*-Octyl-*n*-heptadecane
3. Tri-*n*-octylsilane

The first two were synthesized as described later, while the third was purchased.

Two further compounds were synthesized as models for the kinds of lubricants used as traction fluids:

4. Tricyclohexylmethane
5. 1,1,2-Tricyclohexylethane

So far, actual traction fluids in engineering use have been molecules containing two cyclohexyl groups attached to various kinds of short central backbone, and so the choice of these tricyclohexyl derivatives in this work represented a new step. However, for tricyclohexylmethane at least, there are fairly reliable reports of measurements of its viscosity and lubricating properties under conditions of boundary

layer lubrication, in which it displayed to an unusually high degree the kind of behaviour required for a traction fluid[11]. Tricyclohexylmethane had a high traction coefficient in these tests, becoming suitably viscous and 'sticky', while still providing mechanical protection for the rolling surfaces it was applied to. Therefore these two choices seemed appropriate for investigation, extending the earlier work of Gillies and Sutcliffe on dicyclohexyl traction fluids and related structures.

Since the features of the molecular motion of lubricant molecules that give rise to their special properties evidently rely on the co-operative interaction of the molecules with each other, NMR measurements were made on neat samples of the relevant compounds rather than on a solution of any kind. The experimental details are described at the beginning of Chapter 6. Carbon-13 T_1 relaxation times and NOE factors were measured for each compound and each dynamically equivalent set of carbon atom positions in each, at carbon-13 frequencies of 67.83 and 100.5 MHz, over temperatures ranging from 5 to 10 ^{0}C above their respective melting points, up to 120 to 140 ^{0}C. Using the temperature dependent form of the Lipari and Szabo theory, the parameters describing the motions of the carbon atoms were then obtained, where possible, by suitable fitting of the theoretically predicted values to the experimental data. The analyses are described in Chapters 7 and 8.

1.7 DEUTERIUM NMR

The decision to work with synthetic compounds modelling the structures found in actual lubricants carried with it a further advantage beyond those already mentioned. It was found possible to synthesize samples of site specifically deuterium labelled isotopomers of three of the model compounds that were to be used for carbon-13 measurements:

1D. 9,10-Di-*n*-octyl-*n*-octadecane-9d_1
2D. 9-*n*-Octyl-*n*-octadecane-9d_1
4D. Tricyclohexylmethane-d_1

The relaxation effects observed in NMR of deuterons are completely dominated by the interaction energy of the deuteron quadrupole moment with the electric field gradients present at the site of deuteration. The theoretical equations that can be derived to describe these are similar in general form to those outlined above for carbon-13 relaxation effects. On the assumption of isotropic rotational diffusion, the standard equations for a C-D fragment are derived to be[12]

$$\frac{1}{T_1} = R_1 = \frac{\pi^2}{10}\left(1+\frac{\eta^2}{3}\right)(QCC)^2\left(3J(\omega)+12J(2\omega)\right) \qquad (13)$$

$$\frac{1}{T_2} = R_2 = \frac{\pi^2}{20}\left(1+\frac{\eta^2}{3}\right)(QCC)^2\left(9J(0)+15J(\omega)+6J(2\omega)\right) \qquad (14)$$

where ω is the deuterium resonant angular frequency in the applied field, and QCC is the quadrupolar coupling constant. $J(\omega)$ is the spectral density, given by

$$J(\omega) = \frac{\tau_m}{1+\omega^2\tau_m^2} \qquad (15)$$

where τ_m is a correlation time for the overall molecular rotation. From its theoretical derivation, it should correspond to the τ_m in the equations of Lipari and Szabo for carbon-13 relaxation data. As usual

$$QCC = \frac{e^2qQ}{h} \qquad (16)$$

where h is Plank's constant, e is the electronic charge, and Q the quadrupole moment of the deuteron. The quadrupole interaction energy arises from the molecular electric field gradients at the position of the deuteron; their symmetric matrix $(\partial^2V/\partial x_i\partial x_j)$ can be diagonalized by taking suitable orthogonal coordinates, usually with the one closest to the C-D bond direction as z, in which case the asymmetry parameter is

$$\eta = \frac{V_{xx}-V_{yy}}{V_{zz}} \qquad (17)$$

and

$$eq = V_{zz} \qquad (18)$$

By the substitution of Eq. (7) for τ_m, the dependence on temperature can be introduced, and measurements of deuterium T_1 and T_2 data can then lead to determinations of E_m and τ_m^{298}.

However, Eqs.(13)-(15) take no account of the faster internal motions of the deuterium bond. Assuming that these are sufficiently fast, in the sense that $\tau_i << 1/\omega$, and are also fairly restricted, one can propose the same approximation derived in connexion with the reduced Lipari and Szabo equations in Section 4. This involves introducing a scaling parameter to account for the faster motions by effectively reducing the quadrupolar interaction. Thus one replaces Eq.(15) with:

$$J(\omega) = \frac{S^2\tau_m}{1+\omega^2\tau_m{}^2} \tag{19}$$

or equivalently one can make the substitution:

$$(QCC)^2 \longrightarrow S^2(QCC)^2 \tag{20}$$

The recent paper of Vold et al.[13], reports detailed analyses of motional averaging of deuteron quadrupolar interactions in a flexible molecule, through the use of quadrupole resonance, but the simple assumption made here proved sufficient to allow the analyses of the deuterium relaxation data that were acquired in the present work.

For 9,10-di-*n*-octyl-*n*-octadecane-9d_1 and 9-*n*-octyl-*n*-heptadecane-9d_1, measurements of the deuterium T_1 and T_2 values over a wide range of temperatures at only one frequency (41.4056 MHz) quite unambiguously determined not only the temperature variation of τ_m, but also the value of the factor $(1+\eta^2/3)S^2(QCC)^2$. Thus it was not necessary to make any assumptions about the values of the quadrupole coupling constants, asymmetry parameters, or S^2. The relevant analyses appear in Chapter 7. In the case of tricyclohexylmethane-d_1, similar deuterium NMR measurements were somewhat less satisfactory and there were certain anomalies in the data, but it was still possible to use this information in combination with the carbon-13 data, as discussed in Chapter 8.

1.8 SILICON-29 NMR

In the case of tri-*n*-octylsilane it was obviously possible to supplement the carbon-13 NMR measurements with those of silicon-29 relaxation times and NOE factors. Taking the example of an isolated Si-H fragment, which was in fact the case in question, one would expect a theoretical description exactly analogous to that described by the Lipari and Szabo equations for carbon-13 relaxation. However, the situation is not so simple, since one must take into account the negative gyromagnetic ratio of silicon-29. The paper of Werbelow[14] indicates that the effect of this is a permutation of the weighting factors of the spectral densities in any of the usual expressions for dipolar relaxation. The analogues of the Lipari and Szabo equations for relaxation in an isolated Si-H fragment should therefore become:

$$\frac{1}{T_{1DD}} = R_{1DD} = \frac{(DCC)^2}{4}(6J(\omega_H-\omega_{Si})+3J(\omega_{Si})+J(\omega_H+\omega_{Si})) \tag{21}$$

$$\frac{1}{T_{2DD}} = R_{2DD} = \frac{(DCC)^2}{8}(4J(0)+6J(\omega_H-\omega_{Si})+3J(\omega_{Si})+6J(\omega_H)+J(\omega_H+\omega_{Si})) \tag{22}$$

$$\eta = -\left|\frac{\gamma_H}{\gamma_{Si}}\right| \frac{6J(\omega_H - \omega_{Si}) - J(\omega_H + \omega_{Si})}{6J(\omega_H - \omega_{Si}) + 3J(\omega_{Si}) + J(\omega_H + \omega_{Si})} \tag{23}$$

where $J(\omega)$ is the spectral density,

$$J(\omega) = \frac{2}{5}\left(\frac{S^2\tau_m}{1+\omega^2\tau_m^2} + \frac{(1-S^2)\tau}{1+\omega^2\tau^2}\right), \qquad \text{and} \qquad \frac{1}{\tau} = \frac{1}{\tau_m} + \frac{1}{\tau_i} \tag{24}$$

The various parameters have the same meaning as in the case of carbon-proton dipolar relaxation, and the (signed) dipolar coupling constant is

$$DCC = \left(\frac{\mu_0}{4\pi}\right)\frac{\gamma_{Si}\gamma_H\hbar}{\langle r_{SiH}^3\rangle} \tag{24}$$

Just as in the case of carbon-13 dipolar relaxation, one can consider the case where $\tau_i << 1/(\omega_{Si}+\omega_H)$, and obtain the equations in the case of sufficiently fast restricted internal motion of the Si-H bond by substituting the reduced spectral density

$$J(\omega) = \frac{2}{5}\left(\frac{S^2\tau_m}{1+\omega^2\tau_m^2}\right) \tag{25}$$

It was found that these equations were not sufficient to analyze the 53.5977 MHz silicon-29 T_1 relaxation data for tri-*n*-octylsilane, since the relaxation was found to be predominantly due to spin-rotational coupling at higher temperatures. A similar finding appears in a study, at rather lower temperatures, of silicon-29 relaxation in three low molecular weight liquid silanes[15].

Spin-rotational relaxation arises from the fluctuating local magnetic fields generated by the motion of the charged particles within a molecule, and can be written in terms of the spin-rotation coupling tensor, **C**. Equations describing spin-rotational relaxation rates for isotropic, diffusive, overall motion of a spherically symmetric molecule were derived by Hubbard[16]. The paper of Wang[17] extends this treatment to include anisotropic motion of a symmetric-top molecule, and the expression derived for T_1 in the limit of extreme narrowing is

$$\frac{1}{T_{1SR}} = \frac{1}{T_{2SR}} = R_{1SR} = R_{2SR} = \left(\frac{2kT}{3\hbar^2}\right)\left(I_{\parallel}C_{\parallel}^2\tau_{\parallel} + 2I_{\perp}C_{\perp}^2\tau_{\perp}\right) \tag{26}$$

where $I_{\parallel}$ and $I_{\perp}$ are principal moments of inertia of the molecule, $C_{\parallel}$ and $C_{\perp}$ are components of the spin-rotation coupling tensor, and $\tau_{\parallel}$ and $\tau_{\perp}$ are correlation times for variation of the components of molecular angular velocity, in the directions of the

axis of symmetry, and perpendicular to it, respectively. The derivation of Eq. (26) assumes that the relaxing nucleus lies on the axis of symmetry, as for silicon-29 in tri-*n*-octylsilane.

For a spherically symmetric molecule of moment of inertia I, at temperature T, Hubbard[16] derived a connection between the correlation time for overall molecular reorientation, τ_m, and the correlation time, τ_j, for the variation of the components of molecular angular velocity:

$$\tau_m \tau_j = \frac{I}{6kT} \tag{27}$$

One can expect similar relationships in the case of the symmetric-top molecule, and numerical estimates using the factors in Eq. (27) show that τ_j is at least an order of magnitude smaller than τ_m at the kinds of temperature considered in this work. Therefore if silicon-29 dipolar relaxation is approximately in the region of extreme narrowing, which was apparently the case for tri-*n*-octylsilane above room temperature, any spin-rotational relaxation certainly will be.

The assumption that tri-*n*-octylsilane can be regarded approximately as a spherically symmetric molecule proved adequate for the analysis of the relaxational data in this work. In this case

$$\tau_{\parallel} \approx \tau_{\perp} \propto \frac{1}{T\tau_m} \tag{28}$$

and substitution of Eq. (28) into Eq. (26) leads to an expression for R_1 at extreme (spin-rotational) narrowing of the form

$$\frac{1}{T_{1SR}} = R_{1SR} = \frac{C^2}{\tau_m} \tag{29}$$

where C is some constant. The R_1 relaxation rate, which was the only one measured for tri-*n*-octylsilane in this work, can then be written[16] as the sum of the rates for dipolar and spin rotational relaxation given by Eqs.(21) and (29)

$$R_1 = R_{1DD} + R_{1SR} = R_{1DD} + \frac{C^2}{\tau_m} \tag{30}$$

Using only the reduced form of the spectral densities for the contribution from dipolar relaxation in Eq. (30), a satisfactory description of the observed R_1 relaxation rates in tri-*n*-octylsilane was possible, and E_m could be determined, without having to

know, a priori, the value of the parameter C. The relevant analysis appears in Chapter 7.

REFERENCES FOR CHAPTER 1

[1] D. Klamann, *Lubricants*, Verlag Chemie, Weimheim, 1984

[2] M. Muraki, *Tribology International*, December 1987, 347-354

[3] For an extensive series of engineering measurements of viscosities of lubricant related compounds of both low and high traction coefficients, under conditions of high contact pressures and shearing rates, see K.-H. Hentschel, *J. Synthetic. Lubrication*, 1985, **2**, 143 and 239; also the paper of Muraki, Ref. 2

[4] G. Lipari and A. Szabo, *J. Am. Chem. Soc.*, 1982, **104**, 4546-4570

[5] P. J. Bratt, D. G. Gillies, L. H. Sutcliffe, and A. J. Williams, *J. Phys. Chem.*, 1990, **94**, 2727; P. J. Bratt, D. G. Gillies, A. M. L. Krebber, and L. H. Sutcliffe, *Magn. Reson. Chem.*, 1992, **30**, 1000

[6] D. G. Gillies, S. J. Matthews, and L. H. Sutcliffe, *Magn. Reson. Chem.*, 1990, **28**, 171; D. G. Gillies, S. J. Matthews, and L. H. Sutcliffe, *Magn. Reson. Chem.*, 1991, **29**, 777; D. G. Gillies, S. J. Matthews, and L. H. Sutcliffe, *Magn. Reson. Chem.*, 1991, **29**, 823; D. G. Gillies, S. J. Matthews, and L. H. Sutcliffe, *Magn. Reson. Chem.*, 1992, **30**, 259; D. G. Gillies, S. J. Matthews, L. H. Sutcliffe, and A. J. Williams, *J. Magn. Reson.*, 1990, **86**, 371

[7] L. M. Bull, D. G. Gillies, S. J. Matthews, L. H. Sutcliffe, and A. J. Williams, *Magn. Reson. Chem.*, 1990, **28**, 171

[8] D. G. Gillies, S. J. Matthews, and L. H. Sutcliffe, *Magn. Reson. Chem.*, 1991, **29**, 1221

[9] S. Bagley, H. Kovacs, J. Kowalewski, and G. Widmalm, *Magn. Reson. Chem.*, 1992, **30**, 733

[10] J. Kowalewski and G. Widmalm, *J. Phys. Chem.*, 1994, **98**, 28

[11] E. Kuss, *Ber. Bunsenges. Phys. Chem.*, 1983, **87**, 33; K.-H. Hentschel, *J. Synthetic. Lubrication*, 1985, **2**, 143 and 239

[12] C. Poole and H. Farach, *Theory of Magnetic Resonance*, Wiley-Interscience, 1972; A. Abragam, *Principles of Nuclear Magnetism*, Oxford University Press, 1983; A. Carrington and A. D. McLachlan, *Introduction to Magnetic Resonance*, Harper and Row, 1967

[13] M. S. Greenfield, R. L. Vold, and R. R. Vold, *J. Chem. Phys.*, 1985, **83**(4), 1440

[14] L. Werbelow, *J. Magn. Reson.*, 1984, **57**, 136

[15] K. M. Larsson, J. Kowalewski, and U. Henriksson, *J. Magn. Reson.*, 1985, **62**, 260

[16] P. S. Hubbard, *Phys. Rev.*, 1963, **131**, 1155

[17] C. H. Wang, *J. Magn. Reson.*, 1973, **9**, 75

Chapter 2

SYNTHESES RELATED TO 9,10-DI-*n*-OCTYL-*n*-OCTADECANE

2.1 9,10-DI-*n*-OCTYL-*n*-OCTADEC-9-ENE

The reaction chosen for synthesis of 9,10-di-*n*-octyl-*n*-octadec-9-ene was the reductive coupling of the ketone 9-heptadecanone using the well known McMurry reaction[1]. This involves the generation of a low valent titanium species, under an inert atmosphere, often by the reduction of titanium tetrachloride with zinc in an ethereal solvent. Addition of the appropriate ketone followed by some 10-20 hours of refluxing then effects the desired symmetrical coupling via the oxidation of the titanium species, whose exact nature has been extensively studied, but is still open to some discussion. If the ketone is added at 0 ^{0}C and the reaction then hydrolyzed, the corresponding pinacol can be obtained instead.

It is known that this reaction works through the dimerization of ketyl radicals generated from the ketone on the surface of the titanium metal particles through donation of an electron[2], and this is favoured by the presence of electron withdrawing groups in the ketone which help to stabilize the radical centre, and hindered by substituents with more electropositive nature such as alkyl groups. Aromatic ketones are reported to give especially good results with this reaction. On the other hand it was recognized by McMurry himself that the reaction is often difficult to bring about successfully without special care and precaution in preparing the titanium reagent[3]. Methods described involve rigorous exclusion of moisture and oxygen, and often the use of expensive titanium trichloride as the precursor of the titanium reagent, but for large scale preparations only the procedure using the titanium tetrachloride/zinc system is economic. An ethereal solvent is always reported to be used.

However, in the present case this procedure proved unreliable. Often the greater portion of the ketone used was recovered unchanged through a failure to generate the required titanium species prior to adding the ketone. On other occasions a hydrocarbon oil was produced which contained, according to GC analysis, several different components which it was not possible to separate using standard preparative techniques. Probably this was due to the inductive effect of the long alkyl chains in this ketone slowing the reaction rate, thus leading to predominance of various isomerizations and other side reactions. One of these components was in fact the desired 9,10-di-*n*-octyl-*n*-octadec-9-ene and two others were found out later to be corresponding isomers, but the mixture could not be separated.

In consequence, a series of experiments were carried out to determine if conditions could be found in which this reaction would work reliably and economically

on a large scale, when applied to 9-heptadecanone. The paper of Ledon et al.[4], reported the very effective use of the organo-metallic compound bis(benzene)titanium-$(\eta\text{-}C_6H_6)_2Ti$-for the reductive coupling of ketones.

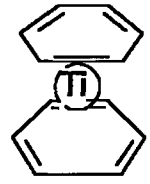

Fig 2.1: The sandwich structure of bis(benzene)titanium proposed by Anthony et. al.[5] The air sensitive solid is red in colour.

This suggested that the use of an aromatic hydrocarbon solvent might provide the answer by generating a more powerfully reducing titanium reagent. At first this proved a failure, and it was impossible to generate the suitable titanium species when the reaction was carried out in toluene. It appeared that titanium tetrachloride was not reduced effectively by zinc in toluene even under vigorous reflux; an orange coloured solution resulted instead of the dense black titanium species which is always quoted in the literature as the required form of titanium for this reaction. In fact there seemed to be very little interaction at all, which was surprising given the reactivity of titanium tetrachloride.

However, by the addition of about 40% by volume of tetrahydrofuran to the toluene a completely different course of events followed, and the titanium tetrachloride was rapidly reduced under reflux to a dense, dark red solution - more probably a colloidal suspension of a low valent titanium species. In any case, addition of 9-heptadecanone in toluene solution followed by reflux for only 90 minutes was sufficient under these conditions to give a 70% yield of the required alkene, 9,10-di-*n*-octyl-*n*-octadec-9-ene,with isomeric impurities amounting to no more than 2% after purification, as determined by GC analysis. It was also found that a much more effective work-up was simply to pour the resulting reaction mixture into very dilute sulphuric acid, whereupon the titanium salts separated at once into the aqueous phase and the organic products were extracted into the toluene with no further work. The recommended method is to neutralize with potassium carbonate solution, which then leads to an awkward filtration of the precipitated titanium salts and an extraction of the organic products into a suitable solvent. The toluene could be recovered; azeotropic distillation was sufficient to dry the solvent for immediate reuse.

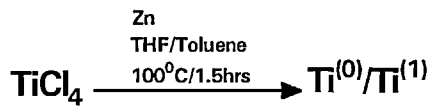

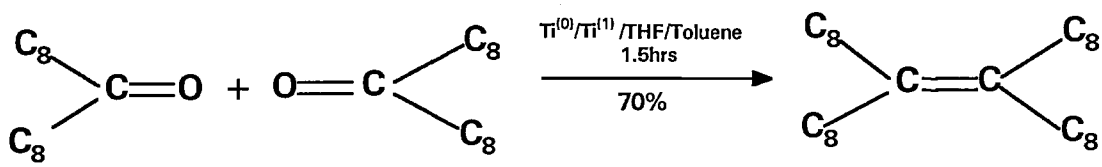

9,10-di-*n*-octyl-*n*-octadec-9-ene: Glassware was oven dried before use; dry toluene of suitable purity was prepared simply by distillation, discarding the first 10% of distillate, which contained all the water present; standard hplc grade THF (Aldrich) could be used as supplied. Zinc grit (Fluka) was also oven dried for 30 minutes before use.

Into a 1 L three-necked round bottom flask, fitted with an efficient mechanical stirrer, reflux condenser, 100 ml dropping funnel protected by a septum, and a gas bubbler/inlet, was placed 25 g (380 mmol) of dry zinc grit, 100 ml of dry THF, and 150 ml of dry toluene. The apparatus was closed and an atmosphere of dry, oxygen free nitrogen established via the gas inlet/bubbler. The mixture was stirred vigorously for 15 minutes to deoxygenate the solvents, while 37.5 g (22.0 ml, 200 mmol) of titanium tetrachloride (Fluka) was transferred into the dropping funnel using a syringe and nitrogen flushing needle.

The flask was then cooled in an ice bath, and the titanium tetrachloride added slowly to the vigorously stirred zinc suspension. The reaction was quite gentle and a yellow solution resulted, the flask filling with yellow fumes and deposits. The ice bath was removed, and the reaction heated gradually to reflux. After refluxing for 30-40 minutes all the fumes and deposits were re-absorbed by the reaction, which turned green, and finally formed a dense, dark red solution. This contained the low valent titanium species required for the subsequent coupling reaction.

The flask was allowed to cool slightly, the stirring was reduced to a steady slow rate, and a solution of 25.4 g (100 mmol) of 9-heptadecanone (>99% purity) in 220 ml of dry toluene run in quite rapidly. After the initial moderately exothermic reaction on adding the ketone solution, the reaction was heated at 100 ^{0}C for 90 minutes.

The contents of the flask were then poured, with frequent shaking, into 200 ml of water, acidified with sulphuric acid. The toluene layer was separated, the aqueous layer extracted twice with fresh toluene, and the combined toluene solutions washed well with water, twice with brine, and dried by standing over anhydrous

potassium carbonate, which also served to neutralize any acid present. After filtration the toluene was removed firstly by distillation, and finally by rotary evaporation. Care was taken not to overheat the crude product during the distillation.

There was obtained about 25 g of pale yellow oil, which according to GC analysis contained some 70 % by weight of the required alkene. Sometimes a small amount of solid material would separate out from this oil on standing for a few days.■

The 9,10-di-*n*-octyl-*n*-octadec-9-ene could not be isolated simply by distillation because it began to isomerize at the boiling point available using standard vacuum distillation apparatus.(About 210 ^{0}C). However, thanks to the absence of any closely related structures in the crude product obtained as above, all the impurities were either polar and could be removed by simple column chromatography, or had lower molecular weight and were successfully removed by short path distillation at moderate temperatures.

Purification of 9,10-di-*n*-octyl-*n*-octadec-9-ene: The crude, neutral, product obtained as above was firstly subjected to a simple distillation at 0.1 mm Hg, taking the pot temperature to a maximum of 120 ^{0}C, which removed a quantity of lower boiling impurities. (These set to a waxy solid on cooling, and probably consisted mostly of 9-heptadecanol; simple reduction of the original ketone is a known side reaction[6]). The residue of oil left in the pot was then divided into two equal portions, and each individually percolated through a 15 cm x 3.5 cm column of silica gel, previously prepared in the usual way by elution with pentane. The elution of the oil was also completed with pentane. All that was required was to collect the initial fractions until there was no further increase in weight of the evaporated elute. This process removed all coloured and polar impurites in the oil. Finally a short path distillation was carried out (in the apparatus described in Appendix 1) at 0.1 mm Hg, taking the flask temperature carefully and slowly to 140 ^{0}C. The oil was cooled before re-admitting air to the flask. The purity of the resulting product could be checked by a simple GC analysis, and if necessary the short path distillation was repeated until all more volatile components were removed. There was finally obtained 14-16 g of water white oil. Carbon-13 and proton NMR spectra corresponded exactly to those expected for the product, 9,10-di-*n*-octyl-*n*-octadec-9-ene, and no other resonances were detectable. Purity by GC analysis was >98%, with traces of two corresponding isomeric alkenes as the remaining components. Yield (averaged over six such syntheses) from the original ketone: 66%.■

2.2 9,10-DI-*n*-OCTYL-*n*-OCTADECANE

Catalytic hydrogenation of 9,10-di-*n*-octyl-*n*-octadec-9-ene gave the required alkane, 9,10-di-*n*-octyl-*n*-octadecane. A final short path vacuum distillation was again used to remove traces of solvents and more volatile impurities from the hydrogenated product, and could be omitted from the procedure for purifying the 9,10-di-*n*-octyl-*n*-octadec-9-ene used in this further reaction:

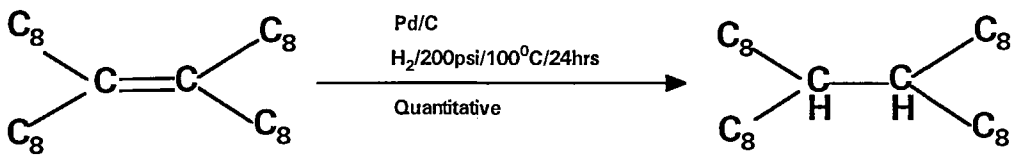

9,10-di-*n*-octyl-*n*-octadecane: 40 g (84 mmol) of 9,10-di-*n*-octyl-*n*-octadec-9-ene was dissolved in a mixture of 160 ml of cyclohexane and 40 ml of glacial acetic acid and hydrogenated for 24 hours at 200 psi and 80 ^{0}C over 2.0 g of 5 % palladium on carbon. After filtration of the catalyst, and drying over anhydrous potassium carbonate, rotary evaporation gave the desired alkane. Complete saturation of all olefinic material was confirmed by proton NMR and GC analysis.

The product was purified in the manner described above for 9,10-di-*n*-octyl-*n*-octadec-9-ene. There was obtained 39 g of water white oil. Proton and carbon-13 NMR spectra agreed exactly with those expected for 9,10-di-*n*-octyl-*n*-octadecane. Purity by GC analysis was >99 %. Yield: almost quantitative.■

2.3 9,10-DI-*n*-OCTYL-*n*-OCTADECANE-9d$_1$

It had been expected that 9,10-di-*n*-octyl-*n*- octadecane-9,10-d$_2$ could be made by catalytic deuterogenation of 9,10-di-*n*-octyl-*n*-octadec-9-ene with deuterium gas. However, an examination of the relevant literature showed that this method would have little chance of success since carbon-hydrogen bonds are activated by the usual heterogeneous metal catalysts, and deuterons would thus be incorporated all over the substrate molecule rather than site specifically at the position of the original double bond[7]. This procedure is only used in special cases where a very active unsaturated centre kinetically favours site specific deuteration. A trial attempt to employ a commercially available homogeneous catalyst to hydrogenate 9,10-di-*n*-octyl-*n*-octadec-9-ene failed, although these catalysts can be used to label a suitable unsaturated centre - often a functionalized one which specifically co-ordinates with the organometallic catalyst molecule[8].

The best hope was to apply the technique of ionic hydrogenation[9]. In this method a double carbon-carbon bond is first protonated by the presence of a suitably

strong acid, and the resulting carbonium ion then traps a hydride ion released from a silane derivative present in the reaction mixture. The acid/silane combination is known as a hydrogenating pair. Use of the corresponding deuteriosilane should result in deuteration instead. Obviously the reaction requires the initially formed carbonium ion to be sufficiently stable to have the opportunity of reacting with the silane present - this means in general that it should be a tertiary carbonium centre. The present case met this requirement, although the actual course of the reaction was found to be more involved than the mechanism would have suggested at first glance, and involved two isomerized alkenes as intermediates:

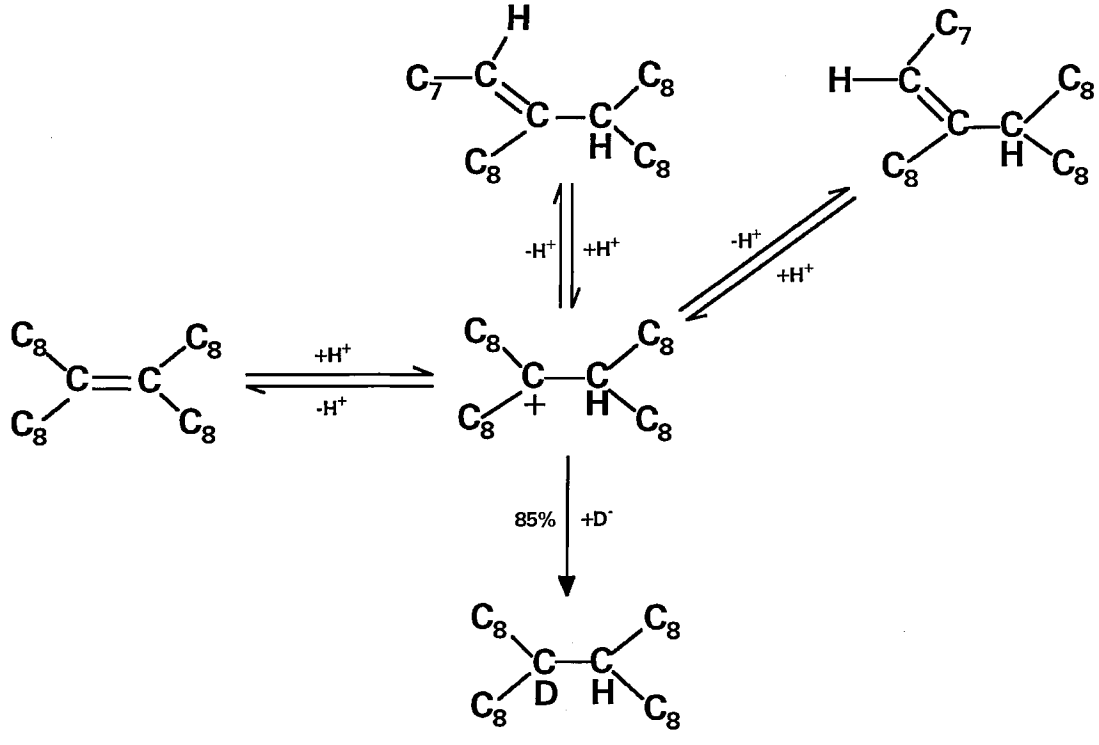

9,10-di-*n*-octyl-*n*-octadecane-9d$_1$: Into a dry 100 ml round bottom flask, fitted with a septum inlet protected by a stop cock, and a teflon coated magnetic stirrer bar, was placed a solution of 5 g (10.5 mmol) of 9,10-di-*n*-octyl-*n*-octadec-9-ene and 1.5 g (12.8 mmol) of triethylsilane-d$_1$ in 25 ml of AR dichloromethane. Using a syringe, 7.0 g of trifluoroacetic acid were then carefully injected into the flask, the stopcock was closed, and the reaction stirred at room temperature for 7 days.

At the end of this time, the septum inlet and stopcock were replaced with a reflux condenser, 5ml each of ether and water added to the mixture, and the reaction carefully neutralized by the addition of solid sodium carbonate. The organic layer was separated and the aqueous layer extracted twice with ether. The combined organic solutions were then washed well with water, twice with brine, and dried by standing over anhydrous sodium sulphate.

The crude product so obtained was purified in the manner described in the synthesis of the ordinary hydrocarbon. There was thus obtained 4.1 g of water white oil; carbon-13 and proton NMR spectra agreed exactly with those expected for the required product, 9,10-di-*n*-octyl-*n*-octadecane-9d_1, and demonstrated the site specific incorporation of the deuterons at the central carbon position. GC analyses were identical with those of the ordinary hydrocarbon, with indicated purity >99.5%. Yield: 82 %.■

Samples of the reaction solution were taken during the course of this synthesis, and analyzed by GC using the conditions appropriate to 9,10-di-n-octyl-n-octadecane. The column was able to resolve 4 components as sharp symmetrical peaks. Two peaks corresponding to 9,10-di-*n*-octyl-*n*-octadecane and 9,10-di-*n*-octyl-*n*-octadec-9-ene were identified by analysis of mixtures with the authentic compounds. There were also two other reaction intermediates generated in a ratio of approximately 2 : 1. Since these were generated within a few hours upon adding the acid to the solution, whereas the subsequent reduction was very slow, one can deduce that they were both products of acid catalyzed isomerization of the original alkene. In view of the unique labelling of the final product alkane at the central carbon position, these intermediates were certainly the two isomeric alkenes (both 9,10-di-*n*-octyl-*n*-octadec-8-ene) indicated in the reaction scheme for the synthesis. Presumably the less sterically hindered "trans" conformation was the one present in greater amount.

A sample taken shortly after the reaction was begun was reduced under rotary evaporation, and analyzed by NMR. The carbon-13 spectrum showed a multiplicity of overlapping resonances, but the proton NMR spectrum (Fig. 2.2) supported the hypothesis of the identity of the two alkenes. At the high field end of the spectrum, one can see the usual alkyl methyl and methylene proton resonances of this type of molecule, and at around 2.0 ppm several poorly defined overlapping resonances attributable to the methylene and methine protons nearest to the double bonds.

However, the decisive factor was the well defined pair of triplet resonances at 5.02 and 5.17 ppm. (Shown magnified in the spectrum). The intensities appear in the ratio of about 2:1, correlating with the GC analysis of the mixture, if one supposes that the two triplets arise from the single **1z** proton in each of the two proposed isomers. (Fig. 2.3). The resonances are each split into a triplet by a ^3J coupling to the two nearest methylene protons on carbon atoms **1a**. This was confirmed when irradiation of the spectrum at around 2.0 ppm caused the simultaneous collapse of the multiplet structure in both resonances, just as one would expect. It was not possible to be sure by NMR alone which resonance belonged to which isomer, but assuming the

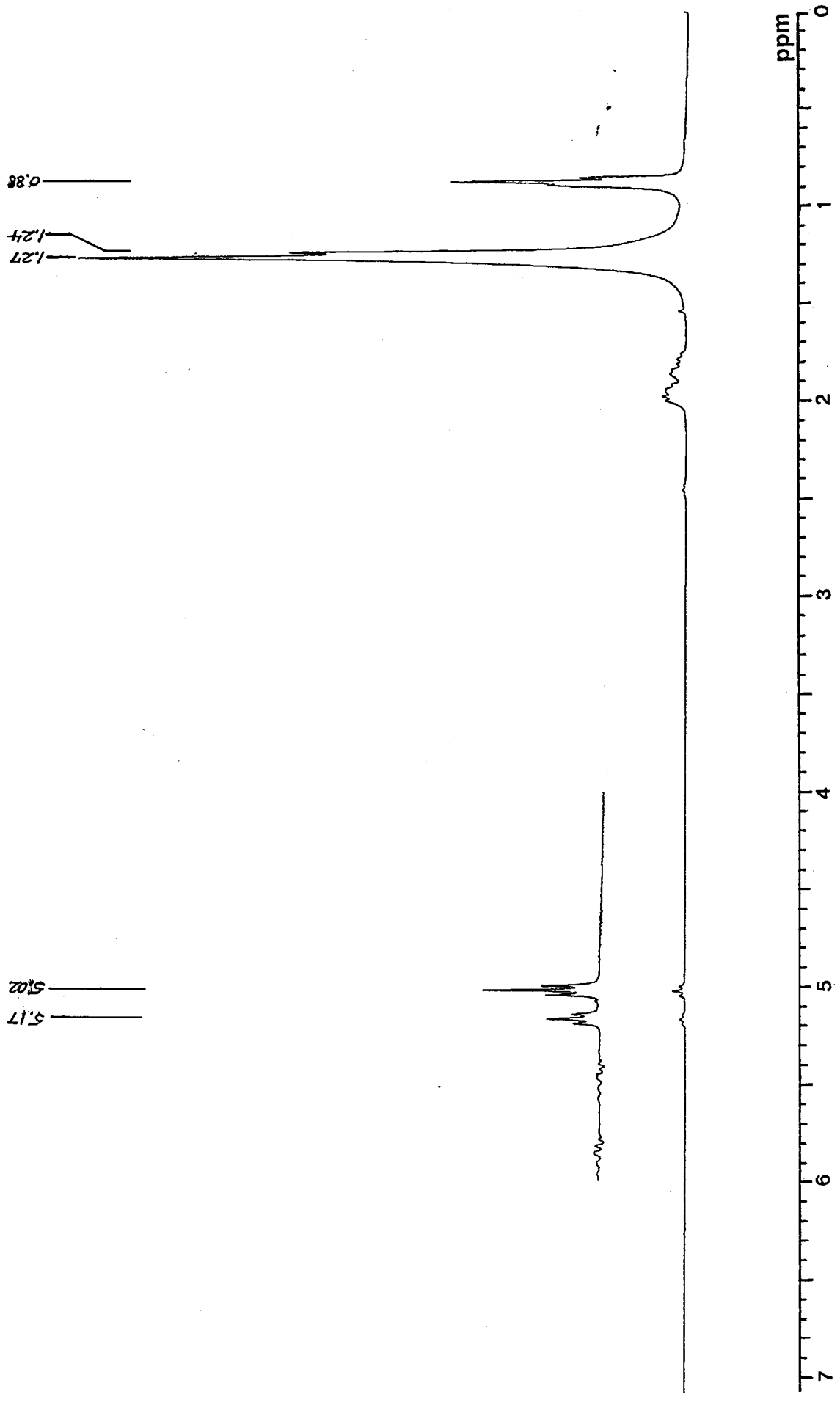

Fig 2.2: The 300 MHz proton spectrum of the non-volatile species present during the synthesis of 9,10-di-*n*-octyl-*n*-octadecane-9d_1.

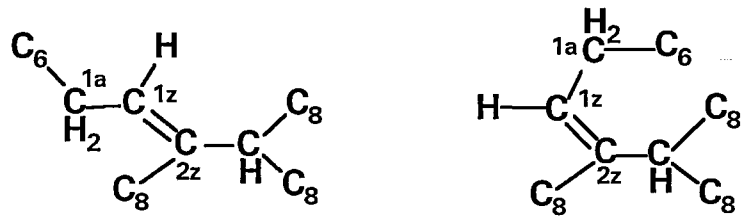

Trans Cis

Fig 2.3: The two isomers of 9,10-di-*n*-octyl-*n*-octadec-8-ene present during the synthesis of 9,10-di-*n*-octyl-*n*-octadecane-9d_1

correlation with the GC result, and that the "trans" isomer was the one present in greater amount, one can assign the resonance at 5.02 ppm to this isomer, and that at 5.17 ppm to the "cis" isomer.

In passing, it is worth noting that the actual reactive intermediates usually assumed to be reduced during this type of ionic reduction are the corresponding trifluoroacetate esters, resulting from direct addition to the double bond, rather than the bare carbonium centre that the simplified diagram suggests. However, in this case these must be present in only very tiny amounts at any moment as kinetic intermediates. The major path seemed to be via the isomerization observed, and the isomerized alkenes were unlikely to have been produced by decomposition of any ester when the samples were removed and analyzed; there was no indication of their presence in the proton spectrum.

These observations indicate the asymmetric position of the double bond to be the more stable one in this structure, and also indicate the relative degree of steric hindrance present in the two possible cis/trans isomers of the asymmetric alkene. Analysis by GC of suitable mixtures indicated that these same two isomeric alkenes were present as two of the impurities produced during the initial attempts to make 9,10-di-octyl-octadec-9-ene using the McMurry reaction. (Along with at least one other major component). Obviously one might expect this, with a prolonged period of refluxing under acidic conditions in the presence of a low valent transition metal. Transition metals are often used to produce such double bond shifts by co-ordination with the pi-electrons of unsaturated bonds[7].

An attempt to isolate 9,10-di-*n*-octyl-*n*-octadec-9-ene by vacuum distillation also caused isomerization. The crude product obtained by the improved method contained no more than 2% of isomers of 9,10-dioctyloctadec-9-ene according to GC analysis. During a simple distillation of this material at 0.1 mm Hg, a distillate was collected at a constant head temperature of 210 ^{0}C, which analysis by GC showed was now changed to a mixture of the required alkene, the two isomers found as above, plus traces of further components which were probably other isomers resulting from

further shifts of the double bond. Interestingly, the two main isomers were once again present in roughly the same ratio of 2:1. Presumably the original alkene rearranged itself continuously in the high temperature of the distillation pot, which was considerably in excess of 210 ^{0}C, distilling over as a constant boiling mixture of components. Traces of acid material or titanium from the coupling reaction may have catalyzed this, but a thermal rearrangement would probably occur in any case under these conditions; the mixture distilled as a noticeably yellow oil, which showed the thermal stress it was under.

It may be that this alkene could be purified by molecular distillation where a lower temperature would avoid any isomerization, but in any case the method actually used was completely satisfactory.

2.4 9-HEPTADECANONE

The syntheses of the compounds related to 9,10-di-*n*-octyl-*n*-octadecane required considerable quantities of 9-heptadecanone, and this was available commercially only at an inflated price. Therefore it was synthesized at moderate cost from nonanoic acid. The reaction used involved the thermal decarboxylation of ferrous nonanoate[10] and was very successful and reliable:

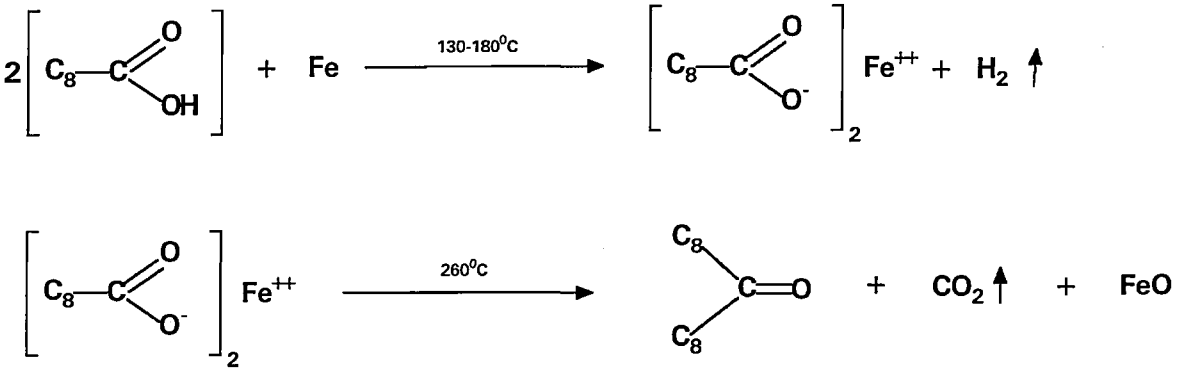

9-heptadecanone: Into a two neck 250 ml round bottomed flask, fitted with a reflux condenser and gas bubbler/inlet, were placed 100 g (633 mmol) of nonanoic acid and 17 g (316 mmol) of hydrogen-reduced iron powder. A thermometer was fitted into the side neck so as to dip into the reaction mixture, and a nitrogen atmosphere established via the bubbler. The nitrogen flow helped to maintain an inert atmosphere, while at the same time allowing for irregular evolutions of gas from the reaction. The flask was then heated to 130 ^{0}C, at which point evolution of hydrogen commenced. The reaction was held at 180 ^{0}C for 1½ hours until the release of hydrogen had slowed to almost nil, and the flask contained the molten green ferrous nonanoate. This was now heated slowly to 260 ^{0}C, when a vigorous release of carbon dioxide began. Heating was

continued for about 1 hour until decarboxylation was complete.The flask was then set for downward distillation through a well lagged simple angled take-off and air condenser, and the crude product distilled out from the flask at over 250 ^{0}C. It was advisable to stir the mixture cautiously through the side neck of the the flask as it was heated towards its boiling point, otherwise the collection of sedimented iron residues could cause a sudden erruption of the contents instead of gentle boiling. The ketone was recrystallized from 400 ml of ethanol/water. (m.p.50.5-51.5 °C). Purity by GC analysis was >99%, and the retention time was identical with that of an authentic sample. The proton NMR spectrum was also identical. Yields: 65-75 g, 80-90% of theoretical.■

2.5 TRIETHYLSILANE-d_1

The labelled silane required for the synthesis of 9,10-di-*n*-octyl-*n*-octadecane-$9d_1$ was economically synthesized by reducing chlorotriethylsilane under reflux in ether with the stoichiometric quantity of lithium aluminium deuteride powder[11]:

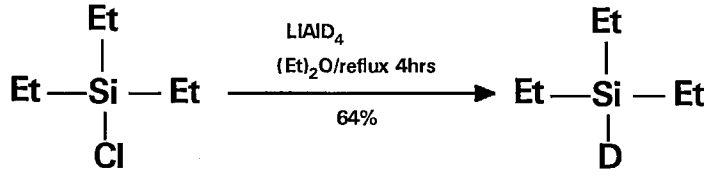

Triethylsilane-d_1: Glassware was oven dried before use. Into a 500 ml two neck round bottom flask, fitted with a reflux condenser, gas bubbler/inlet, dropping funnel and magnetic stirring, was placed a suspension of 4 g (95 mmol) of fresh lithium aluminium deuteride powder in 220 ml of sodium-dried ether, and an inert atmosphere of dry nitrogen estblished via the gas inlet. The dropping funnel was carefully filled with 50 g (330 mmol) of chlorotriethylsilane (the liquid could be transfered by pouring carefully), and sealed under positive nitrogen pressure, using a septum and flushing needle. With cooling in a bath of cold oil, the chlorotriethylsilane was added at a slow rate to the stirred suspension of deuteride during about 5 minutes. The oil bath was heated slowly, and the reaction brought to reflux for 4 hours. Any remaining unreacted deuteride was then destroyed by the cautious addition of first moist ether, then water, and finally sufficient dilute sulphuric acid to dissolve the precipitated salts. The flask was cooled as required. The aqueous layer was separated, and extracted three times with ether. The combined ether layers were washed with water, twice with brine and finally dried over anhydrous sodium sulphate. After filtration, the ether was removed by careful distillation, and the crude product itself distilled through a 5 cm

column of glass helices to give 24.6 g of triethylsilane-d_1 as a water white liquid, boiling at 107/109 ^{0}C. Yield: 64%. The IR spectrum taken as a liquid film showed the presence of the Si-D bond absorption (stretching frequency) at 1550 cm^{-1}, and the absence of any Si-H bond absorption at 2100 cm^{-1}. Although the lithium aluminium deuteride used was nominally only of 98% isotopic purity, the reduced silane appeared from the IR spectrum and subsequent use to be practically 100% labelled. One can surmise that the formation of a Si-D bond may be favoured energetically compared with the formation of a Si-H bond during this reduction.■

Triethylsilane-d_1 was also used as the source of deuterons in reactions described in Chapters 3 and 4 for the syntheses of 9-*n*-octyl-*n*-heptadecane-9d_1 and tricyclohexylmethane-d_1

REFERENCES FOR CHAPTER 2

[1] T. Mukaiyama, T. Sato, and J. Hanna, *Chemistry Letters*, 1973, 1041; J. E. McMurry, *Acc. Chem. Res.*, 1974, 7, 283; A. Ishida and T. Mukaiyama, *Chemistry Letters*, 1976, 1127; D. Lenoir, *Synthesis*, 1977, 553; J. E. McMurry, M. P. Fleming, K. L. Kees, and L. R. Krepski, *J. Org. Chem.*, 1978, **43**, 3255; J. E. McMurry, *Acc. Chem. Res.*, 1983, **16**, 405; D.Lenoir, *Synthesis*, 1989, 883.

[2] R. Dams, M. Malinowski, I. Westdorp, and H. Y. Geise, *J. Org. Chem.*, 1982, **47**, 248

[3] J. E. McMurry, T. Lectka, and J. G. Rico, *J. Org. Chem.*, 1989, **54**, 3748

[4] H. Ledon, I. Tkatchenko, and D. Young, *Tet. Lett.*, 1979, **2**, 173.

[5] M. T. Anthony, M. L. H. Green, and D. Young, *J. Chem. Soc., Dalton Transactions*, 1975, 1419

[6] J. Leimer and P. Weyerstahl, *Chem. Ber.*, 1982, **115**, 3697

[7] J. March, *Advanced Organic Chemistry*, Wiley

[8] R. R. Schrock and J. A. Osborn, *J. Am. Chem.Soc.*, 1976, **98** , 2134 and 2143; M. D. Fryzuk, and B. Bosnich, *J. Am. Chem. Soc.*, 1977, **99**, 6262; J. M. Brown and R. G. Naik, *J. Chem. Soc., Chem. Commun.*, 1982, 348; T. Hayashi, N. Kawamura, and Y. Ito, *J. Am. Chem. Soc.*, 1987, **109**, 7876.

[9] D. N. Kursanov, Z. N. Parnes, and N. M. Loim, *Synthesis*, September 1974, 633; F. A. Carey, and H. S. Tremper, *J. Org. Chem.*, 1971, **36**, 758

[10] R. Davis, C. Granito, and H. P. Schultz, *Organic Syntheses*, Coll. Vol. **V**, 589; R. Davis, and H. P. Schultz, *J. Org. Chem.*, 1962, **27**, 854

[11] M. P. Doyle, C. C. McOsker, and C. T. West, *J. Org. Chem.*, 1976, **41**, 1393

NMR SPECTRA

9,10-DI-*n*-OCTYL-*n*-OCTADEC-9-ENE

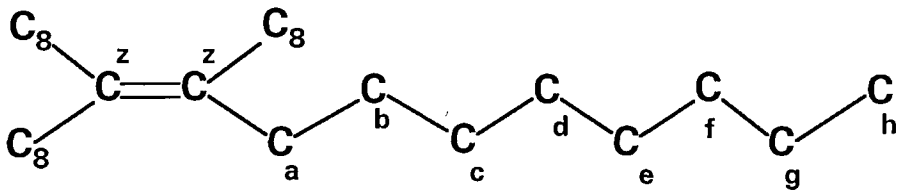

Spectrum 2.1 shows the completely proton decoupled carbon-13 resonances of 9,10-di-*n*-octyl-*n*-octadec-9-ene. The two central carbons **z** appear strongly shifted downfield at 133.444 ppm. The four methyl groups **h** appear at 14.129 ppm, and the four nearest methylene carbons, **g**, appear at 22.771 ppm, while the remaining seven equivalent sets of methylene carbons of the *n*-octyl chains are revealed as individual resonances in the expansion, Spectrum 2.2. Spectrum 2.3 is a proton decoupled carbon-13 SEFT spectrum of this alkene, with delay τ = 8 ms, thereby allowing phase sensitive detection of the various carbon resonances. The methylene groups and the two central carbons **z** appear with normal phase, while the single resonance of the four methyl groups **h** appears with inverted phase.

Spectrum 2.4 is the proton spectrum of the alkene, which shows some distinguishing features. An expansion appears in Spectrum 2.5. The triplet methyl resonances appear at 0.88 ppm, and at 1.27 ppm the large resonance of the methylene protons on carbons **b** to **g**. The eight methylene protons on carbons **a** appear as a broadened triplet feature centred at 1.94 ppm. The three peak integrals obtained for this spectrum were in almost the exact ratio expected for this structure.

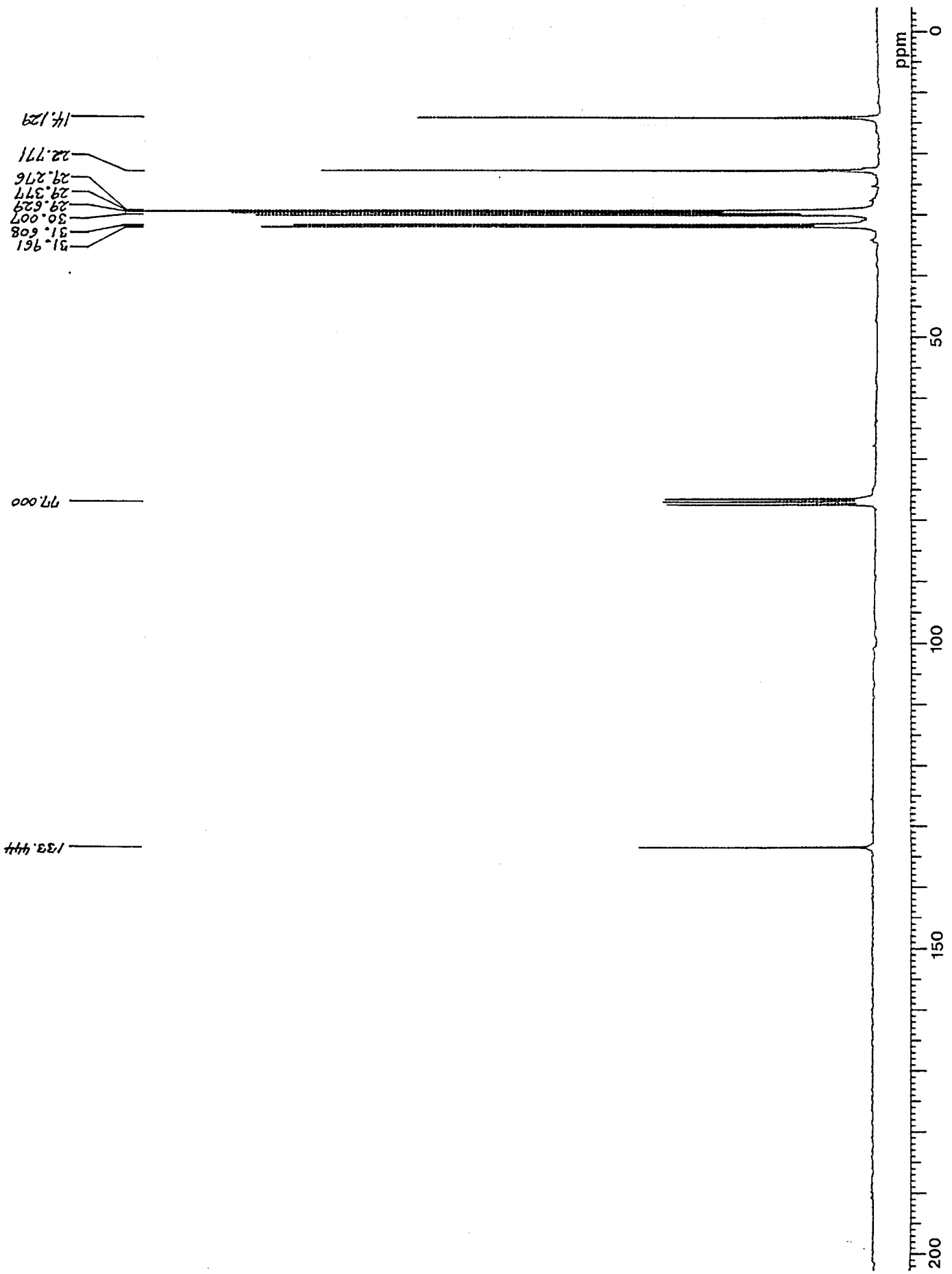

2.1: The 67.83 MHz proton decoupled carbon-13 spectrum of 9,10-di-*n*-octyl-*n*-octadec-9-ene.

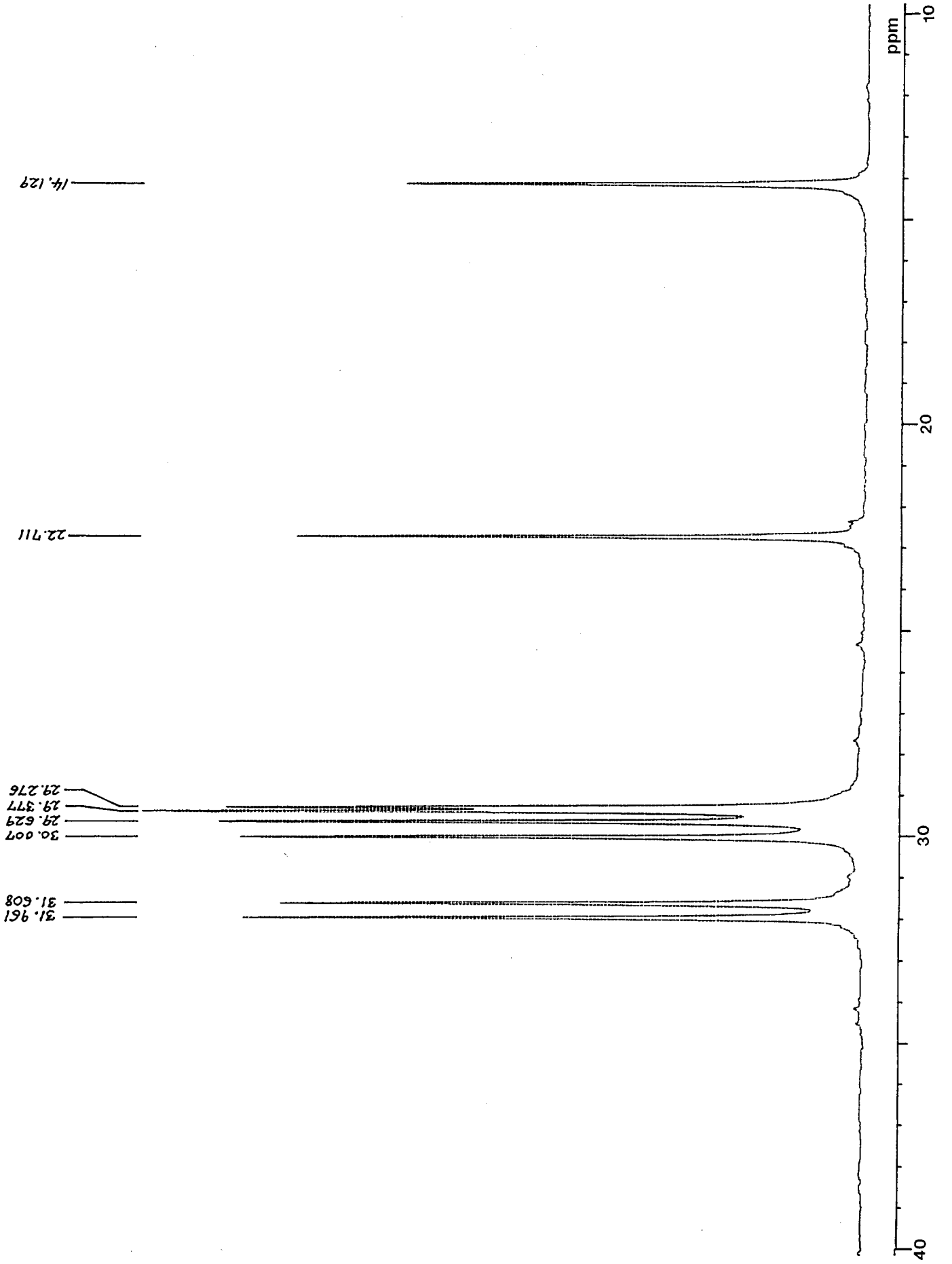

2.2: The 67.83 MHz proton decoupled carbon-13 spectrum of 9,10-di-*n*-octyl-*n*-octadec-9-ene (expansion).

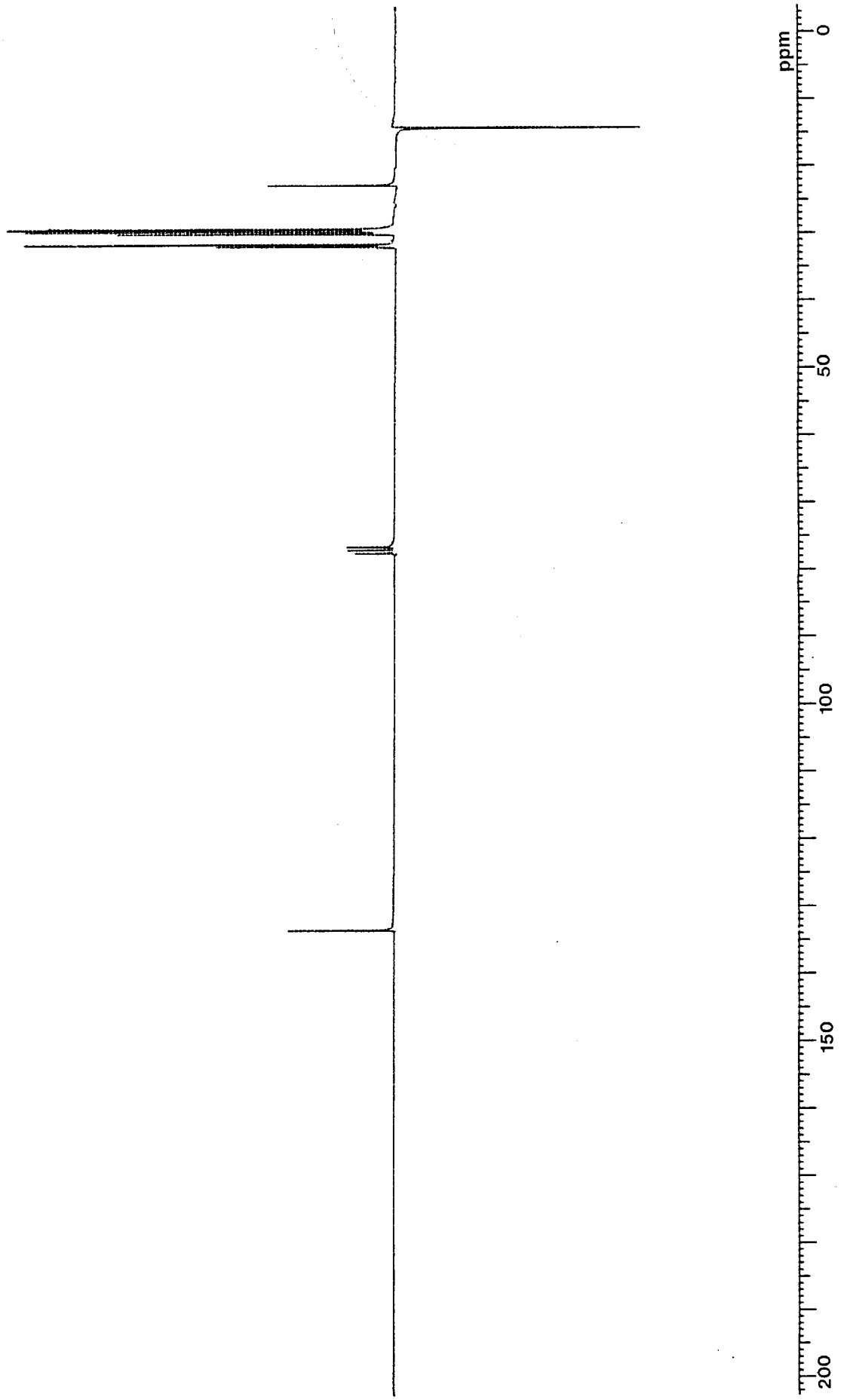

2.3: The 67.83 MHz proton decoupled SEFT spectrum of 9,10-di-*n*-octyl-*n*-octadec-9-ene.

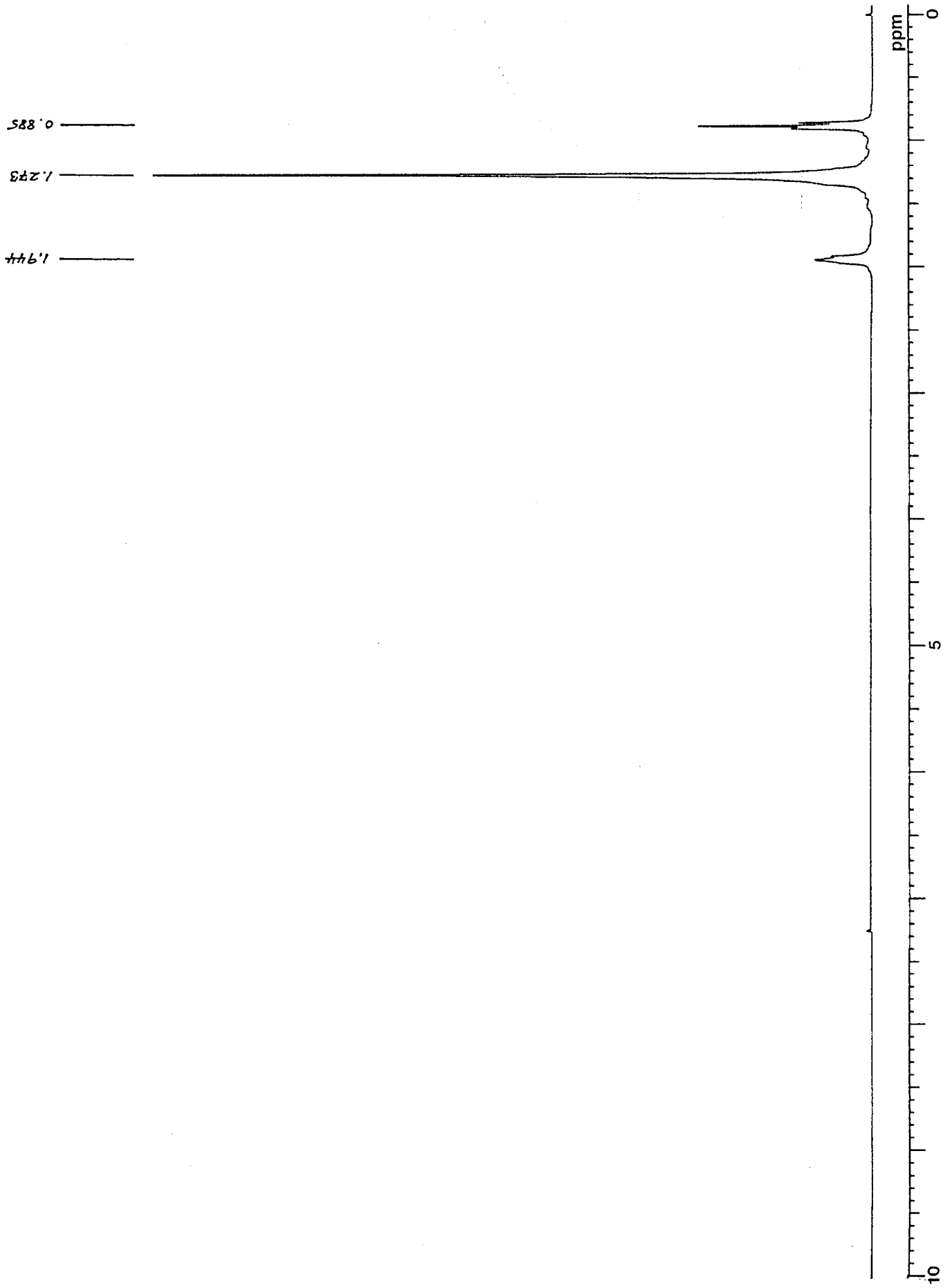

2.4: The 269.7 MHz proton spectrum of 9,10-di-*n*-octyl-*n*-octadec-9-ene.

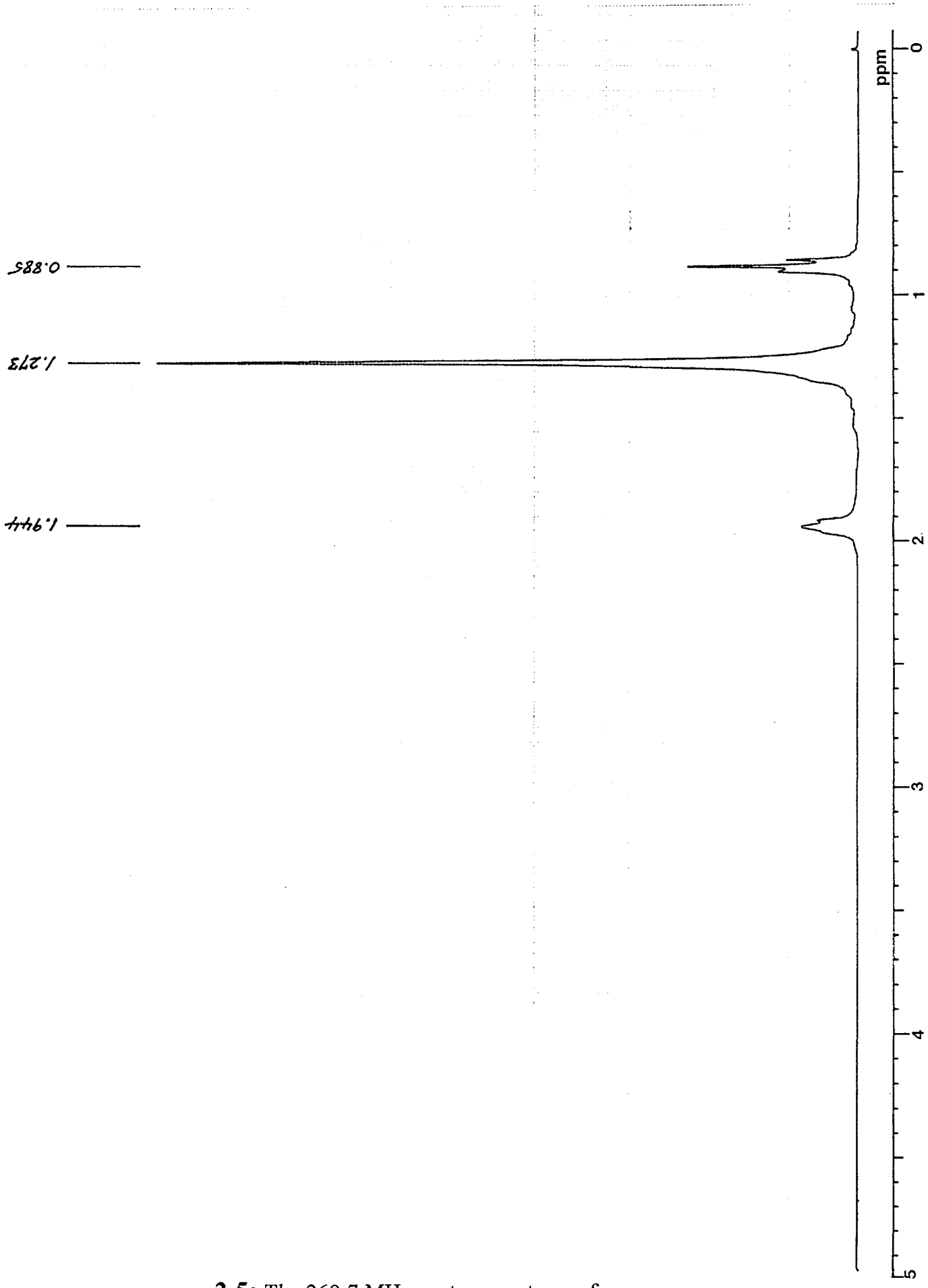

2.5: The 269.7 MHz proton spectrum of 9,10-di-*n*-octyl-*n*-octadec-9-ene (expansion).

9,10-DI-*n*-OCTYL-*n*-OCTADECANE AND 9,10-DI-*n*-OCTYL-*n*-OCTADECANE-9d_1

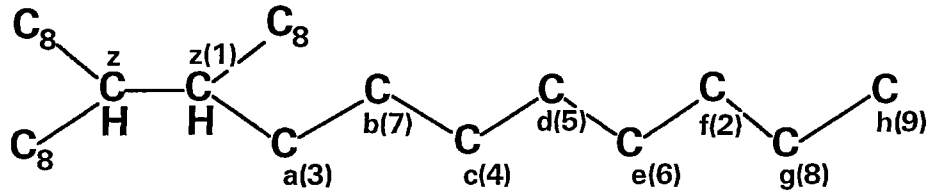

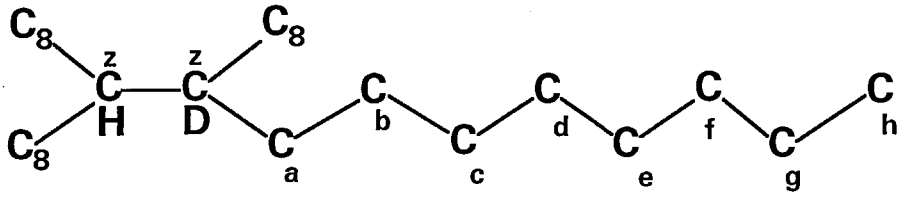

Spectrum 2.6 shows the completely proton decoupled carbon-13 resonances of 9,10-di-*n*-octyl-*n*-octadecane. The two central carbons **z** appear at 39.496 ppm, the four methyl groups **h** at 14.116 ppm, and the seven equivalent sets of methylene carbons of the *n*-octyl chains are spread out in between. The off-resonance decoupled spectrum, 2.7, confirms this, wherein the resonances are identified by their multiplicities.

Spectrum 2.8 shows the completely decoupled spectrum of the corresponding isotopomer, 9,10-di-*n*-octyl-*n*-octadecane-9d_1. At 39.421 ppm can be seen the resonance of the one remaining protonated carbon atom **z**, while next to it, at slightly higher field appears the small coupled triplet of the adjoining deuterated **z** carbon atom. These features are expanded in Spectrum 2.9, where there can now be seen the splitting of the resonance near 30.66 ppm, due to unequal deuteration shifts in the *n*-octyl chains on either side of the deuterated carbon centre. From this one can assign the resonance at 30.675 ppm in Spectrum 2.6, to the four carbon atoms **a**. A further expansion, Spectrum 2.10, shows the broadening of the resonance at 28.167 ppm, again caused by unequal, but much smaller, deuteration shifts in the *n*-octyl chains. This allows one to conclude that the resonance at 28.167 ppm in Spectrum 2.6 belongs to the four carbon atoms **b**. One can also assign the resonance at 22.711 ppm to the four **g** carbon atoms.

The remaining carbon atom resonances in the octyl chains can be assigned with the help of the T_1 data that were later acquired. Assuming that the longitudinal relaxation times will increase with increasing mobility as one moves further towards the methyl ends of the chains, and choosing a frequency and temperature combination (for example, 68.83 MHz and 40 ^{0}C) at which this association of the resonances agrees for the assignments that have already been deduced as above, leads to the

assignment of the three remaining positions; **c**, 30.121 ppm; **d**, 29.692 ppm; **e**, 29.390 ppm; **f**, 31.961 ppm.

The carbon atoms are also numbered in the order in which their resonances appear in the standard spectrum, starting from the low field end.

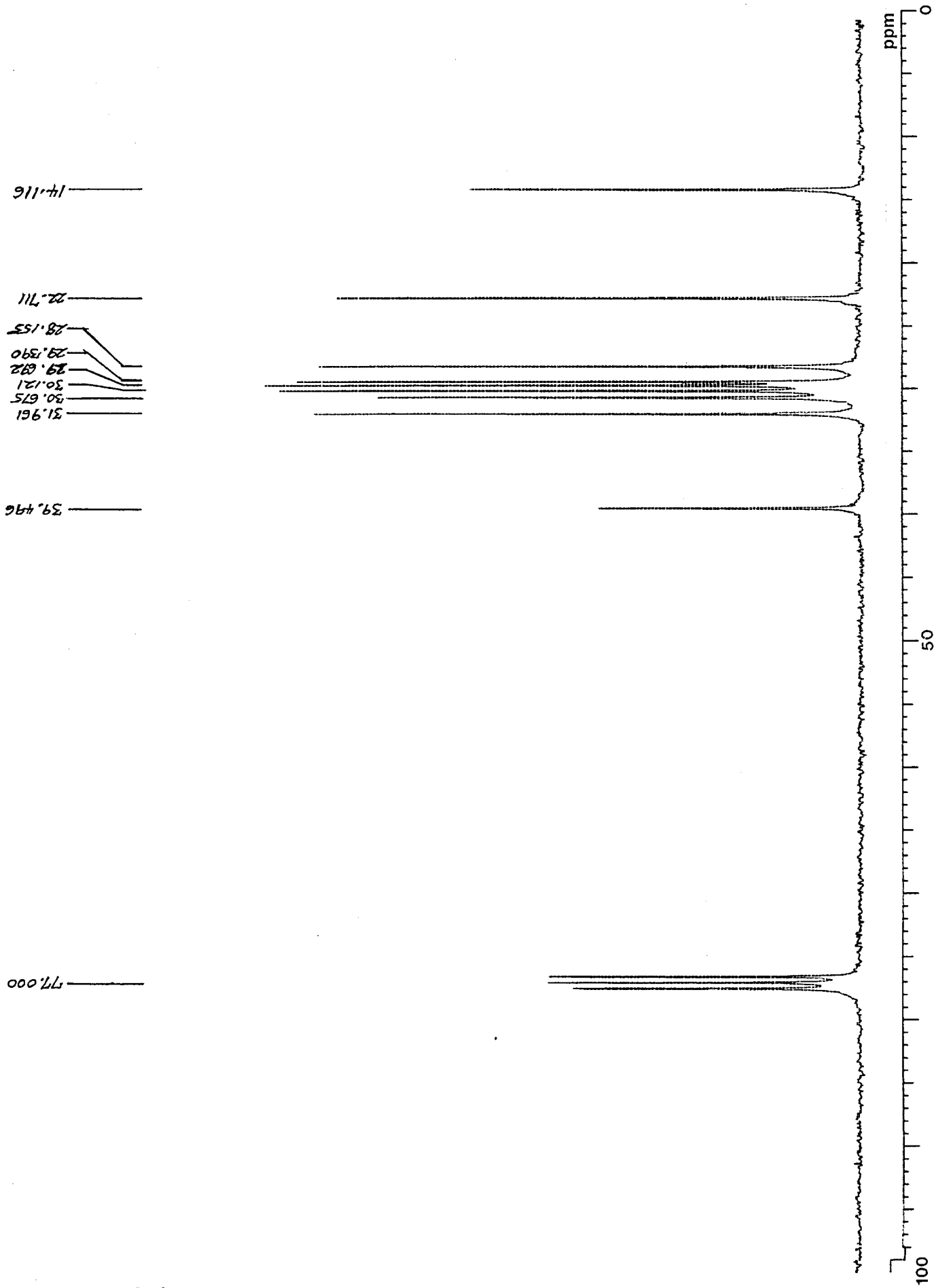

2.6: The 67.83 MHz proton decoupled carbon-13 spectrum of 9,10-di-*n*-octyl-*n*-octadecane.

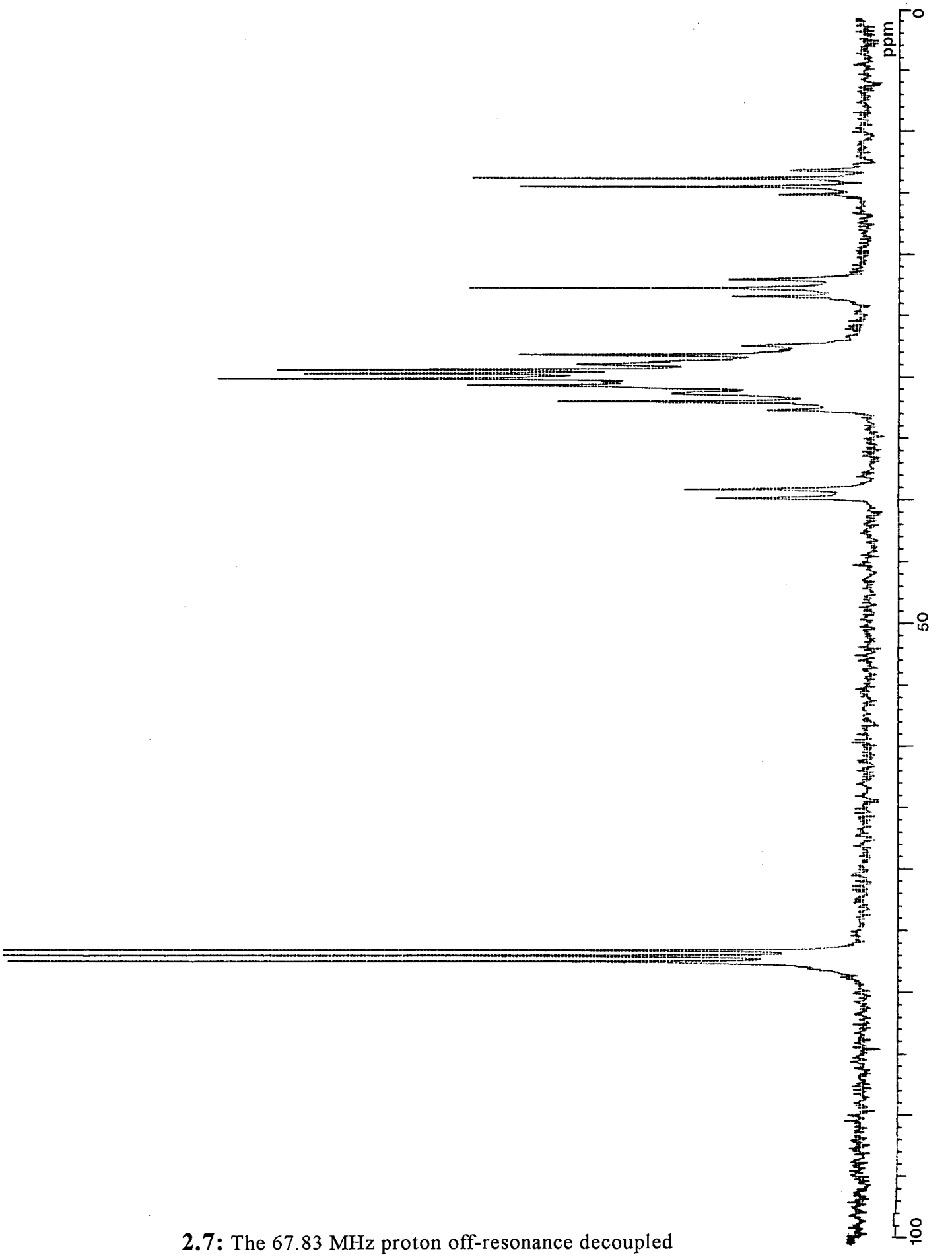

2.7: The 67.83 MHz proton off-resonance decoupled carbon-13 spectrum of 9,10-di-*n*-octyl-*n*-octadecane.

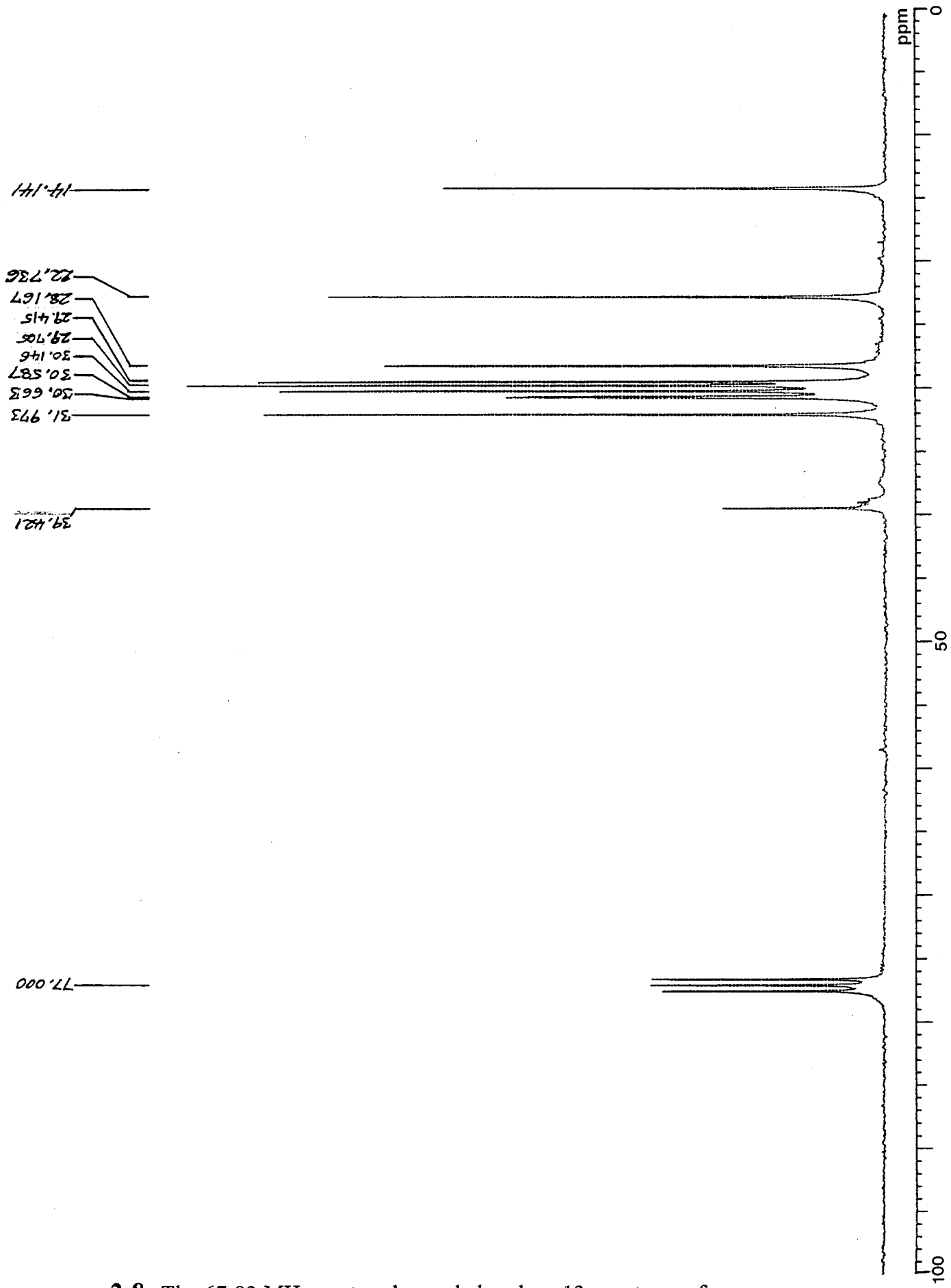

2.8: The 67.83 MHz proton decoupled carbon-13 spectrum of 9,10-di-*n*-octyl-*n*-octadecane-9d$_1$.

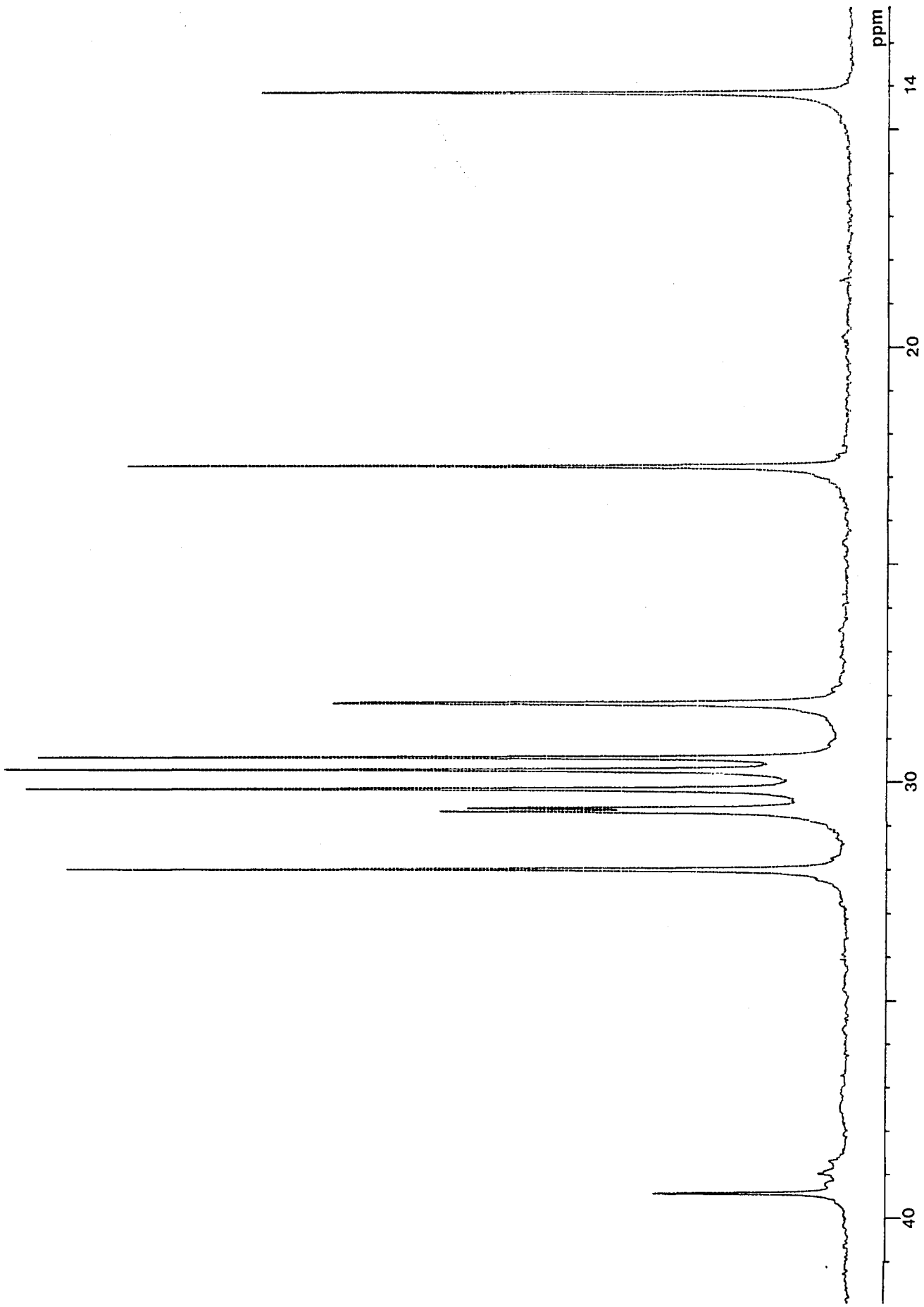

2.9: The 67.83 MHz proton decoupled carbon-13 spectrum of 9,10-di-*n*-octyl-*n*-octadecane-9d_1 (expansion).

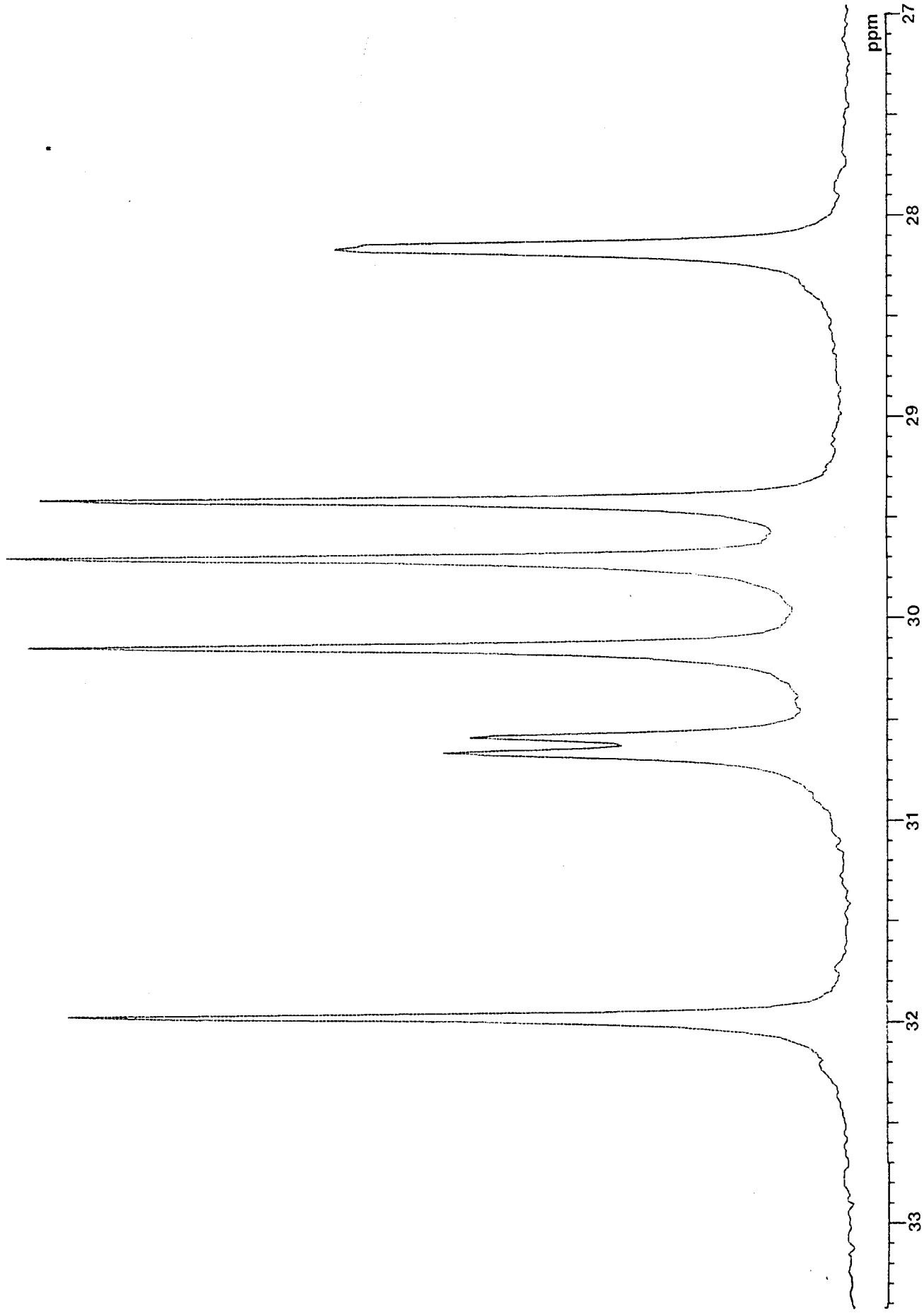

2.10: The 67.83 MHz proton decoupled carbon-13 spectrum of 9,10-di-*n*-octyl-*n*-octadecane-9d_1 (expansion).

Chapter 3

SYNTHESES RELATED TO 9-*n*-OCTYL-*n*-HEPTADECANE

3.1 9-*n*-OCTYL-*n*-HEPTADECANE

The alkane 9-*n*-octyl-*n*-heptadecane has been reported previously by Challenger and Pantony, and the synthesis described there was followed[1]. This involved the catalytic dehydration of 9-*n*-octyl-*n*-heptadecan-9-ol by refluxing in the presence of iodine to give 9-*n*-octyl-*n*-hepatdec-8-ene, and the catalytic hydrogenation of this to give the required alkane. Fractional distillations under vacuum were used to obtain a pure sample of this material. A standard Grignard reaction between *n*-octyl magnesium bromide and diethyl carbonate, using the procedure of Moyer and Marvel[2], gave the tertiary alcohol 9-*n*-octyl-*n*-heptadecan-9-ol:

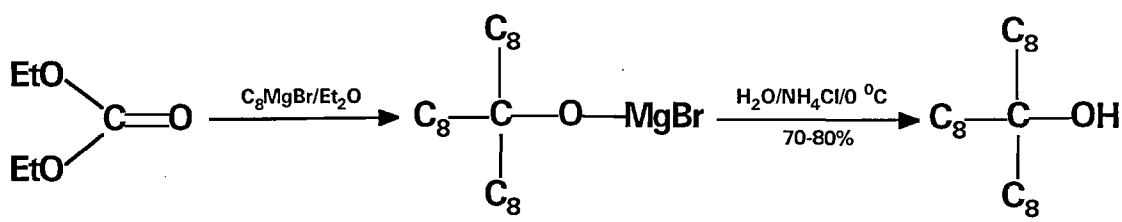

9-*n*-octyl-*n*-heptadecan-9-ol: Glassware was oven dried before use. Into a three-necked 1 l flask, fitted with magnetic stirring, a double coil condenser, a 250 ml addition funnel (protected with a drying tube), a septum inlet and a gas bubbler/inlet, were placed 13.5 g (550 mmol) of magnesium turnings and 100 ml of dry ether. The apparatus was closed, an atmosphere of dry nitrogen established, and 5 ml of *n*-octyl bromide injected into the flask. After about 10 minutes of gentle warming the reaction commenced. At this point stirring was started and a solution of 106 g (550 mmol) of *n*-octyl bromide in 125 ml of dry ether added as rapidly as the refluxing of the ether would allow. After addition was complete the flask was warmed in a water bath for 30 minutes to complete the reaction.

A solution of 18.5 g (167 mmol) of diethyl carbonate in 23 ml of dry ether was then added slowly to the Grignard reagent with rapid stirring. The reaction was vigorous and addition required about 45 minutes. A slightly higher yield was obtained, at the cost of extending the time required for the synthesis, by adding the diethyl carbonate at such a rate that the reaction did not reflux, remaining only slightly above room temperature. After the addition was complete the flask was heated in a water bath for a further 1 hour.

The reaction mixture was hydrolyzed by pouring it, with frequent shaking, into a 2 l conical flask containing 125 ml of saturated ammonium chloride solution and 250 g of crushed ice. The ether layer was separated and the aqueous layer extracted twice with ether. (The ether used to extract the aqueous layer could be obtained by distilling the ether from the first separated layer). The combined ethereal solutions were then washed well with water and dried with brine. Removal of the ether by distillation and rotary evaporation gave around 65 g of crude tri-n-octyl carbinol as a viscous oil, which contained 70-80 % by weight of the required alcohol, by GC analysis; a yield overall of 70-80% based on the diethyl carbonate used.

The product could be dried by standing over anhydrous potassium carbonate, which also gradually removed the yellow colour present.■

It was possible to isolate an analytical sample of 9-*n*-octyl-*n*-heptadecan-9-ol by chromatography over silica gel, eluting with pentane/chloroform, followed by short path distillation to remove the remaining volatile impurities, in the manner used to purify 9,10-di-*n*-octyl-*n*-octadec-9-ene in Chapter 2. Purity by GC analysis was >99%, and the carbon-13 and proton NMR spectra of this alcohol agreed exactly with those expected, and are reproduced at the end of this chapter. However, for the synthesis of 9-*n*-octyl-*n*-heptadecane it was not necessary to isolate the pure alcohol.

The crude alcohol was dehydrated by refluxing it with a catalytic amount of iodine[3] in a fractional distillation apparatus, and the desired dehydrated product isolated by distilling it directly out of the reaction, followed by a further fractional distillation. One notes that because of the symmetrical structure of the alcohol only one possible dehydration product would be expected, namely 9-*n*-octyl-*n*-heptadec-8-ene. Despite being a tertiary alcohol, it was found that the reaction required several hours of heating to effectively complete the dehydration of all the 9-*n*-octyl-*n*-heptadecan-9-ol. The alcohol contaminated the required alkene if it was not effectively dehydrated before fractioning the product out of the flask:

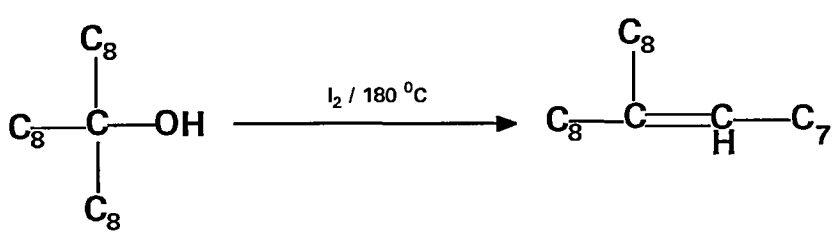

9-*n*-octyl-*n*-heptadec-8-ene: The standard fractionating apparatus described in Appendix 1 was assembled, using an electrically heated 35 cm x 1.7 cm column, filled with 4 mm glass Raschig rings. Into the boiler was placed 65 g of crude

9-*n*-octyl-*n*-heptadecan-9-ol, together with a few small iodine crystals. The column was also flooded with a part of this solution of the alcohol and iodine before beginning the reaction. The pressure was reduced to 0.2 mm Hg and the contents of the distillation pot brought to the boil. The mixture was then refluxed into the (unheated) fractionating column for 4 hours, after which time the column was gradually heated, the pressure reduced further and the product boiling at around 180 °C / 0.1 mm Hg collected. The important thing was to ensure that the iodine did not evaporate away before dehydration was complete, hence the usefulness of the unheated fractionating column.

The oil obtained was again fractionally distilled in the same apparatus, and 36.5g of colourless oil was obtained, boiling at 167-170 °C/0.07 mm Hg. A proton NMR spectrum of this oil agreed with the expected product of dehydration, 9-*n*-octyl-*n*-heptadec-8-ene, and purity by GC analysis was >99%.■

Catalytic hydrogenation of 9-*n*-octyl-*n*-heptadec-8-ene gave the desired alkane 9-*n*-octyl-*n*-heptadecane:

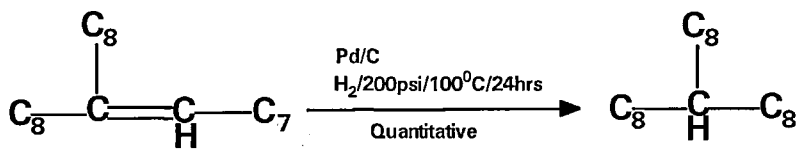

9-*n*-octyl-*n*-heptadecane: 9-*n*-octyl-*n*-heptadec-8-ene (36.5 g) was dissolved in 100 ml of a 50/50 mixture of cyclohexane and glacial acetic acid and hydrogenated for 24 hours at 200 psi and 80 °C over 2g of 5% palladium-on-carbon, with magnetic stirring. After removal of the catalyst and volatile solvents there was obtained 36g of colourless oil. This was fractionated under vacuum through a 35 x 1.7 cm heated column of 4 mm Raschig rings, to give 33 g of colourless oil boiling at 159/161 °C / 0.1 mm Hg. Proton and carbon-13 NMR agreed exactly with the desired product, 9-octyl-heptadecane. Purity by GC analysis was >99%.■

3.2 9-*n*-OCTYL-*n*-HEPTADECANE-9d$_1$

The same reaction[4] that had been applied to synthesize 9,10-di-*n*-octyl-*n*-octadecane-9d$_1$ was used to synthesize the isotopomer 9-*n*-octyl-*n*-heptadecane-9d$_1$. All that was required was to replace the substrate with the appropriate alkene, 9-*n*-octyl-*n*-heptadec-8-ene, obtained as described above by the dehydration of 9-*n*-octyl-*n*-heptadecan-9-ol:

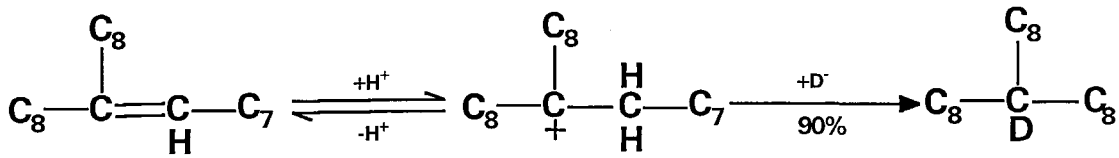

9-*n*-octyl-*n*-heptadecane-9d$_1$: Into a dry 100 ml round bottom flask, fitted with a septum inlet protected by a stop cock, and a PTFE coated magnetic stirrer bar, was placed a solution of 5 g (14.3 mmol) of 9-*n*-octyl-*n*-heptadec-8-ene and 2.0 g (17.1 mmol) of triethylsilane-d$_1$ in 25 ml of AR dichloromethane. Using a glass syringe, 7.0 g of trifluoroacetic acid were then carefully injected into the flask, the stopcock was closed, and the reaction stirred at room temperature for 7 days.

At the end of this time, the septum inlet and stopcock were replaced with a reflux condenser, 5 ml each of ether and water added to the mixture, and the reaction carefully neutralized by the addition of solid sodium carbonate. The organic layer was separated and the aqueous layer extracted with ether. The combined organic solutions were then washed well with water, twice with brine, and dried by standing over anhydrous sodium sulphate.

The crude product from the reaction was purified by elution through a column of silica gel, and short path distillation at 0.1 mm Hg / 100 ^{0}C, in the manner described in Chapter 2 for 9,10-di-*n*-octyl-*n*-octadec-9-ene, to obtain 4.2 g of water white oil. It would probably have been possible to isolate the deuterated product by fractional distillation in this case, but it was decided not to take the least risk of any exchange of the tertiary deuteron during the long period of high temperature refluxing required during such a distillation. Analyses by GC were identical to those of the ordinary hydrocarbon, and the indicated purity was >98 %. The carbon-13 NMR spectra agreed precisely with those expected for the compound, and demonstrated the site specific incorporation of the deuterons at the centres of the molecules.■

REFERENCES FOR CHAPTER 3

1 F.Challenger and D.A.Pantony, *J. Inst. Ptrlm.*, 1954, **40**, 37

2 W.W.Moyer and C.S.Marvel, *Organic Syntheses*, Coll. Vol. **II**, 602

3 For reactions using iodine to dehydrate tertiary alcohols see: H. Hibbert, *J. Am. Chem. Soc.*, 1915, **37**, 1748; F. C. Whitmore and H. M. Woodburn, *J. Am. Chem. Soc.*, 1933, **55**, 361; F. C. Whitmore and F. E. Williams, *J. Am. Chem. Soc.*, 1933, **55**, 406; J. M. Church, F. C. Whitmore, and R. V. McGrew, *J. Am. Chem. Soc.*, 1934, **56**, 176; A. C. Cope and S. W. Fenton, *J. Am. Chem. Soc.*, 1951, **73**, 1673; A. C. Cope and H. C. Campbell, *J. Am. Chem. Soc.*, 1952, **74**, 179

[4] D. N. Kursanov, Z. N. Parnes, and N. M. Loim, *Synthesis*, September 1974, 633; F. A. Carey and H. S. Tremper, *J. Org. Chem.*, 1971, **36**, 758

NMR SPECTRA

9-*n*-OCTYL-*n*-HEPTADECAN-9-OL AND 9-*n*-OCTYL-*n*-HEPTADEC-9-ENE

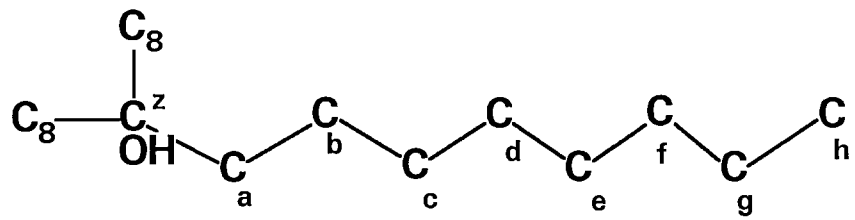

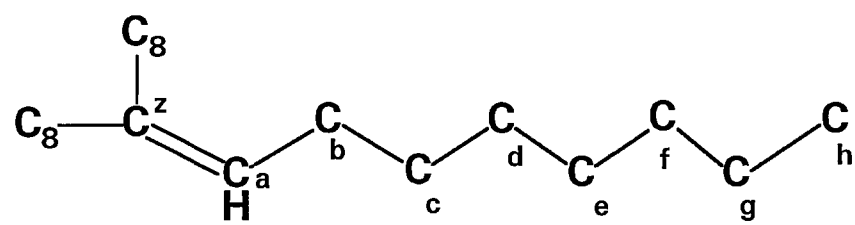

Spectrum 3.1 shows the completely proton decoupled carbon-13 resonances of 9-*n*-octyl-*n*-heptadecan-9-ol. The central carbon **z** appears at 74.429 ppm, the three methyl groups **h** at 14.091 ppm, and the seven equivalent sets of methylene carbons of the *n*-octyl chains are spread out in between. The resonance at 39.295 ppm can be assigned to carbon positions **a**, and one can assign the resonances at 22.686 ppm to the three carbon atoms **g**. The off-resonance decoupled spectrum, 3.2, confirms this, wherein the resonances are identified by their multiplicities.

Spectrum 3.3 is the proton spectrum of this alcohol, and it is just possible to discern some separation of the methylene protons at 1.270 and 1.374 ppm, while the methyl groups appear at 0.877 ppm.

Spectrum 3.4 is the proton spectrum of the product of dehydration of this alcohol, 9-*n*-octyl-*n*-heptadec-8-ene. The methyl groups appear at 0.88 ppm, and the methylene groups in positions **c** to **g** as the broad feature at 1.27 ppm. The three methylene groups proximal to the double bond appear at 1.94 ppm, as a rather indistinct multiplet, while the sole ethylenic proton, **a**, appears as a well defined triplet at 5.08 ppm, coupled to two methylene protons in the **b** position on the closest octyl chain. The constant is the usual one of about 6 Hz.

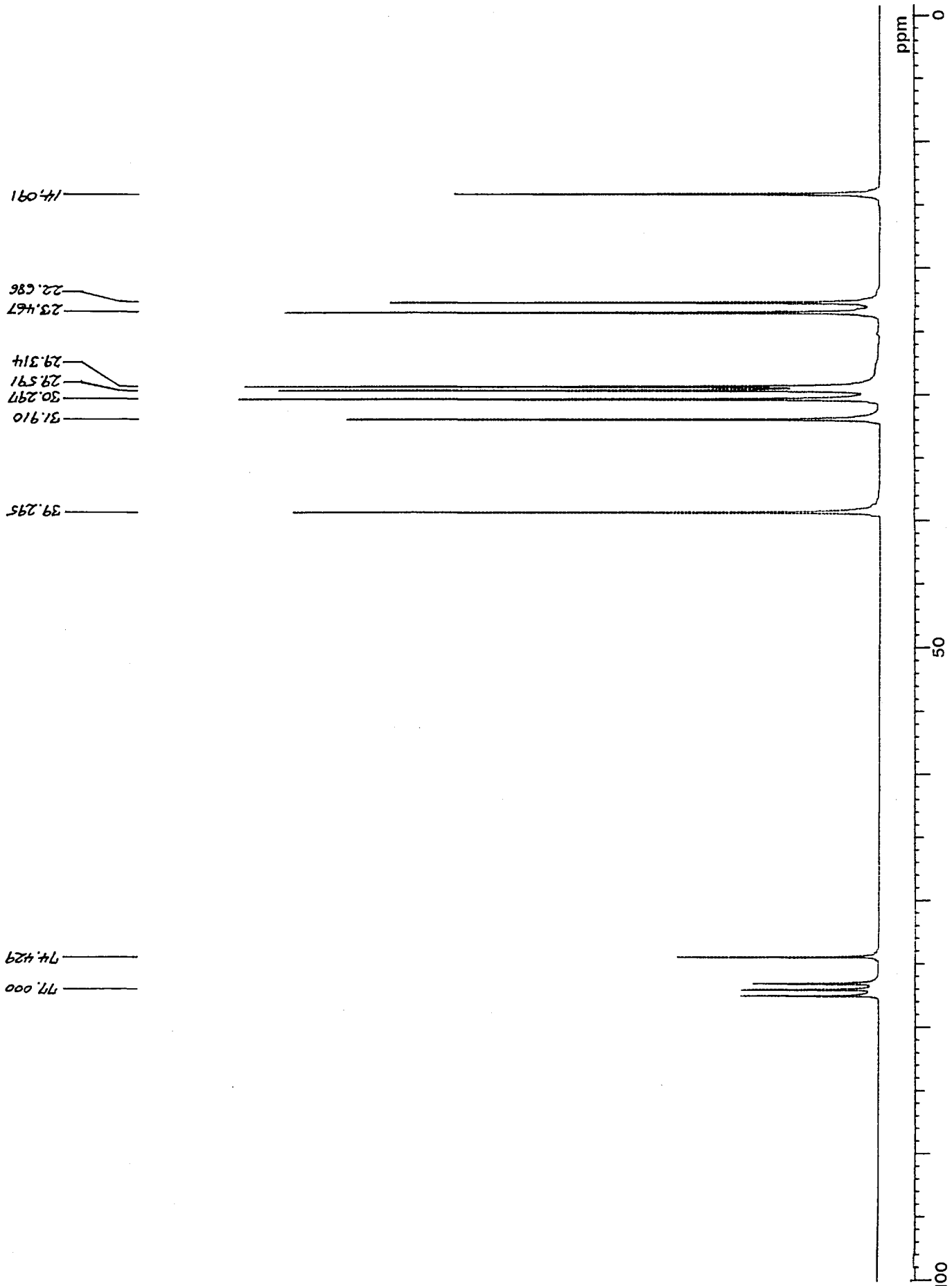

3.1: The 67.83 MHz proton decoupled carbon-13 spectrum of 9-*n*-octyl-*n*-heptadecan-9-ol.

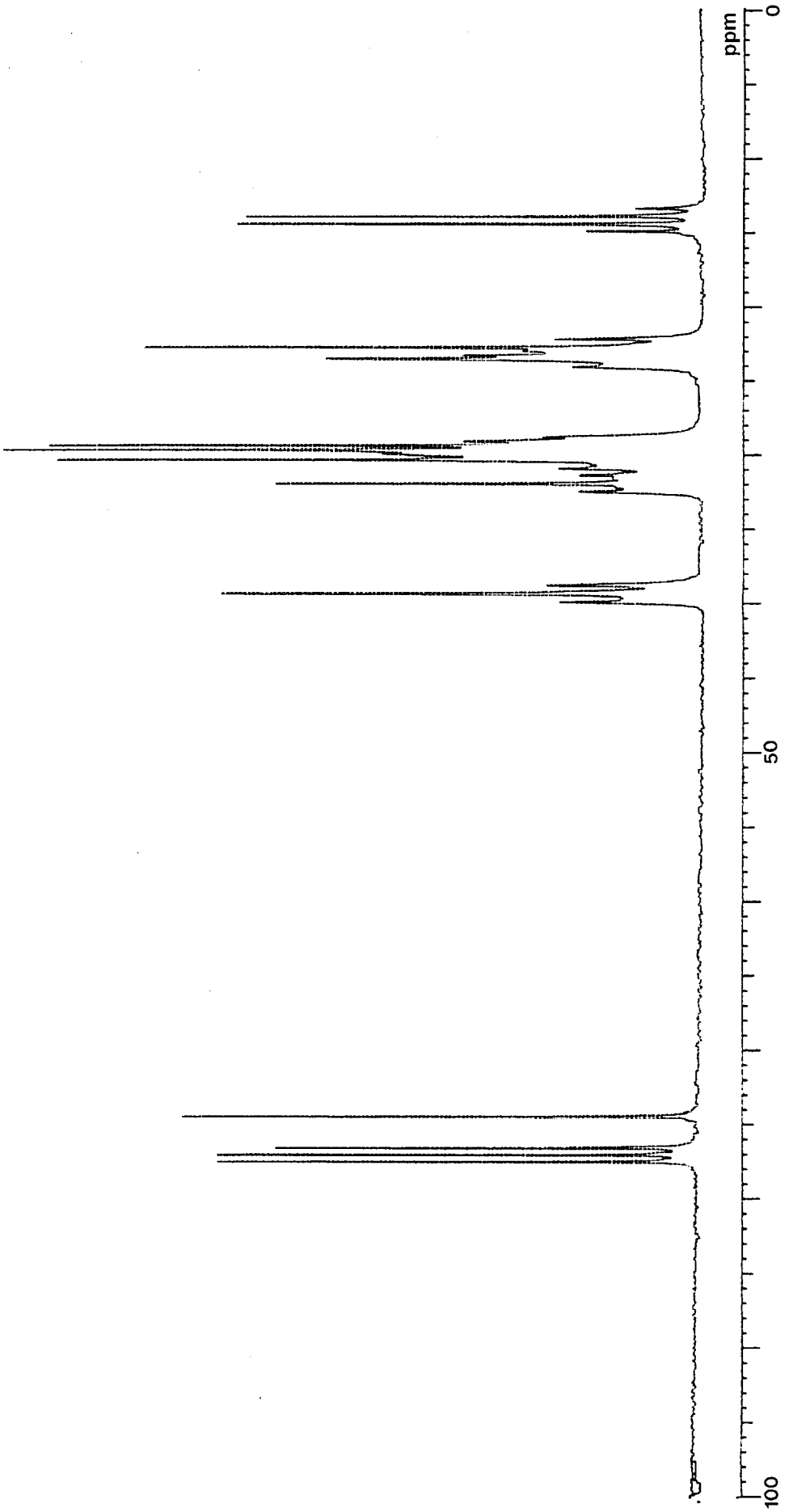

3.2: The 67.83 MHz off-resonance decoupled carbon-13 spectrum of 9-*n*-octyl-*n*-heptadecan-9-ol.

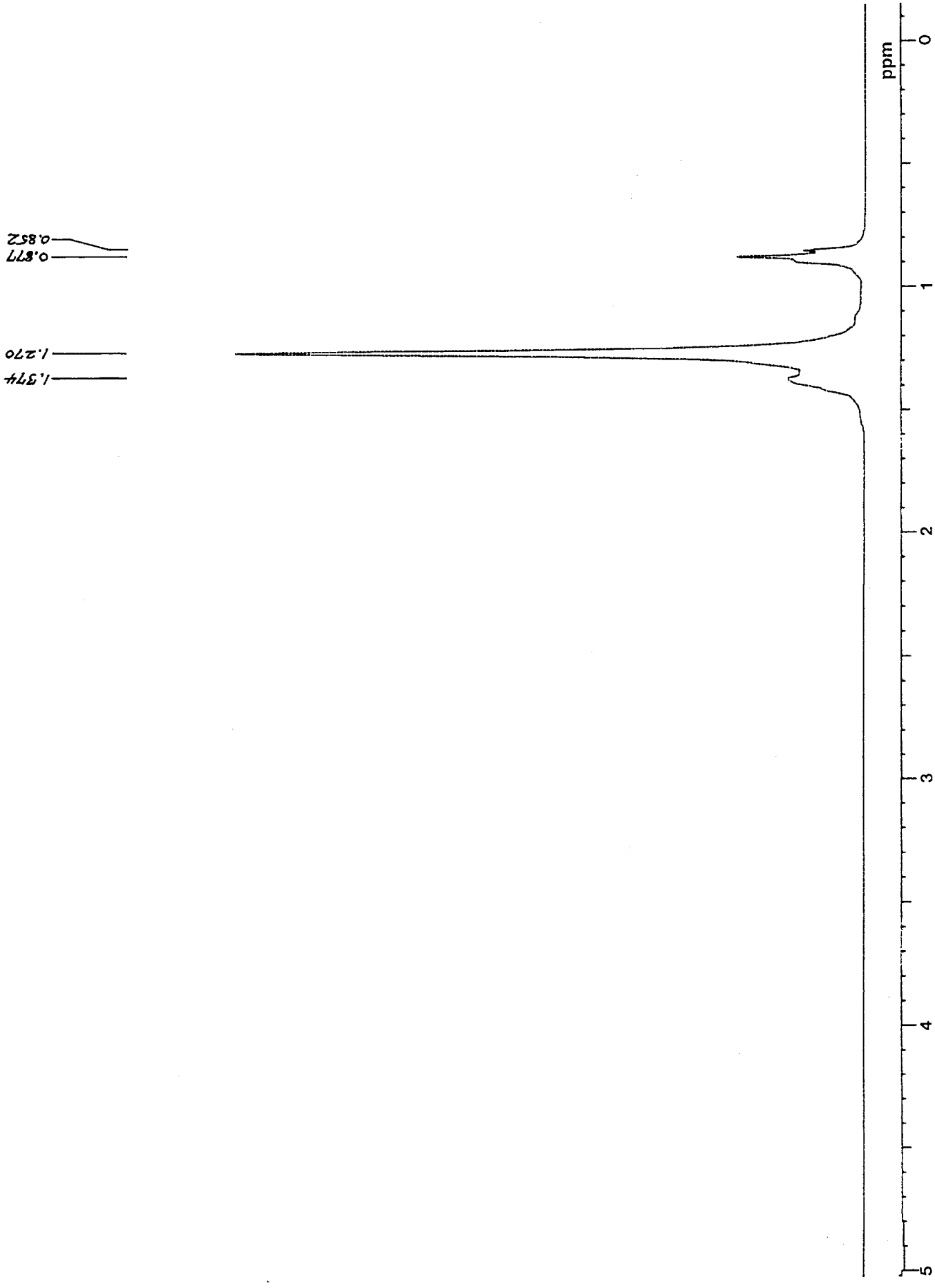

3.3: The 269.7 MHz proton spectrum of 9-*n*-octyl-*n*-heptadecan-9-ol.

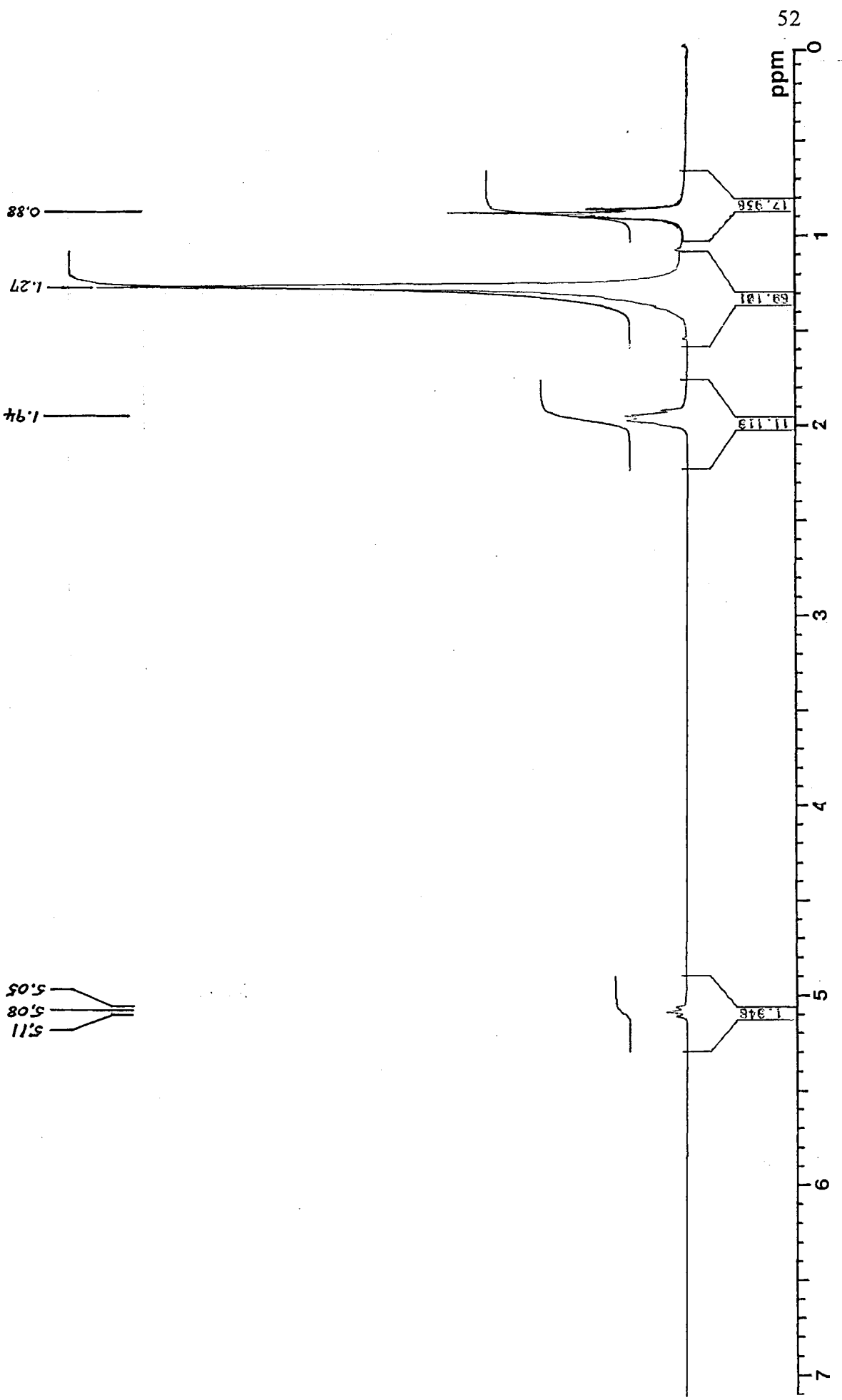

3.4: The 300.1 MHz proton spectrum of 9-*n*-octyl-*n*-heptadec-8-ene.

9-*n*-OCTYL-*n*-HEPTADECANE AND
9-*n*-OCTYL-*n*-HEPTADECANE-9d_1

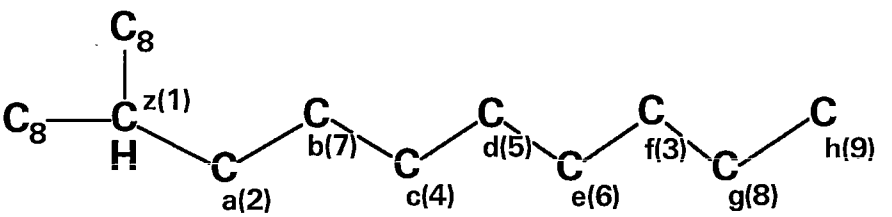

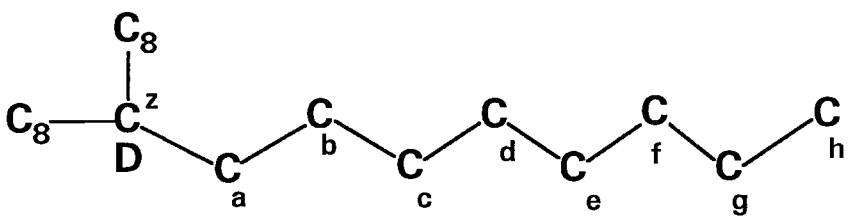

Spectrum 3.5 shows the completely proton decoupled carbon-13 resonances of 9-*n*-octyl-*n*-heptadecane. The central carbon **z** appears at 37.430 ppm, the three methyl groups **h** at 14.141 ppm, and the seven equivalent sets of methylene carbons of the *n*-octyl chains are spread out in between. One can assign the resonances at 22.736 ppm to the three carbon atoms **g**. The off-resonance decoupled spectrum, 3.6, confirms this, wherein the resonances are identified by their multiplicities.

Spectrum 3.7 shows the completely decoupled spectrum of the corresponding isotopomer, 9-*n*-octyl-*n*-heptadecane-9d_1. At 36.850 ppm can be seen the small triplet resonance of the central deuterated carbon atom, **z**. (And no trace of any protonation at this position in the sample). Spectrum 3.8 was that obtained from a roughly 2:3 mixture of the original alkane with its monodeuterated isotopomer, and the features of this spectrum therefore imitate those observed in the case of 9,10-di-*n*-octyl-*n*-octadecane-9d_1. The resonance of the protonated carbons **z** appears just next to the small triplet from the same position in the deuterated molecules. In an expansion, Spectrum 3.9, two distinct resonances appear at 33.624 ppm and 33.750 ppm. One concludes that the resonance at 33.750 ppm is that of the three **a** carbons in the undeuterated molecules, and that at 33.624 ppm comes from the same positions, slightly shifted, in the deuterated molecules. Therefore one can assign the three **a** carbons to the peak at 33.725 ppm in the spectrum of the unlabelled compound. The deuteration of the centre of this molecule provides no further certain assignments.

The remaining carbon atom resonances in the octyl chains can be assigned with the help of the T_1 data that were later acquired, in the same way as described for 9,10-

di-*n*-octyl-*n*-octadecane, assuming that in general the T_1 values will increase as one moves closer to the methyl groups of the chains. Choosing a suitable frequency and temperature combination (68.83 MHz and 40 ^{0}C) leads to the assignment of the three remaining positions; **b**, 26.743 ppm; **c**, 30.196 ppm; **d**, 29.717 ppm; **e**, 29.415 ppm; **f**, 31.961 ppm.

The carbon atoms are also numbered in the order in which their resonances appear in the standard spectrum, starting from the low field end. One notes that the order and chemical shifts agree almost exactly with those deduced for 9,10-di-*n*-octyl-*n*-octadecane, except the order in which **a** and **f** appear in the spectra is reversed.

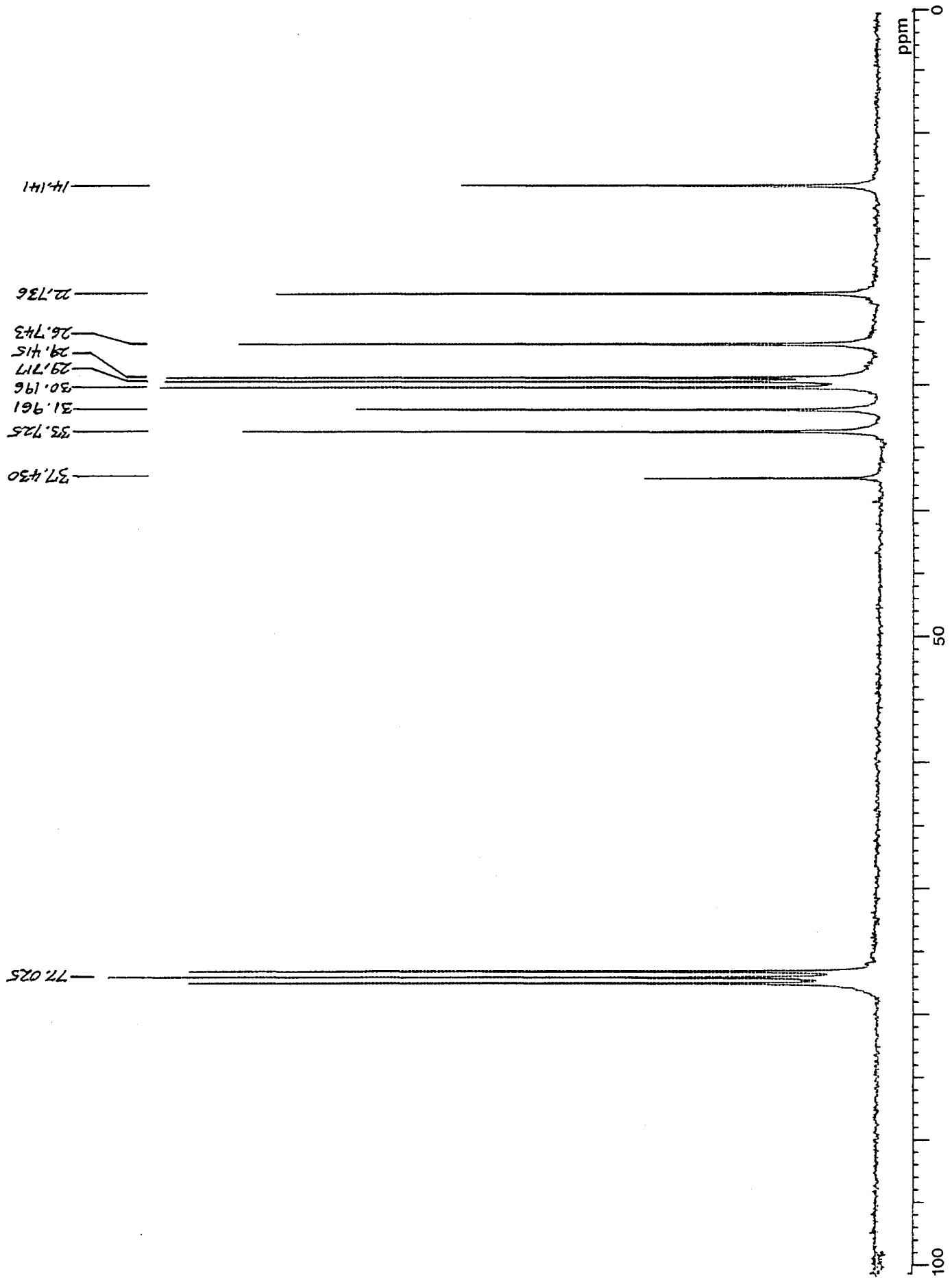

3.5: The 67.83 MHz proton decoupled carbon-13 spectrum of 9-*n*-octyl-*n*-heptadecane.

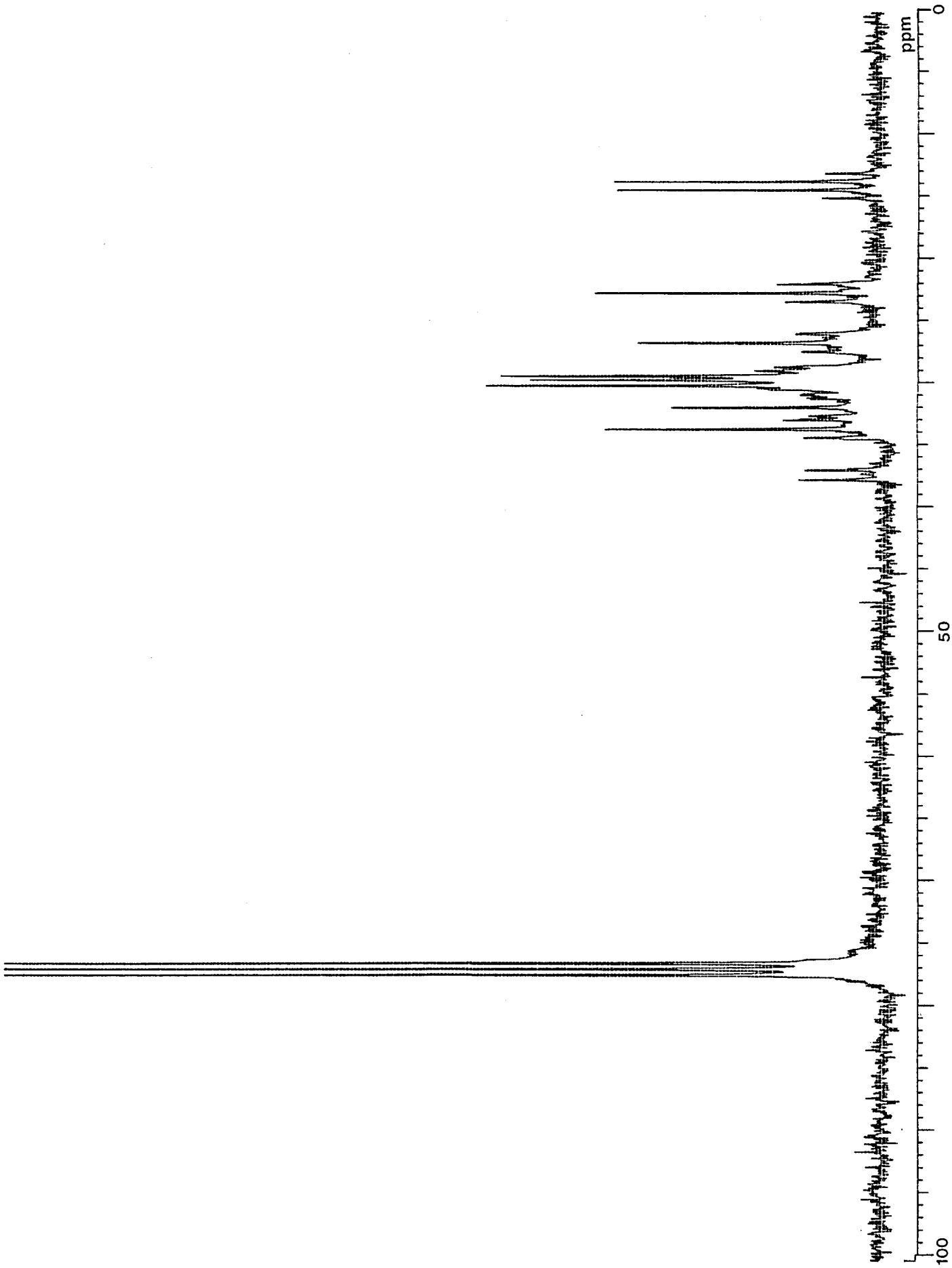

3.6: The 67.83 MHz off-resonance decoupled carbon-13 spectrum of 9-*n*-octyl-*n*-heptadecane.

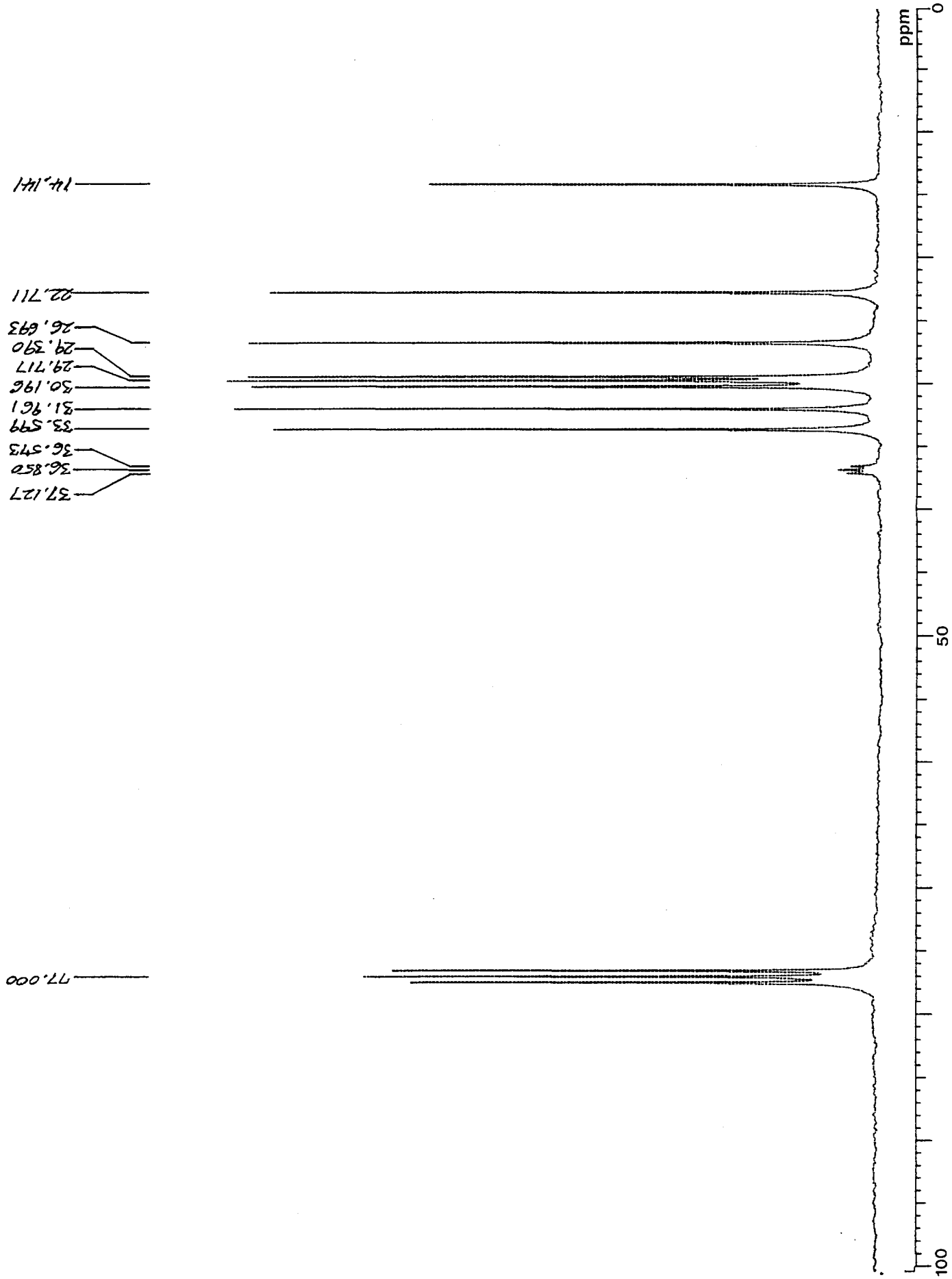

3.7: The 67.83 MHz proton decoupled carbon-13 spectrum of 9-*n*-octyl-*n*-heptadecane-9d$_1$.

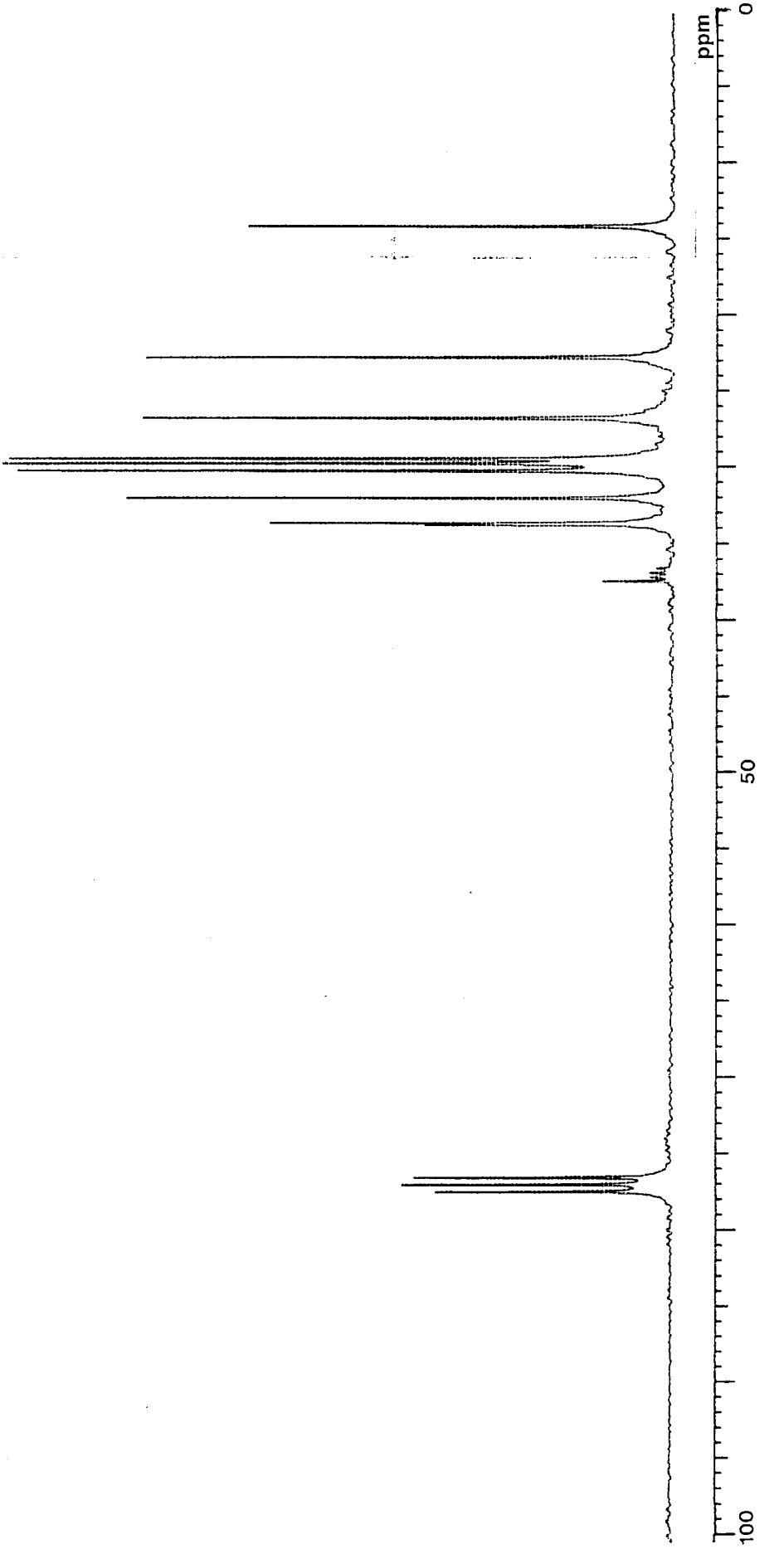

3.8: The 67.83 MHz proton decoupled carbon-13 spectrum of a mixture of 9-*n*-octyl-*n*-heptadecane and 9-*n*-octyl-*n*-heptadecane-9d_1 in the proportion of roughly 2:3.

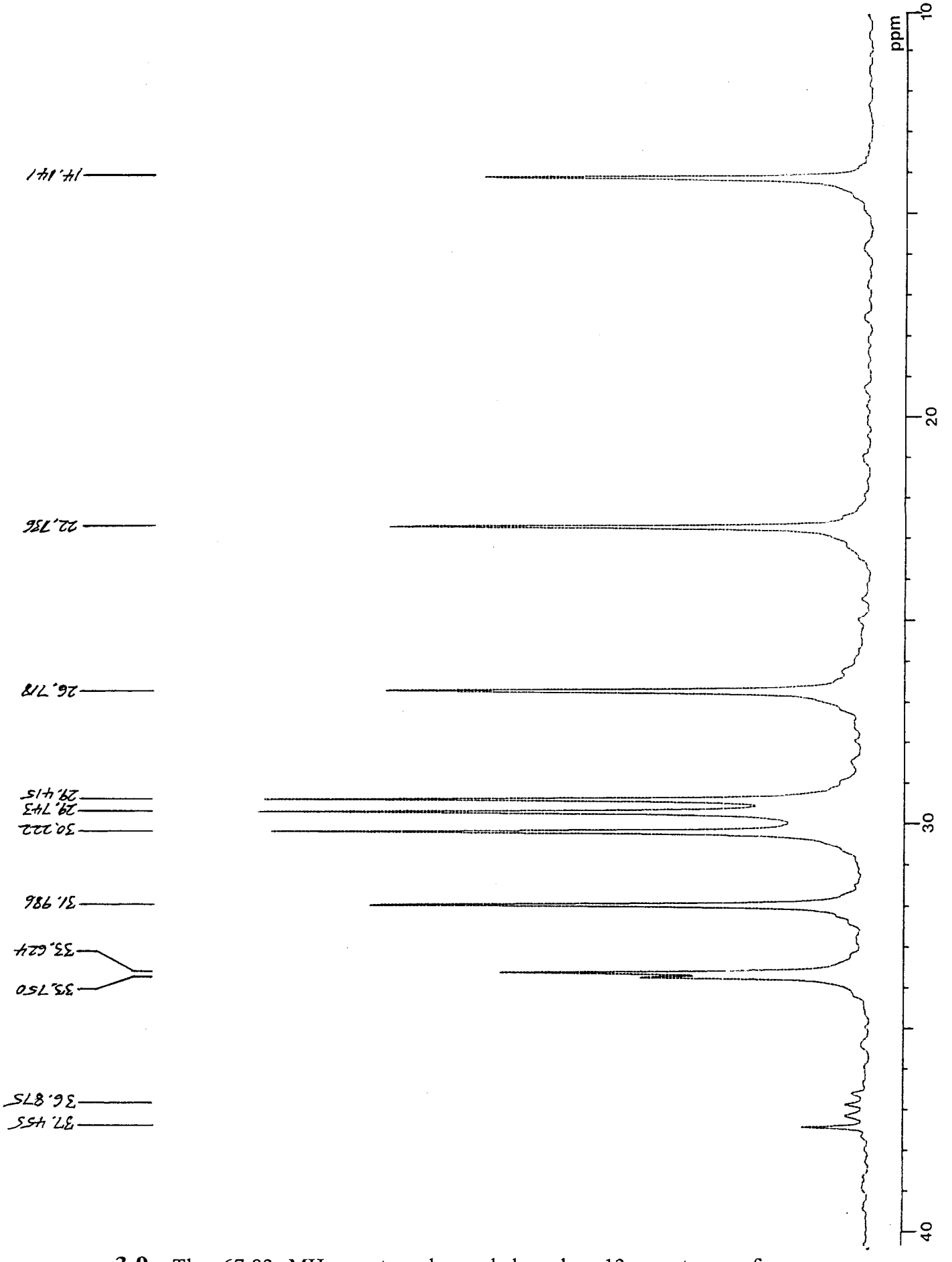

3.9: The 67.83 MHz proton decoupled carbon-13 spectrum of a mixture of 9-*n*-octyl-*n*-heptadecane and 9-*n*-octyl-*n*-heptadecane-9d$_1$ in the proportion of roughly 2:3 (expansion).

TRI-*n*-OCTYLSILANE

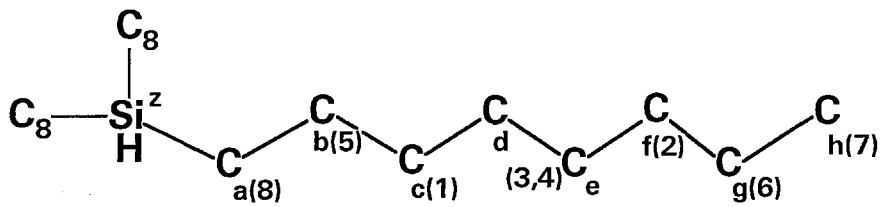

Spectrum 3.10 shows the completely proton decoupled carbon-13 resonances of tri-*n*-octylsilane. The three methyl groups **h** appear at 14.114 ppm, while the three methylene groups **a** appear at 11.364 ppm, strongly shifted upfield by the electropositive nature of the neighbouring central silicon atom, **z**. One can also assume that the **g** carbon atoms appear at 22.710 ppm, as usual. The remaining resonances of the *n*-octyl chains appear, in some order, from 33.410 to 22.710 ppm. These occur in equivalent groups of three, with two very close resonances at 29.342 ppm and 29.292 ppm, shown expanded in Spectrum 3.11. This corresponds to a separation of 3 to 4 Hz. (The resolution of the spectrum was 0.5 Hz). The off-resonance decoupled spectrum, 3.12, confirms these assignments, wherein the resonances are identified by their multiplicities.

Spectrum 3.13 is a proton decoupled carbon-13 SEFT spectrum of this silane with delay τ = 8 ms, thereby allowing phase sensitive detection of the various carbon resonances. The methylene groups appear with normal phase, while the single resonance of the three methyl groups **h** appears with inverted phase.

The remaining carbon atom resonances in the octyl chains can be assigned with the help of the T_1 data that were later acquired, making the same assumptions as used for 9-*n*-octyl-*n*-heptadecane. On this basis, and again choosing a suitable frequency and temperature combination (68.83 MHz and 40 ^{0}C) leads to the assignment of the five remaining positions; **b**, 24.719 ppm; **c**, 33.410 ppm; **d** and **e** closely spaced at 29.312 and 29.292 ppm; **f**, 31.970 ppm.

The carbon atoms are also numbered in the order in which their resonances appear in the standard spectrum, starting from the low field end. One notes how the presence of the silicon atom and the folding of the octyl chain resonances back onto themselves alter the appearance and assignments of this spectrum as compared to the corresponding hydrocarbon analogue, 9-*n*-octyl-*n*-heptadecane.

The few small unidentified resonances in this spectrum show that the silane supplied could probably be best described as only of technical grade purity. Analysis by GC gave a single rather broad peak, on which one could just detect a few slight distortions in the symmetrical shape, from overlapping components. This tended to suggest that the impurities were close homologues, or probably isomers of tri-*n*-

octylsilane; for example, with 2-*n*-octyl groups substituted for 1-*n*-octyl groups on the silicon atom.

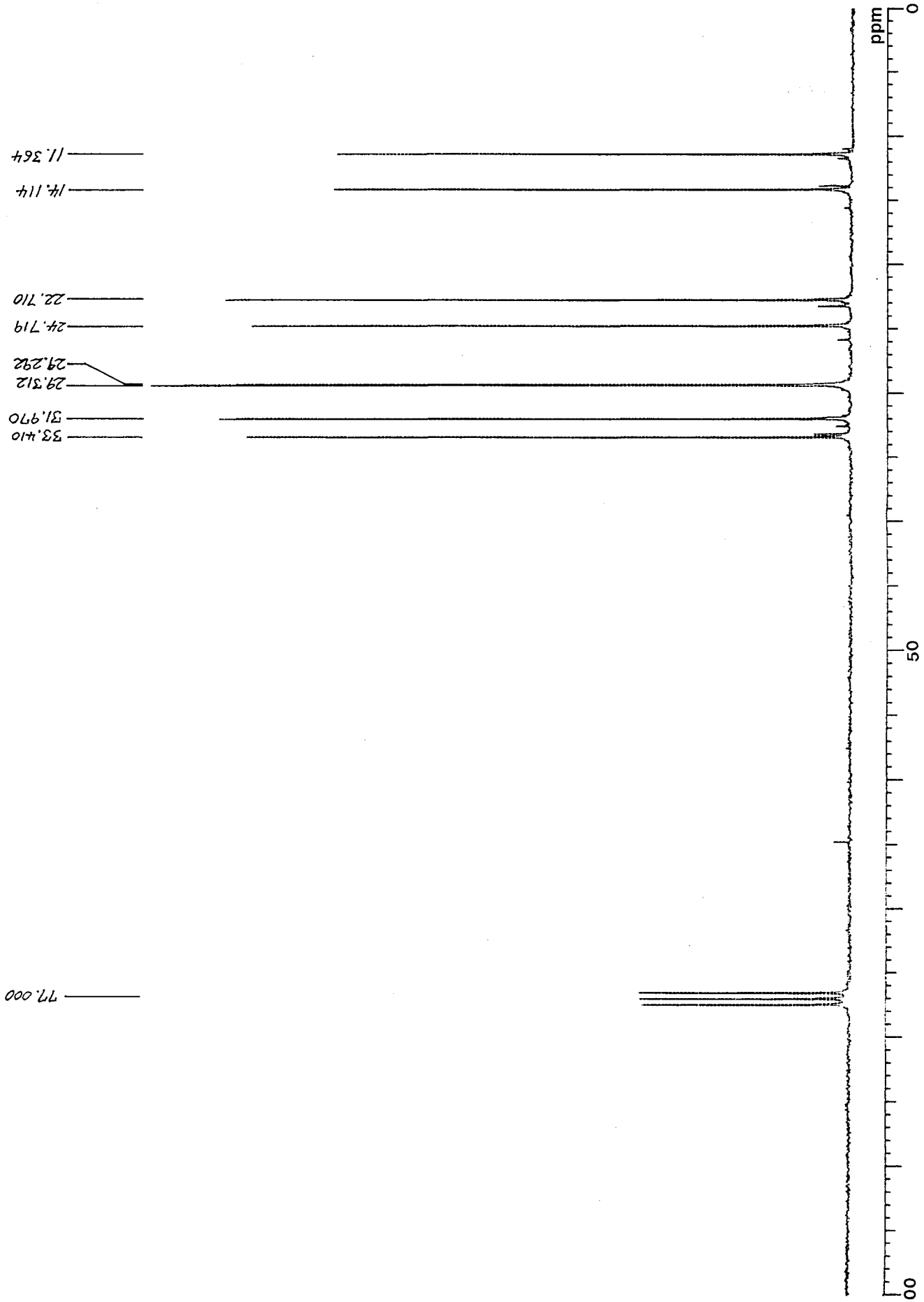

3.10: The 67.83 MHz proton decoupled carbon-13 spectrum of tri-*n*-octylsilane.

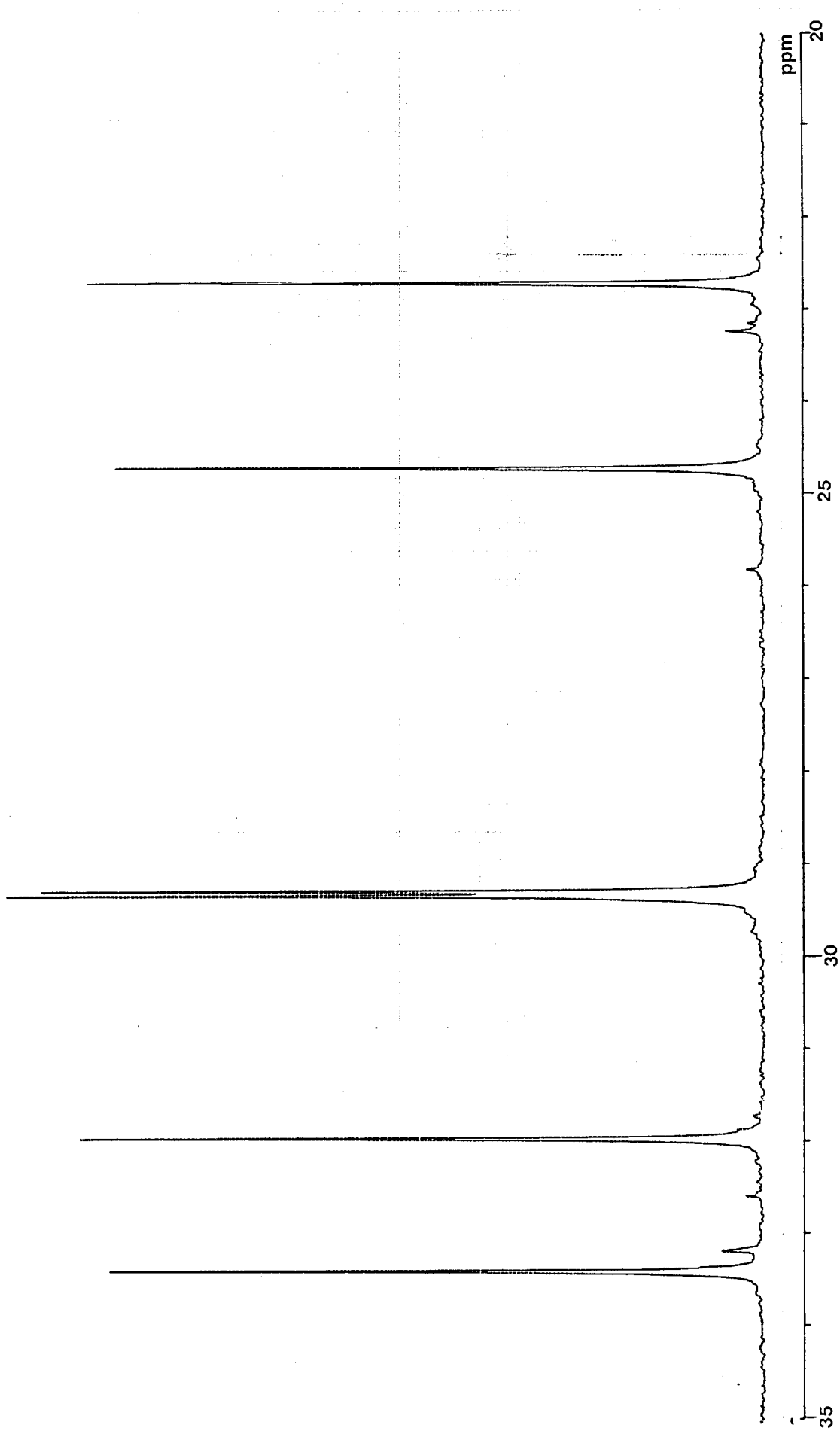

3.11: The 67.83 MHz proton decoupled carbon-13 spectrum of tri-*n*-octylsilane (expansion).

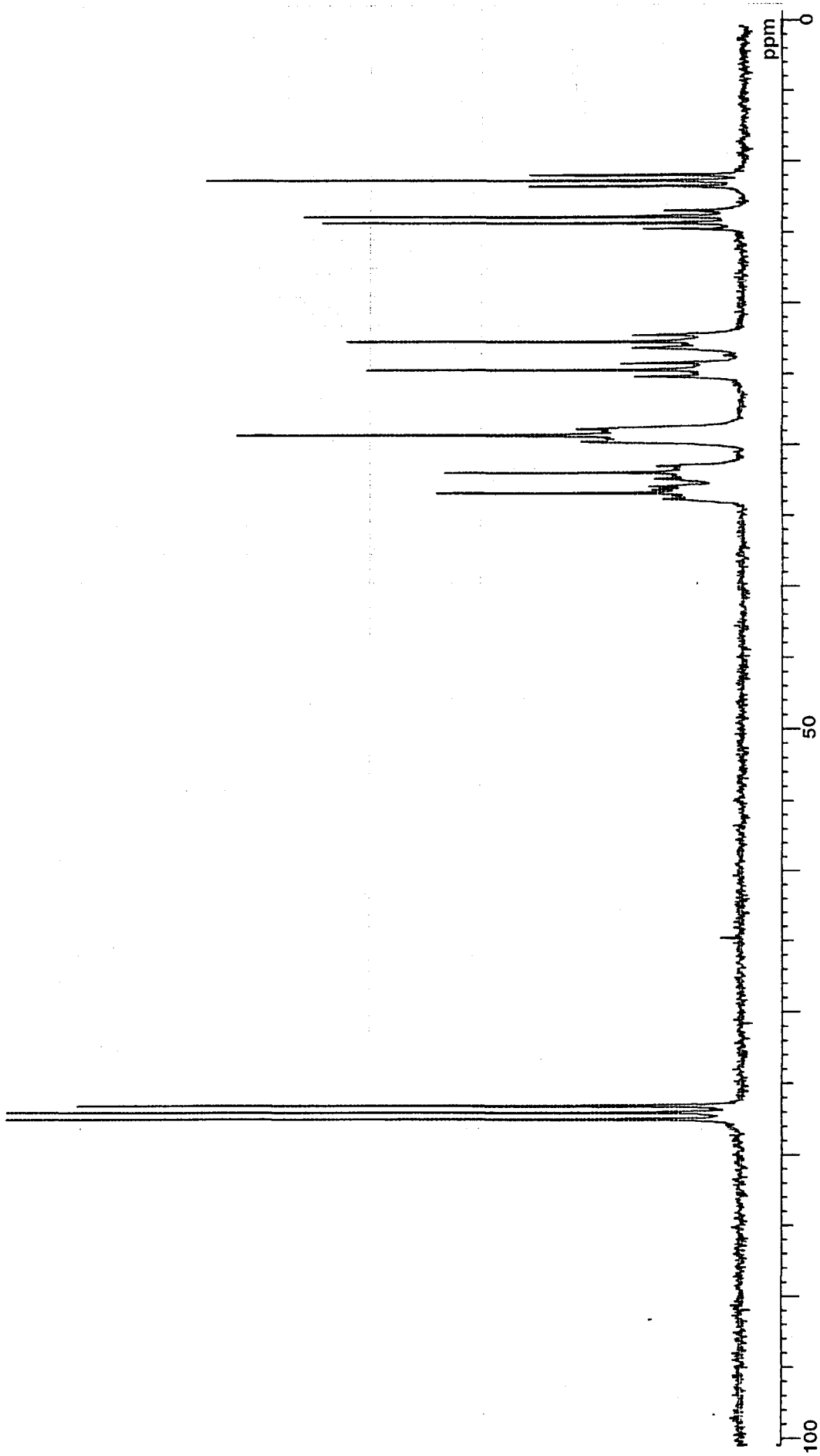

3.12: The 67.83 MHz off-resonance decoupled carbon-13 spectrum of tri-*n*-octylsilane.

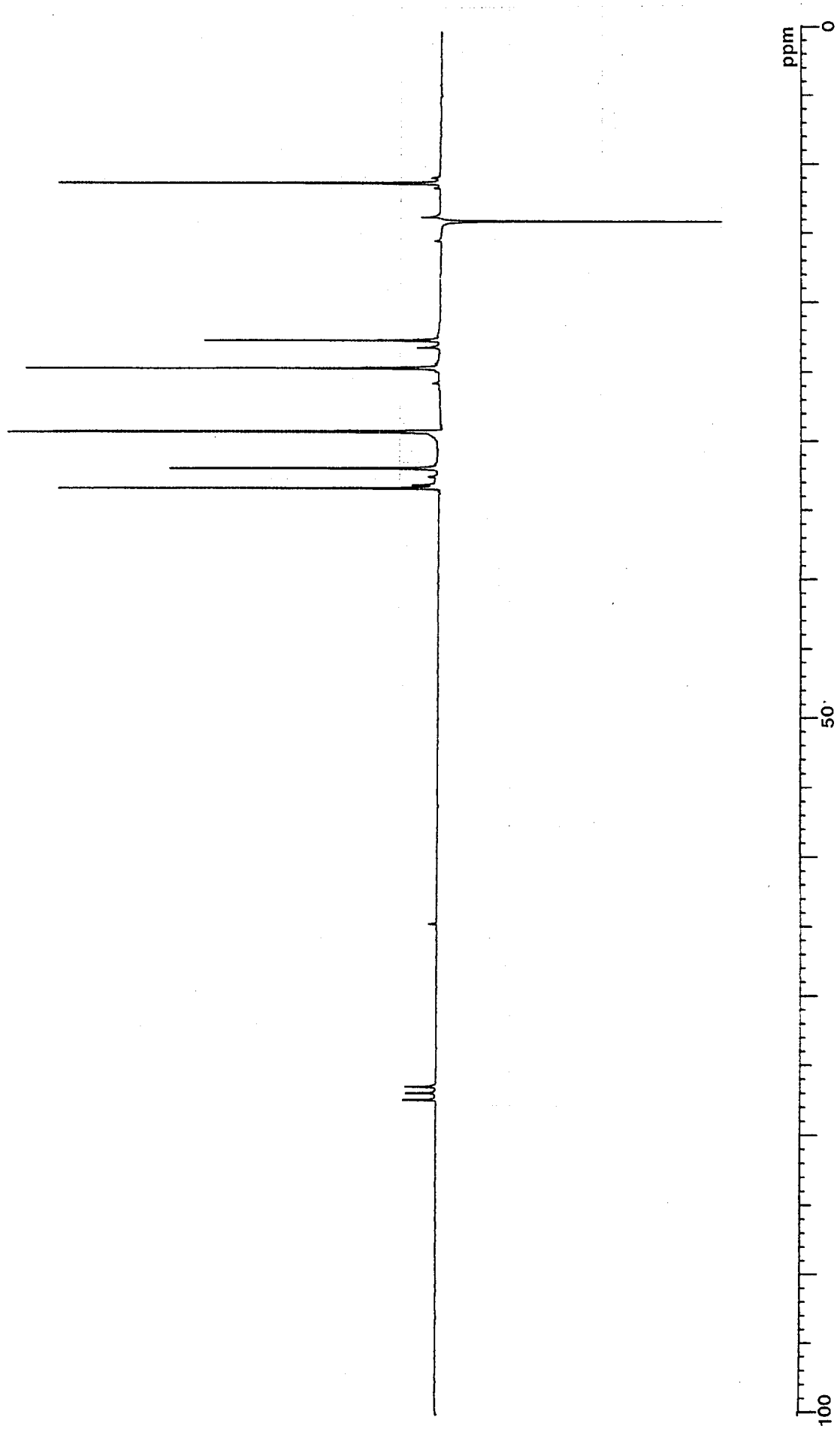

3.13: The 67.83 MHz proton decoupled SEFT spectrum of tri-*n*-octylsilane.

Chapter 4

SYNTHESES RELATED TO TRICYCLOHEXYLMETHANE

4.1 TRICYCLOHEXYLMETHANE AND 1,1,2-TRICYCLOHEXYLETHANE

Tricyclohexylmethane and 1,1,2-tricyclohexylethane are both known compounds, having been synthesized during the late 1920's and 1930's during investigations of the newly discovered Raney nickel and platinum black hydrogenation catalysts. These syntheses were used as a guide. It was now possible to be certain that pure samples of the required compounds had been obtained, by using GC and NMR methods that were not available to earlier investigators. Some of the reported data concerning tricyclohexylmethane were found to be inaccurate or incomplete, and therefore further studies of this and related structures were carried out which have led to the X-ray crystallographic and ESR results detailed in the next chapter.

Tricyclohexylmethane was synthesized in the obvious way by the complete catalytic hydrogenation of triphenylmethane. Reliable earlier reports were those of Adams and Marshall[1], who used platinum black at room temperature and low pressure for this purpose, and Adkins, Zartman and Cramer[2], who used an active Raney Nickel at around 1200 psi and 150 ^{0}C. The last mentioned paper investigates the increasing difficulty involved in successfully perhydrogenating a series of polyaromatic structures, where the steric hindrance of the cyclohexyl groups that are formed gradually limits co-ordination with the catalytic surface. However, it was found that the perhydrogention of triphenylmethane can be conveniently accomplished with a standard W2 Raney nickel if the following slightly unconventional procedure is followed:

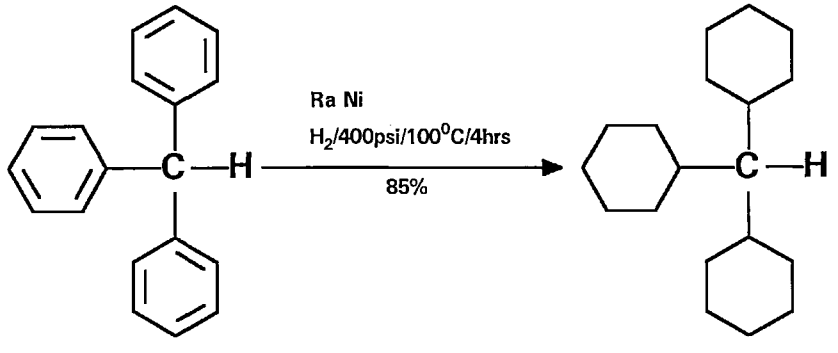

Tricyclohexylmethane: 10g (41 mmol) of triphenylmethane was dissolved, with warming, in a mixture of 5 ml of toluene and 95 ml of cyclohexane, and the solution poured into a 500 ml capacity Parr pressure vessel.

Meanwhile, a 5 ml quantity of activated Raney nickel slurry was washed fifteen times with distilled water, twice with absolute ethanol, once with isopropanol and finally twice with cyclohexane; using at least 20 ml of solvent for each washing. About 4 ml (6g) of nickel slurry remained.

A small amount of glass wool was then gently teased out and submerged in the reaction solution so as to form a fine network throughout and the prepared nickel poured into the solution, covering the glass wool with the slurry.

The solution was hydrogenated at 400 psi, and 100 °C. Rapid uptake of hydrogen started at around 95 °C and the vessel was repressurized with hydrogen as necessary until the hydrogenation was complete. This usually required from three to five hours. The vessel was gently rocked from time to time, to ensure the contents were mixed, but no other form of agitation was used.At the end of this time, the nickel was filtered off, the solution dried over magnesium sulphate, and the solvent removed.

The resulting colourless oil slowly solidified to a hard crystalline mass, which GC analysis showed was 85% of tricyclohexylmethane and 15% of a hydrocarbon product of smaller molecular weight. The solid was recrystallized from absolute ethanol to give 7 g of white crystals of tricyclohexylmethane. (m.p. 57.5/58.5 °C). Purity by GC analysis was >99.5%. Yield: 70%. The compound crystallized as long needles from a dilute solution, and in a more irregular habit from a concentrated one.■

Activated Raney nickel slurry, equivalent to W2 Raney nickel, was obtained from Sigma Chemicals and was used straight from the bottle for these hydrogenations over a period of several months without loss of effectiveness; standard laboratory glass wool was obtained from BDH and used without any special preparation.

The exact volume and constitution of the solvent was not critical, but the use of more toluene reduced the volume needed to dissolve the substrate. The toluene was hydrogenated simultaneously to methylcyclohexane. A generous quantity of nickel is indicated above, but a smaller proportion would have been adequate.

4.2 1,1,2-TRICYCLOHEXYLETHANE

It was found that the same procedure used to perhydrogenate triphenylmethane could be used to perhydrogenate triphenylethylene, to give the required 1,1,2-tricyclohexylethane. The compound is reported in the early work of Zartman and Adkins[3]:

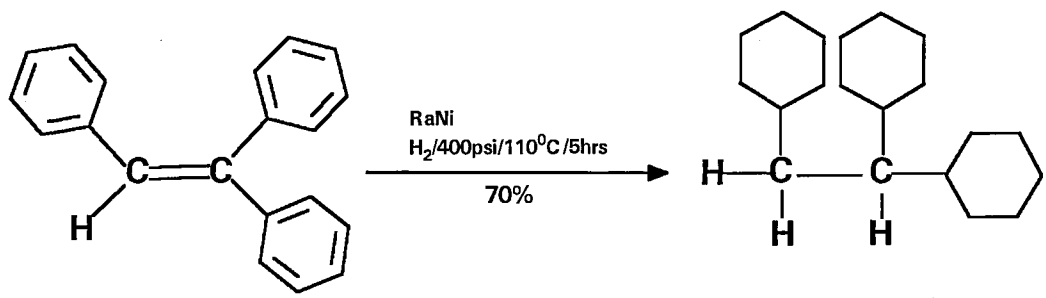

1,1,2-tricyclohexylethane: 10 g of triphenylethylene was dissolved in 100 ml of cyclohexane, and hydrogenated over 6 g of W2 Raney nickel supported on glass wool, according to the procedure described for the synthesis of tricyclohexylmethane, at 120 °C / 400 psi for 5 hours. Removal of the catalyst and solvent gave 10 g of viscous oil, which analysis by GC showed to contain some 70% of the desired product, together with two alkanes of lower molecular weight produced by hydrogenolysis. In all, 40 g of triphenylethylene were hydrogenated by this method, and the total crude product fractionated under vacuum through a heated 35 x 1.7 cm column of 4 mm glass Raschig rings to give 29.2 g of viscous water white oil, boiling at 143 °C / 0.2 mm Hg. Carbon-13 and proton NMR spectra agreed exactly with the desired product 1,1,2-tricyclohexylethane. Purity by GC analysis was > 98%. Yield overall: 64%.■

4.3 TRICYCLOHEXYLMETHANE-d_1

As in the synthsis of the isotopomers of the *n*-alkyl structures described in Chapters 2 and 3, the position to be labelled was a tertiary one, and therefore it was hoped that a similar approach via ionic deuteration would be appropriate. However, one was dealing here with a very different type of tertiary centre with high steric hindrance, and the presence of three neighbouring tertiary positions on the attached cyclohexyl rings gave strong potential for rearrangements of, and eliminations from, a central carbonium ion. Nevertheless the attempt was begun.

The indicated precursor was tricyclohexylmethanol. This cannot be synthesized via any of the usual Grignard methods except in very poor yields[4] - 10% or less - due to the strong steric inhibition of the usual mechanisms by the three cyclohexyl groups. A procedure using sodium is reported to give a yield of 19% from cyclohexyl

bromide[5]. However, the synthesis of hindered tertiary alcohols is also possible via organoborane chemistry[6].

Tricyclohexylborane was made by the standard hydroboration of cyclohexene in THF solution. This was then reacted with a carbene centre generated internally in the reaction mixture by proton abstraction from α,α-dichloromethyl methyl ether[7], using a solution in hexane of lithium 3-methyl-3-pentoxide as base. Following co-ordination of the carbene with tricyclohexylborane, a transfer of the cyclohexyl groups from the boron to the co-ordinated carbon centre takes place in the usual sort of fashion for borane type syntheses. Oxidation of the resulting methyl tert-alkylchloroboronic ester with alkaline hydrogen peroxide and a simple vacuum distillation gave tricyclohexylmethanol in 55% yield from the original cyclohexene:

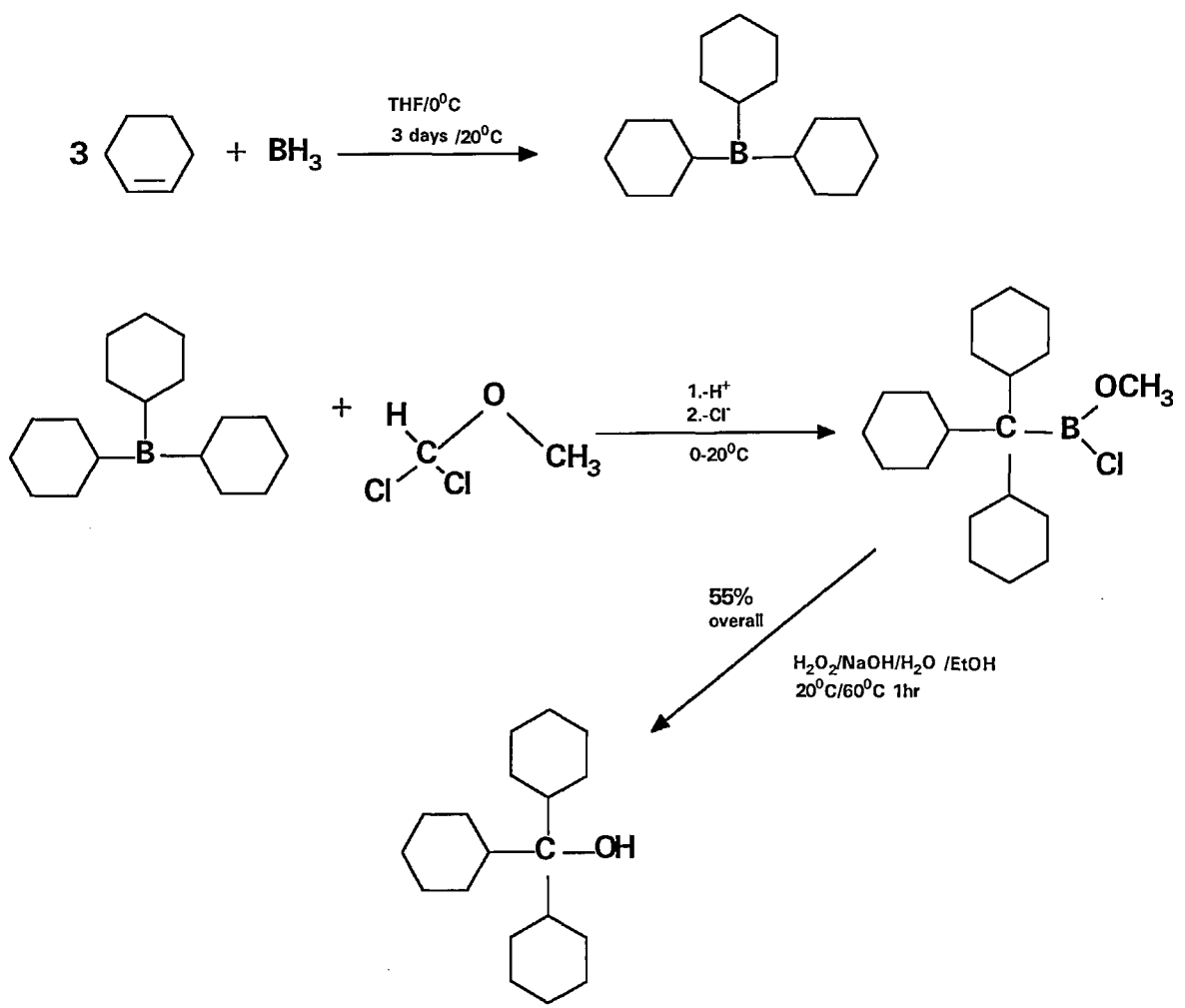

The actual yield from tricyclohexylborane is reported[7] to exceed 90%, but the hydroboration of cyclohexene in THF solution does not proceed to completion[6], and this explains the reduced yield for this method. A better procedure would be to carry out the hydroboration in diglyme and isolate the borane before using it for the alcohol synthesis. However, the method described here gave a reasonable yield and has the

merit of being a simple one pot synthesis using a standard commercially available solution of borane-THF complex.

Tricyclohexylmethanol: Glassware was oven dried before use. Into a three-necked 1 l round bottom flask, equipped with a magnetic stirrer bar, septum inlet, bypassed 100 ml dropping funnel sealed by a septum, reflux condenser, and gas bubbler/inlet was placed a solution of 24.6 g (300 mmol) of cyclohexene in 40 ml of dry THF. The apparatus was closed and a steady slow stream of dry, oxygen free nitrogen established through it. The flask was then cooled in a bath of iced water, while 100 ml of a 1 M solution of borane-THF complex in THF was transferred by cannula under nitrogen pressure from a sure-seal type bottle into the dropping funnel. The borane-THF complex solution was added drop-wise over a period of 30 minutes to the stirred, cooled solution of cyclohexene, as a dense white precipitate of dicyclohexyl borane dimer gradually formed. The reaction was then allowed to warm to room temperature, and stirred for 3 days. A clear colourless solution resulted, which tested neutral to litmus paper and gave no reaction with methanol.

The flask was again cooled in a water bath to 10 ^{0}C, and 10.7 g (110 mmol) of α,α-dichloromethyl methyl ether transferred into the reaction by syringe, followed by the fairly rapid addition of a solution of 100 mmol of lithium 3-methyl-3-pentoxide in 60 ml of hexane. The reaction was allowed to warm to room temperature and stirred for 2 hours.

The gas bubbler was then removed, 150 ml of ethanol and 24 g of solid sodium hydroxide added, and oxidation accomplished by the cautious addition of 80 ml of 30% hydrogen peroxide solution. The initially exothermic reaction was controlled at just beneath its reflux temperature by judicious application of an ice-water bath, and the oxidation finally completed by warming to 60 ^{0}C for 1 hour.

The organic layer was separated, and the aqueous layer extracted three times with ether. The combined organic fractions were washed with water, twice with brine and dried over anhydrous potassium carbonate. Filtration and rotary evaporation of the solvents gave a viscous oil, from which some large crystals of tricyclohexylmethanol slowly separated.

Simple vacuum distillation of this product, using a well lagged head and an air cooled condenser, gave 15 g of tricyclohexylmethanol boiling at about 160 ^{0}C / 0.14 mm Hg. Carbon-13 and proton NMR spectra agreed exactly with those expected. Purity by GC analysis was >98%. Yield: 55%. The alcohol formed a viscous resin on cooling, which gradually changed to a hard crystalline mass over a few days. Crystallization from benzene gave a powder, m.p. 94.5 ^{0}C.■

A hexane solution of the alkoxide required for this synthesis was easily prepared by the reaction of a 1.6 M solution of *n*-butyl lithium with one equivalent of 3-methyl-3-pentanol[8]:

Lithium 3-methyl-3-pentoxide: An oven dried 250 ml two-necked round bottom flask was fitted with a septum inlet, magnetic stirring, and an air condenser protected by a calcium chloride guard tube, and 62 ml of a 1.6M solution of *n*-butyl lithium in hexane were transferred into the flask by cannula under nitrogen pressure. The flask was cooled in an ice bath, while 12 g (100 mmol) of 3-methyl-3-pentanol were slowly injected through the septum using a syringe. The reaction was vigorous, and the hexane boiled. The final point of neutralization of the *n*-butyl lithium was reached when the yellow colour vanished. The resulting (roughly 1.6M) solution of 100 mmol of lithium 3-methyl-3-pentoxide could be sealed and kept for use, if necessary.■

From tricyclohexylmethanol it was possible to prepare tricyclohexyl-methylchloride by reaction with phosphorus pentachloride in a buffered chloroform solution, but the reaction was very susceptible to slight changes in reagent concentrations and conditions. The paper of Carman and Shaw[9] describing this method gives yields of 80%, or more, even in cases involving the replacement of tertiary hydroxyl groups in various difficult positions, and the reduced yield in the present case is an indication of the problems of operating on a hindered centre.

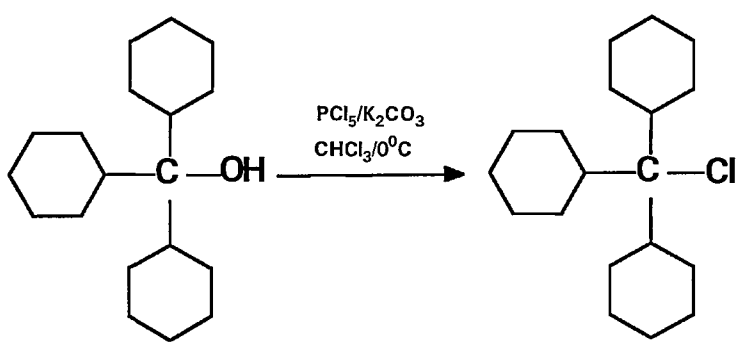

Neunhoeffer[4] reported that tricyclohexylmethylbromide was successfully synthesized by stirring tricyclohexylmethanol with an excess of acetyl bromide in ether at 0 °C; the bromide gradually crystallizing out over a few days. An attempt to follow

Neunhoffer's method using acetyl chloride was negative, and the alcohol was recovered from the solution unchanged.

Tricyclohexylmethylchloride: Into a 50 ml flask fitted with a calcium chloride guard tube was placed 8 ml of dry chloroform, 2.0 g (10 mmol) of phosphorous pentachloride and 0.28 g (2 mmol) of anhydrous potassium carbonate. The stirred suspension was cooled to 0 ^{0}C and a solution of 1.0 g (3.6 mmol) of tricyclohexylmethanol in 4 ml of dry chloroform added in 1 ml portions over 5 minutes. Stirring was continued for 5 more minutes, and then the reaction allowed to warm to room temperature during a further 5 to 10 minutes. The white precipitate was quickly filtered off, and the filtrate concentrated under vacuum at 45 ^{0}C to give about 1.3 g of a pale yellow solid. This was dissolved by gentle heating under reflux in a solution of 0.25 ml of acetyl chloride in 8 ml of dry ethyl acetate. Upon cooling sparkling white crystals of tricyclohexylmethylchloride formed which were filtered off and washed with ice cold ethyl acetate. Yield: 55%, 0.6 g, m.p. about 130 ^{0}C, but the crystals began to decompose and fracture before this temperature was reached. Tricyclohexylmethylchloride required C, 76.85; H, 11.20%, and combustion analysis gave C, 76.1; H, 11.3%. Carbon-13 and proton NMR spectra agreed exactly with those expected for the compound. The crystals were stable indefinitely at room temperature, under dry conditions. The crude material isolated during the reaction transforms itself during about one day into a sticky resin from which no chloride can be isolated.■

It is possible to exchange a tertiary halide atom with hydride (or in this case deuteride) derived from triethylsilane in the presence of a catalytic amount of aluminium chloride[10]. It was found that the reaction could be made to succeed with tricyclohexylmethylchloride as well, without resorting to unusual types of reaction conditions to stabilize the carbonium centre:

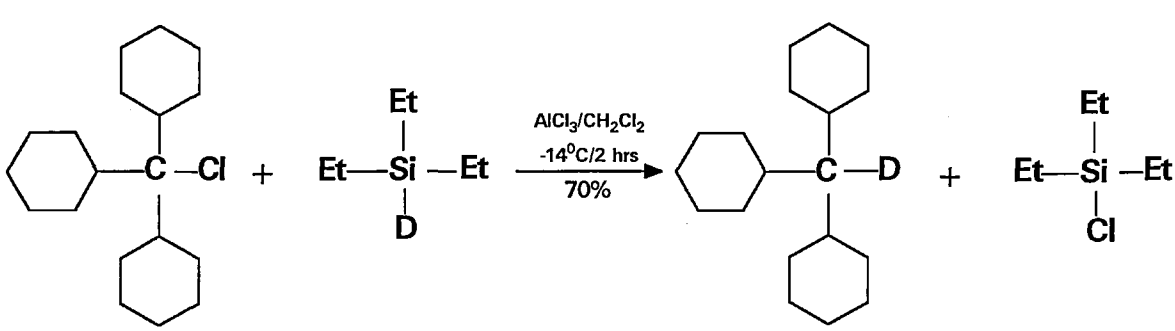

By using a considerable excess of the silane, the tricyclohexyl carbonium ion formed could be trapped by deuteride ion before it had time to suffer rearrangement and decomposition. The effective concentration of the silane was also increased considerably because the chloride crystallized out from solution almost completely at the temperature of the reaction; on the other hand the tricyclohexylmethane produced remained in solution throughout.

Tricyclohexylmethane-d_1: A solution of 1.0 g (3.4 mmol) of tricyclohexylmethylchloride and 0.8 g (6.8 mmol) of triethylsilane-d_1 in AR dichloromethane was cooled with an ice/ammonium chloride freezing mixture to -14 ^{0}C until most of the chloride had crystallized out. A knife point of aluminium chloride powder was then added and stirring continued for 4 hours. The reaction was diluted with 5 ml of ether and 5 ml of water, followed carefully by addition of enough anhydrous sodium carbonate to neutralize the reaction. The aqueous layer was separated off, the organic phase washed with water, twice with brine and then dried over anhydrous sodium sulphate. After filtration the solvents were rotary evaporated off, and all volatile material removed by distilling the oily product up to 80 ^{0}C at 0.15 mm Hg. The remaining oil solidified on cooling to a crystalline mass. Recrystallization of this from absolute ethanol gave 500 mg of amorphous white crystals of tricyclohexylmethane-d_1. Carbon-13 and proton NMR spectra agreed exactly with those expected for this compound, and purity by GC analysis was >98%. Yield: 56%. This crystallization was more difficult than that of the corresponding hydrocarbon obtained by hydrogenation, because of the presence of the closely related structure dicyclohexylcyclohexenylmethane as the main impurity in the product. It was necessary to induce crystallization at the critical moment during cooling of the solution by vigorous scratching of the flask, otherwise an oily dispersion would form.■

4.4 THE DECOMPOSITION OF TRICYCLOHEXYLMETHYLCHLORIDE IN CHLOROFORM SOLUTION

Tricyclohexylmethylchloride spontaneously decomposes when kept in solution in chloroform for some 7 days at room temperature, with the release of hydrogen chloride. A sample was kept in deuteriochloroform in a 10 mm NMR tube for this length of time, during which the carbon-13 spectrum changed from the simple one of the pure chloride to a much more complex pattern. This was analyzed with the help of the corresponding proton and carbon-proton correlated spectra, as described in the final section of this chapter. The NMR analysis confirmed the conjecture of Neunhoffer[4], who apparently observed a similar decomposition of the bromide, that the product was dicyclohexylcyclohexenylmethane. Analysis of the solution by GC

showed that this was essentially the sole product, since there were only traces of other components. The alkene is a solid of low melting point, and the slow evaporation of a solution in hexane gave some crystals suitable for X-ray structural analysis.

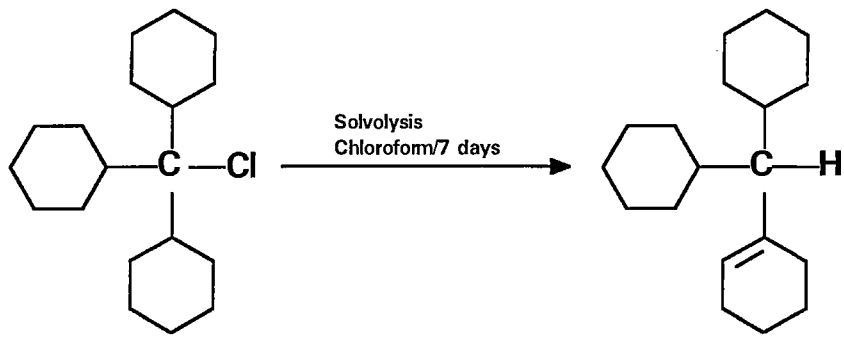

The treatment of a solution of tricyclohexylmethanol in dichloromethane with a few drops of trifluoroacetic acid at room temperature rapidly dehydrated the alcohol, and produced the same alkene as the major product. However, in this case there were also a few percent of at least two other products, according to GC analysis, and these were probably isomers with the double bond shifted to other positions in one cyclohexyl ring. Probably the conditions of acid catalyzed dehydration lead to more possibilities for isomerization of the initial alkene product.

4.5 THE HYDROGENATION OF TRIPHENYLMETHANE OVER RANEY NICKEL

Since the procedure described in Section 4.1 for the hydrogenation of triphenylmethane (and triphenylethylene) had proved so successful, it was of some interest to obtain quantitative proof that the hydrogenation had proceeded more rapidly than under the usual conditions of using a stirred catalyst. Therefore the hydrogenation was conducted twice, using identical solutions of 5 g of triphenylmethane, and as far as possible, identical conditions of temperature and hydrogen pressure (100 ^{0}C, 400 psi); in the one case with a stirred W2 Raney nickel catalyst, and in the other an identical amount (2 g) of the same W2 catalyst , employed as a dispersion supported on glass wool as described earlier. The catalyst was washed and prepared in the same way for each experiment.

Samples from the hydrogenated solution were analyzed by GC at regular intervals during the course of each hydrogenation. Tables 4.1 and 4.2 give masses of the higher boiling components present during the reductions as percentages of the original triphenylmethane, determined by FID detection from the peak areas. This had

proved a reliable measure of the mass of any given component present for these types of homologous hydrocarbons, without the need for response compensation. Where possible the components present were identified by analysis of suitable mixtures with authentic samples. The results are plotted in Figs 4.1 and 4.2, together with the estimated actual curves. Since the equipment did not allow for access without actually halting the hydrogenation, conditions were far from ideal, and samples could only be taken at rather long intervals, but the results were nevertheless of interest.

In the case of the nickel/glass wool combination, the reduction was complete after less than 6 hours, whereas in the case of the stirred catalyst, the main product after more than 30 hours was dicyclohexylphenylmethane, with only a tiny percentage of tricyclohexylmethane. A saturated product of smaller molecular weight was detectable in the faster hydrogenation, which was a product of hydrogenolysis of the substrate.

This was identified as dicyclohexylmethane by carbon-13 NMR analysis of the oily residue remaining after the recrystallization of the tricyclohexylmethane. The proton decoupled spectrum is shown in Fig. 4.3, while Fig. 4.4 shows a corresponding SEFT spectrum. The marked resonances belong to tricyclohexylmethane, (cf. the relevent spectra at the end of this chapter), while the remaining peaks are those expected for dicyclohexylmethane, in the proportion indicated by GC analysis.

Despite the evidence for the increased rate and completeness of reduction over the supported nickel, it still seems a surprising thing to observe. On the other hand, the increase of catalytic activity with suitable dispersion is very well known, and silica itself is often used in all manner of forms as such a support[11]. Only recently a surprising series of papers[12] has reported the use of silica in "foot-print catalysis", where the hydroxyl groups on the surface of silica particles are regio-selectively substituted and/or removed by prior treatments. The silica thus produced goes on to display certain specificities in the catalysis of various hydrolytic reactions.

In the present case, the chemical and physical properties of the glass wool surface may be such as to interact with closely adherent nickel particles to generate more effective catalytic sites. Some evidence for this was that the reaction over the supported catalyst showed a clear delay of up to 60 minutes on each occasion, before a sudden rapid uptake of hydrogen began. In the case of the stirred reaction, the uptake began at once, as one would normally expect. The supported reaction failed, of course, if the catalyst was previously shaken off the glass wool surface to the bottom of the pressure vessel. Obviously, it would be appropriate to test this hypothesis by substituting various different types of glass, and other surfaces as the support for the nickel, but time did not allow for this.

Hours	Unknown	dicyclohexyl-phenylmethane	Tricyclohexyl-methane	Unknown	Triphenyl-methane
0	0.00	0.00	0.00	0.00	100.00
6	17.70	21.33	0.00	49.03	11.42
11	19.79	39.07	0.00	36.32	3.99
18	12.07	79.77	0.00	7.18	0.00
24	0.00	97.36	2.64	0.00	0.00
30	0.00	96.92	3.08	0.00	0.00

Table 4.1: The hydrogenation of triphenylmethane over stirred Raney nickel at 400 psi / 100 ^{0}C.

Hours	Dicyclohexyl-methane	dicyclohexyl-phenylmethane	Tricyclohexyl-methane	Triphenyl-methane
1	0.00	0.00	0.00	100.00
4	8.15	38.02	53.83	0.00
7	14.30	0.00	85.70	0.00
12	14.30	0.00	85.70	0.00
19	14.30	0.00	85.70	0.00
25	14.30	0.00	85.70	0.00
30	14.30	0.00	85.70	0.00

Table 4.2: The hydrogenation of triphenylmethane over Raney Nickel supported on glass wool at 400 psi / 100 ^{0}C.

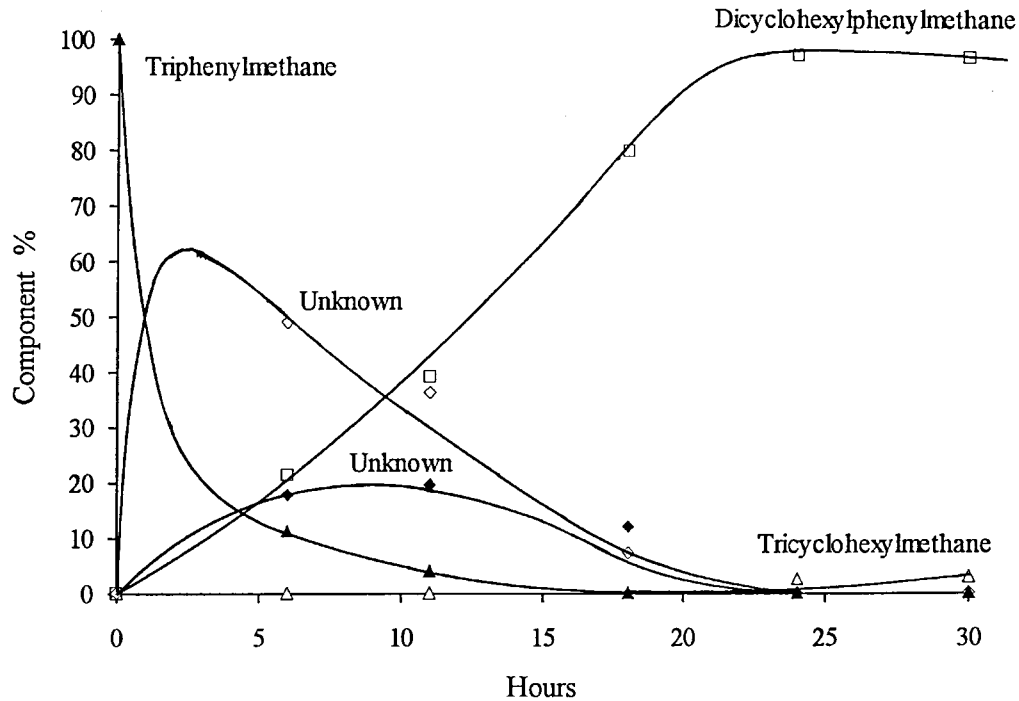

Fig. 4.1: The hydrogenation of triphenylmethane over stirred Raney nickel at 400 psi / 100 ^{0}C.

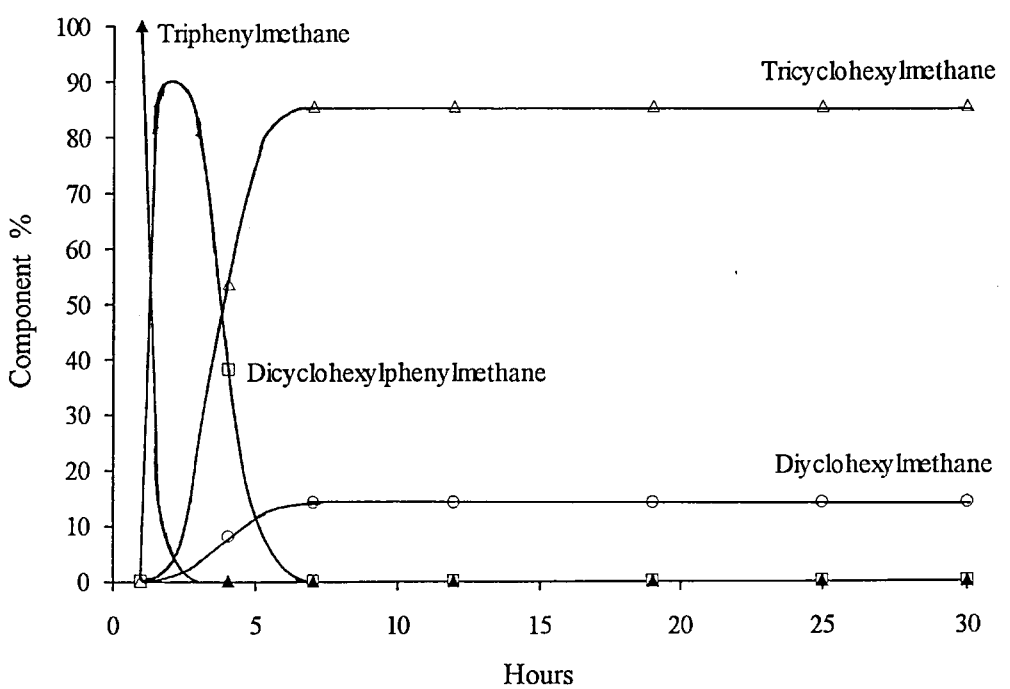

Fig. 4.2: The hydrogenation of triphenylmethane over Raney nickel supported on glass wool at 400 psi / 100 ^{0}C.

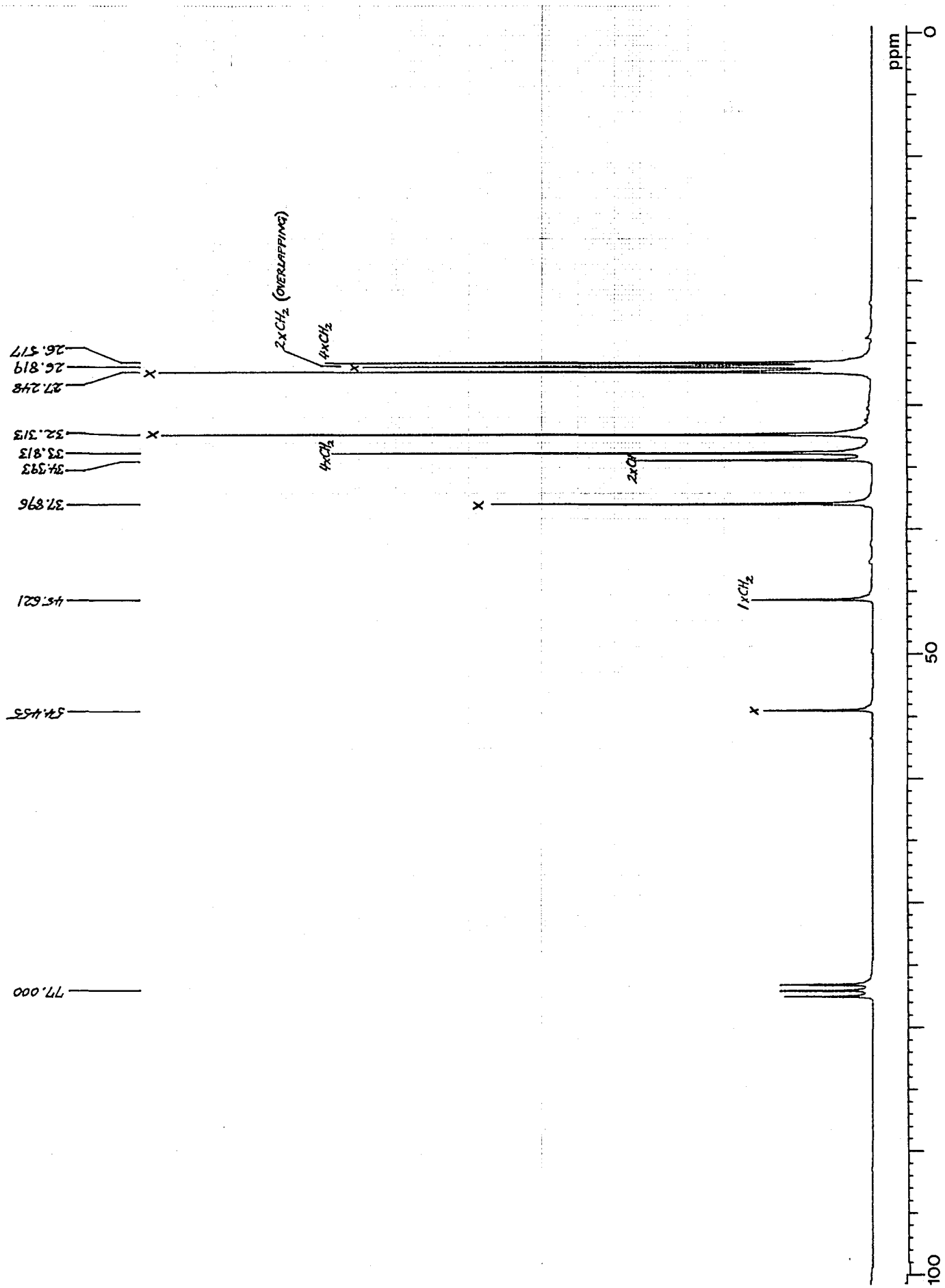

Fig. 4.3: The 67.83 MHz proton decoupled carbon-13 spectrum of the residue after recrystallization of tricyclohexylmethane synthesized using the Raney nickel / glass wool combination.

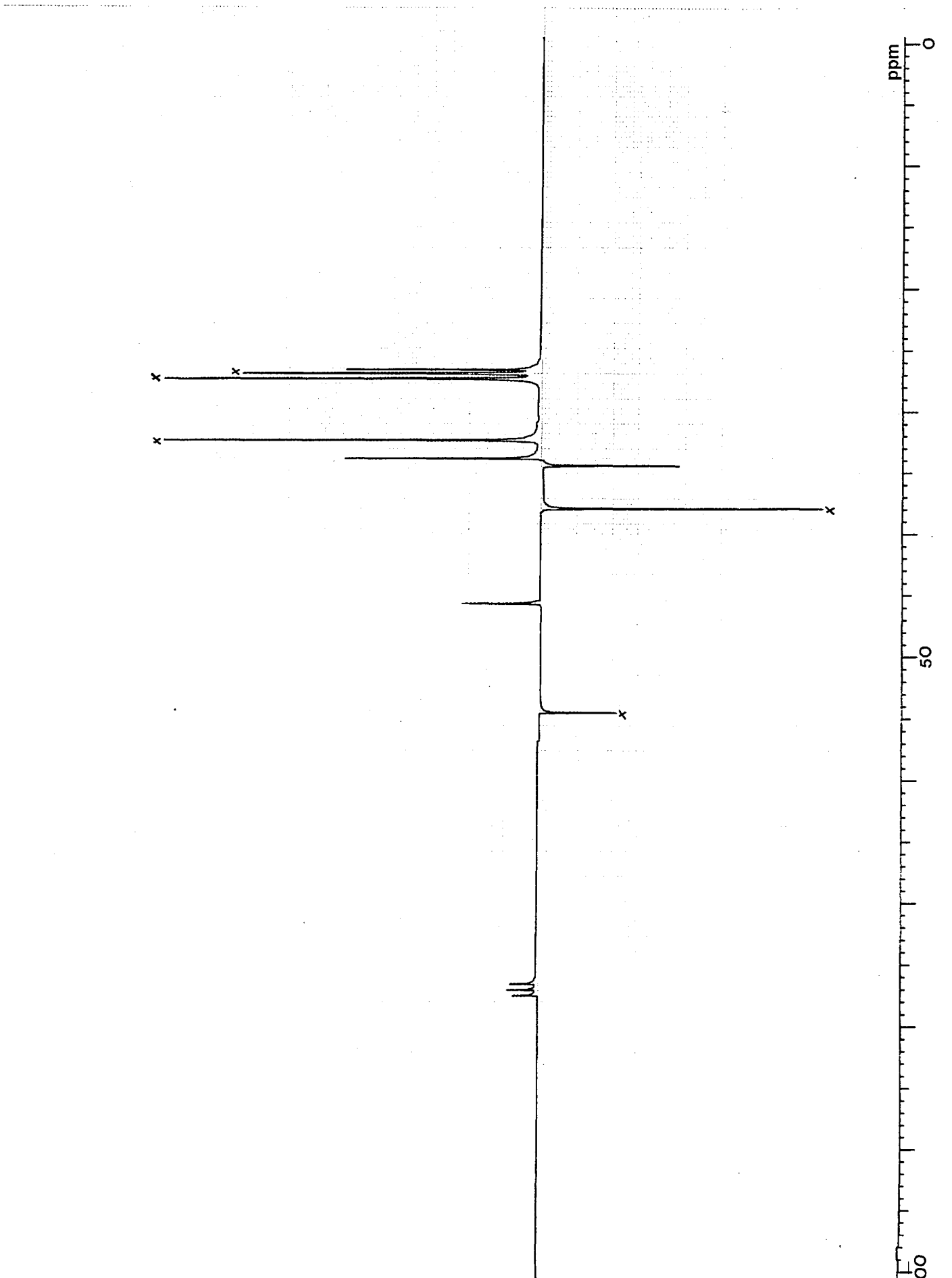

Fig. 4.4: The 67.83 MHz proton decoupled SEFT spectrum of the residue after recrystallization of tricyclohexylmethane synthesized using the Raney nickel / glass wool combination.

The stirred reaction itself presented some points of interest, since there were at least five detectable intermediates between triphenylmethane and tricyclohexylmethane in this case, and thus the reduction does not proceed with each aromatic ring being saturated stepwise[13], essentially at one go. Obviously it must be the steric requirements of the molecule, and its reduction intermediates, that gradually make complete reduction of a remaining aromatic ring more difficult. At least one must be a derivative of cyclohexene, or even cyclohexadiene. From the rate curves, it is evident that these intermediates cannot be directly obtained by restricting the hydrogen uptake.

A similar result appears in a more recent paper dealing with the hydrogenation of trypticene over palladium and ruthenium catalysts[14]. (At higher temperatures and pressures than were employed here). In this case the rigid bicyclic structure gave a large number of possible stereo-isomeric forms of the totally saturated product, eicosahydro-9,10[1',2']-benzenoanthracene, and of various partially saturated intermediates; and these were only isolated after extensive work.

The stirred reaction was not allowed to continue for more than 30 hours, and it was not determined whether the reduction to tricyclohexylmethane would eventually reach the same equilibrium as in the faster reaction. Presumably, eventually it would do so.

4.5 ATTEMPTS TO SYNTHESIZE TRICYCLOHEXYLMETHYLAMINE

Several attempts were made to synthesize tricyclohexylmethylamine, but without success. An amine of a similar type of symmetrical structure, amantadine, or 1-adamantyl amine[15], is one of the few drugs with a proven anti-viral action.

The synthesis of tert-alkyl amines is one of the more difficult chemical problems, and in this case the inherent instability of the tricyclohexylmethyl carbonium ion and the steric hindrance to any kind of nucleophilic substitution at the central carbon atom presented a challenge. Indeed, it might be that this amine is incapable of existing as a stable molecule.

One possibility was to synthesize tricyclohexylacetic acid, and obtain the required amine from the thermal rearrangement of the corresponding acyl azide - the Curtius reaction[16] - but an attempt to obtain tricyclohexylacetic acid by the catalytic hydrogenation of triphenylacetic acid failed using platinum oxide catalyst even at high pressure and temperature. This acid may be inaccessible by hydrogenation because of steric factors, although dicyclohexylacetic acid can be obtained by the same method[17].

Another experiment attempted the catalytic exchange of chloride ion from tricyclohexylmethylchloride with azide ion from sodium azide in the presence of zinc chloride[18], to give tricyclohexylmethylazide; the amine could then be obtained by hydrogenation of this. The results were negative. The interesting method of White and

Ellinger[19] using dimethylsulfamoyl chloride also failed, although the sodium alkoxide was apparently formed by reaction of tricyclohexylmethanol with sodium hydride without any concomitant dehydration.

In the end, the most promising approach seemed to be the Ritter reaction[20]. This involves generating the tricylohexylmethyl carbonium ion, and trapping it in situ with an appropriate nitrile. The resulting amide could then be hydrolyzed to give the amine. This method, with several variations quoted in the literature[21], is a standard synthesis of 1-adamantyl amine from adamantan-1-ol, where it works quite well. The reaction is outlined in Fig. 4.5.

An initial attempt to proceed directly from tricylclohexylmethanol by treating this with trifluoroacetic acid in the presence of excess acetonitrile (as a co-solvent with dichloromethane) failed, and only resulted in dehydrating the alcohol to give the alkene mentioned before, dicyclohexylcyclohexenylmethane. However, in view of the successful monodeuteration accomplished earlier by catalytic exchange of chloride and deuteride ions between tricyclohexylmethylchloride and triethylsilane-d_1, in which the desired carbonium centre was certainly involved, an approach starting from the chloride seemed a possibility. The paper of Bach et al.[22] reports several successful Ritter reactions using nitronium ions to generate carbonium centres by electrophilic abstraction of halide ions from organo-halides.

A solution of tricyclohexylmethylchloride in a mixture of dichloromethane and acetonitrile was cooled to -10 ^{0}C, under anhydrous conditions, and a molar equivalent of nitronium tetrafluoroborate added. There was an almost instantaneous generation of a vivid cherry red colour, which persisted for about 5 minutes, then changed to a blue/green colour for some time, and finally vanished to give a feintly yellow solution. Without the chloride present, a control experiment gave no colour changes. It is very likely that the bright red colour was due to the presence of the desired tricyclohexylmethyl carbonium ion, in some state of combination. The formation of brightly coloured carbonium salts (halochromism) occurs when some organohalides and alcohols, in particular triphenylmethanol, are treated with strong acids, and it is believed the same phenomenon occurred in this case. Neunhoeffer reported that tricyclohexylmethanol gave brick-red crystals of a chromate salt when stirred in solution with chromic anhydride[4]. No such colours were observed in any of the other reactions involving tricyclohexylmethylchloride, or the parent methanol. Also, the tricyclohexylmethyl free radical (described in Chapter 5) was apparently not coloured either.

Thus there was some evidence for the generation of the tricyclohexylmethyl carbonium ion as a persistent entity under these conditions. Neutralization of the reaction, and evaporation of the solvents produced a brown glassy solid, quite unlike either the original chloride, or the alkene produced by simple solvolysis of the chloride

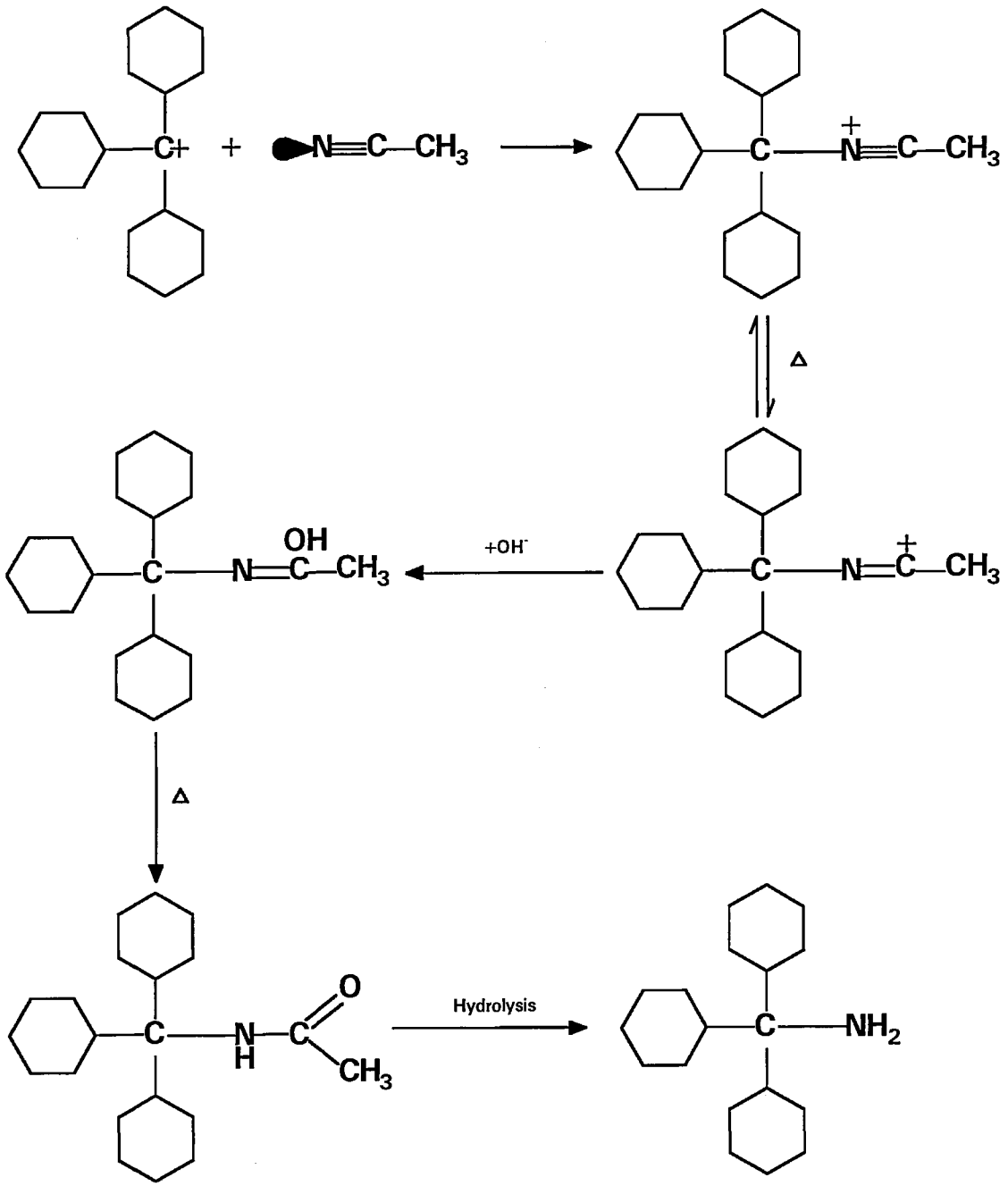

Fig. 4.5: Outline of the proposed synthesis of tricyclohexylmethylamine using a Ritter reaction

as described earlier. Analysis by proton NMR indicated the presence of cyclohexyl structures, but no further detail could be established. Attempts at crystallization were unsuccessful. The material was hydrolyzed by boiling for 2 hours in alcoholic potassium hydroxide, but the solution darkened considerably, and unfortunately no identifiable products could be isolated from the resulting viscous residue.

Despite this unhappy outcome, the method seems worth investigating. It may be possible to employ nitrosonium ion to displace the chloride ion from the substrate[23], in which case possible oxidative damage to the tricyclohexyl structure would be minimized. The use of dichloromethane to facilitate the solution of the tricyclohexylmethylchloride might have interfered with the course of the trapping of the carbonium centre by the acetonitrile. It may be possible simply to use a suspension of the chloride in acetonitrile. (cf. the deuteration reaction in Section 4.3). Using hydrogen cyanide as the nitrile nucleophile would reduce factors of steric hindrance and lead to greater ease of hydrolysis of the resulting amide produced. Finally, an acid catalyzed hydrolysis might be preferable.

4.6 DICYCLOHEXYL ETHER

It was thought this compound might be required, and accordingly the procedure for its synthesis was determined. The obvious route was the catalytic hydrogenation of diphenyl ether, but this is impractical using the usual catalysts because of the extensive hydrogenolysis of the ether linkage that occurs during the attempt. However the paper of Takagi et al.[24], details the remarkable success attained in the perhydrogenation of this and several related substrates using rhodium and ruthenium hyroxide blacks, and their procedure was used here:

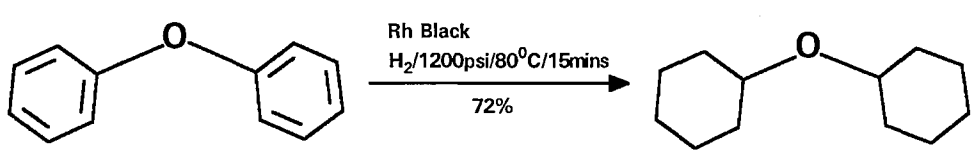

Dicyclohexyl ether: Rhodium(II) chloride (100 mg) was dissolved in 10 ml of distilled water and warmed in an oil bath to 90 ^{0}C. About 1 ml of 10% sodium hydroxide solution (2g, 50 mmol, in 20 ml of distilled water) was then added drop wise to the vigorously stirred chloride solution. The red colour of the chloride vanished and a fine yellow precipitate of rhodium hydroxide formed. This was filtered off under gravity, washed well with distilled water and dried over silica gel in a vacuum desiccator. The dried lumps were crushed to give a fine powder.

A solution was made of 5 g (29 mmol) of diphenyl ether in 40 ml of cyclohexane and placed in a Parr pressure vessel. A few drops of glacial acetic acid were then added, together with 25 mg of the prepared rhodium hydroxide catalyst, and the reaction hydrogenated at 1200-1500 psi and 80 ^{0}C for 15 minutes, with magnetic stirring. The catalyst, now changed to a black powder, was filtered from the solution and removal of the solvent gave a colourless oil. Analysis by GC showed a large proportion of a new product with a retention time about 1 minute less than phenyl ether, together with some cyclohexanol and traces of other products. Distillation under water pump vacuum gave 3.8 g of cyclohexyl ether boiling at 147-160 ^{0}C. Carbon-13 and proton NMR spectra agreed with those expected for dicyclohexylether, and purity by GC analysis was >95%. Fractional distillation would be necessary to obtain an analytical sample. Yield: 72%. The material is a limpid liquid, with a peculiar sweet smell.[25]■

REFERENCES FOR CHAPTER 4

[1] R. Adams and R. L. Shriner, *J. Am. Chem. Soc.*, 1923, **45**, 2171; R. Adams and J. R. Marshall, *J. Am. Chem Soc.*, 1928, **50**, 1970

[2] H. Adkins, W. H. Zartman, and H. Cramer, *J. Am. Chem. Soc.*, 1931, **53**, 1425

[3] W. H. Zartman and H. Adkins, *J. Am. Chem. Soc.*, 1932, **54**, 1668

[4] O. Neunhoeffer, *Liebigs Anal.*, 1934, **509**, 115

[5] P. D. Bartlett and A. Schneider, *J. Am. Chem. Soc.*, 1945, **67**, 141

[6] H. C. Brown, *Boranes in Organic Chemistry*, Cornell University Press, 1972

[7] H. C. Brown and B. A. Carlson, *J. Org. Chem.*, 1973, **38**, 2422; H. C. Brown, J-J. Katz, and B. A. Carlson, *J. Org. Chem.*, 1973, **38**, 3968; H. C. Brown, B. A. Carlson, and R. H. Prager, *J. Am. Chem. Soc.*, 1971, **93**, 2070

[8] B. A. Carlson and H. C. Brown, *Organic Synthses*, Coll. Vol. **VI**, 137

[9] R. M. Carman and I. M. Shaw, *Aust. Jour. Chem.*, 1976, **29**, 133

[10] M. P. Doyle, C. C. McOsker, and C. T. West, *J. Org. Chem.*, 1976, **41**, 1393

[11] M. Arai, Y. Ikushima, and Y. Nishiyama, *Bull. Chem. Soc. Jpn.*, 1986, **59**, 347

[12] T. Shimada, R. Hirose, and K. Morihara, *Bull. Chem. Soc. Jpn.*, 1994, **67**, 227, and a series of previous papers referred to therein.

[13] Compare this with results based on hydrogen uptake and fractional distillation in the 1949 paper of H. A. Smith, D. M. Alderman, C. D. Shacklett and C. M. Welch, *J. Am. Chem. Soc.*, 1949, **71**, 377

[14] M. Farina, C. Morandi, E. Mantica, and D. Botta, *J. Org. Chem.*, 1977, **42**, 2399, and a sequence of related papers by these authors on this subject

[15] J. Kirschbaum, *Analytical Profiles of Drug Substances*, 1983, **12**, 1-36

[16] C. Kaiser and J. Weinstock, *Organic Syntheses*, **51**, 48

[17] H. A. Smith, D. M. Alderman, C. D. Shacklett, and C. M. Welch, *J. Am. Chem. Soc.*, 1949, **71**, 377

[18] J. A. Miller, *Tet. Lett.*, 1975, **34**, 2959

[19] E. H. White and C. A. Ellinger, *J. Am. Chem. Soc.*, 1965, **87**, 5261

[20] N. W. Werner and J. Casanova Jr., *Organic Syntheses*, Coll. Vol. **V**, 273

[21] A. Kalir and D. Balderman, *Organic Syntheses*, **60**, 104

[22] R. D. Bach, J. W. Holubka, and T. A. Taaffer, *J. Org. Chem.*, 1979, **44**, 1739

[23] G. A. Olah, B. G. B. Gupta, and S. Narang, *Synthesis*, April 1979, 274

[24] Y. Takagi, T. Naito, and S. Nishimura, *Bull. Chem. Soc. Jap.*, 1965, **38**, 2119; see also S. Nishimura, *Bull. Chem. Soc. Jap.*, 1961, **34**, 1544; Y. Yokoyama, H. Mabuchi, H. Shoji, and N. Saito, *Bull. Chem. Soc. Jap.*, 1963, **36**, 353

[25] W. Ipatiew and O. Philipow, *Ber.*, 1908, **41**, 1001

NMR SPECTRA

TRICYCLOHEXYLMETHANE AND TRICYCLOHEXYLMETHANE-d_1

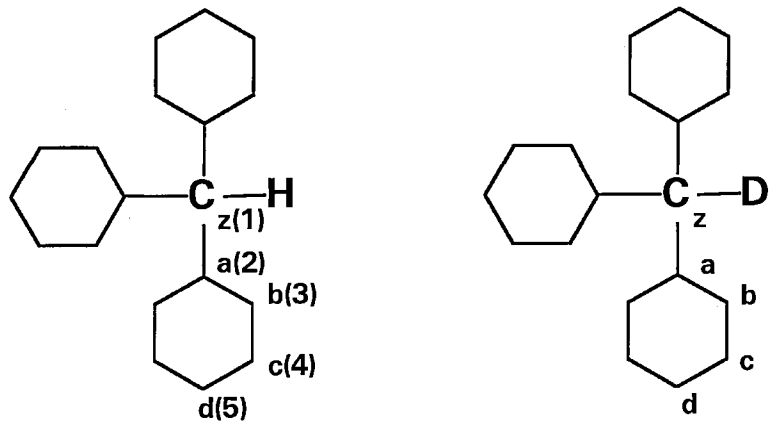

Spectrum 4.1 is the proton decoupled carbon-13 spectrum of tricyclohexylmethane, and the easy assignment of the resonances is as given in the paper published on the compound; position **z**, 54.453 ppm; **a**, 37.895 ppm; **b**, 32.310 ppm; **c**, 27.241 ppm; **d**, 26.809 ppm. Spectrum 4.2 is the corresponding off-resonance proton decoupled carbon-13 spectrum, which confirms these assignments. Spectrum 4.3, shows the proton decoupled carbon-13 spectrum of the corresponding isotopomer, tricyclohexylmethane-d_1. At 53.812 ppm one can observe the small triplet from the central deuterium labelled carbon atom, **z**. Just next to it, and slightly downfield, one sees the tiny residual peak arising from a small percentage of protonated carbon atoms in position **z**. This is present in this case because some of the deuterons have been incorporated during the synthesis at the neighbouring tertiary positions, **a**, in the molecule; a consequence of the special structural features in this molecule. The corresponding labelling at the **a** carbon atoms is masked in the spectrum by the large resonances of the protonated atoms. Otherwise, the rest of the spectrum is as in that of the un-labelled compound.

The carbon atoms are also numbered in the order in which their resonances appear in the standard spectrum, starting from the low field end.

Spectrum 4.4 is the proton spectrum of tricyclohexylmethane, shown expanded as Spectrum 4.5. Proton **z**, appears as a quartet at 0.74 ppm, coupled to the adjoining **a** protons on the three cyclohexyl rings. These three axial protons, **a**, appear as (triply coincident) doublets of triplets centred at 1.46 ppm, near to the equatorial proton resonances. This splitting can be analyzed in terms of couplings to proton **z** and two equivalent equatorial ring protons, of about 4 Hz each, and a larger coupling of about 12 Hz to two equivalent axial ring protons. The remaining axial protons of the

cyclohexyl rings appear at 1.0-1.3 ppm, and the equatorial protons at 1.5-1.8 ppm. The coupling of 4 Hz between the **z** and **a** protons indicates that the torsional motions of the cyclohexyl rings about the bonds to the central atom are restricted, even in solution. What kind of average conformation this corresponds to, and the nature of the internal motions present in this molecule in the liquid state, are problems taken up in Chapter 8 along with the analyses of the NMR relaxation measurements.

Spectrum 4.6 is the proton spectrum of tricyclohexylmethane-d_1, and an expansion appears as Spectrum 4.7. One sees the resonance from the central methine proton at 0.74 ppm is essentially absent, as expected. A tiny residual resonance appears (starred) from the remaining protonated positions that were noted above in the carbon-13 spectrum. It is also possible to see the collapse of the original splitting pattern in the resonances that remain for the **a** proton positions, at 1.46 ppm, due to the removal of part of the coupling system. There are also some small changes in the other resonances in the spectrum, which cannot be interpreted easily, and which probably result from a combination of deuteration shifts and changes in coupling constants.

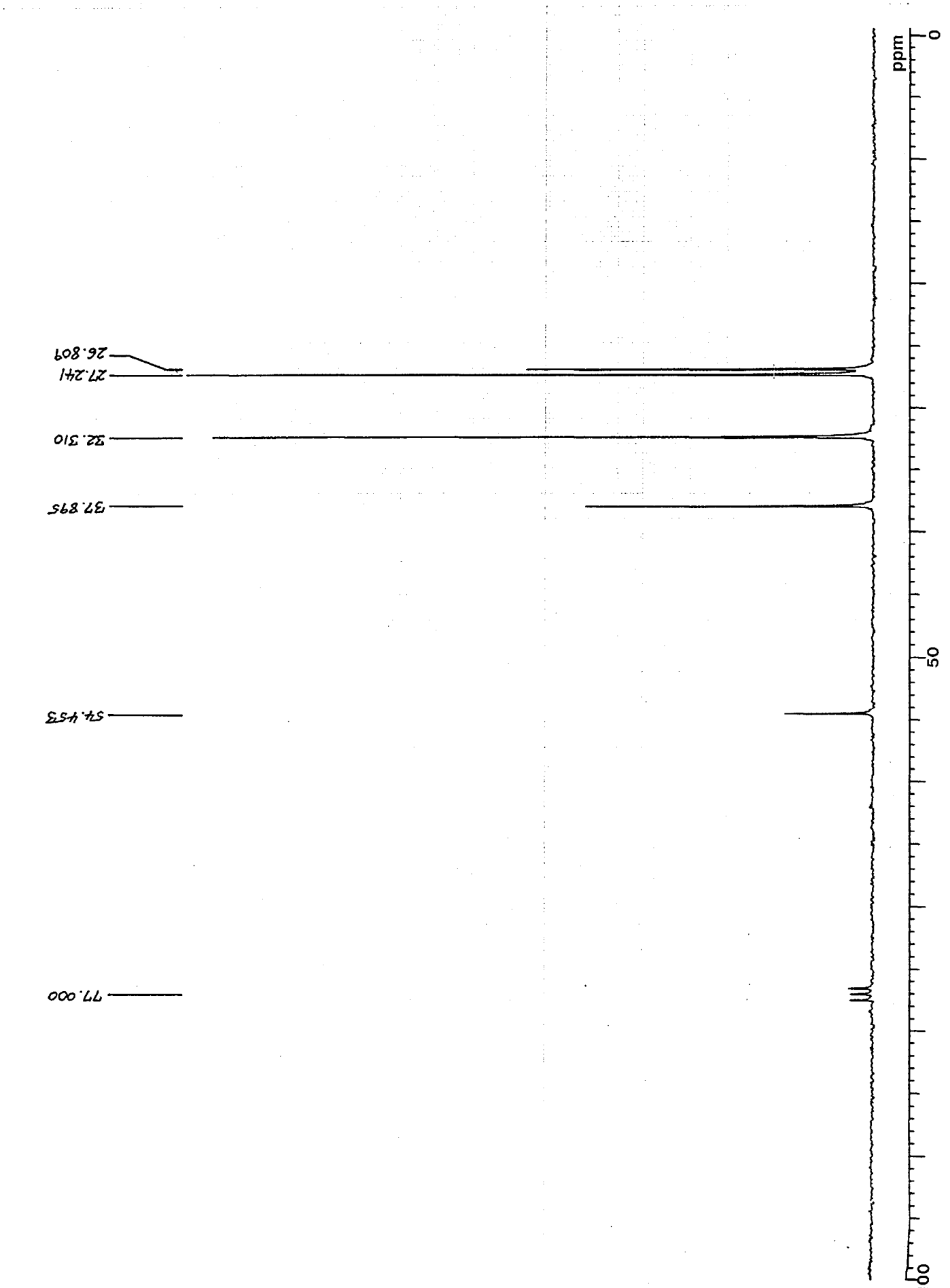

4.1: The 67.83 MHz proton decoupled carbon-13 spectrum of tricyclohexylmethane.

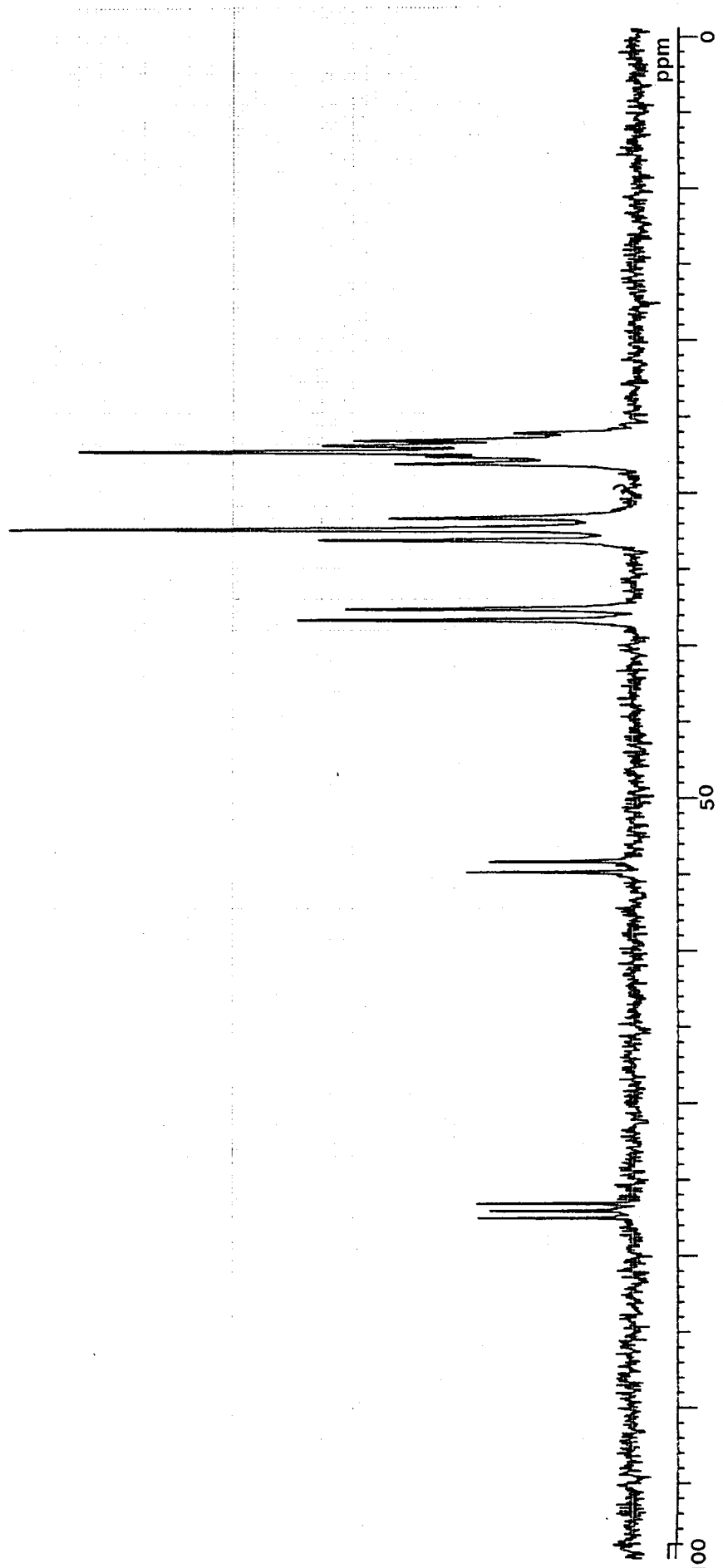

4.2: The 67.83 MHz off-resonance decoupled carbon-13 spectrum of tricyclohexylmethane.

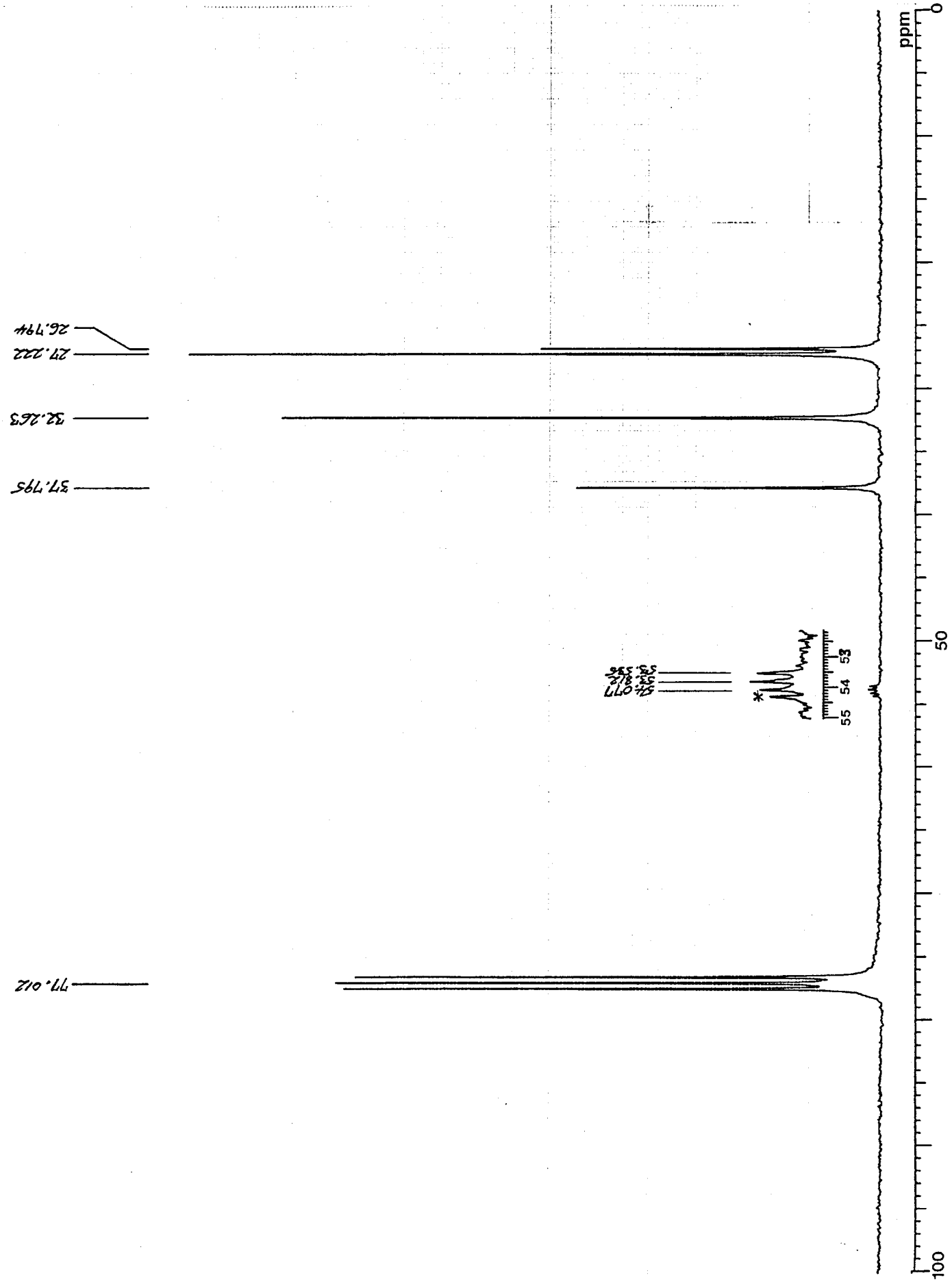

4.3: The 67.83 MHz proton decoupled carbon-13 spectrum of tricyclohexylmethane-d_1.

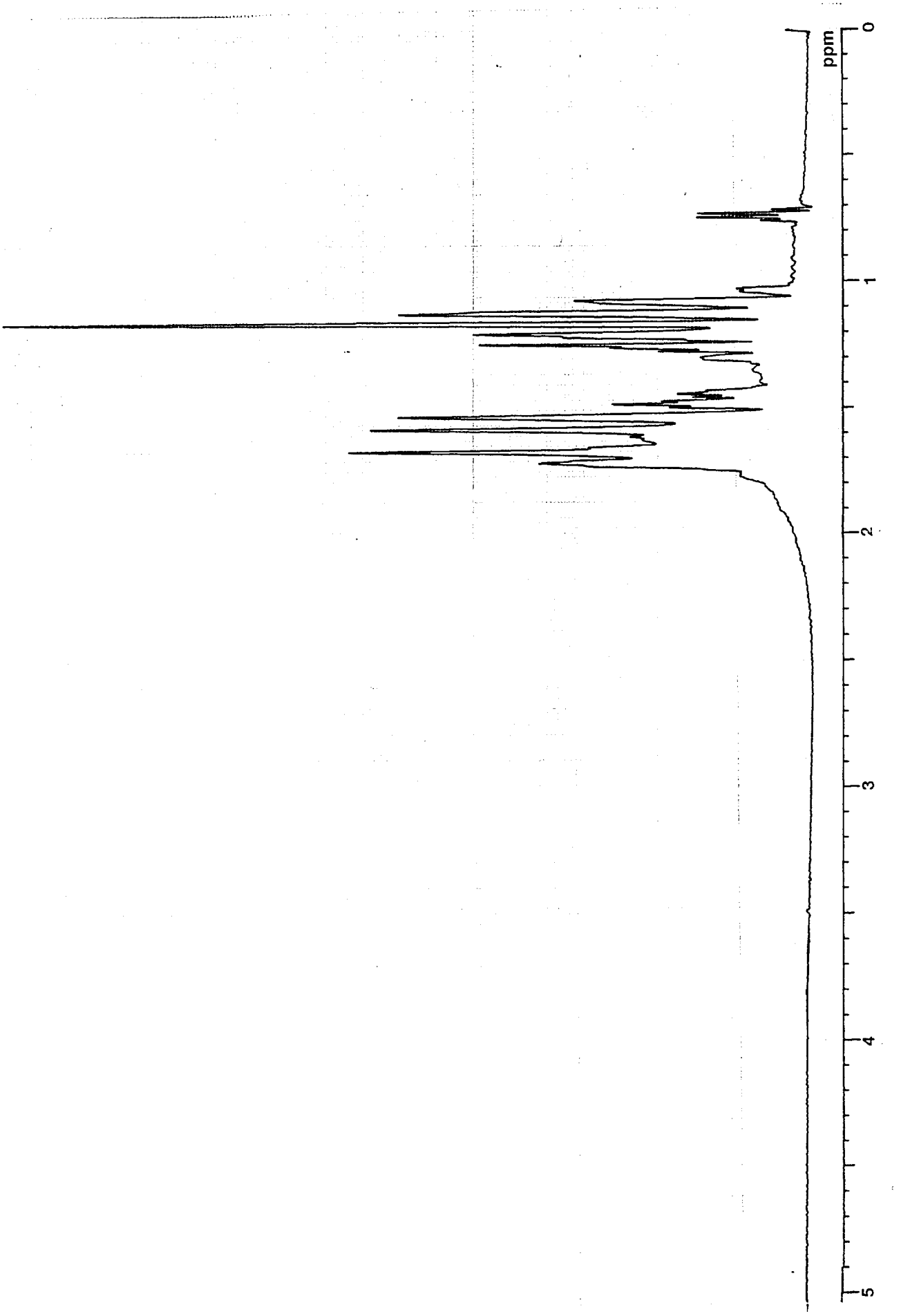

4.4: The 269.7 MHz proton spectrum of tricyclohexylmethane.

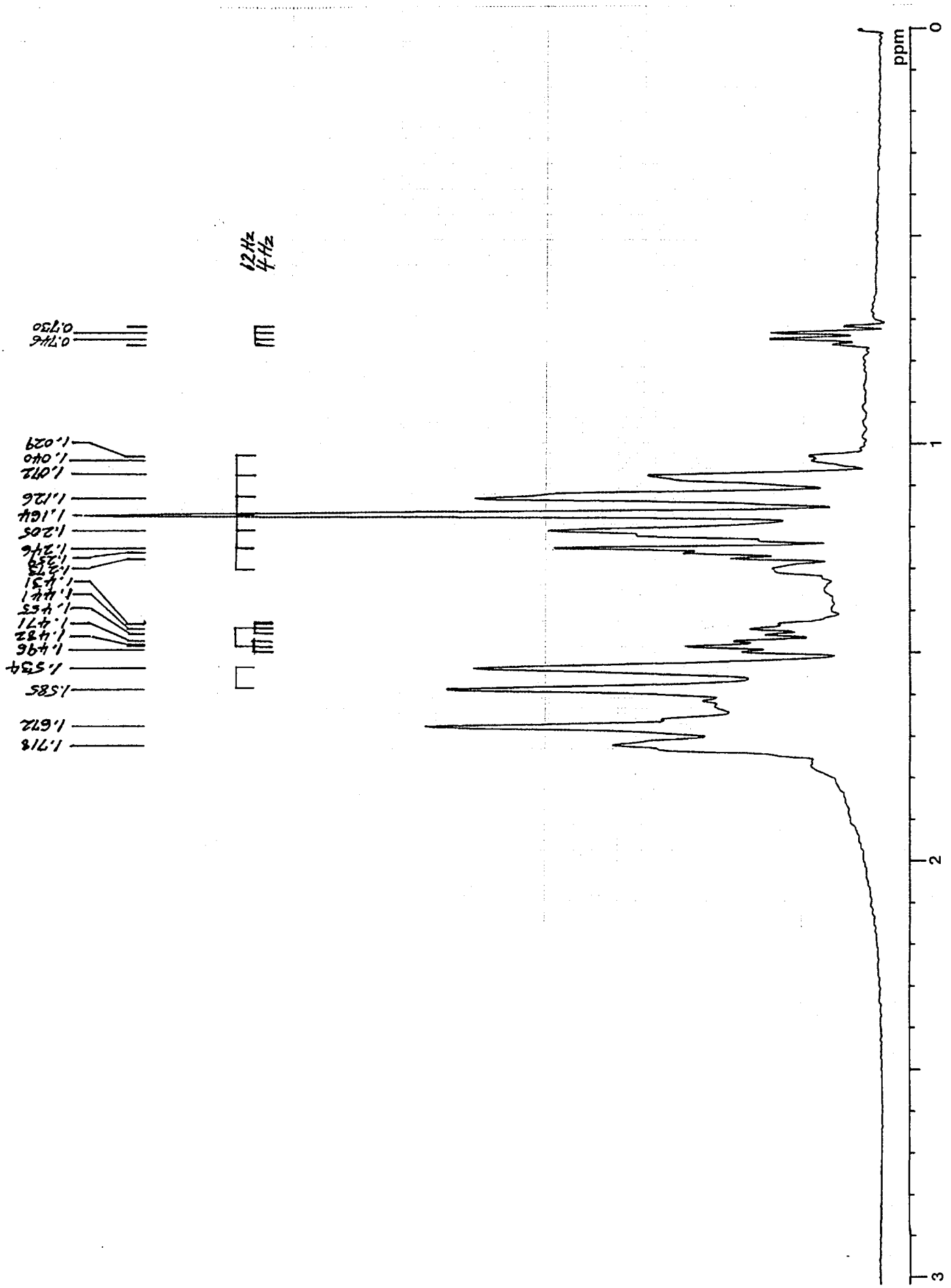

4.5: The 269.7 MHz proton spectrum of tricyclohexylmethane (expansion).

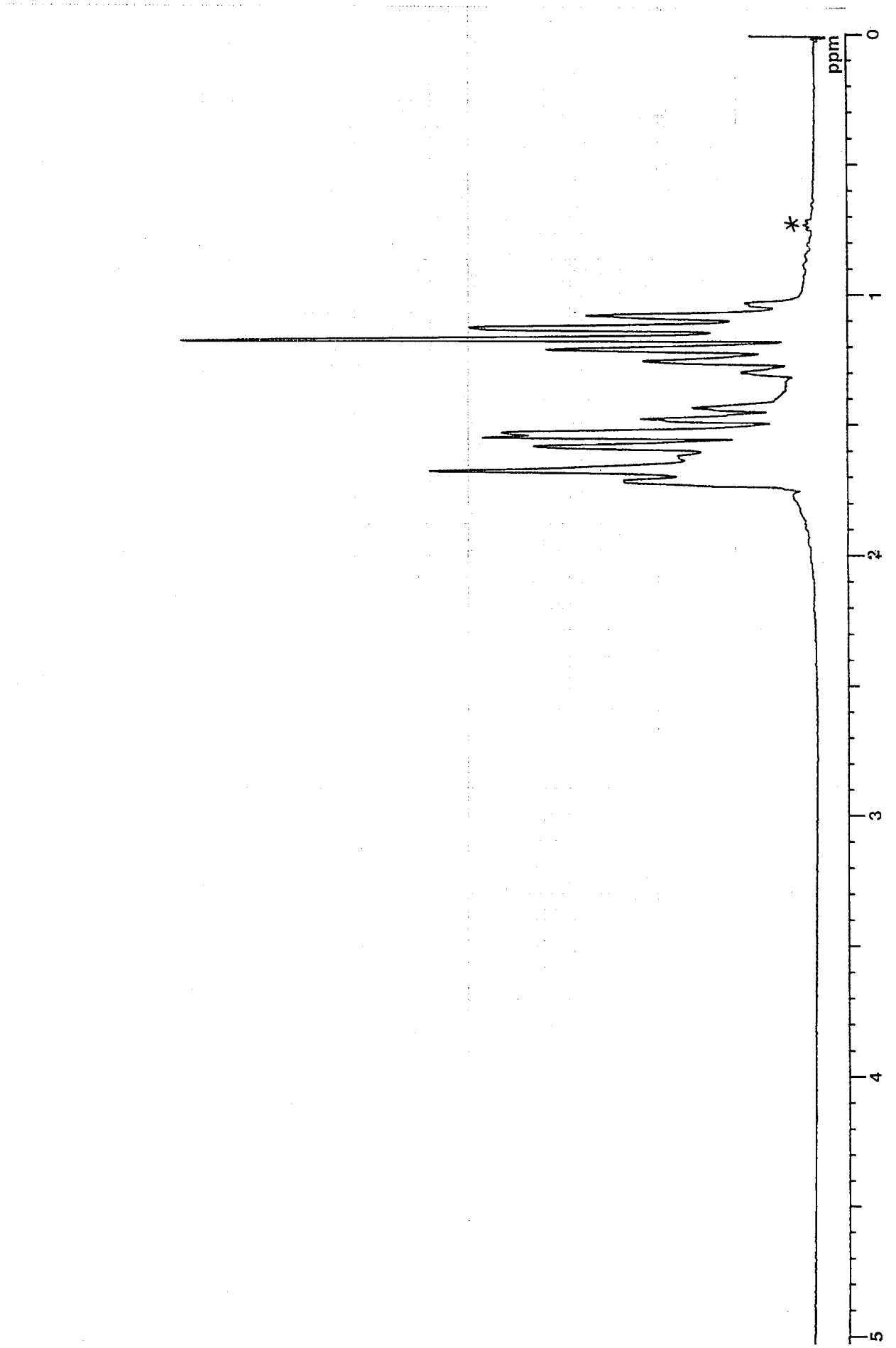

4.6: The 269.7 MHz proton spectrum of tricyclohexylmethane-d_1.

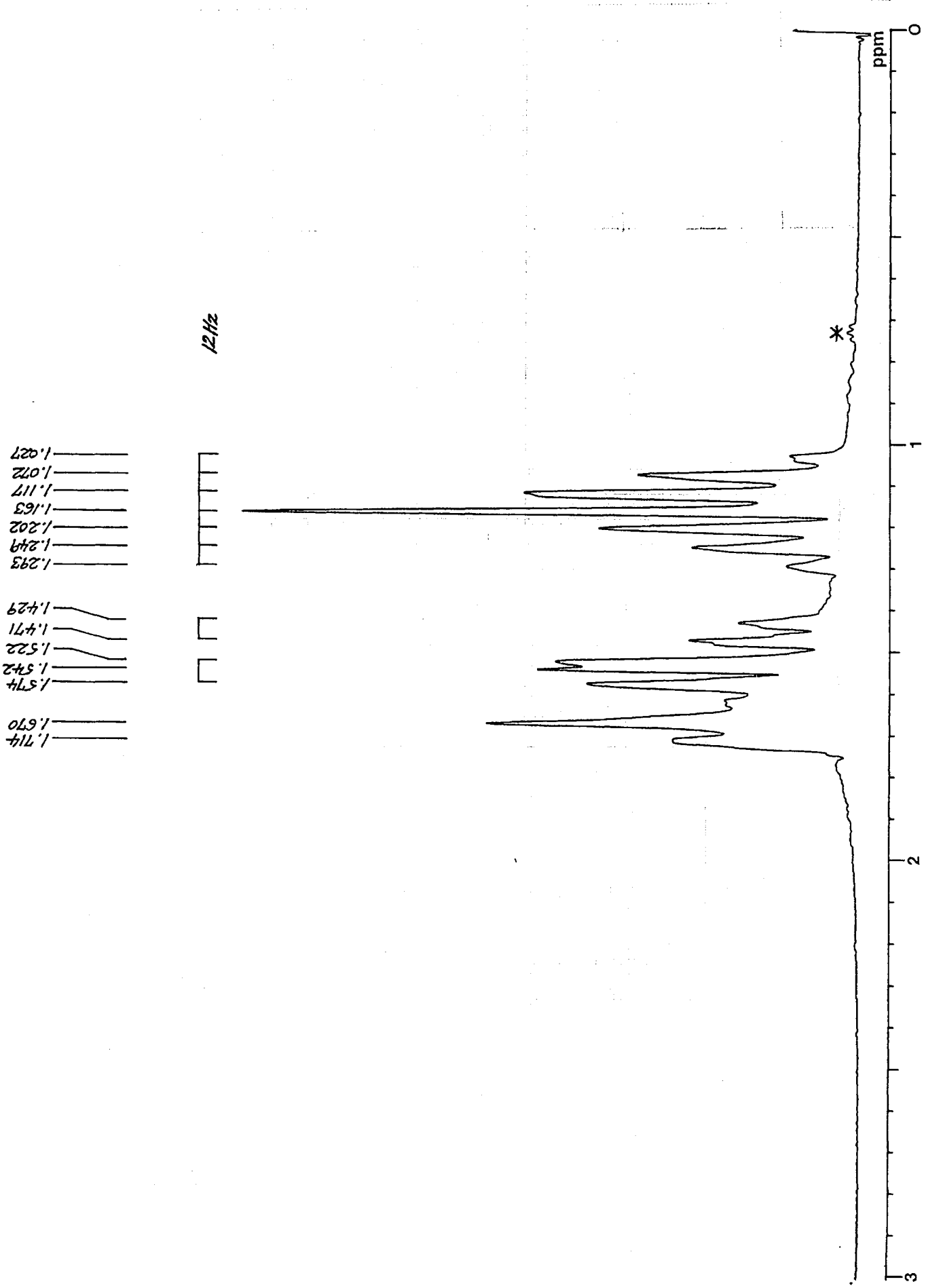

4.7: The 269.7 MHz proton spectrum of tricyclohexylmethane-d_1 (expansion).

TRICYCLOHEXYLMETHANOL AND TRICYCLOHEXYLMETHYLCHLORIDE

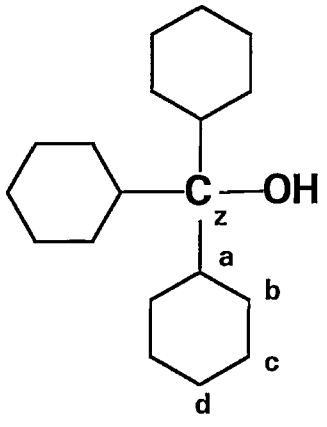

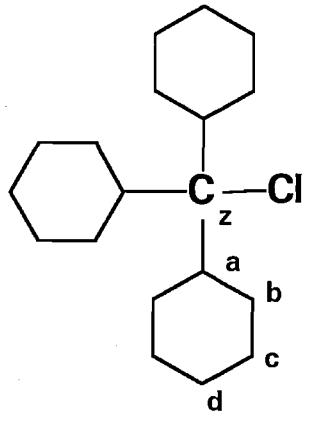

Spectrum 4.8 is the proton decoupled carbon-13 spectrum of tricyclohexylmethanol, which can be assigned as follows; position **z**, 77.781 ppm; **a**, 44.008 ppm; **b**, 28.331 ppm; **c**, 27.449 ppm; **d**, 26.019 ppm. One notes the expected downfield shift of carbons **a**, as compared with tricyclohexylmethane, and a small upfield shift in carbons **c**. Spectrum 4.9 shows the proton decoupled SEFT spectrum, with delay τ = 8 ms, in which the phases of the resonances confirm these assignments.

The proton spectrum, 4.10, has no distinguishing features, except for the usual division into axial and equatorial resonances. The three axial protons in positions **a** probably belong to the downfield resonances, as they do even in tricyclohexylmethane.

Spectrum 4.11 is the proton decoupled carbon-13 spectrum of tricyclohexylmethylchloride, which is very similar to the parent alcohol, and can be assigned as follows; position **z**, 90.811 ppm; **a**, 46.553 ppm; **b**, 29.995 ppm; **c**, 27.600 ppm; **d**, 26.743 ppm.

Spectrum 4.12 is the proton spectrum of tricyclohexylmethylchloride. The resonances can be assigned to axial (1.1 - 1.4 ppm) and equatorial (1.6 - 2.0 ppm) proton positions in the cyclohexyl rings; except that the three axial protons in positions **a** will again belong to the downfield portion of the spectrum. The resonance at 0.74 ppm in the spectrum of tricyclohexylmethane is, of course, absent in the proton spectra of tricyclohexylmethanol and tricyclohexylmethylchloride.

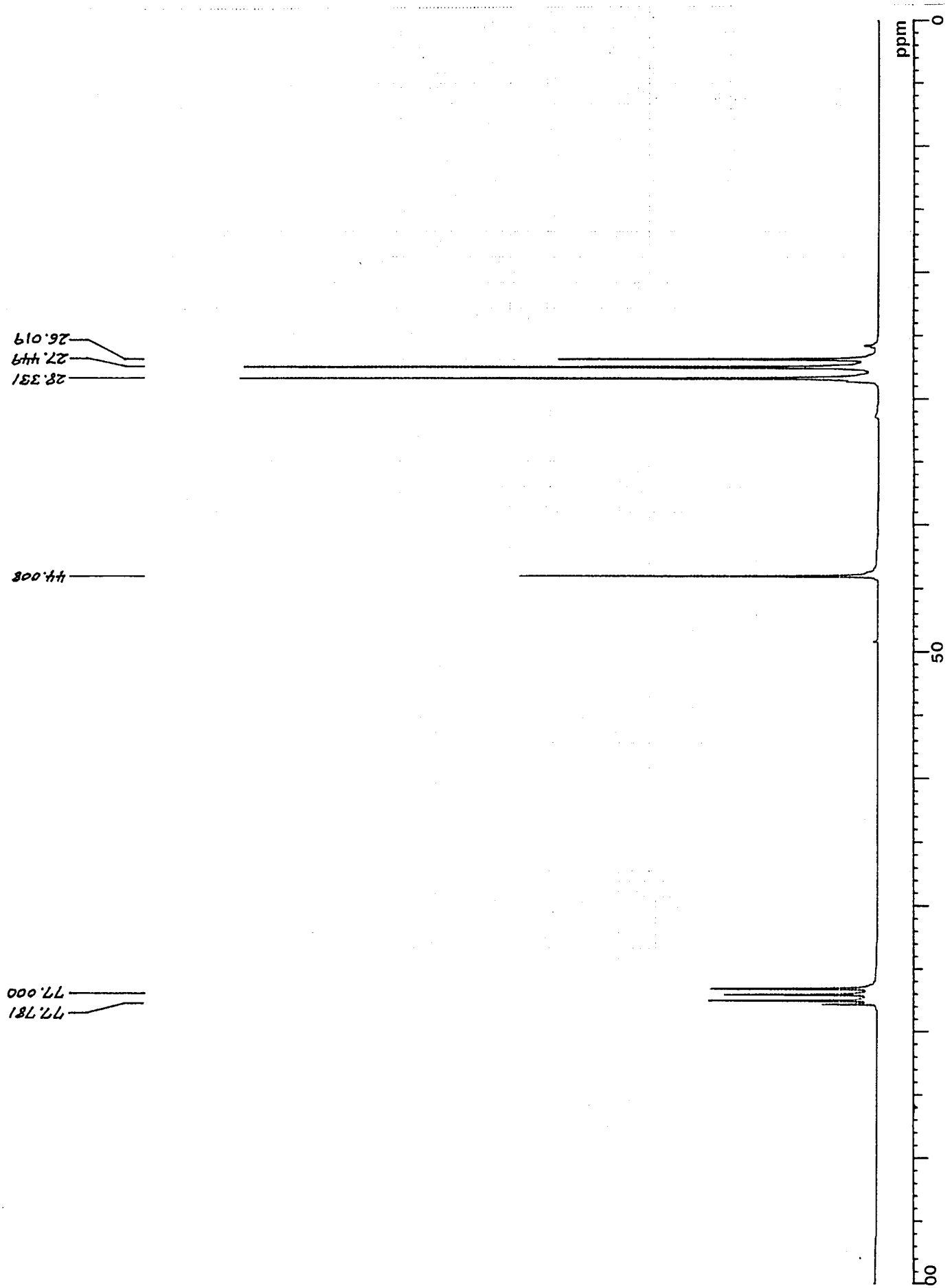

4.8: The 67.83 MHz proton decoupled carbon-13 spectrum of tricyclohexylmethanol.

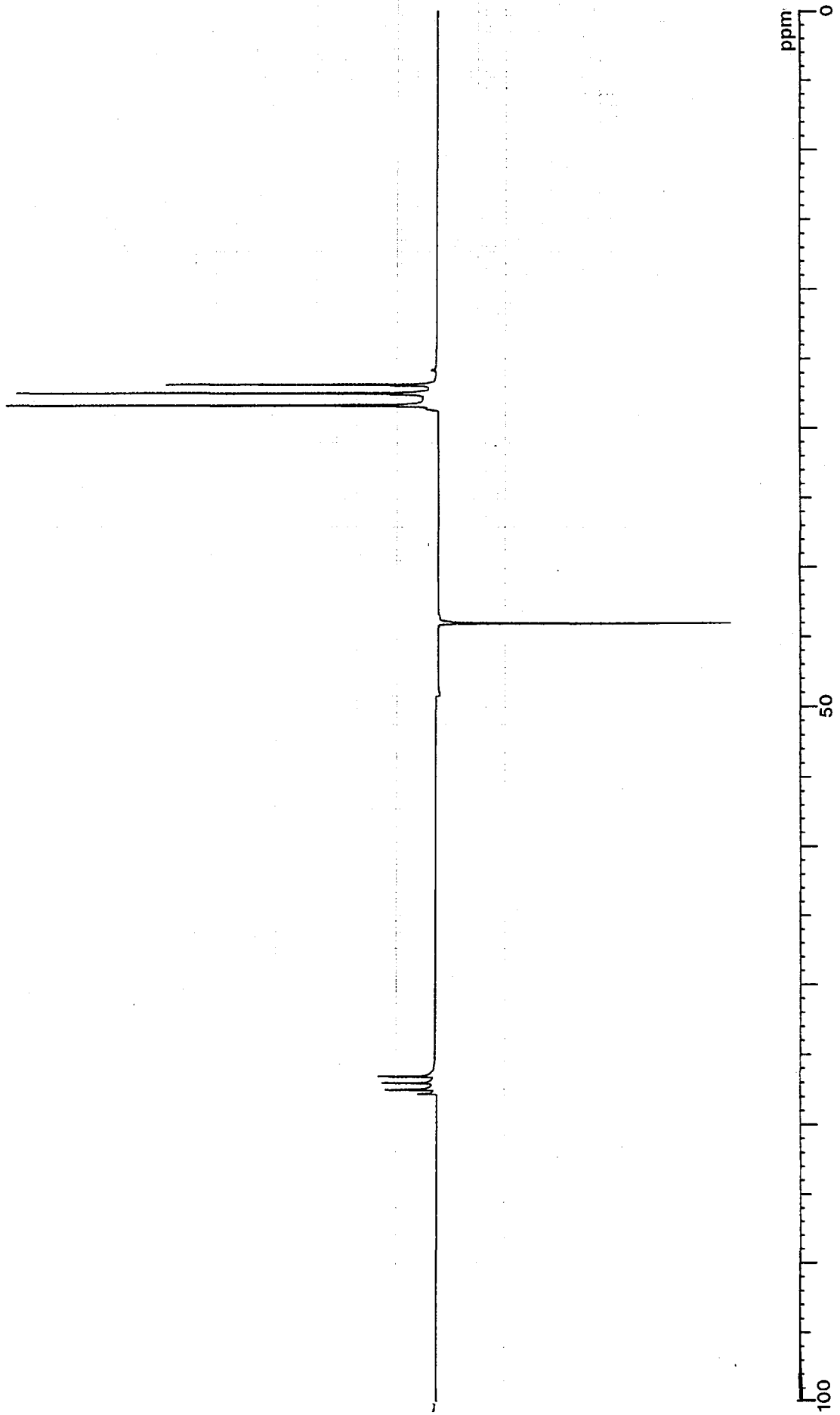

4.9: The 67.83 MHz proton decoupled SEFT spectrum of tricyclohexylmethanol.

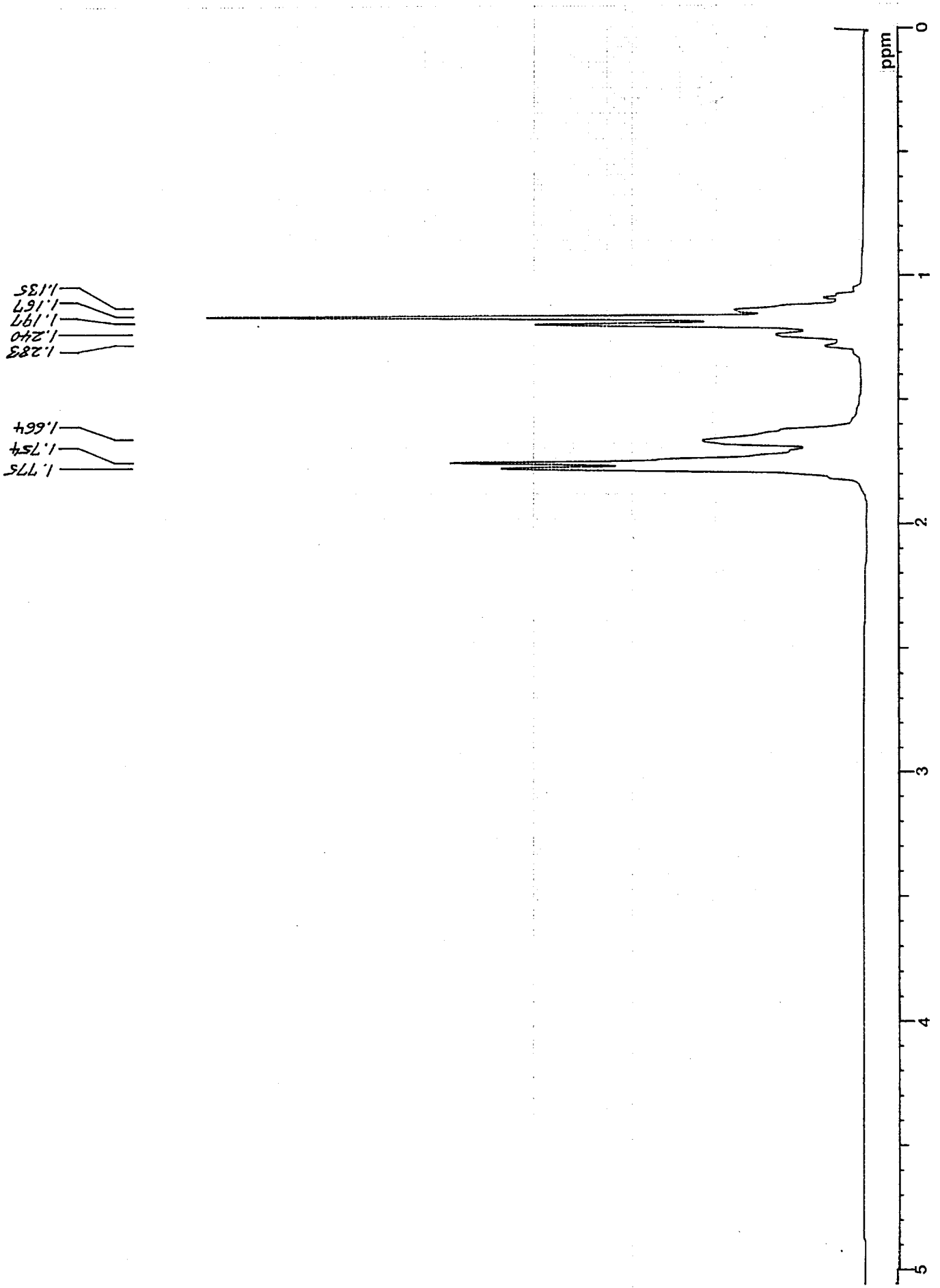

4.10: The 269.7 MHz proton spectrum of tricyclohexylmethanol.

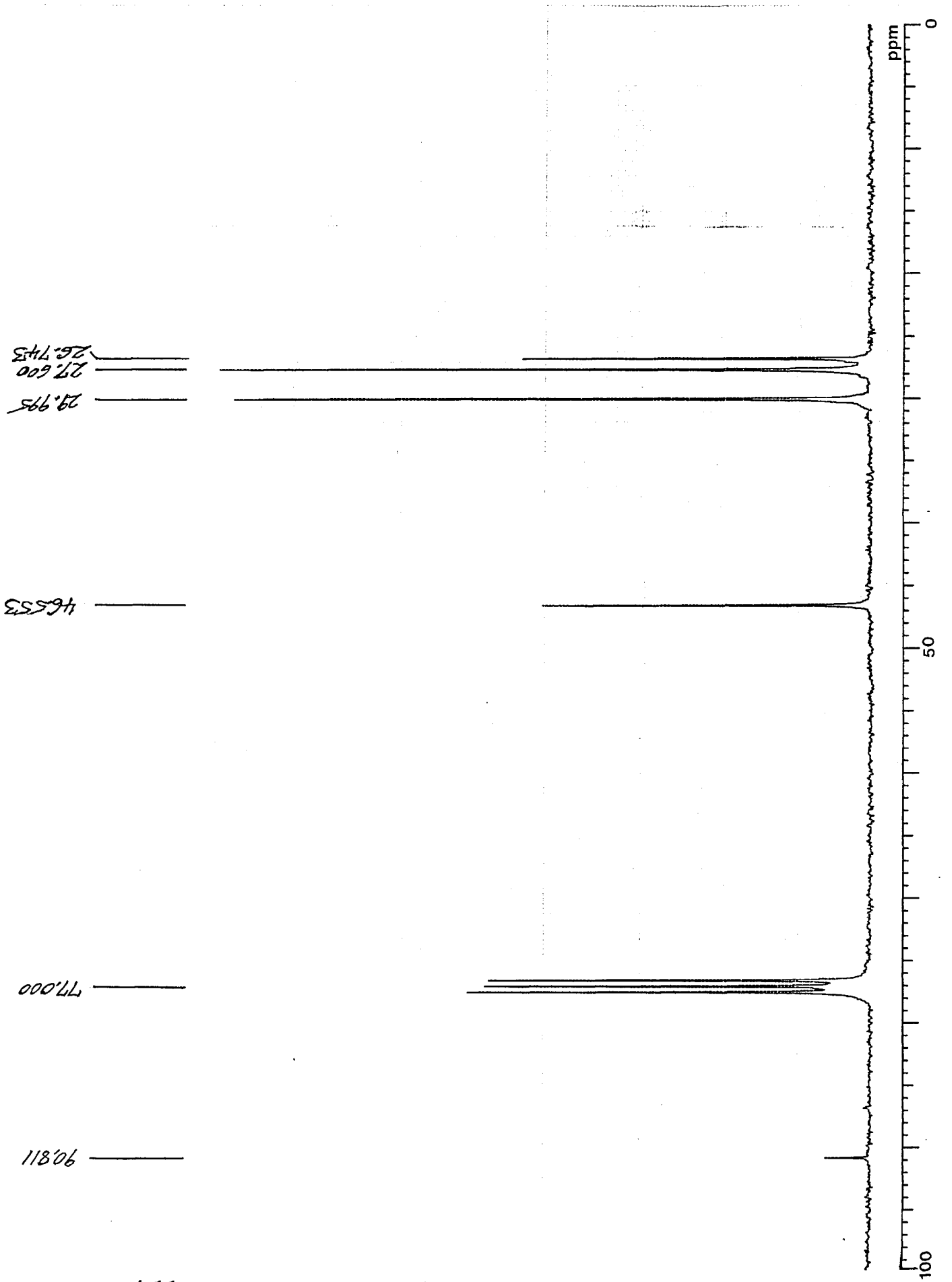

4.11: The 67.83 MHz proton decoupled carbon-13 spectrum of tricyclohexylmethylchloride.

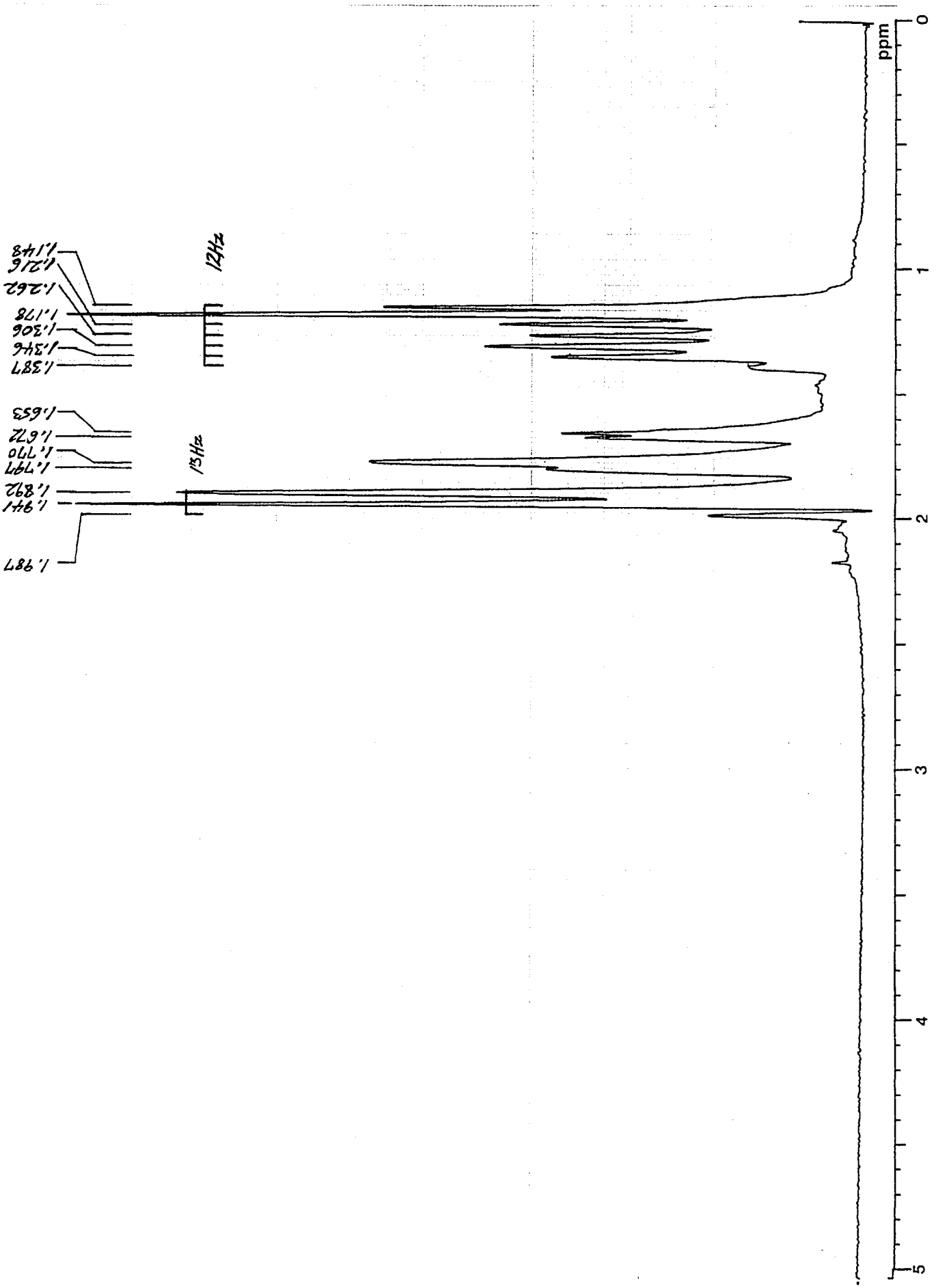

4.12: The 269.7 MHz proton spectrum of tricyclohexylmethylchloride.

DICYCLOHEXYLCYCLOHEXENYLMETHANE

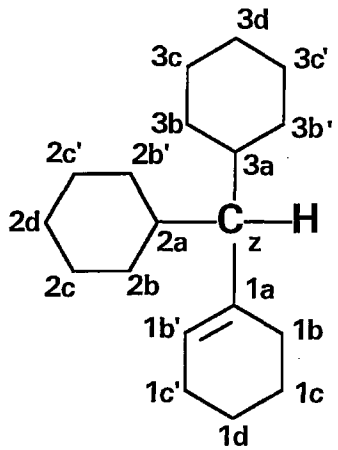

The product of the slow solvolysis of tricyclohexylmethylchloride in chloroform solution was identified using a combination of 1D and 2D NMR spectroscopy. Although the structure had been suspected by Neunhoeffer, these NMR results confirmed it.

Spectrum 4.13 shows the proton decoupled carbon-13 spectrum of the compound, while Spectrum 4.14 is an off-resonance decoupled spectrum. At once, one can suspect the presence of a single double bond in the molecule, from the two resonances far downfield, at 123.123 and 138.220 ppm; and also its position, since from the off-resonance decoupled spectrum it is apparent that one carbon is protonated, and the other, further downfield, is not. The likeliest possibility, given the compound's origin from tricyclohexylmethane, is the indicated structure, assigning carbon **1a** at 138.220 ppm, and carbon **1b'** at 123.123 ppm. Following on from this, one can also assign the central carbon **z** to the methine resonance at 58.450 ppm (similar to tricyclohexylmethane) and the two methine carbons **2a** and **3a** to the resonance at 37.581 ppm.

Spectrum 4.15 is the proton NMR spectrum, and shows a complicated pattern of cycloaliphatic resonances from 0.8 to 1.8 ppm. However a single peak appears at 5.25 ppm, belonging to proton **1b'**. One notes the broad appearance and lack of resolved splittings of this proton in a cyclohexenyl ring. Two similar features appear at 2.00 and 1.84 ppm, each about twice the area of the resonance at 5.25 ppm. One can assign these to the protons at positions **1b** and **1c'**.

These assignments were confirmed by a (proton decoupled) carbon-13-proton correlation spectrum at 7.05 T, Spectrum 4.16. Carbon **1b'** correlates to the resonance at 5.25 ppm as expected, and carbons **z**, **2a** and **3a** correlate to single resonances at about 1.46 ppm. The single features at 2.00 and 1.84 ppm correlate to the small carbon resonances at 25.408 and 29.894 ppm respectively, which do not have the usual axial/equatorial proton correlation pattern apparent for the other

carbon resonances in this region. Thus one can assign these two resonances, and the corresponding proton features, to the carbons **1b** and **1c'** of the cyclohexenyl ring, probably in this order. The remaining two carbons of the cyclohexenyl ring appear at 23.391 and 22.912 ppm, again correlated to only a single proton region at 1.53 ppm.

The remaining resonances of the two cyclohexyl rings are left, displaying a pattern also seen later in phenyldicyclohexylmethane, with equivalent pairs of carbons **2b/3b** and **2b'/3b'**, at 32.162 and 30.222 ppm, in some order, and carbons **2c/3c**, **2c'/3c'**, **2d**, and **3d**, squashed together at 26.95 ppm. The corresponding axial and equatorial proton resonances appear as expected. The approximate integrals of the various portions of the proton spectrum were close to those required for the structure.

The equivalences that occur in the carbon-13 resonances of the cyclohexyl rings can be expected to be as indicated, rather than between similar positions in each individual ring, from simple consideration of the diastereomeric possibilities resulting from the substitution pattern of the central carbon position, **z**. Thus, for example, one expects the equivalence **2b/3b**, rather than **2b/2b'**. The existence of further equivalence in the simpler spectra of the tricyclohexylmethyl derivatives is an interesting problem, apparently related nature of the internal motions and the resultant averaging of conformations in these molecules. In the case of 1,1,2-tricyclohexylethane, mentioned later in this section, one cyclohexyl ring shows the pattern of extra equivalences, while the other two, with a pattern of equivalence similar to that found in the two cyclohexyl rings of the present example, do not. These questions are discussed further in Chapter 8.

Overlap of the central proton resonance at 1.46 ppm precludes obtaining any information about the angular motion of the cyclohexyl and cyclohexenyl groups in this molecule from the coupling constants of the central **z** proton, but once again it seems likely that they are restricted some way, as was the case in tricyclohexylmethane.

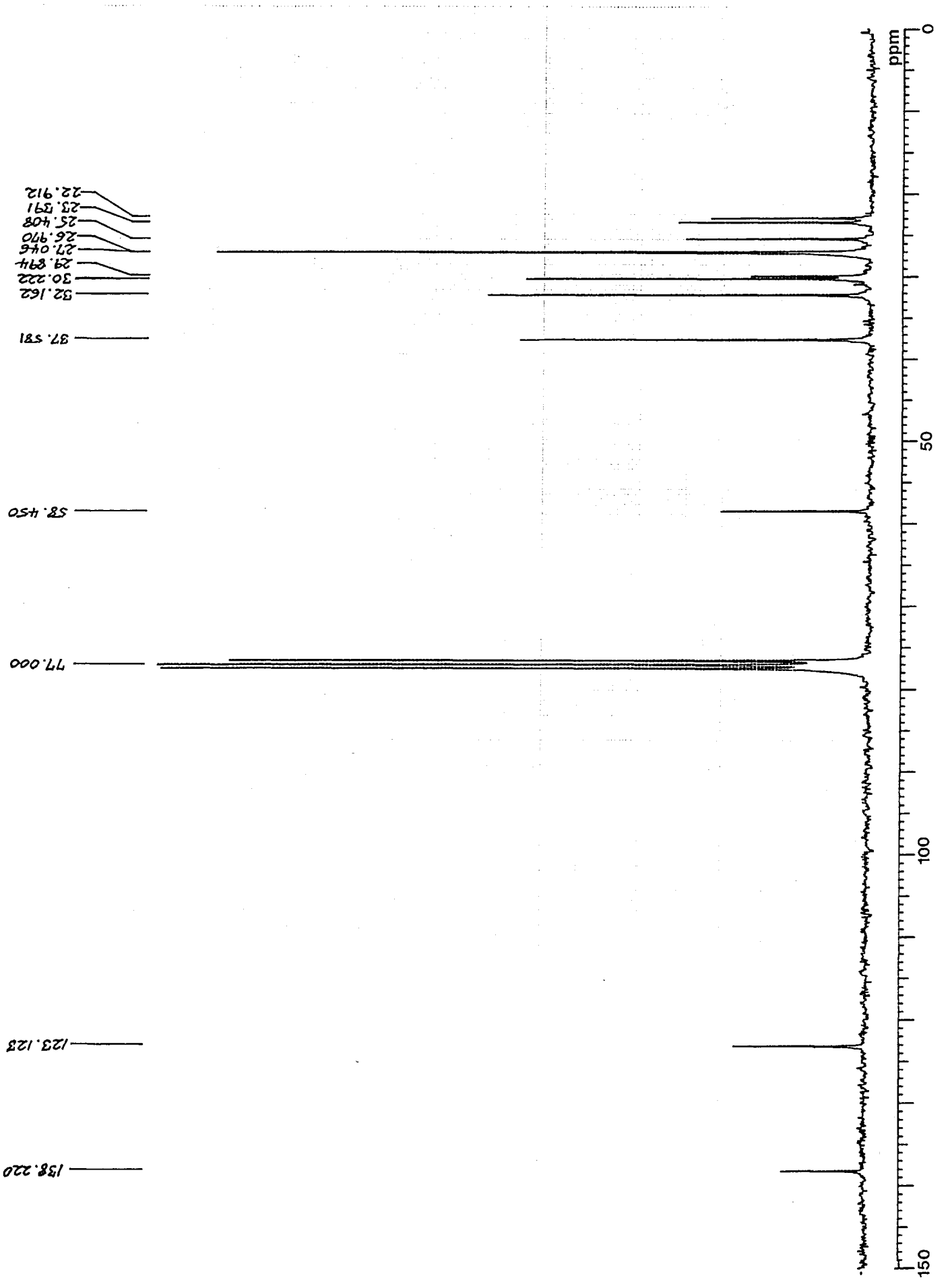

4.13: The 67.83 MHz proton decoupled carbon-13 spectrum of dicyclohexylcyclohexenylmethane.

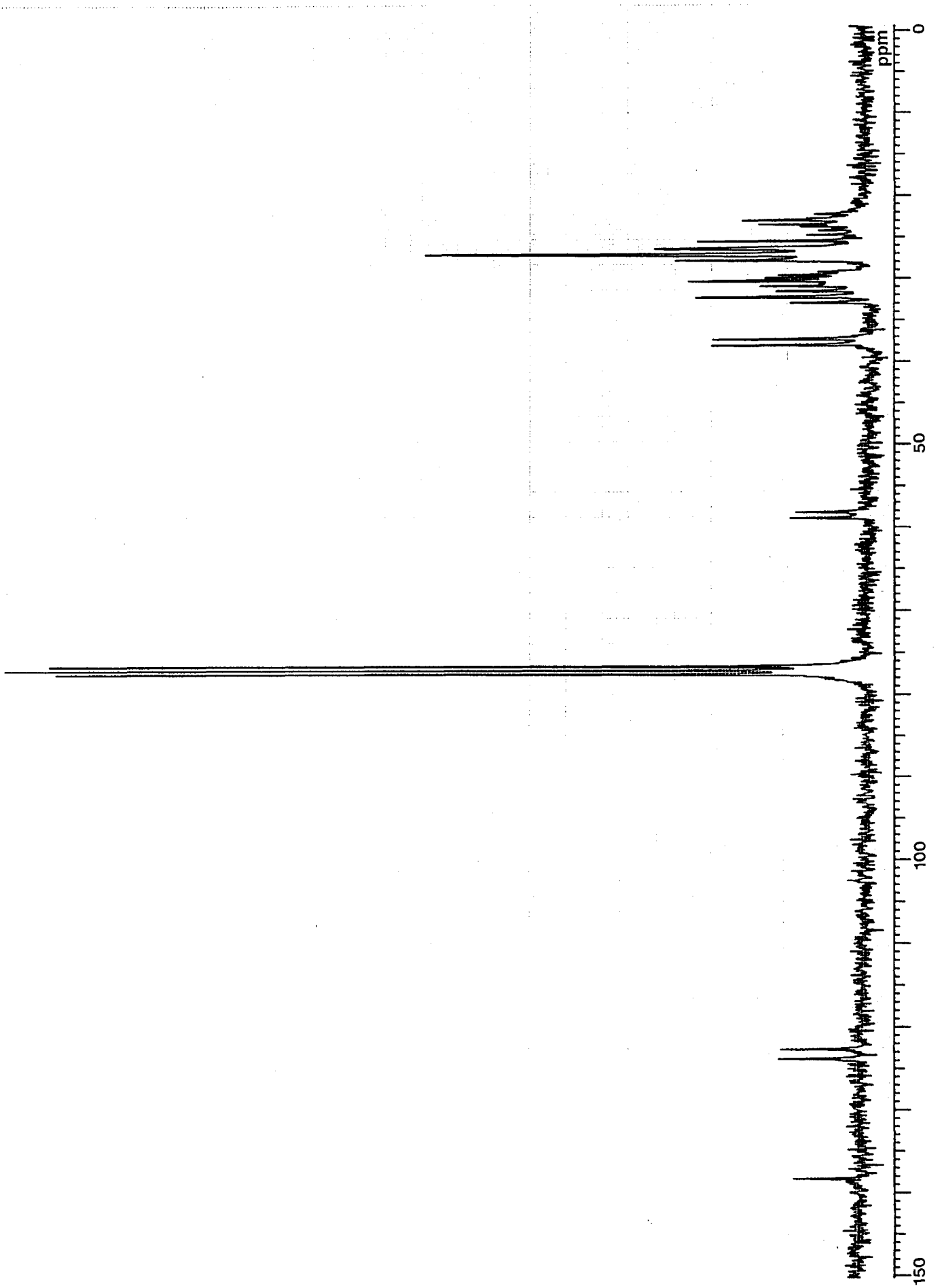

4.14: The 67.83 MHz off-resonance decoupled carbon-13 spectrum of dicyclohexylcyclohexenylmethane.

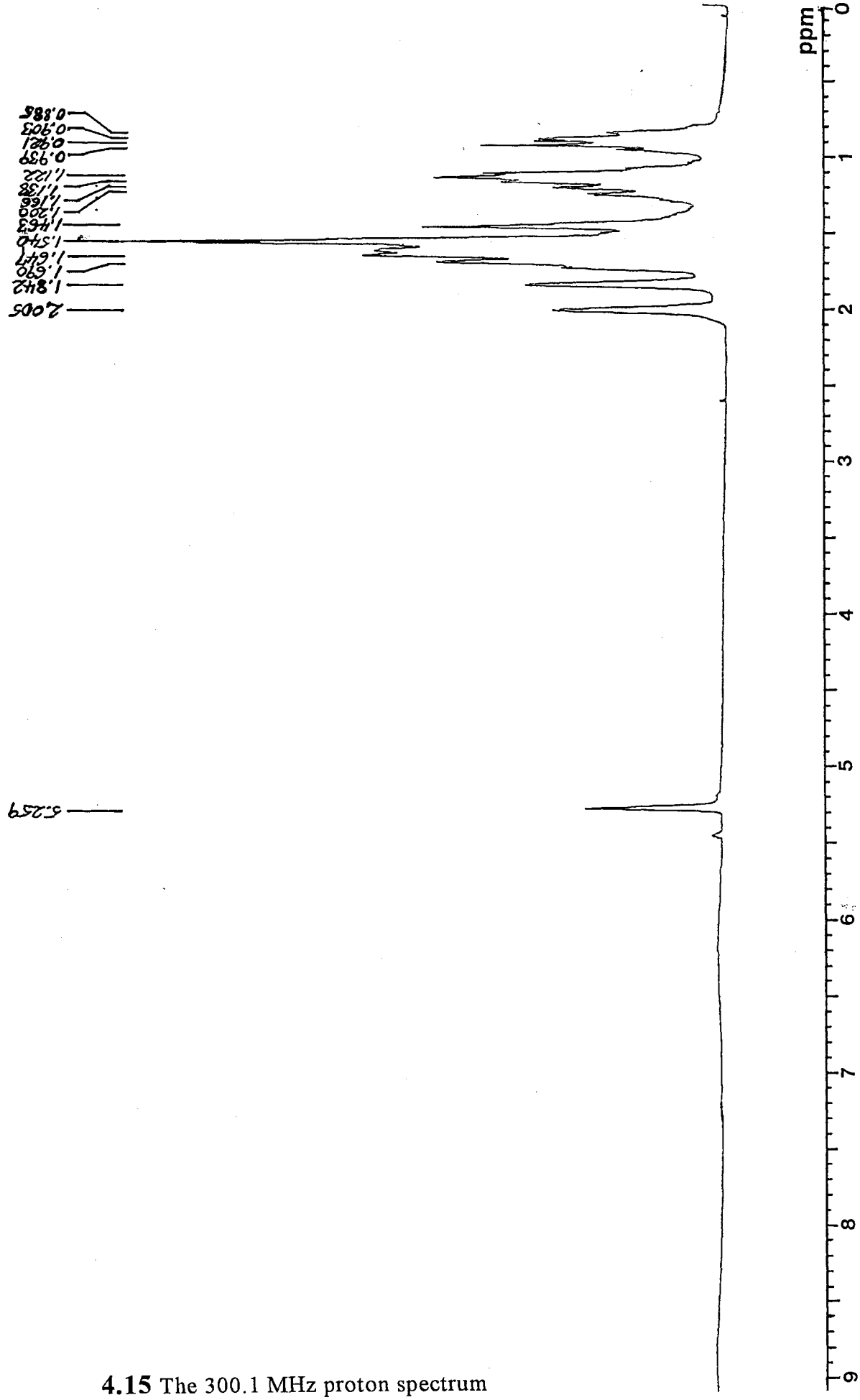

4.15 The 300.1 MHz proton spectrum of dicyclohexylcyclohexenylmethane.

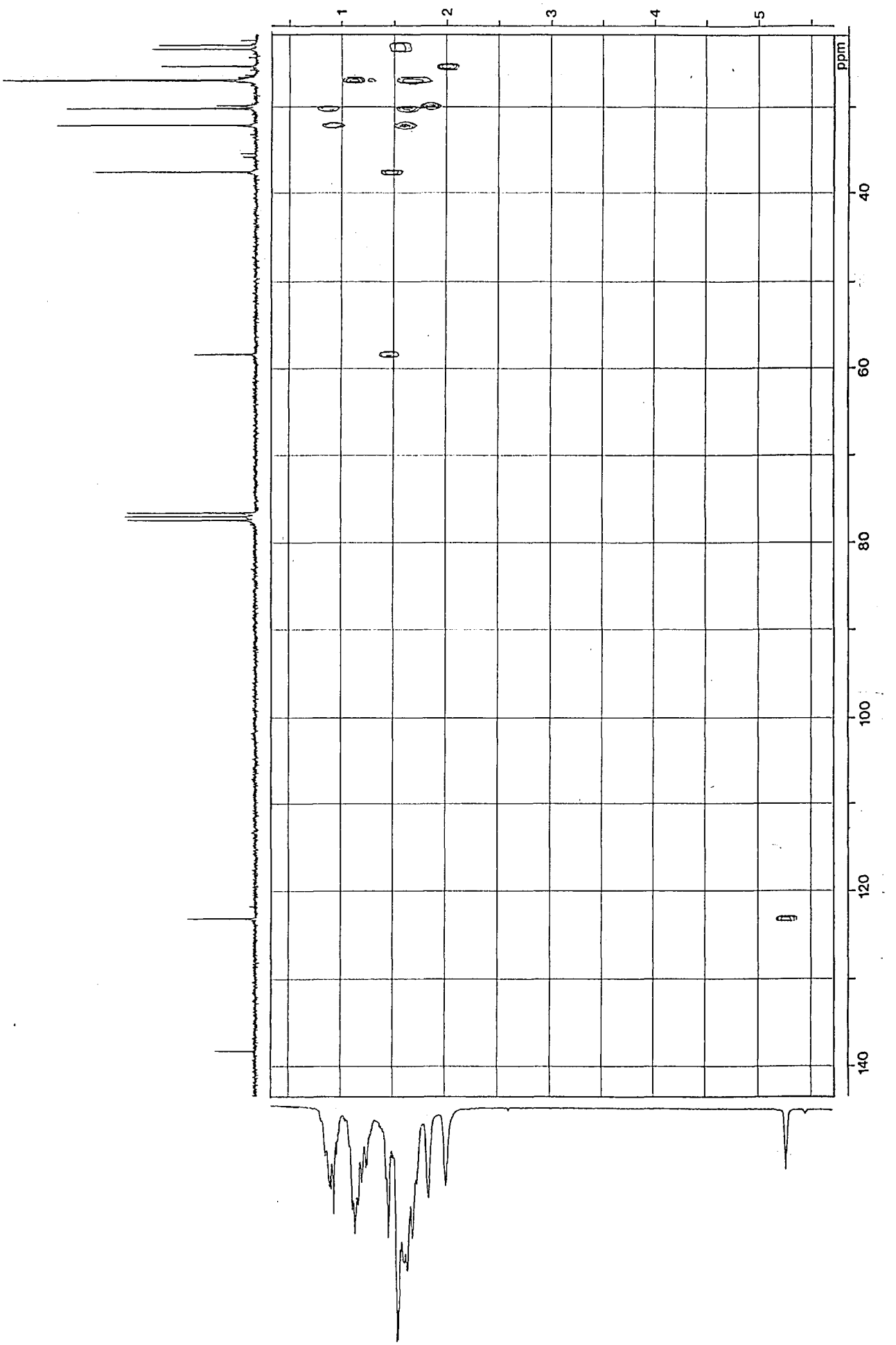

4.16: The proton decoupled carbon-13 — proton correlation spectrum of dicyclohexylcyclohexenylmethane at 7.05 T.

DICYCLOHEXYLPHENYLMETHANE

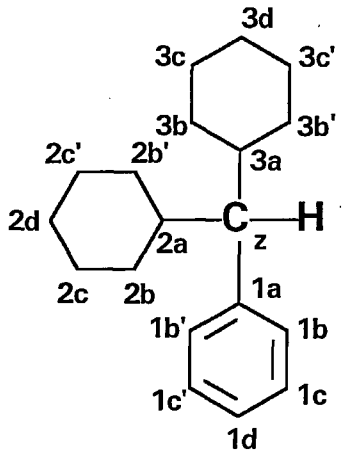

The product of the slow hydrogenation of triphenylmethane over stirred Raney nickel catalyst (purity >98% by GC analysis) was identified by a combination of 1D and 2D NMR spectroscopy. Spectrum 4.17 shows the proton decoupled carbon-13 spectrum of the compound, while Spectrum 4.18 is a proton decoupled carbon-13 SEFT spectrum, with evolution time τ = 8 ms, allowing phase sensitive detection of the resonances. One can see the aromatic resonances of the compound from 124 to 143 ppm, and from the SEFT spectrum one can assign the resonance at 142.505 ppm to the quarternary carbon **1a**, while the remaining aromatic carbons appear in some way as two pairs of identical chemical shift, and one single resonance. The resonance at 57.920 ppm can be assigned, as a methine resonance, to the central carbon **z**. The remaining resonances cannot be definitely assigned from the 1D spectrum alone.

Spectrum 4.19 is the proton NMR spectrum, and clearly shows the aromatic and cycloaliphatic regions, the last of which is expanded in Spectrum 4.20. However only one resonance can be immediately assigned; the triplet centred at 2.2 ppm belongs to the **z** proton at the molecular centre, with couplings to two protons, **2a** and **3a**, on the attached cyclohexyl rings.

Spectrum 4.21 shows a (proton decoupled) carbon-13-proton correlated spectrum of the compound at a field of 7.05 T. Using this it is possible to assign the remaining carbon resonances, and identify various groups of proton resonances present. The **2a** and **3a** methine carbons of the two cyclohexyl rings must appear coincidentally at 38.060 ppm, where they correlate with only a single proton resonance at about 1.8 ppm. Carbons **2b/3b** and **2b'/3b'** appear as two sets of pairs with the same chemical shifts, in some order at 32.189 and 29.747 ppm, where they correlate with their respective sets of axial and equatorial protons at 0.8 ppm, and 1.55 and 1.75 ppm. The remaining carbons **2c/3c**, **2c'/3c'**, **2d** and **3d**, appear crowded together around 26.7 ppm, correlating with their axial and equatorial protons. One can

expect the equivalences of the carbon resonances in the two cyclohexyl rings to follow the pattern suggested for dicyclohexylcyclohexenylmethane, for similar reasons.

The quarternary aromatic carbon **1a** is at 142.505 ppm, with no correlations, as required. The remaining five aromatic carbons appear correlated to the aromatic protons, as expected, at 127.382, 129.726, and 125.542 ppm. Presumably they occur as two sets of pairs for carbons **1b** and **1c**, and a single resonance for carbon **1d**. It is hard to imagine any other arrangement, and the aromatic proton resonance splits into two areas in the ratio of ratio 3:2, just as this would require. The remaining integrals from the proton spectrum coincide very closely with those expected.

The coupling constant of protons **2a** and **3a** to proton **z** is around 10 Hz, which indicates that the torsional motions of the cyclohexyl rings about the bonds to the central atom are restricted in some way even in solution, as was the case for tricyclohexylmethane.

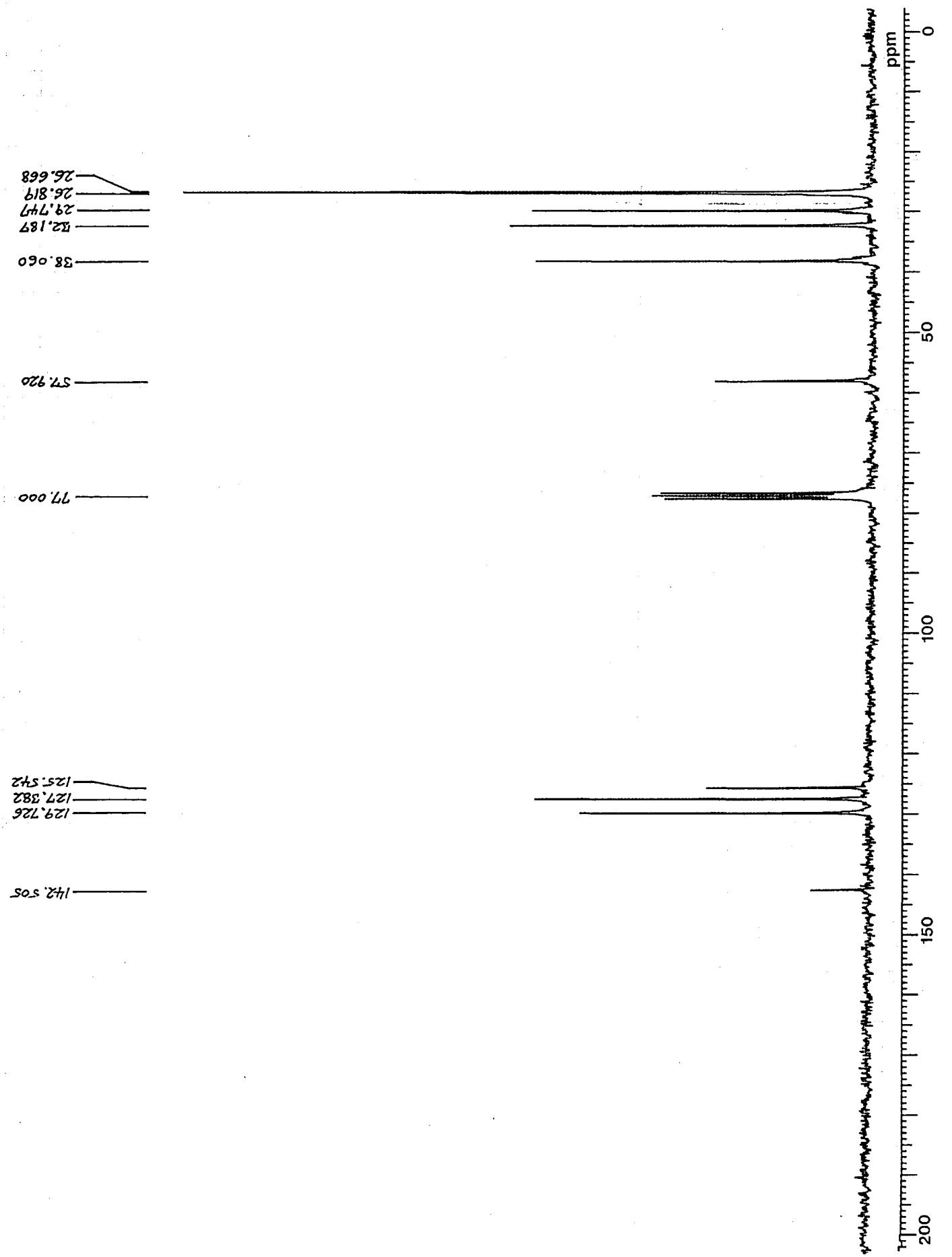

4.17: The 67.83 MHz proton decoupled carbon-13 spectrum of dicyclohexylphenylmethane.

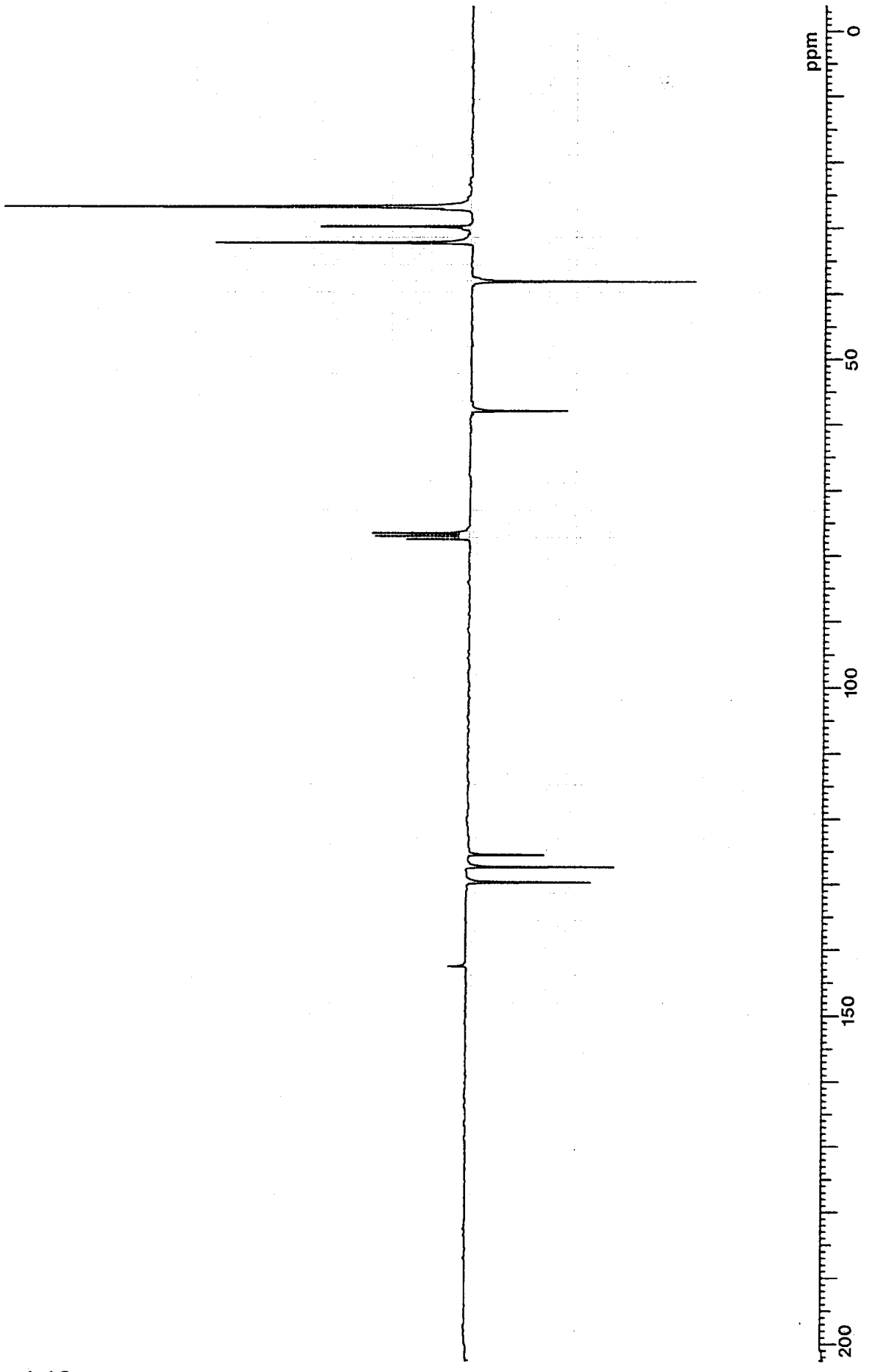

4.18: The 67.83 MHz proton decoupled SEFT spectrum of dicyclohexylphenylmethane.

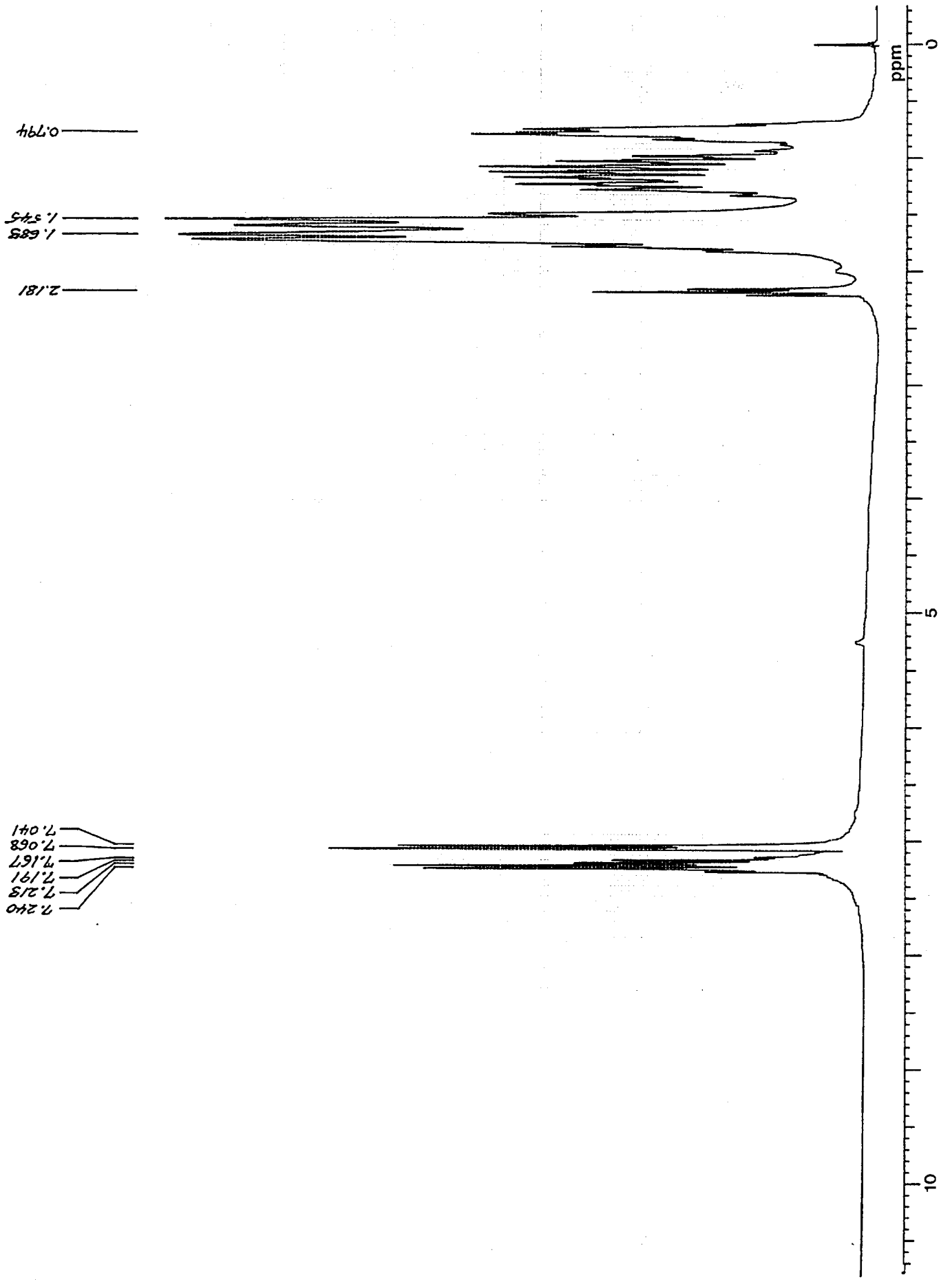

4.19: The 269.7 MHz proton spectrum of dicyclohexylphenylmethane.

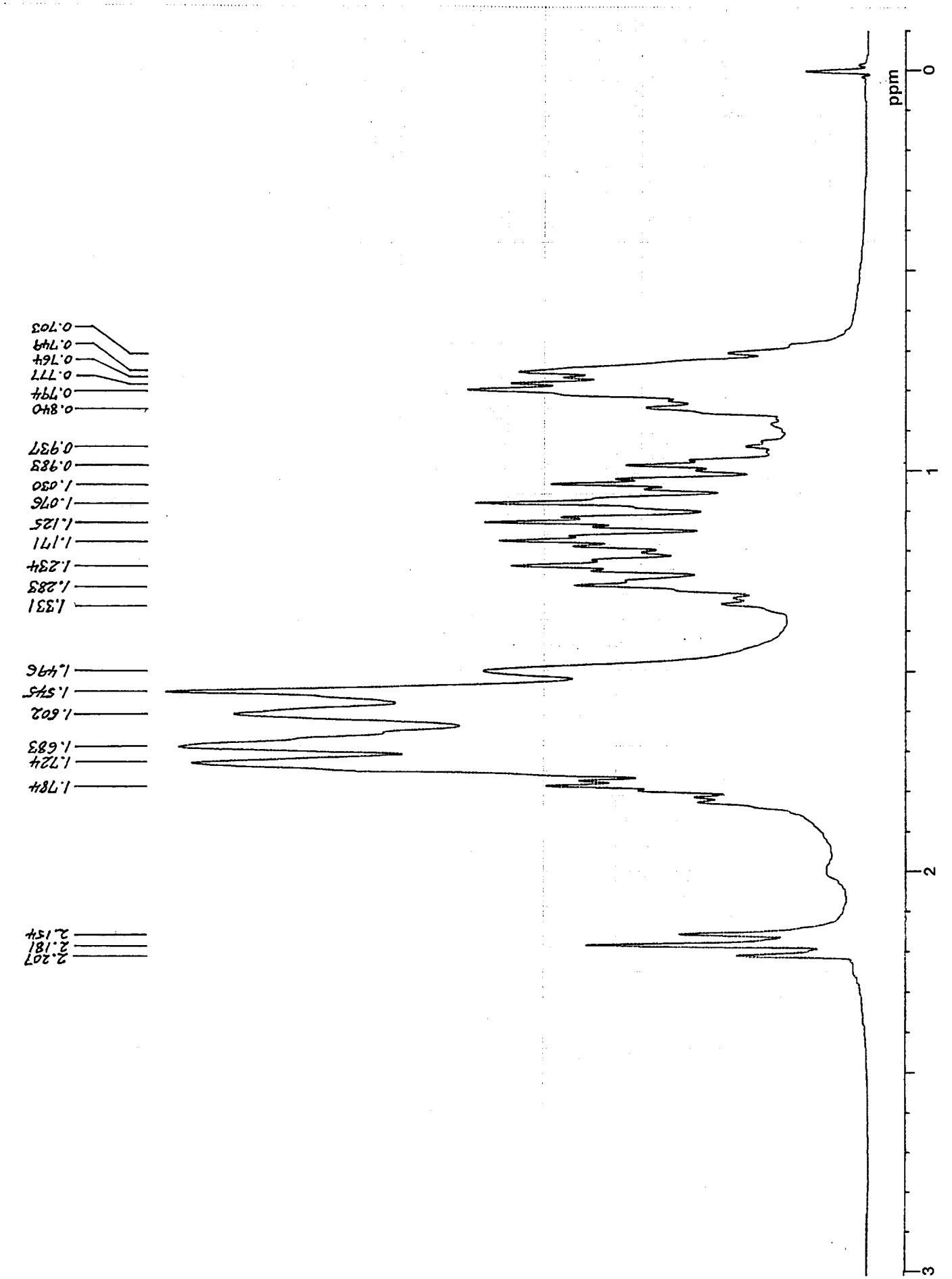

4.20: The 269.7 MHz proton spectrum of dicyclohexylphenylmethane (expansion).

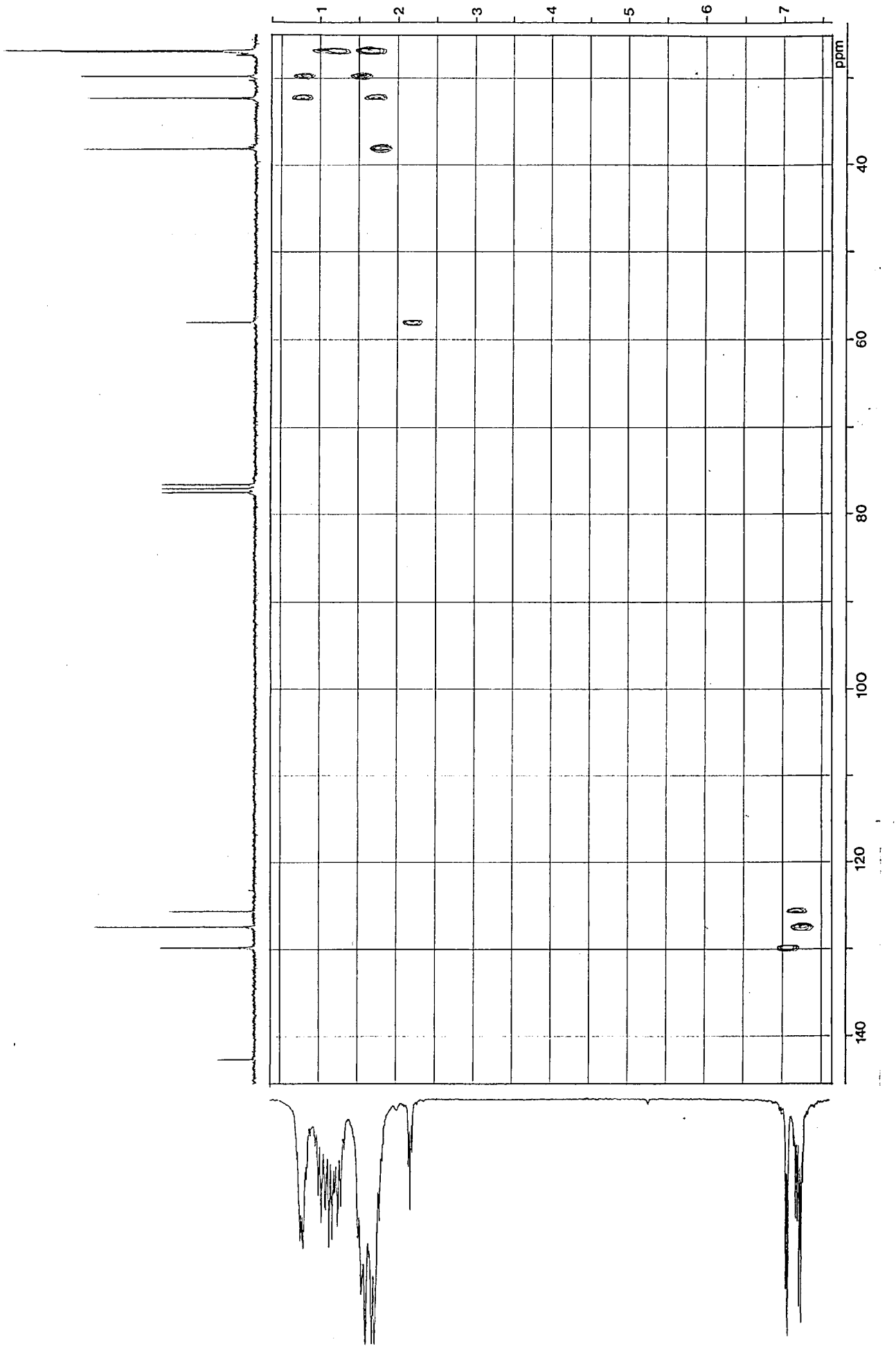

4.21: The proton decoupled carbon-13 — proton correlation spectrum of dicyclohexylphenylmethane at 7.05 T.

1,1,2-TRICYCLOHEXYLETHANE

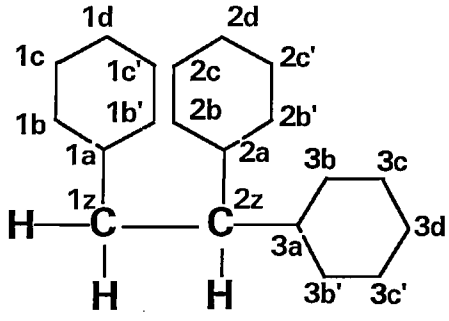

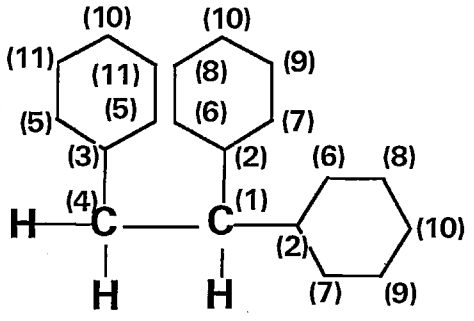

Spectrum 4.22 shows the proton decoupled carbon-13 spectrum of 1,1,2-tricyclohexylethane, and Spectrum 4.23 an expansion of this. Spectrum 4.24 is a proton decoupled carbon-13 SEFT spectrum of the same compound, with evolution time τ = 8 ms, thereby allowing phase sensitive detection of the resonances. Methylene groups appear with normal phase here, while the methine carbons in the molecule are inverted. By this means, and by comparison to the much simpler and known assignments for tricyclohexylmethane, it is relatively easy to arrive at assignments of the four resonances at the low field part of the spectrum. Carbon **2z** appears at 45.671 ppm, and carbon **1z** at 36.473 ppm. (By inspection of phases in the SEFT spectrum). The resonance at 40.051 ppm comes from two carbon atoms, **2a** and **3a,** and carbon **1a** appears at 37.43 ppm.

Three equivalent pairs of carbon atoms, **1b/1b'**, **2b/3b**, **2b'/3b'**, appear, in some order, from 29.0 to 34.0 ppm, and from an examination of the proton decoupled carbon-13 spectrum at 100.5 MHz and 80 ^{0}C it was found that the resonance at 26.869 ppm splits into two separate peaks, with sizes in the approximate ratio of 2:1. However, the precise assignments of the high field part of the spectrum cannot be made from the 1D spectra alone.

The correct assignments were revealed by the acquisition of a 100.5 MHz 2D INADEQUATE spectrum of the compound at 80 ^{0}C, reproduced here as Spectrum 4.25. Using the known assignments of the low field region of the 1D spectrum, the connectivity of the rings can be traced from carbon position **2z** outwards, as indicated. The remaining ring carbons are thus assigned as follows; **1b/1b'**, 33.927 ppm; **1c/1c'**, 26.617 ppm; **2b/3b**, 32.910 ppm; **2b'/3b'**, 29.919 ppm; **2c/3c**, 27.197 ppm; **2c'/3c'**, 26.995 ppm; **1d**, **2d** and **3d** at 26.869 ppm. One can assume the **d** carbons of rings **2** and **3** appear as the larger, and the **d** carbon of ring **1** as the smaller, of the two close resonances at 26.896 ppm.

These assignments assume that the equivalences observed in the carbon-13 resonances for rings **2** and **3** follow the pattern found previously in the cases of dicyclohexylcyclohexenylmethane and dicyclohexylphenylmethane, for similar reasons,

while the motional averaging in ring **1** leads to further equivalence, as in the cases of the tricyclohexylmethyl derivatives. Presumably, the relative correlations of the chemical shifts with the primed and unprimed positions in rings **2** and **3** can be correlated with average spatial configuration of this molecule in the liquid state.

The carbon atoms are also numbered in the order in which their resonances appear in the standard spectrum, starting from the low field end. Some of the carbon-13 chemical shifts present in the 2D INADEQUATE spectrum of the neat liquid hydrocarbon at 80 ^{0}C differ noticeably from those in the standard spectrum, in deuteriochloroform solution at 25 ^{0}C; the corresponding standard shifts of each resonance are the ones mentioned in the discussion of the assignments.

In the proton NMR spectrum, Spectrum 4.28, also shown expanded as Spectrum 4.29, the broad regions corresponding to the equatorial and axial protons appear as in the other compounds. An apparent triplet resonance appears at 0.809 ppm, which can be assigned to the proton in position **2z**, by analogy with tricyclohexylmethane. It may be possible to interpret this resonance in terms of two identical couplings of about 11 Hz to protons **2a** and **3a**, and two smaller unresolved couplings to the **1z** protons. If this is correct, then this gives some information about the average orientations of rings **2** and **3** with respect to the rest of the molecule, and demonstrates the restriction of their torsional motions about the **z-a** bonds.

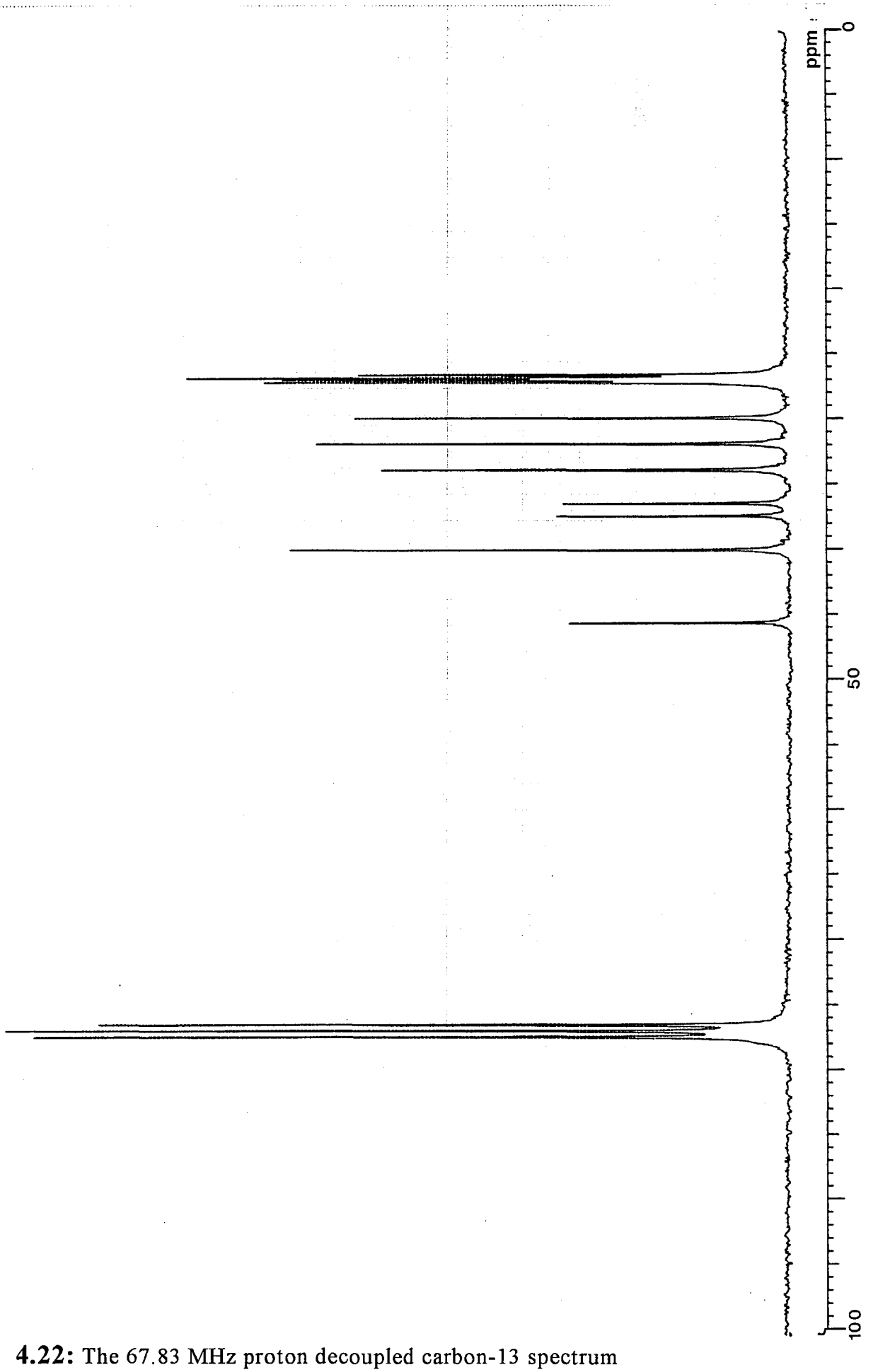

4.22: The 67.83 MHz proton decoupled carbon-13 spectrum of 1,1,2-tricyclohexylethane.

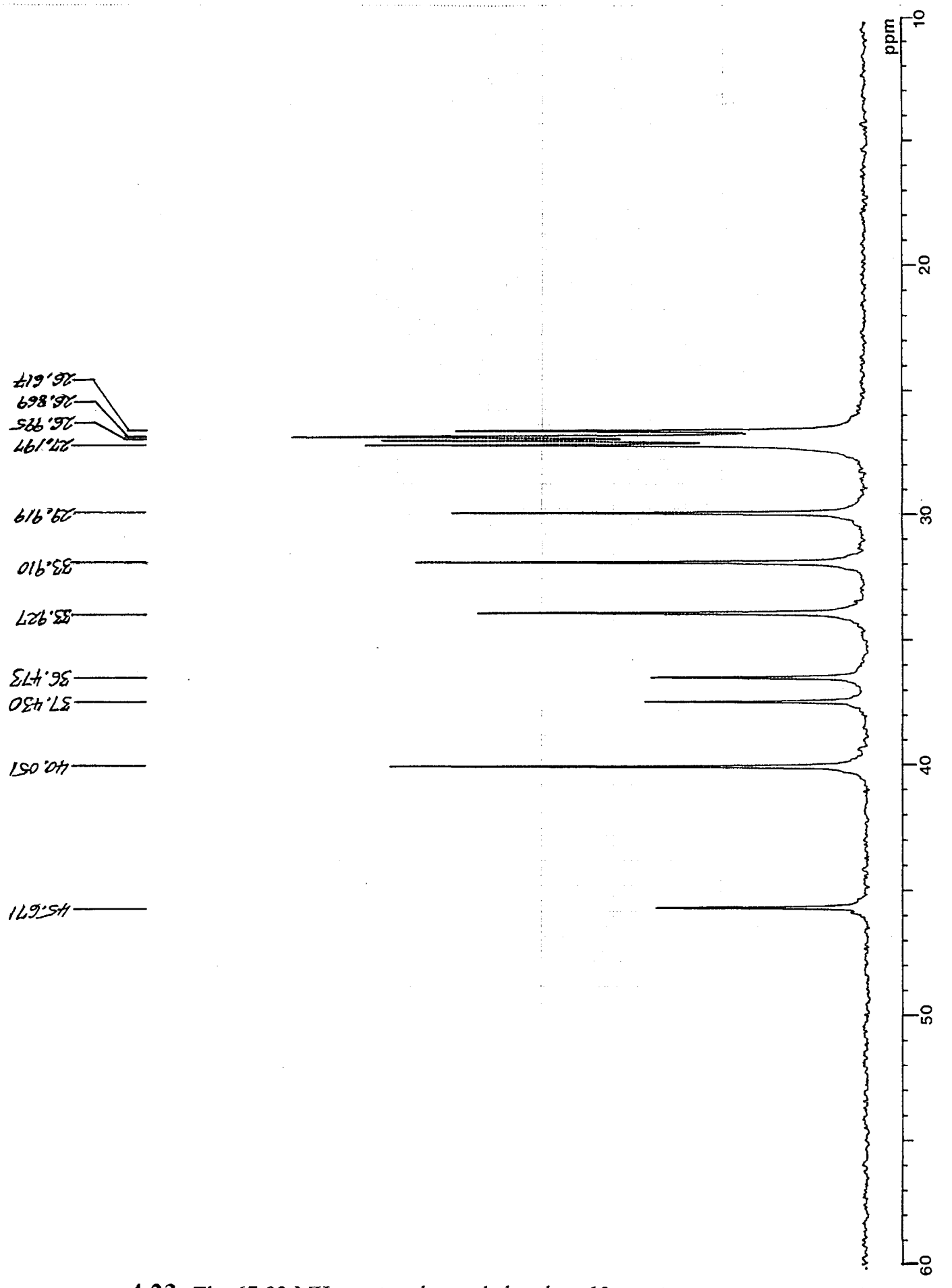

4.23: The 67.83 MHz proton decoupled carbon-13 spectrum of 1,1,2-tricyclohexylethane (expansion).

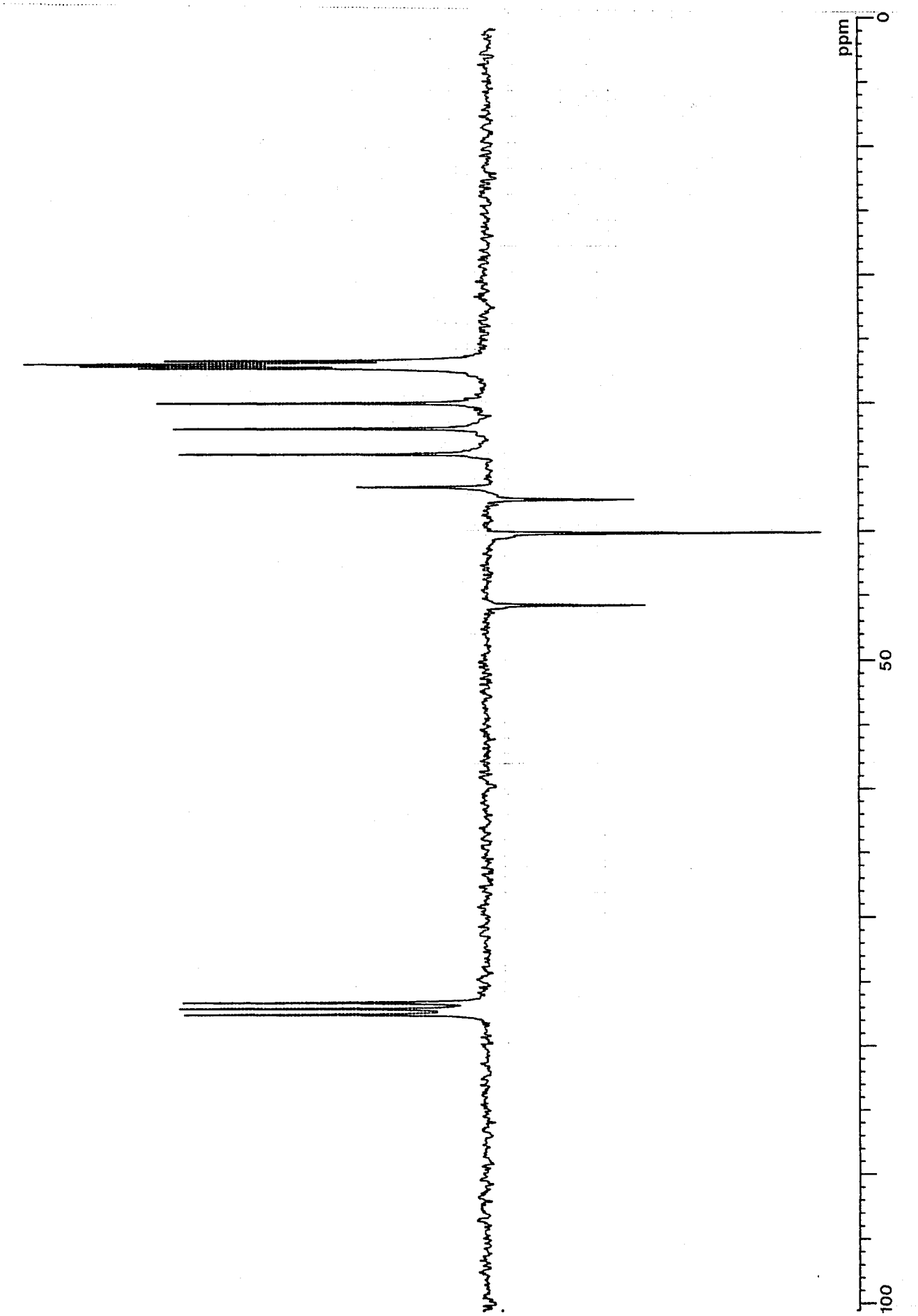

4.24: The 67.83 MHz proton decoupled SEFT spectrum of 1,1,2-tricyclohexylethane.

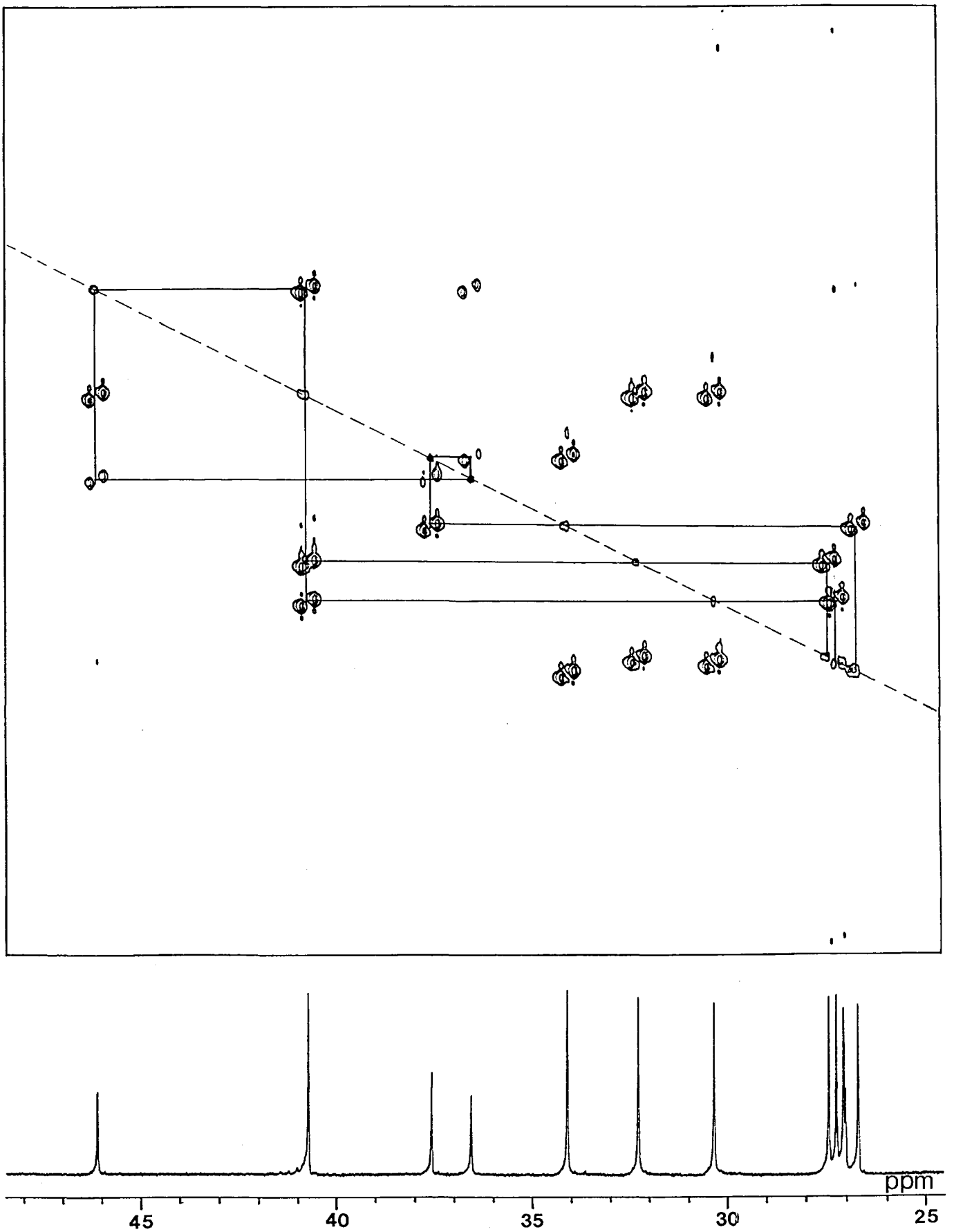

4.25: The 100.5 MHz proton decoupled 2D INADEQUATE spectrum of 1,1,2-tricyclohexylethane at 80 ^{0}C (acquired on a neat sample of the hydrocarbon).

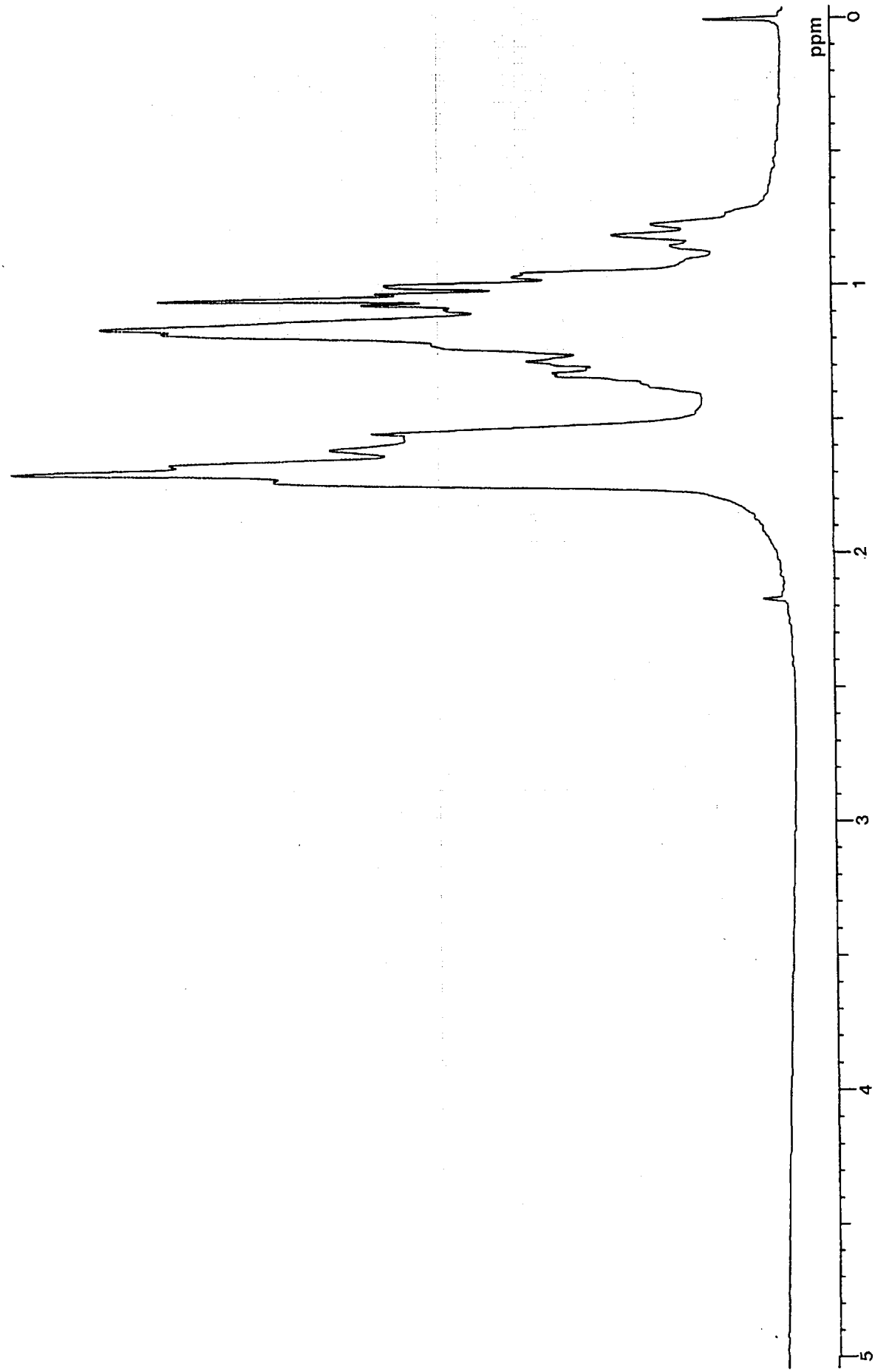

4.26: The 269.7 MHz proton spectrum of 1,1,2-tricyclohexylethane.

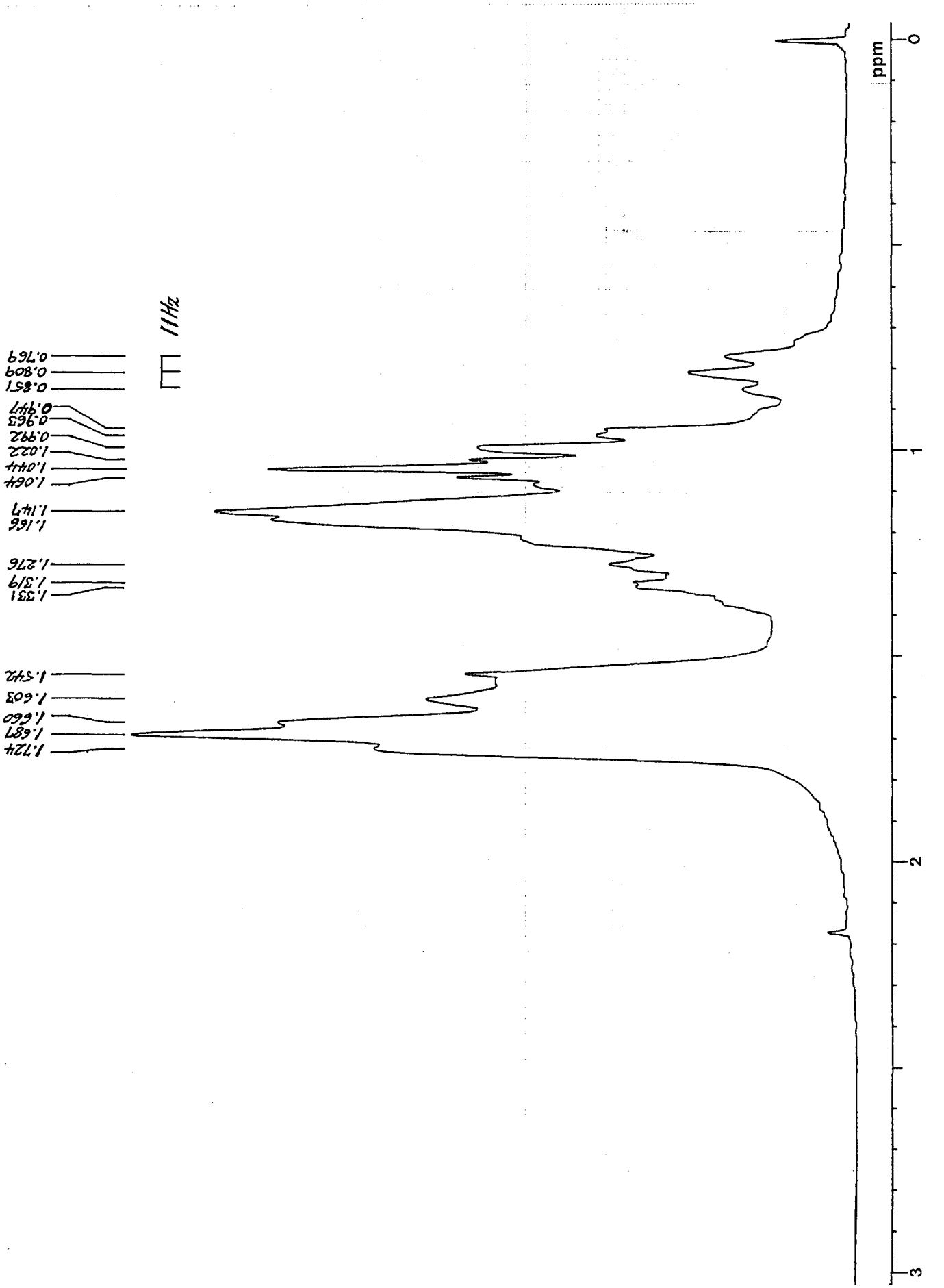

4.27: The 269.7 MHz proton spectrum of 1,1,2-tricyclohexylethane (expansion).

DICYCLOHEXYL ETHER

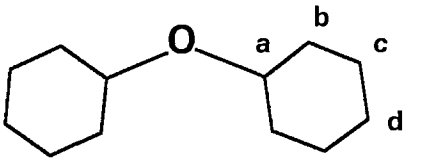

Spectrum 4.28 is the proton decoupled carbon-13 spectrum of dicyclohexylether, and the obvious assignment of the resonances is as follows: position **a**, 74.681 ppm; **b**, 33.271 ppm; **c**, 24.525 ppm; **d**, 25.786 ppm. Spectrum 4.29 is the corresponding off-resonance proton decoupled carbon-13 spectrum, which confirms these assignments.

Spectrum 4.30 is the proton spectrum of dicyclohexylether. One can assign the resonances from 1.13 to 1.32 ppm to most of the axial protons in the two rings. The two (probably axial) protons, **a**, appear as the complex feature from 3.27 to 3.36 ppm, which appears to be, but may not actually be, a septet with a regular splitting of about 4 Hz between each peak. The remaining three prominent resonances appear with areas in about the ratio of 2:2:1, which suggests their assignment to the equatorial protons in the rings: position **b**, 1.85 ppm; **c**, 1.74 ppm; **d**, 1.52 ppm. This interpretation therefore assumes that it is the equatorial positions in the rings that experience deshielding from the oxygen atom, whereas the axial protons are relatively unaffected.

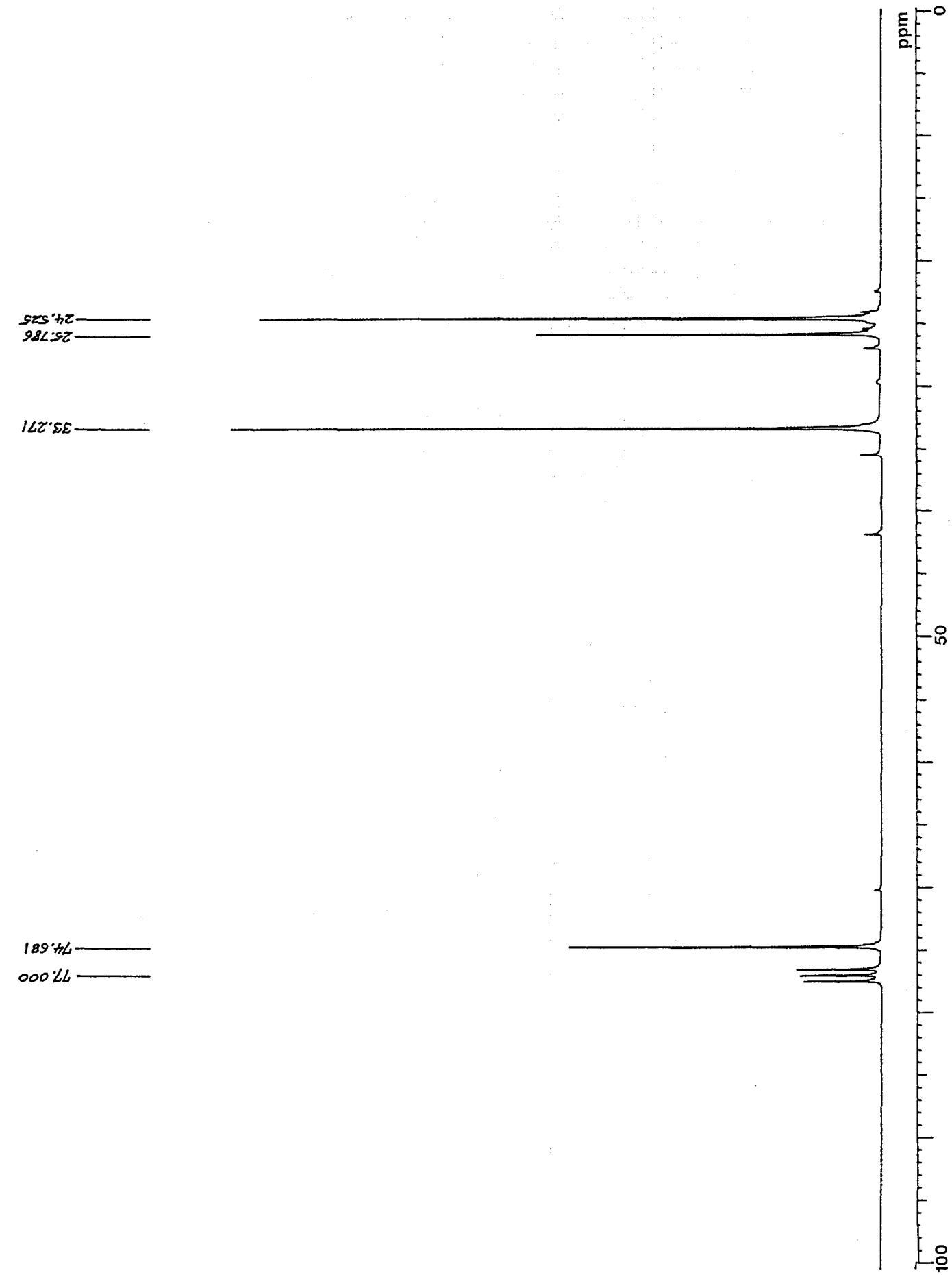

4.28: The 67.83 MHz proton decoupled carbon-13 spectrum of dicyclohexylether.

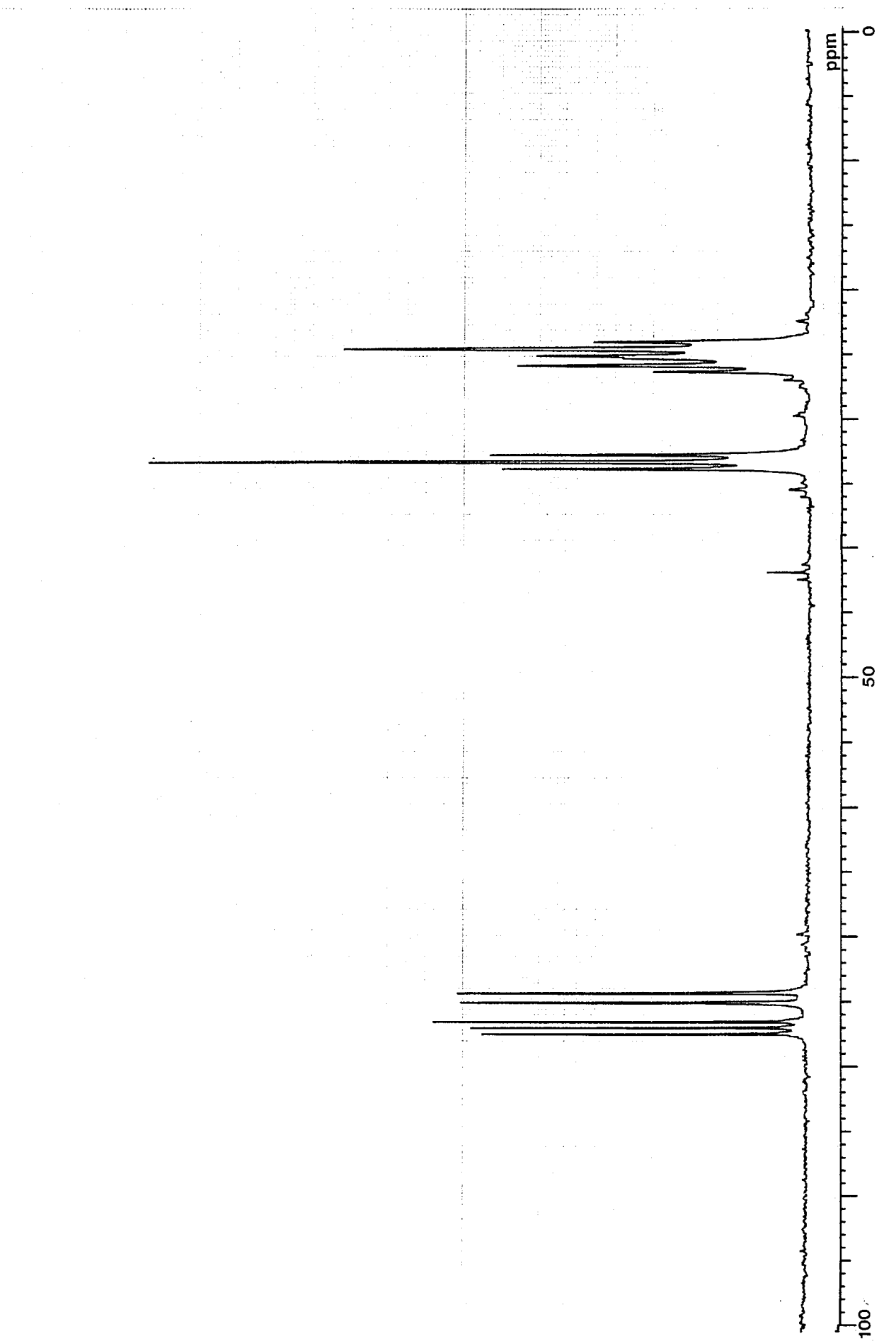

4.29: The 67.83 MHz off-resonance decoupled carbon-13 spectrum of dicyclohexylether.

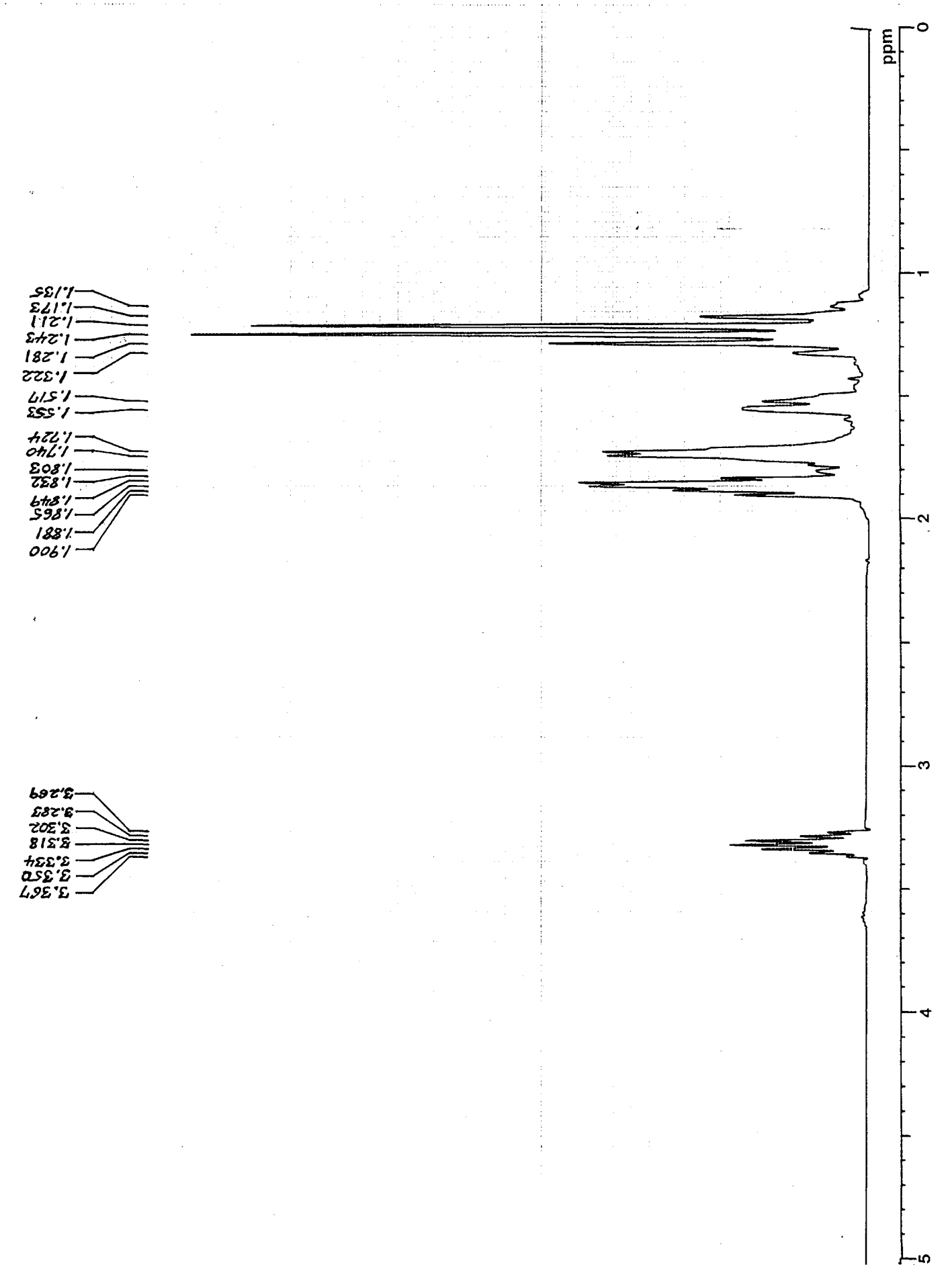

4.30: The 269.7 MHz proton spectrum of dicyclohexylether.

Chapter 5

TRICYCLOHEXYLMETHANE, TRICYCLOHEXYLMETHYLCHLORIDE, AND TRICYCLOHEXYLMETHYL: X-RAY CRYSTALLOGRAPHIC AND ESR STUDIES

5.1 THE STRUCTURE OF TRICYCLOHEXYLMETHANE

The structure of tricyclohexylmethane was determined by X-ray crystallography and the full data were given in a published paper, reproduced here as Appendix 3. The structure and the packing in the unit cell are shown in Figs. 5.1 and 5.2, respectively.

The compound crystallizes from ethanol with a simple orthorhombic structure, symmetry group P $2_1,2_1,2_1$. The crystal is chiral, with all the molecules assuming the same handed arrangement of the three cyclohexyl rings about the central carbon atom. It also contains an unusually large amount of "empty space", since the volume per carbon atom (neglecting the much smaller hydrogen atoms) works out at 22.2 $Å^3$, whereas one expects about 18 $Å^3$ from previously determined structures for hydrocarbons. Despite this (or perhaps because of this) the crystals themselves are very hard and brittle. There is even an increase in volume when the solid melts, of some 10 %.

Presumably all these observations are linked to the disposition of the hydrogen atoms around the three cyclohexyl groups. One imagines the interplay between the steric factors tending to keep the molecules apart and the electronic van der Waals forces between the many carbon-hydrogen bonds of different molecules which are responsible for transition to the crystalline state. In connexion with this one might mention that although the compound crystal*i*zes readily enough on cooling a solution in ethanol, it solidifies very slowly from the pure melt at room temperature, where the steric interaction of the cyclohexyl rings in unordered neighbouring molecules must delay the process. Cooling the melt to room temperature gives a very viscous liquid, and this solidifies over about 30 minutes.

5.2 THE STRUCTURE OF TRICYCLOHEXYLMETHYLCHLORIDE

The structure of tricyclohexylmethylchloride was also determined by X-ray crystallography, and the full data obtained are reproduced here as Appendix 4. Crystals suitable for this were obtained by the slow evaporation at room temperature of a dilute solution of the chloride in hexane containing a small proportion of chloroform. The structure and the packing in the unit cell are shown in Figs. 5.3 and 5.4, respectively.

The space group of the structure is Pmna; slightly more complicated than that of tricyclohexylmethane, and involving reflections and translations of the generating unit. The crystal is not chiral, but instead each molecule is arranged so as to have a plane of symmetry passing directly through its "vertical" axis, as indicated in Fig 5.3. The dihedral angle between the least-squares planes of atoms C11-C16, and C21-C22, is 127.3^0. Thus the minor change in substitution at the centre of this structure alters the whole aspect of the crystal structure from that obtained in the case of tricyclohexylmethane. If one imagines perturbing the molecules by slightly rotating two cyclohexyl rings in each one by a few degrees, it is clear that the transition to an analogous asymmetrical chiral structure can be realised, but how that relates to the crystal structure as a whole would be a testing matter to determine. A feature retained in the chloride is the rather large volume per carbon atom, at 21.3 $Å^3$

The bond angles around the central carbon atoms are distorted from the normal tetrahedral angles more than in tricyclohexylmethane, but contrary to what one might have anticipated, the molecule appears "squashed and flattened"; the three rings are splayed out towards the chlorine atom at the central point of attachment, and the bonding of the three proximal tertiary carbon atoms is also similarly affected. In a way one can see here the approach to the flat geometry of the tricyclohexylmethyl radical described below, and perhaps an explanation of instability of the chloride in solution, assuming the effect is not caused solely by the crystal field forces. The rhombohedral crystals were hard, and also beautifully refractive; very probably due to the mirror plane symmetry of the constituent molecules.

It was not possible to assess the behaviour on melting, since the chloride began to fracture and decompose from around 90 ^{0}C, up to the temperature at which a general melting began at around 130 ^{0}C. The cooled material solidified, but was not the original chloride.

5.3 THE TRICYCLOHEXYLMETHYL RADICAL

A series of four papers on tricyclohexylmethane, tricyclohexylmethanol, and related molecules, published by Neunhoeffer and co-workers[1] during 1934/1936 were originally part of an attempt to produce the tricyclohexylmethyl radical, but they failed to produce any conclusive evidence for its existence by chemical methods.

However, the radical was discovered during the course of the present work, and successfully studied over a wide temperature range using a combination of ESR spectroscopy and theoretical calculations. Halogen abstraction using trimethyl tin radicals in decalin solution at room temperature generated the tricyclohexylmethyl radical from tricyclohexylmethylchloride; stabilized by the steric hindrance of the three cyclohexyl rings, the radical had a half life of some 30 minutes. The paper that has

been published describing this work is reproduced here as Appendix 5. The computed structure of the radical, together with the ESR spectrum, are shown in Fig. 5.5.

The radical was shown to have 3-fold (C_{3h}) rotational symmetry; the three bonds joining the cyclohexyl rings to the central carbon atom appear to be in a coplanar configuration in the temperature range of 200 to 455 K, and the average position of the C-H vectors on the α-carbons lie in this same plane, each with the same rotational sense. It was also observed that the ESR spectrum of the radical disappeared at 200 K, but could be restored simply by warming. From this the inference was made that the radicals dimerize at 200 K, and thus the first evidence has been obtained to show the probable existence of hexacyclohexylethane at this temperature. Any kind of head-to-tail arrangement, as was found in the case of the dimerization of triphenylmethyl radicals[2], seems unlikely in this case. One can only speculate how the radicals are arranged when they pair, but evidently the bond formed between the two central carbon atoms must be very weak because of the steric effects of the six rings.

REFERENCES FOR CHAPTER 5

[1] O. Neunhoeffer, *Justus Liebigs Ann. Chem.*, 1934, **509**, 115; O. Neunhoeffer and F. Nerdel, *Justus Liebigs Ann. Chem.*, 1936, **526**, 47; O. Neunhoeffer, *Justus Liebigs Ann. Chem.*, 1936, **526**, 58; O. Neunhoeffer and R. Schluter, *Justus Liebigs Ann. Chem.*, 1936, **526**, 65

[2] H. Lankamp, W. Th. Nauta, and C. MacLean, *Tetrahedron Lett.*, 1968, 249; H. A. Staab, H. Brettschneider, and H. Brunner, *Chem. Ber.*, 1970, **103**, 1101; H. Volz, W. Lotch, and H.-W. Schnell, *Tetrahedron*, 1970, **26**, 5343; for reviews, see V. D. Scholle and E. G. Rozantsev, *Russ. Chem. Rev.*, 1973, **42**, 1011, and J. M. McBride, *Tetrahedron*, 1974, **30**, 2009

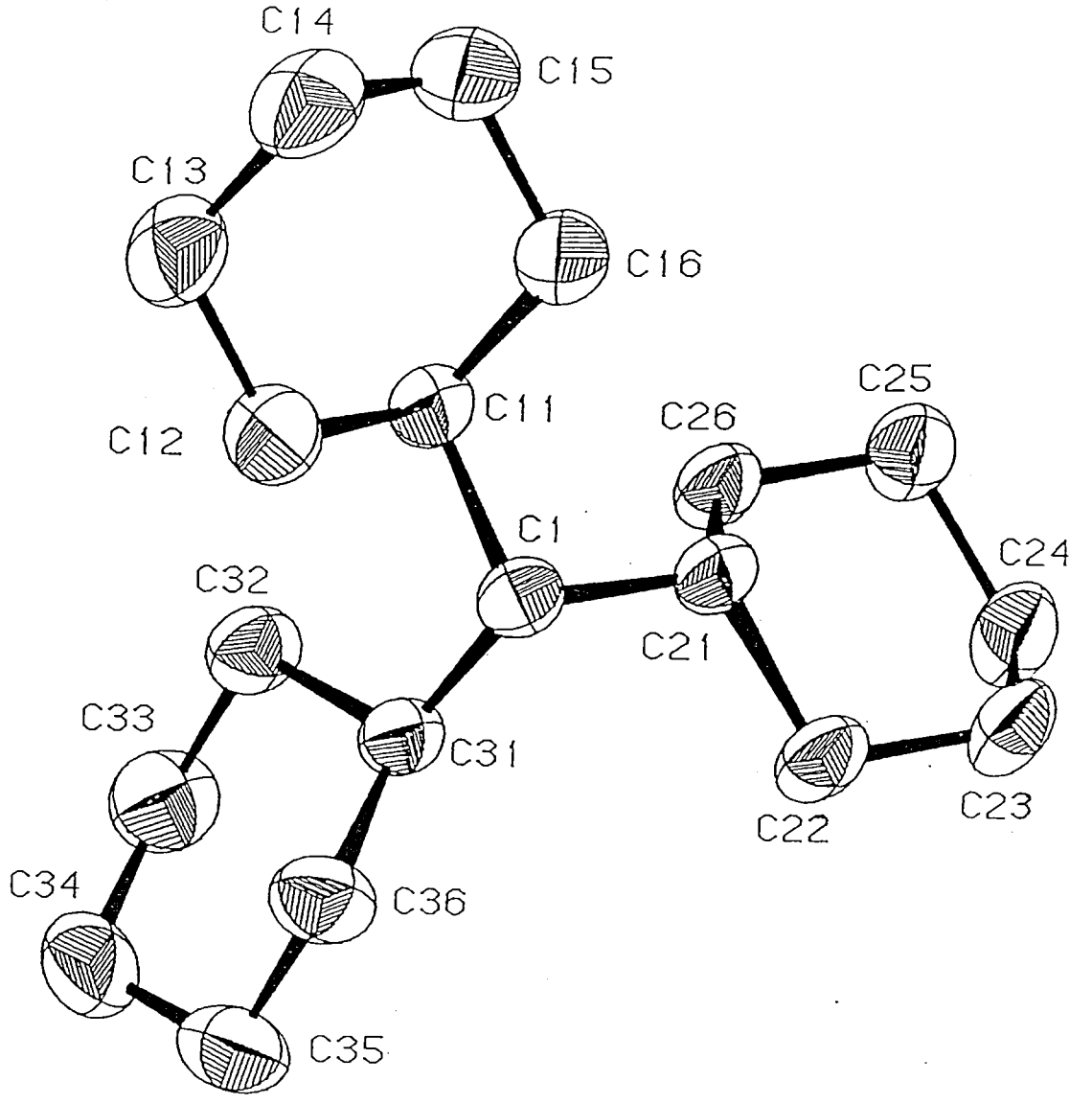

Fig 5.1: The structure of tricyclohexylmethane determined by X-ray crystallography.

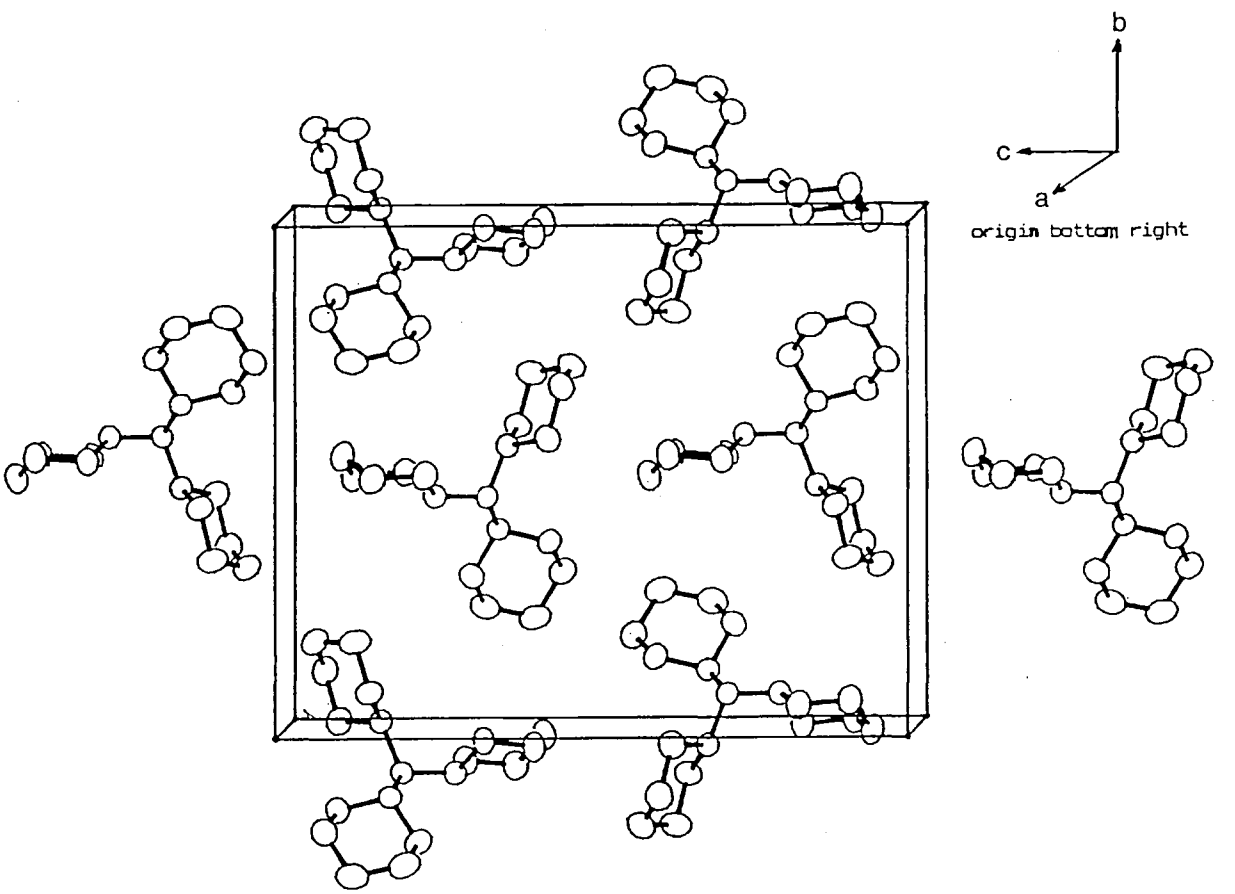

Fig 5.2: The packing of tricyclohexylmethane within the unit cell.

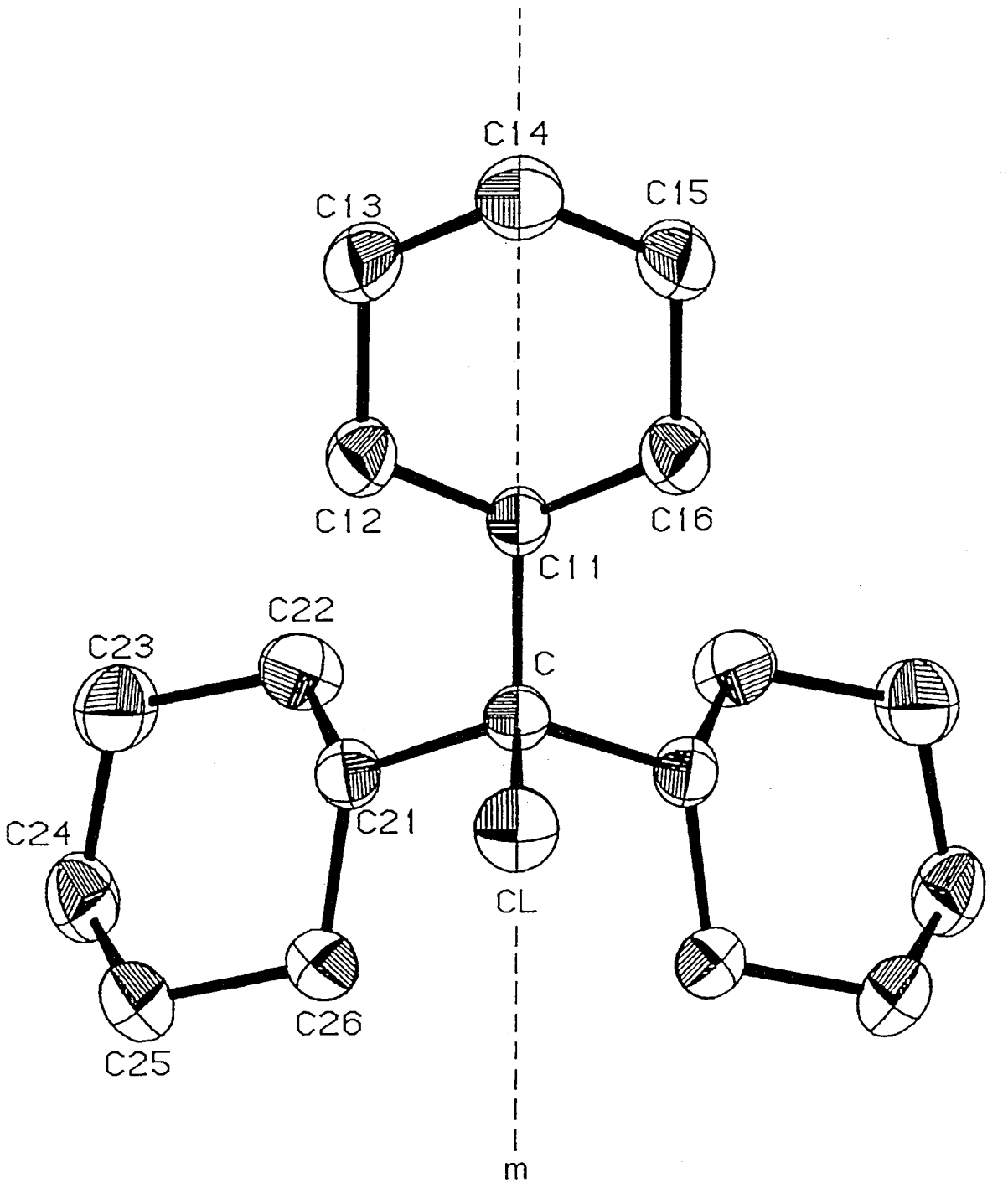

Fig 5.3: The structure of tricyclohexylmethylchloride determined by X-ray crystallography.

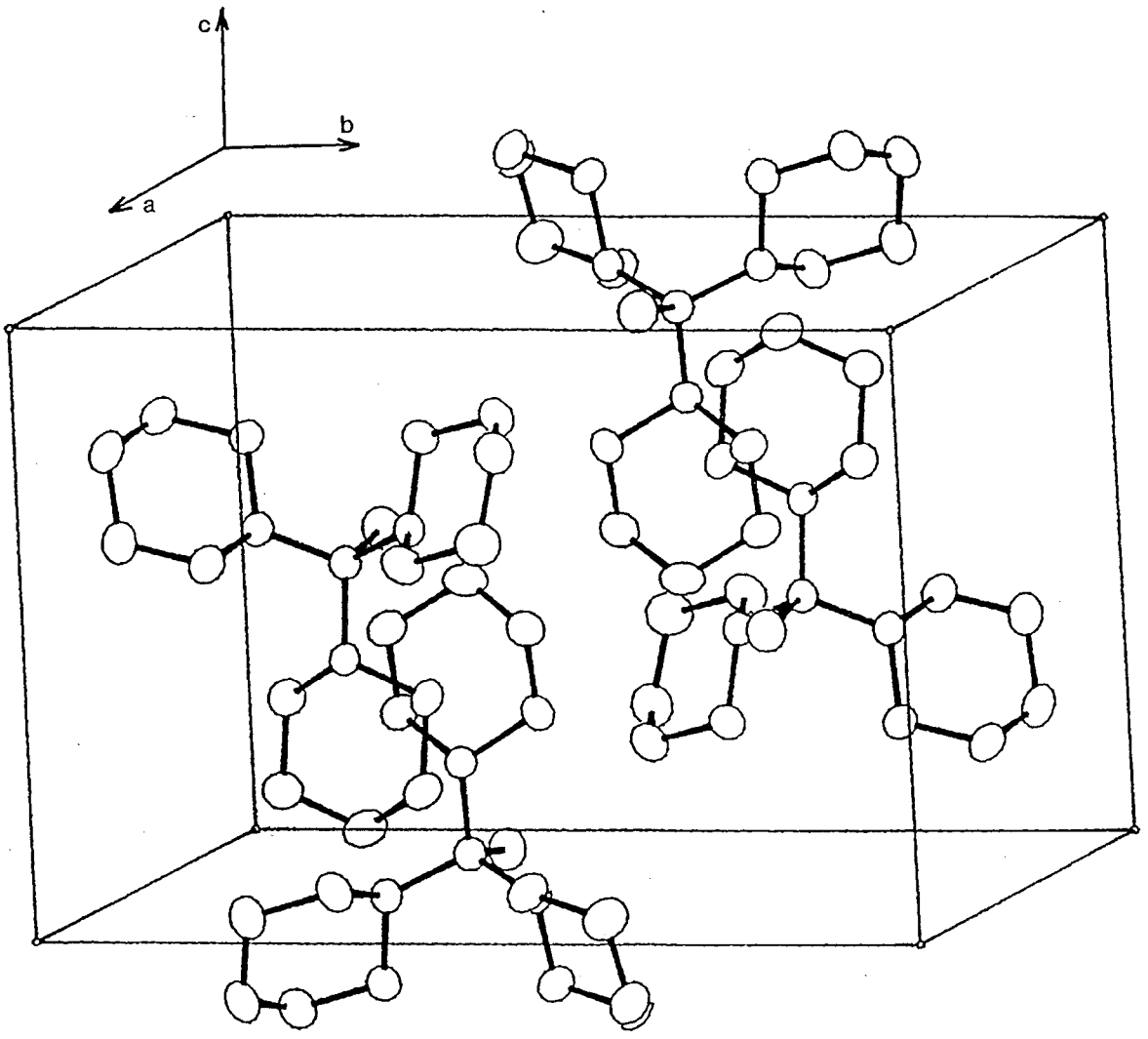

Fig 5.4: The packing of tricyclohexylmethylchloride within the unit cell.

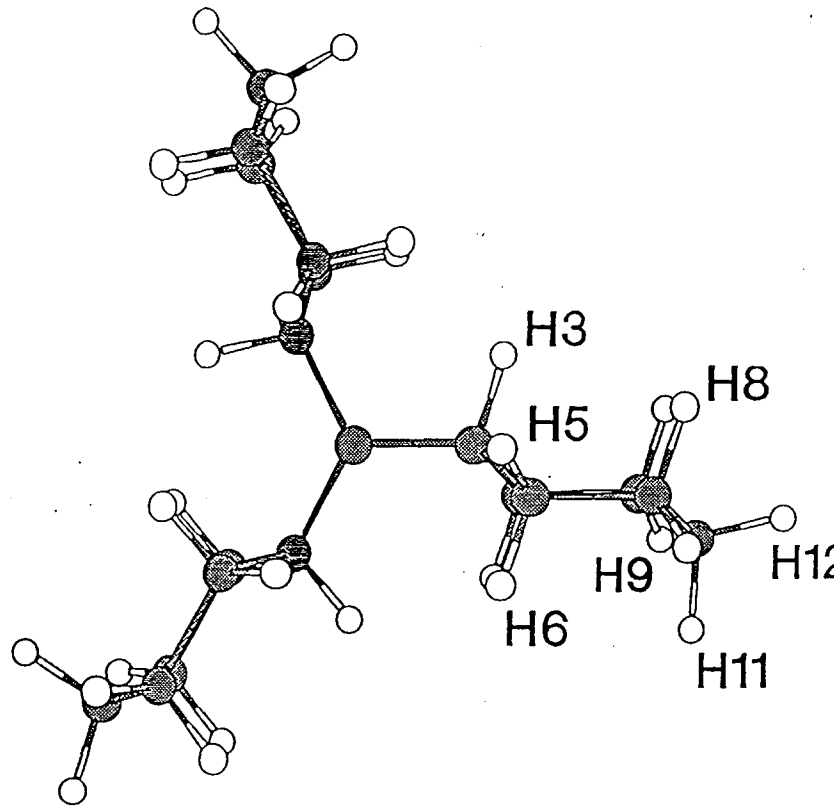

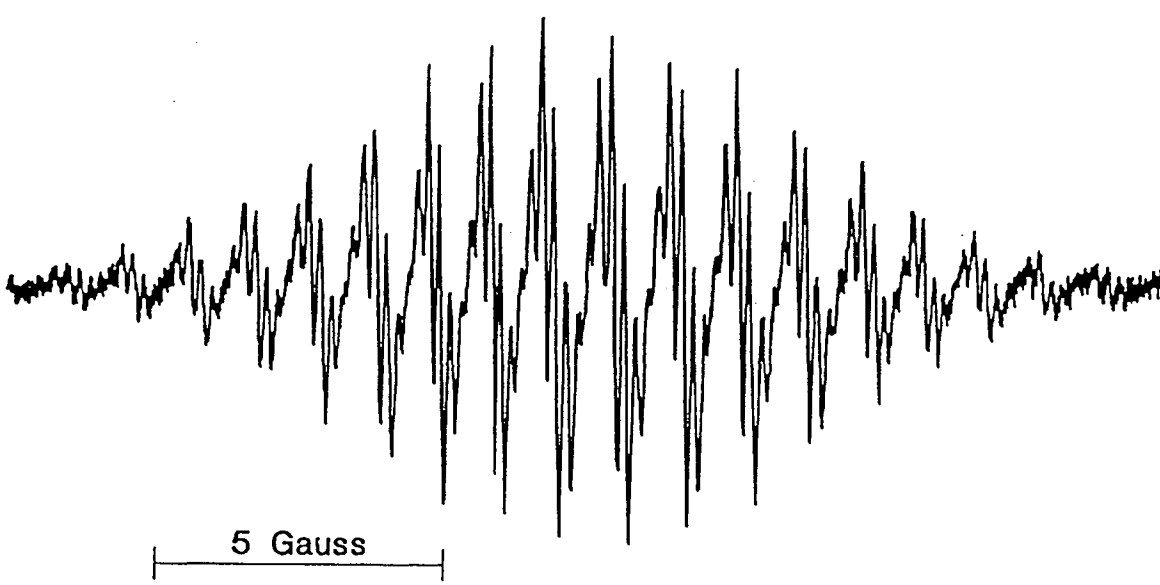

Fig 5.5: The computed minimum energy conformation of tricyclohexylmethyl (above), and the experimental X-band ESR spectrum in decalin solution at 455 K, at a modulation amplitude of 0.05 G (below).

Chapter 6

SAMPLE PREPARATION AND NMR MEASUREMENTS; COLLECTED TABLES OF DATA

6.1 SAMPLE PREPARATION

Five model lubricant compounds were selected from the syntheses described earlier as the subjects of these measurements. Three *n*-octyl derivatives were chosen as representative of the 'normal' type of lubricating oil:

1. 9,10-Di-*n*-octyl-*n*-octadecane
2. 9-*n*-Octyl-*n*-heptadecane
3. Tri-*n*-octylsilane

Two hydrocarbons, each containing three cyclohexyl groups, were chosen as representative of 'traction fluid' lubricants:

4. Tricyclohexylmethane
5. 1,1,2-Tricyclohexylethane

The four liquid samples, of compounds 1, 2, 3 and 5, were sealed inside 17.5 cm x 8 mm od thin walled NMR tubes. Suitable 20 cm tubes were purchased ready made from Messrs. Wilmad, with a constriction 2.5 cm from the open end. Each tube was attached via a greaseless PTFE rotoflow gas tap to a ground glass joint. The hydrocarbon was transferred using a syringe or lengthened glass pipette directly to the bottom of the tube, to a depth of 4.5 cm, taking care not to wet the area of the constriction. The whole assembly was then attached to a vacuum line, the sample degassed using from 5 to 10 freeze-pump-thaw cycles, and the tube finally detached and sealed under vacuum by application of a small blow-torch flame at the constricted point.

The sample of tricyclohexylmethane was prepared inside a 17.5 cm x 8 mm od tube of borosilicate glass with wall thickness of about 1.5 mm, specially prepared for the purpose. This was necessary since the solid hydrocarbon shattered a standard NMR tube as it melted. The thicker walled tube resisted the expansion of the sample easily. The powder of the solid sample was transferred to the bottom of the tube assembly by stroking with a fine file, and the sample degassed thereafter as described above. In fact simply melting the solid under vacuum once removed nearly all the dissolved gas, as far as could be ascertained by observing the sample's behaviour

Deuterium NMR measurements were carried out on three monodeuterated isotopomers of the samples:

1D. 9,10-Di-*n*-octyl-*n*-octadecane-9d_1
2D. 9-*n*-Octyl-*n*-octadecane-9d_1
4D. Tricyclohexylmethane-d_1

The first two samples were prepared as described for the corresponding hydrocarbons. In the case of the last sample, tricyclohexylmethane-d_1, a borosilicate tube of 5 mm od. x 17.5 cm length and internal diameter of about 2 mm was used, since the amount of available isotopomer was limited. About 200 mg gave a sample 5 cm in length when melted. Otherwise the sample was degassed and sealed as described for the larger sample of the ordinary hydrocarbon, and the thick walled tube was not shattered by the expansion on melting.

Silicon-29 NMR measurements could, of course, be carried out on the sample of tri-*n*-octylsilane already prepared.

6.2 CARBON-13 NMR MEASUREMENTS

Carbon-13 T_1 relaxation rates and NOE values were determined over a wide range of temperatures for each of the samples at 67.83 MHz and 100.53 MHz, using Jeol FX270 and GX400 spectrometers, respectively. For all measurements the sample tube was placed concentrically inside a commercial thick walled 10 mm tube, and the intervening annulus filled with an appropriate deuterated solvent, which was used as a field lock. At 25 ^{0}C and above this was dimethylsulphoxide-d_6, and at temperatures below 25 ^{0}C, acetone-d_6 was employed. The field was shimmed beforehand on a sample of deuterium oxide, and this gave good resolution for the spectrum of the actual sample combination in all cases; spectra were acquired without any sample rotation, to minimize possible effects originating from convective currents. For the same reason at least 20 minutes were allowed for temperature equilibration before acquiring measurements, and at the higher temperatures, where the samples became much less viscous and relaxation times longer, up to 45 minutes were allowed. The standard manufacturer's variable temperature equipment was used throughout, and gave control to $\pm$0.5 ^{0}C

T_1 relaxation times were determined using a standard inversion-recovery sequence, with an 8-phase acquisition cycle. The spectra were acquired with complete proton decoupling, as described in Section 6.5, in connection with temperature calibration. A spectral width of 3000 Hz and 8 K data points were used at 67.83 MHz, and 6000 Hz and 16 K data points at 100.53 MHz. It was possible, for the compounds investigated, to cover the entire ranges of the individual magnetisation curves using

15 - 20 carefully chosen relaxation delays, ranging up to approximately 10 times the longest T_1 value under measurement. A generous delay time of 5 - 10 T_1 values was allowed between each scan. The 180^0 pulse lengths were individually determined at each temperature, on each sample, by seeking a null-point spectrum. Typical 180^0 pulse lengths ranged from 38-42 μs on the FX270 spectrometer, and from 32-42 μs on the GX400 spectrometer. The pulse lengths increased as the temperature was raised, particularly using the 10 mm probe of the GX400 spectrometer.

The number of scans was chosen to reduce noise in the transformed spectra to an acceptable level, and typically this required only 16 scans at 67.83 MHz, and 8 scans at 100.53 MHz, because of the large sample sizes being employed. Application of a suitable exponential window was used to further reduce baseline noise, and increase accuracy of the calculated peak heights. Scatter in the data points was usually traceable to baseline noise, and could be removed by repeating the measurement with more scans. The magnetisation curves for each resonance were then determined in the usual way from the peak heights, and the T_1 values obtained by least squares optimization of the fit of the usual three parameter exponential function[1].

On the FX270 spectrometer, the inversion of magnetization obtained was at least 90% across the entire sample spectrum in all cases, and for many of the experiments was uniformly around 95%. The fits of the exponential curves to the measured magnetization were generally very good, with $r^2 \geq 0.97$. The poorer fits usually occurred in experiments which extended over longer time periods, and were probably due to drift in the spectrometer circuitry, although relaxation delays were always randomized to minimize this effect. Repetition of a selected number of experiments on different samples, and at different temperatures, produced T_1 values which were consistent to ±5%.

On the GX400 spectrometer, the results were quite remarkably good. The inversion of magnetization was always in excess of 95%, and the fitted magnetization curves passed almost exactly through each measured value. when the experiment had been correctly prepared and executed; even for the longer experiments, with longer relaxation times. Repetition of a number of experiments on different samples, and at different temperatures, produced T_1 values which were consistent to ±3%.

The NOE factors were determined using standard inverse-gated decoupling sequences. The details of the proton decoupling used appear in Section 6.5. Fully proton decoupled scans were acquired first, followed by an equal number of scans with gated decoupling. The equal pulse lengths in both experiments were chosen to be close to 90^0, and the delay time between each scan was generous, at 10-15 T_1 values. The NOE factors were determined, wherever possible, from ratios of the corresponding, individually calculated peak areas; not the heights, which were found to be unreliable in these cases. Where peak overlap prevented the direct use of integrals themselves, the area of the entire peak combination was apportioned in each

spectrum according to the ratio of the peak heights. Peak heights were used directly only where overlap from the residual lock solvent signal made this unavoidable.

To improve the accuracy of the integration of the peak areas as much as possible, at least double the number of scans that had been satisfactory for the corresponding T_1 measurements were employed; double the number of data points were used, and suitable exponential windows were applied (equally to each spectrum, of course) to enhance the signal-to-noise ratio, and increase the number of data points per peak as much as possible, after taking into consideration the problem of peak overlap.

The area of each peak obtained from a given spectrum depended on the accuracy and skill of the human integrator, since all the integrals were manually performed and corrected for baseline drift, using the standard integration packages. However, it was found that the areas were consistent to at least ±5% upon repeated processing. This means that the ratios of areas of the "with" and "without" NOE peak areas could be expected to be accurate only to ±10%. The scatter of the calculated NOE factors in the data plots in Appendices 6-10 can be largely ascribed to this source. The actual error may not be quite as large as this might suggest, and the values can probably be taken to be generally accurate to ±0.1. The error varies depending on the size of the NOE factor, at least in theory being proportionately larger for the smaller factors, than for the larger ones.

There appears to be a systematic error in the results from the GX400 spectrometer at higher temperatures, where the NOE factors appear consistently low. This may be instrumental in origin, since these measurements had to be made overnight, under automatic control. This meant that the pulse lengths were not ideal, and longer experiments, with larger numbers of scans, had to be pre-programmed, which may have led to increased error from spectrometer drift. Similar measurements under direct operator control on the FX270 spectrometer were quite satisfactory.

6.3 DEUTERIUM NMR MEASUREMENTS

Deuterium T_1 relaxation times were determined for the prepared samples of the monodeuterated isotopomers at 41.405 MHz using the same Jeol FX270 spectrometer used previously for the carbon-13 work. The general conditions and methods were as described for carbon-13 measurement in Section 6.2, but special care was taken over these deuterium measurements, to ensure the highest possible accuracy and reliability. The samples were loaded into the spectrometer exactly as for the ordinary hydrocarbons, without sample rotation, but with the corresponding protonated solvent, instead of the deuterated one, filling the annulus around the inner tube; the spectra were acquired without a field lock. The T_1 values were determined over the same range of temperatures as for the corresponding carbon-13 work, and at

least 1 hour was always allowed for temperature equilibration before commencing measurement.

Values of T_1 relaxation times values were determined using a standard inversion-recovery sequence, with an 8-phase acquisition cycle. The spectra were acquired with noise modulated proton decoupling to maintain uniformity with the measurements made on the ordinary hydrocarbons, although this had no noticeable effect to the appearance of the deuterium spectrum in any case. The spectral width was adjusted for each measurement to be 3-4 times the width of the resonance line. Typically, this meant using 4K data points, and a spectral width of 2 kHz. The pulse point was always placed to one side of the resonance, and 180^0 pulse lengths were 40-50 μs, depending on the temperature. Each experiment utilized 15 relaxation delays, up to about 10 times the T_1 value, carefully chosen to cover the full variation of the magnetization curve, with a delay of 20, or more, T_1 values between the scans.

The number of scans required for each spectrum was at least 64, and 4 dummy scans were introduced before each acquisition. Application of a suitable exponential window was used to reduce baseline noise to a minimum, and increase accuracy of the calculated peak heights. Special care was taken to correctly phase the resonances, particularly as they became very broadened at lower temperatures in the case of the *n*-octyl compounds. The magnetisation curve for the resonance was then determined in the usual way from the peak heights, and the T_1 values obtained by least squares optimization of the fit of the usual three parameter exponential function[1].

The inversion of magnetization obtained was always at least 95%, and the fits of the exponential functions to the measured magnetization were excellent, with $r^2 \geq 0.98$ at all temperatures, for all three compounds. Repetition of a selected number of experiments, at different temperatures, produced T_1 values which were consistent to ±3%. The fits tended to be slightly poorer at the lower temperatures, where the T_1 values were of the order of milliseconds. Relaxation delays of only several hundred microseconds were used in these experiments, and small errors in the delay timing may have given slightly poorer data.

Half height deuterium line widths were measured directly from the dispersive resonances, and the actual line width found after subtracting the broadening due to the exponential window that had been applied. The inhomogeneity of the applied field, and the effect of the decoupler noise modulation, were insignificant contributions to the deuterium line widths in these examples except at the highest temperatures, as a simple analysis showed.

An examination was made of some typical line widths in the carbon-13 spectra of the same samples, under identical conditions to those described above, (in particular, without sample rotation), at temperatures where extreme narrowing had been shown to apply, and the assumption of $T_1 \approx T_2$ could be made. After subtracting the natural line width corresponding to this, the residual line width was 2-3 Hz for the

8 mm / 10 mm tube combination, and 1-2 Hz for the 5 mm / 10 mm combination used for tricyclohexylmethane-d_1. These would correspond to contributions of at most 1-2 Hz, and about 1 Hz, respectively, to the deuterium NMR line widths, where broadening due to the applied proton decoupling would also be smaller. Therefore, the measured deuterium line widths were corrected by reducing those of 9,10-di-*n*-octyl-*n*-octadecane-9d_1 and 9-*n*-octyl-*n*-heptadecane-9d_1 uniformly by 1.5 Hz, and those of tricyclohexylmethane-d_1 by 1 Hz.

Transverse T_2 relaxation times were computed from the corrected line widths using the usual formula for a Lorenztian resonance:

$$T_2 = \frac{1}{\pi \nu_{1/2}}$$

The resulting T_2 values are given in the tables in Section 6.7, and comparison with the T_1 values in extreme narrowing at the higher temperatures, justify the corrections made to the line widths. The line widths are believed accurate to ±2 Hz, which is small as a percentage of the larger line widths encountered. It was found during the subsequent analyses of the data that the proportionately larger errors in the line widths at higher temperatures for 9,10-di-*n*-octyl-*n*-octadecane-9d_1 and 9-*n*-octyl-*n*-heptadecane-9d_1 were not significant in the extraction of the required parameters describing τ_m. For example, increasing the inhomogeneity correction by 1 Hz across the entire range of line width data changed the resulting parameters of the optimum fits of the theoretical curves (E_m, τ_m^{298}, and K^2) by less than 0.1%.

In the case of tricyclohexylmethane-d_1, at the higher temperatures it was possible to detect the signal from the minor component with labelling on a tertiary centre next to the central carbon atom, and so in this case half-height half-line widths were measured for the side of the main resonance that was not affected by overlap with the minor component, and doubled. Despite this precaution, the line width data were not compatible with the theoretical picture assumed here, as is discussed in detail in Chapter 8, and were not actually utilized for the motional analyses.

6.4 SILICON-29 NMR MEASUREMENTS

Silicon-29 T_1 relaxation times were determined for the sample of tri-*n*-octylsilane at 53.5977 MHz using the same Jeol FX270 spectrometer used previously for the carbon-13 work. The general conditions and methods were as described for carbon-13 measurement in Section 6.2, but special care was taken over these measurements, to ensure the highest possible accuracy and reliability. The sample was loaded into the spectrometer exactly as for the carbon-13 measurements. The T_1

values were determined over the same range of temperatures, and at least 1 hour was always allowed for temperature equilibration before commencing measurement.

Values of T_1 relaxation times values were determined using a standard inversion-recovery sequence, with an 8-phase acquisition cycle. The spectra were acquired with complete proton decoupling, to maintain uniformity with the carbon-13 measurements. This generally resulted in a considerable improvement of signal-to-noise, by removal of the large proton couplings to the silicon atom, despite the negative NOE produced. The spectral width was usually 200 Hz, and 2K data points were used. This gave a long acquisition time of 5.12 s, and heavy exponential windows were applied to remove the noise resulting from this, and broaden the narrow resonance. The pulse point was always placed to one side of the resonance, and 180^0 pulse lengths were 40-55 μs, depending on the temperature. Each experiment utilized 15 relaxation delays, distributed at random, up to about 10 times the T_1 value, and carefully chosen to cover the full variation of the magnetization curve, with a delay of 5 T_1 values between scans.

The number of scans was chosen to reduce baseline noise to a few percent of the largest resonance observed, and depended quite strongly on the temperature. At higher temperatures, the NOE factor became less negative and signal-to-noise deteriorated somewhat, requiring some 64-96 scans, and experiments running for up to 10 hours due to the long T_1 times. The magnetisation curve for the resonance was determined in the usual way from the peak heights, and the T_1 values obtained by least squares optimization of the fit of the usual three parameter exponential function[1].

The inversion of magnetization obtained was at least 90%, and the fits of the exponential functions to the measured magnetization were very good for the shorter experiments, with $r^2 \geq 0.98$, but slightly less so for the higher temperature measurements, where the magnetization curve contained more scatter, probably due to drifting spectrometer conditions during the long experiments. Nevertheless, repetition of a few of the experiments produced T_1 values which were consistent to ±5%.

The silicon-29 resonance was only a few Hertz wide at all temperatures, and therefore T_2 values were not available from line width measurements of the kind used for the deuterium measurements in Section 6.3.

6.5 TEMPERATURE CALIBRATION

The measurements with the FX270 spectrometer employed 5 W of noise modulated continuous wave decoupling, while the GX400 spectrometer employed a low power composite pulse Waugh sequence. In the case of the GX400 bilevel decoupling was used during the acquisition of the NOE enhanced spectra in the with/without NOE pairs, while constant power decoupling was applied for the T_1 measurements. Since the accuracy of the conclusions to be drawn from the measured

data would depend strongly on the temperatures at which the various measurements took place, some care was given to this question. However, sample heating by the decoupling irradiation was found to be minimal.

A sample was prepared consisting of a similar arrangement to that used for the actual measurements, with the appropriate lock solvent, a sample of 9,10-dioctyloctadecane, and a very small (1 mm) copper-constantan thermocouple dipping into the sample to exactly the depth of the irradiation coils of the probe in use. This assembly was loaded into the spectrometer, and attached by a long extension to a calibrated digital meter. (Comark). The strong magnetic field did not affect the reading at room temperature. The sample temperature could then be measured at the various set temperature readouts on the spectrometer variable temperature controller that were to be used in the actual experiments.

The effect of irradiation on the sample temperature was determined in a simple manner; the irradiation was switched on for some minutes, and then abruptly stopped. After a few seconds the reading of the digital meter stabilized and the sample temperature could be quickly ascertained, before it began to relax to the original reading, which required several minutes. On both the FX270 and GX400 10 mm probes, the introduction of the thermocouple into the sample did not noticeably change the tuning and matching of the irradiation coil from that normally present during this work. Therefore the power absorbed by the sample with the thermocouple present could be expected to be close to that absorbed by a normal sample, and any heating effect caused by the presence of the small metallic thermocouple could be neglected.

It was found in the case of the FX270 that irradiation caused an increase of a few degrees only at each set temperature, whereas for the GX400 the change averaged around one degree. The temperatures determined in this way are believed to be accurate to ± 1 ^{0}C. The sample temperatures during gated decoupling would differ from the ones determined in this way for continuous decoupling, but evidently by no more than about 1 ^{0}C. Since this represented only a small part of the overall possible error in such NOE measurements, it was assumed that the temperatures under continuous decoupling were the ones to attach to the NOE data, and this has been done in the tables that follow.

Thus the complication of the use of chemical shift thermometry was not required in this work, and it is doubtful if it could give any more accurate results. In any case, several of the original papers dealing with the question of sample temperature under irradiation also found that the heating of non-polar samples such as hydrocarbons was always negligible[2].

6.6 CARBON-13 T_1 RELAXATION TIME AND NOE DATA

The carbon-13 T_1 relaxation time and NOE data that were obtained are recorded in the tables appearing on the following pages, and grouped according to compound in the order:

1. 9,10-Di-*n*-octyl-*n*-octadecane	Tables 6.1-6.4
2. 9-*n*-Octyl-*n*-heptadecane	Tables 6.5-6.8
3. Tri-*n*-octylsilane	Tables 6.9-6.12
4. Tricyclohexylmethane	Tables 6.13-6.16
5. 1,1,2-Tricyclohexylethane	Tables 6.17-6.20

Corrected temperatures are recorded in degrees Centigrade, and Kelvin, and relaxation times in seconds to three decimal places. Data acquired for overlapping carbon-13 resonances are included when they can be assumed to be representative for each individual carbon position, on the basis of expected dynamic equivalence, or the trend of the data at temperatures where the peaks could be resolved individually.

The carbon-13 resonances are given in the tables in the order in which they appear in the standard spectra shown in the earlier chapters, numbering upwards consecutively from the low field side. For the convenience of the reader, the diagrams showing the correspondence of these numberings to the carbon assignments in these five compounds are reproduced at the start of the tables as Fig 6.1.

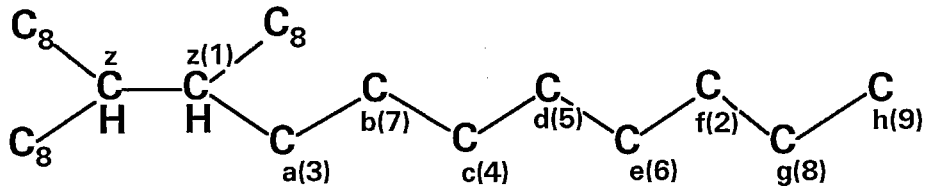

9,10-di-*n*-octyl-*n*-octadecane

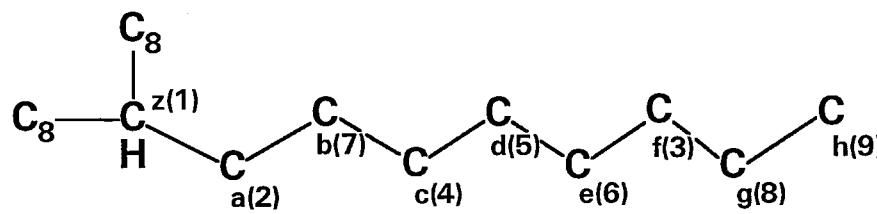

9-*n*-octyl-*n*-heptadecane

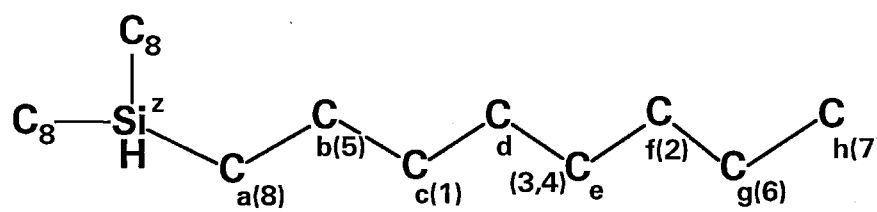

Tri-*n*-octylsilane

Fig 6.1: Carbon-13 peak positions and assignments.

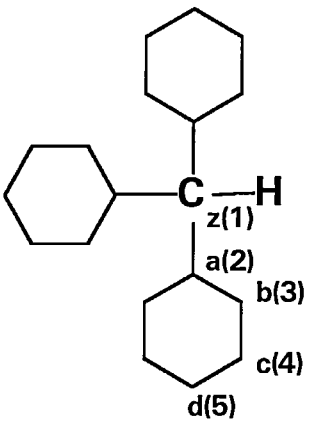

Tricyclohexylmethane

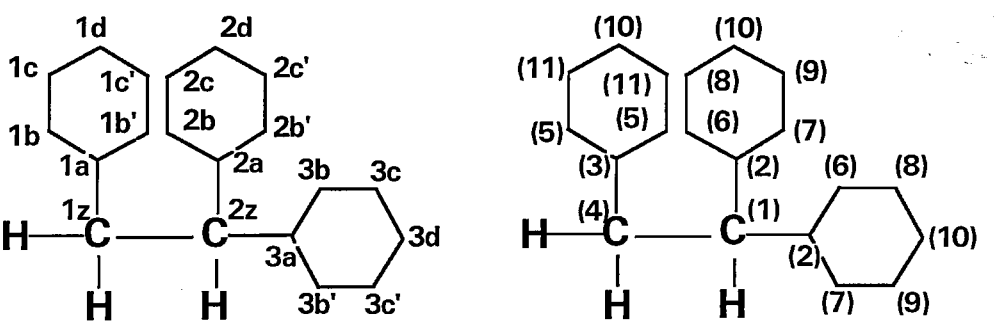

1,1,2-tricyclohexylethane

Fig 6.1 Carbon-13 peak positions and assignments. (continued)

Temperature		Peak position								
^{0}C	K	1	2	3	4	5	6	7	8	9
118.3	391.5	0.500	3.719	0.443	1.224	1.804	2.603	0.742	5.177	6.624
99.9	373.1	0.408	3.146	0.341	1.118	1.613	2.183	0.613	4.507	7.246
81.0	354.2	0.273	2.353	0.232	0.743	1.163	1.698	0.418	3.595	5.456
61.1	334.3	0.198	1.620	0.171	0.450	0.730	0.970	0.280	2.462	4.345
41.7	314.9	0.164	0.880	0.131	0.306	0.466	0.588	0.204	1.375	2.748
27.0	300.2	0.145	0.625	0.112	0.240	0.325	0.444	0.166	0.929	1.986
14.0	287.2	0.152	0.493	0.113	0.210	0.272	0.371	0.152	0.720	1.565
5.0	278.2	0.174	0.403	0.115	0.185	0.244	0.279	0.151	0.579	1.274
-4.7	268.5	0.205	0.324	0.167	0.167	0.200	0.229	0.147	0.451	1.016
-14.1	259.1	0.322	0.277	0.278	0.161	0.180	0.200	0.155	0.360	0.829

Table 6.1: Carbon-13 T_1 relaxation times of 9,10-di-*n*-octyl-*n*-octadecane at 67.83 MHz.

Temperature		Peak position								
^{0}C	K	1	2	3	4	5	6	7	8	9
133.1	406.3	0.649	4.564	0.577	1.602	2.344	3.179	0.983	6.208	7.484
111.4	384.6	0.464	3.799	0.407	1.203	1.808	2.501	0.718	5.617	8.089
89.1	362.3	0.354	2.646	0.294	0.838	1.254	1.735	0.507	4.029	6.461
66.0	339.2	0.272	1.779	0.227	0.595	0.849	1.173	0.370	2.719	4.783
43.6	316.8	0.220	1.122	0.179	0.406	0.567	0.756	0.263	1.674	3.176
26.7	299.9	0.225	0.776	0.165	0.322	0.425	0.550	0.227	1.150	2.229
12.1	285.3	0.271	0.616	0.192	0.293	0.371	0.447	0.228	0.878	1.754
2.6	275.8	0.336	0.498	0.212	0.260	0.313	0.372	0.227	0.685	1.410
-6.8	266.4	0.429	0.410	0.232	0.237	0.273	0.317	0.228	0.545	1.118
-16.5	256.7	0.607	0.351	—	0.236	0.246	0.282	0.234	0.454	0.921

Table 6.2: Carbon-13 T_1 relaxation times of 9,10-di-*n*-octyl-*n*-octadecane at 100.53 MHz.

Temperature		Peak position								
^{0}C	K	1	2	3	4	5	6	7	8	9
118.3	391.5	1.52	1.80	1.76	1.85	1.87	1.87	1.79	1.59	1.67
99.9	373.1	1.70	1.84	1.83	1.89	1.90	1.94	1.89	1.84	1.80
81.0	354.2	1.31	1.72	1.60	1.69	1.75	1.76	1.51	1.77	1.81
61.1	334.3	1.18	1.75	1.30	1.55	1.66	1.72	1.34	1.76	1.86
41.7	314.9	0.81	1.70	0.93	1.42	1.56	1.63	1.12	1.73	1.92
27.0	300.2	0.45	1.28	0.46	0.88	0.99	1.04	0.66	1.36	1.50
14.0	287.2	0.54	1.26	0.52	0.92	1.02	1.13	0.78	1.44	1.64
5.0	278.2	0.35	1.26	0.49	0.86	0.97	1.07	0.80	1.34	1.52
-4.7	268.5	0.37	1.10	—	0.72	0.84	0.94	0.75	1.20	1.50
-14.1	259.1	0.47	1.18	—	0.88	0.90	0.97	0.89	1.34	1.62

Table 6.3: Carbon-13 NOE factors of 9,10-di-*n*-octyl-*n*-octadecane at 67.83 MHz.

Temperature		Peak position								
^{0}C	K	1	2	3	4	5	6	7	8	9
119.3	392.5	1.39	1.61	1.56	1.51	1.54	1.54	1.68	1.67	1.61
100.1	373.3	1.45	1.62	1.45	1.61	1.65	1.70	1.59	1.82	1.68
80.0	353.2	1.16	1.65	1.22	1.40	1.50	1.55	1.36	1.78	1.90
60.0	333.2	0.86	1.58	0.91	1.24	1.35	1.41	1.08	1.66	1.77
40.3	313.5	0.57	1.56	0.67	1.11	1.26	1.33	0.92	1.59	1.81
25.7	298.9	0.38	1.42	0.60	1.08	1.23	1.31	0.83	1.54	1.72
10.9	284.1	0.49	1.49	0.66	0.98	1.08	1.22	0.92	1.52	1.91
1.5	274.7	0.47	1.34	0.65	0.89	1.03	1.06	0.88	1.40	1.92
-8.1	265.1	0.44	1.31	—	0.74	0.94	0.94	0.82	1.30	1.63
-17.9	255.3	0.38	1.10	—	0.68	0.76	0.88	0.81	1.20	1.60

Table 6.4: Carbon-13 NOE factors of 9,10-di-*n*-octyl-*n*-octadecane at 100.53 MHz.

Temperature		Peak position								
^{0}C	K	1	2	3	4	5	6	7	8	9
118.3	391.2	1.541	1.165	4.128	2.302	2.829	3.565	1.662	5.611	6.507
99.9	373.1	1.153	0.838	3.915	1.605	2.331	2.776	1.167	5.214	7.039
81.0	354.2	0.792	0.610	3.370	1.268	1.773	2.251	0.832	4.184	6.021
61.1	334.3	0.472	0.352	1.945	0.700	0.984	1.432	0.490	2.855	4.574
41.7	314.9	0.348	0.255	1.365	0.514	0.662	0.857	0.368	1.840	3.306
27.0	300.2	0.239	0.184	0.915	0.373	0.493	0.643	0.255	1.292	2.429
14.0	287.2	0.210	0.159	0.687	0.289	0.376	0.483	0.201	1.025	2.017
5.0	278.2	0.159	0.120	0.511	0.213	0.277	0.349	0.164	0.748	1.529
-4.7	268.5	0.146	0.109	0.398	0.186	0.242	0.297	0.147	0.562	1.170
-14.1	259.1	0.144	0.109	0.332	0.172	0.207	0.243	0.141	0.450	0.889
-20.2	253.0	0.161	0.106	0.284	0.159	0.182	0.215	0.129	0.381	0.798

Table 6.5: Carbon-13 T_1 relaxation times for 9-*n*-octyl-*n*-heptadecane at 67.83 MHz.

Temperature		Peak position								
^{0}C	K	1	2	3	4	5	6	7	8	9
133.1	406.3	1.679	1.274	5.157	2.413	3.152	3.907	1.782	6.471	7.213
111.4	384.6	1.304	0.950	4.295	1.802	2.462	3.142	1.319	5.515	6.616
89.1	362.3	0.884	0.667	3.510	1.322	1.847	2.387	0.943	4.967	7.115
66.0	339.2	0.602	0.451	2.572	0.930	1.315	1.718	0.647	3.754	6.191
43.6	316.8	0.369	0.288	1.605	0.587	0.826	1.085	0.405	2.347	3.883
26.7	299.9	0.296	0.223	1.002	0.407	0.546	0.697	0.299	1.458	2.629
12.1	285.3	0.250	0.188	0.778	0.332	0.439	0.568	0.246	1.108	2.091
2.6	275.8	0.223	0.164	0.558	0.269	0.333	0.411	0.209	0.779	1.467
-6.8	266.4	0.220	0.154	0.489	0.242	0.298	0.358	0.195	0.652	1.270
-16.5	256.7	0.247	0.154	0.394	0.223	0.258	0.304	0.192	0.514	1.000
-21.1	252.1	0.277	0.157	0.353	0.213	0.243	0.281	0.191	0.465	0.849

Table 6.6: Carbon-13 T_1 relaxation times for 9-*n*-octyl-*n*-heptadecane at 100.53 MHz.

Temperature		Peak position								
^{0}C	K	1	2	3	4	5	6	7	8	9
118.3	391.5	1.97	1.89	1.81	1.91	1.92	1.91	1.81	1.93	1.84
99.9	373.1	1.90	1.91	1.99	1.98	2.02	2.02	2.05	1.94	1.86
81.0	354.2	2.00	2.06	2.15	2.09	2.07	2.11	2.08	2.07	2.12
61.1	334.3	1.92	1.79	1.82	1.75	1.78	1.76	1.63	1.67	1.72
41.7	314.9	1.73	1.62	1.83	1.66	1.72	1.72	1.62	1.88	1.95
27.0	300.2	1.26	1.35	1.64	1.45	1.56	1.58	1.45	1.73	1.86
14.0	287.2	1.00	1.11	1.45	1.09	1.19	1.21	1.12	1.63	1.82
5.0	278.2	0.80	0.98	1.45	0.97	1.09	1.19	0.93	1.50	1.73
-4.7	268.5	0.59	0.79	1.27	0.89	1.00	1.03	0.86	1.45	1.67
-14.1	259.1	0.68	0.69	1.21	0.94	1.04	1.06	0.84	1.25	1.55
-19.0	254.2	0.37	0.70	1.20	0.92	0.99	0.98	0.83	1.21	1.51

Table 6.7: Carbon-13 NOE factors for 9-*n*-octyl-*n*-heptadecane at 67.83 MHz.

Temperature		Peak position								
^{0}C	K	1	2	3	4	5	6	7	8	9
119.3	392.5	1.68	1.71	1.64	1.68	1.71	1.72	1.62	1.71	1.72
100.1	373.3	1.88	1.82	1.80	1.85	1.86	1.83	1.83	1.78	1.76
80.0	353.2	1.92	1.84	1.91	1.77	1.79	1.78	1.82	1.98	1.93
60.0	333.2	1.60	1.69	1.80	1.68	1.72	1.76	1.56	1.80	1.87
40.3	313.5	1.55	1.53	1.65	1.52	1.60	1.64	1.51	1.76	1.87
25.7	298.9	1.19	1.26	1.59	1.30	1.45	1.49	1.27	1.76	1.96
10.9	284.1	0.82	1.03	1.47	1.04	1.13	1.13	1.10	1.57	1.98
1.5	274.7	0.62	0.89	1.58	0.98	1.05	1.10	0.96	1.54	1.83
-8.1	265.1	0.57	0.86	1.22	0.97	1.07	1.11	0.94	1.53	1.88
-17.9	255.3	0.48	0.71	1.20	0.91	0.93	1.00	0.84	1.30	1.69
-22.9	250.3	0.47	0.60	1.10	0.85	0.88	0.92	0.85	1.31	1.71

Table 6.8: Carbon-13 NOE factors for 9-*n*-octyl-*n*-heptadecane at 100.53 MHz.

Temperature		Peak position							
^{0}C	K	1	2	3	4	5	6	7	8
118.3	391.5	2.805	4.084	3.251	3.575	2.469	4.528	4.707	1.990
99.9	373.1	1.816	3.576	2.385	2.906	1.890	4.575	5.552	1.478
81.0	354.2	1.446	2.779	1.781	1.978	1.433	3.353	3.785	1.167
61.1	334.3	1.073	2.476	1.456	1.730	1.026	3.343	4.938	0.785
41.7	314.9	0.786	1.879	1.145	1.229	0.726	2.634	4.061	0.555
27.0	300.2	0.513	1.130	— 0.722 —		0.485	1.605	2.810	0.384
14.0	287.2	0.425	0.923	— 0.573 —		0.392	1.314	2.263	0.307
5.0	278.2	0.383	0.745	— 0.495 —		0.360	1.053	1.994	0.288
-4.7	268.5	0.290	0.579	— 0.395 —		0.279	0.811	1.596	0.224
-14.1	259.1	0.238	0.452	— 0.312 —		0.232	0.603	1.239	0.185
-23.9	249.3	0.215	0.357	— 0.247 —		0.208	0.467	0.882	0.173

Table 6.9: Carbon-13 T_1 relaxation times for tri-*n*-octylsilane at 67.83 MHz.

Temperature		Peak position							
^{0}C	K	1	2	3	4	5	6	7	8
133.1	406.3	2.993	4.988	3.589	4.153	2.817	5.810	6.108	2.238
111.4	384.6	2.488	4.978	3.233	3.743	2.323	6.378	6.872	1.764
89.1	362.3	1.868	4.111	2.436	2.973	1.742	5.630	7.635	1.339
66.0	339.2	1.348	3.138	1.811	2.169	1.257	4.391	6.735	0.975
43.6	316.8	0.905	2.021	1.201	1.367	0.847	2.851	4.621	0.679
26.7	299.9	0.619	1.307	— 0.834 —		0.586	1.831	2.965	0.460
12.1	285.3	0.473	0.971	— 0.647 —		0.450	1.360	2.408	0.359
2.6	275.8	0.396	0.762	— 0.525 —		0.377	1.050	1.885	0.299
-6.8	266.4	0.336	0.593	— 0.424 —		0.324	0.819	1.501	0.262
-16.5	256.7	0.285	0.476	— 0.352 —		0.277	0.630	1.110	0.233
-26.4	246.8	0.245	0.378	— 0.288 —		0.240	0.475	0.881	0.210

Table 6.10: Carbon-13 T_1 relaxation times for tri-*n*-octylsilane at 100.53 MHz.

Temperature		Peak position							
^{0}C	K	1	2	3	4	5	6	7	8
118.3	391.5	1.81	1.91	— 1.71 —		1.82	1.72	1.58	1.61
99.9	373.1	1.83	1.84	— 1.96 —		1.78	1.76	1.81	1.75
81.0	354.2	1.82	1.80	— 1.83 —		2.08	1.86	1.92	1.87
61.1	334.3	1.84	2.00	— 1.94 —		1.79	1.77	1.85	1.70
41.7	314.9	1.62	1.80	— 1.62 —		1.58	1.92	1.68	1.63
27.0	300.2	1.63	1.59	— 1.57 —		1.49	1.73	1.77	1.20
14.0	287.2	1.43	1.73	— 1.33 —		1.42	1.81	1.90	1.43
5.0	278.2	1.24	1.48	— 1.21 —		1.27	1.61	1.81	1.22
-4.7	268.5	1.26	1.44	— 1.05 —		1.07	1.47	1.83	1.08
-14.1	259.1	1.10	1.31	— 0.97 —		1.10	1.37	1.82	1.12
-23.9	249.3	1.04	1.15	— 0.96 —		1.12	1.24	1.56	1.00

Table 6.11: Carbon-13 NOE factors for tri-*n*-octylsilane at 67.83 MHz.

Temperature		Peak position							
^{0}C	K	1	2	3	4	5	6	7	8
119.3	392.5	1.69	1.81	— 1.77 —		1.94	1.72	1.66	1.88
100.1	373.3	1.68	1.75	— 1.67 —		1.65	1.79	1.93	1.68
80.0	353.2	1.81	1.86	— 1.81 —		1.81	1.75	1.90	1.98
60.0	333.2	1.63	1.80	— 1.67 —		1.69	2.01	1.87	1.71
40.3	313.5	1.57	1.71	— 1.61 —		1.51	1.81	1.73	1.52
25.7	298.9	1.43	1.68	— 1.55 —		1.56	1.83	1.85	1.23
10.9	284.1	1.33	1.72	— 1.18 —		1.43	1.93	1.84	1.41
1.5	274.7	1.57	1.67	— 0.98 —		1.34	1.74	2.01	1.13
-8.1	265.1	1.30	1.74	— 1.14 —		1.38	1.77	1.86	1.14
-17.9	255.3	1.21	1.35	— 1.03 —		1.29	1.60	1.84	1.18
-27.8	245.4	1.09	1.29	— 0.94 —		1.11	1.42	1.69	0.99

Table 6.12: Carbon-13 NOE factors for tri-*n*-octylsilane at 100.53 MHz.

Temperature		Peak position				
^{0}C	K	1	2	3	4	5
137.0	410.2	1.574	1.567	0.968	0.993	0.847
127.7	400.9	1.310	1.260	0.743	0.756	0.692
118.3	391.5	1.125	0.972	0.604	0.610	0.513
109.3	382.5	0.946	0.846	0.512	0.547	0.464
99.9	373.1	0.736	0.667	0.407	0.412	0.362
89.9	363.1	0.506	0.512	0.308	0.311	0.250
81.0	354.2	0.323	0.326	0.211	0.210	0.188
71.0	344.2	0.261	0.259	0.161	0.162	0.154
61.1	334.3	0.195	0.195	0.122	0.123	0.114

Table 6.13: Carbon-13 T_1 relaxation times for tricyclohexylmethane at 67.83 MHz.

Temperature		Peak position				
^{0}C	K	1	2	3	4	5
133.1	406.3	1.466	1.383	0.821	0.831	0.707
122.4	395.6	1.176	1.132	0.680	0.686	0.584
111.4	384.6	0.950	0.898	0.531	0.540	0.456
100.5	373.7	0.699	0.676	0.397	0.403	0.341
89.1	362.3	0.515	0.522	0.312	0.315	0.269
77.6	350.8	0.367	0.383	0.220	0.225	0.196
66.0	339.2	0.279	0.299	0.170	0.172	0.153

Table 6.14: Carbon-13 T_1 relaxation times for tricyclohexylmethane at 100.53 MHz.

Temperature		Peak position				
^{0}C	K	1	2	3	4	5
137.0	410.2	1.81	1.98	1.97	1.96	1.98
118.3	391.5	1.81	1.98	1.94	1.99	2.02
99.9	373.1	1.88	1.90	1.87	1.76	1.71
89.9	363.1	1.71	1.81	1.86	1.85	1.88
81.0	354.2	1.87	1.79	1.74	1.74	1.72
76.0	349.2	2.06	1.84	1.91	1.94	1.94
71.0	344.2	1.65	1.44	1.67	1.48	1.40
66.0	339.2	1.28	1.26	1.37	1.35	1.23
61.1	334.3	1.12	1.19	1.23	1.24	1.13

Table 6.15: Carbon-13 NOE factors for tricyclohexylmethane at 67.83 MHz.

Temperature		Peak position				
^{0}C	K	1	2	3	4	5
138.5	411.7	1.92	1.74	1.80	1.71	1.99
128.9	402.1	1.88	1.78	1.82	1.78	2.07
119.3	392.5	1.63	1.81	1.81	1.80	1.76
109.7	382.9	1.63	1.77	1.80	1.82	1.91
100.1	373.2	1.60	1.96	1.92	1.81	1.71
90.0	363.2	1.79	1.61	1.79	1.74	1.75
80.0	353.2	1.74	1.50	1.59	1.62	1.34
70.0	343.2	1.37	1.32	1.38	1.34	1.21
60.0	333.2	0.86	0.87	1.03	0.95	0.87

Table 6.16: Carbon-13 NOE factors for tricyclohexylmethane at 100.53 MHz.

Temperature		Peak position										
°C	K	1	2	3	4	5	6	7	8	9	10	11
137.0	410.2	1.343	1.448	1.644	0.839	1.145	1.007	1.004	1.010	1.011	0.823	1.154
127.7	400.9	1.044	1.182	1.338	0.681	0.831	0.759	0.764	0.779	0.784	0.632	0.884
118.3	391.5	0.926	1.058	1.083	0.560	0.741	0.656	0.656	0.658	0.640	0.529	0.732
109.3	382.5	0.819	0.903	0.944	0.495	0.666	0.597	0.604	0.593	0.586	0.486	0.660
99.9	373.1	0.568	0.645	0.700	0.346	0.440	0.407	0.408	0.393	0.393	0.330	0.458
89.9	363.1	0.388	0.483	0.512	0.252	0.326	0.294	0.291	0.295	0.288	0.237	0.324
81.0	354.2	0.322	0.398	0.423	0.196	0.270	0.235	0.232	0.235	0.227	0.191	0.259
71.0	344.2	0.219	0.278	0.303	0.144	0.182	0.163	0.161	0.157	0.156	0.137	0.178
61.1	334.3	0.178	0.227	0.239	0.111	0.147	0.133	0.133	0.130	0.129	0.115	0.146
51.7	324.9	0.145	0.177	0.194	0.088	0.112	0.106	0.106	0.099	0.104	0.092	0.117
41.7	314.9	0.153	0.165	0.190	0.083	0.106	0.093	0.091	0.099	0.091	0.091	0.110

Table 6.17: Carbon-13 T_1 relaxation times for 1,1,2-tricyclohexylethane at 67.83 MHz.

Temperature		Peak position										
°C	K	1	2	3	4	5	6	7	8	9	10	11
133.1	406.3	1.176	1.345	1.444	0.701	0.932	0.813	0.817	0.815	0.814	0.661	0.932
122.4	395.6	0.956	1.102	1.201	0.576	0.762	0.669	0.678	0.676	0.666	0.543	0.755
111.4	384.6	0.744	0.872	0.928	0.443	0.591	0.523	0.526	0.522	0.516	0.418	0.587
100.5	373.7	0.556	0.672	0.702	0.337	0.445	0.394	0.399	0.403	0.399	0.326	0.445
89.1	362.3	0.449	0.540	0.568	0.265	0.356	0.316	0.321	0.320	0.318	0.261	0.355
77.6	350.8	0.331	0.408	0.445	0.202	0.267	0.238	0.240	0.239	0.239	0.201	0.267
66.0	339.2	0.253	0.316	0.345	0.158	0.207	0.183	0.183	0.184	0.184	0.161	0.204
54.6	327.8	0.214	0.261	0.287	0.133	0.165	0.151	0.149	0.147	0.146	0.138	0.165
43.6	316.8	0.222	0.239	0.267	0.133	0.157	0.138	0.139	0.145	0.142	0.143	0.150

Table 6.18: Carbon-13 T_1 relaxation times for 1,1,2-tricyclohexylethane at 100.53 MHz.

Temperature		Peak position										
°C	K	1	2	3	4	5	6	7	8	9	10	11
137.0	410.2	1.95	1.72	1.99	2.01	2.04	2.05	2.02	1.97	1.98	1.99	1.99
118.3	391.5	1.82	1.78	1.89	2.02	1.93	1.99	2.01	1.93	1.95	1.95	1.95
99.9	373.1	1.68	1.76	1.92	1.98	1.94	1.94	2.03	1.94	1.93	1.95	1.96
81.0	354.2	1.70	1.54	1.55	1.55	1.82	1.70	1.78	1.66	1.64	1.64	1.66
71.0	344.2	1.52	1.40	1.65	1.65	1.65	1.66	1.63	1.63	1.65	1.54	1.62
66.0	339.2	1.28	1.28	1.31	1.31	1.38	1.39	1.41	1.41	1.40	1.26	1.36
61.1	334.3	—	—	—	—	—	—	—	—	—	—	—
56.5	329.7	0.99	1.00	0.93	0.98	1.09	1.12	1.13	1.16	1.12	0.96	1.10
51.7	324.9	0.68	0.80	0.73	0.78	0.85	0.88	0.93	0.94	0.94	0.78	0.93
46.7	319.9	0.51	0.66	0.63	0.62	0.71	0.71	0.75	0.71	0.68	0.57	0.71
41.7	314.9	0.34	0.56	0.48	0.50	0.63	0.62	0.59	0.63	0.60	0.56	0.67

Table 6.19: Carbon-13 NOE factors for 1,1,2-tricyclohexylethane at 67.83 MHz.

Temperature		Peak position										
°C	K	1	2	3	4	5	6	7	8	9	10	11
138.5	411.7	1.79	1.79	1.75	1.91	1.90	1.90	1.93	1.79	1.78	1.80	1.82
128.9	402.1	1.67	1.81	1.65	1.79	1.71	1.78	1.84	1.87	1.90	1.92	1.96
119.3	392.5	1.69	1.82	1.80	1.86	1.82	1.84	1.86	1.80	1.79	1.78	1.79
109.7	382.9	1.79	1.79	1.93	2.10	1.79	1.76	1.76	1.75	1.71	1.73	1.76
100.1	373.3	1.66	1.80	1.60	1.61	1.77	1.75	1.87	1.83	1.82	1.76	1.78
90.0	363.2	1.68	1.72	1.78	1.87	1.75	1.77	1.82	1.78	1.78	1.74	1.77
80.0	353.2	1.56	1.61	1.50	1.68	1.57	1.60	1.57	1.63	1.61	1.53	1.61
70.0	343.2	1.24	1.33	1.06	1.24	1.34	1.40	1.41	1.32	1.34	1.18	1.31
60.0	333.2	0.87	1.00	0.91	0.99	0.97	0.96	1.01	1.03	1.03	0.86	1.02
50.1	323.3	0.55	0.64	0.61	0.65	0.68	0.72	0.75	0.70	0.72	0.60	0.75
40.3	313.5	0.32	0.55	0.53	0.53	0.67	0.57	0.58	0.51	0.50	0.45	0.62

Table 6.20: Carbon-13 NOE factors for 1,1,2-tricyclohexylethane at 100.53 MHz.

6.7 DEUTERIUM T_1 RELAXATION TIME AND LINE WIDTH DATA

The deuterium relaxation times and half height line widths that were obtained at 41.4056 MHz for the three monodeuterated isotopomers are given in the tables appearing on the following pages, in the order:

1D. 9,10-Di-*n*-octyl-*n*-octadecane-9d_1	Table 6.21
2D. 9-*n*-Octyl-*n*-heptadecane-9d_1	Table 6.22
4D. Tricyclohexylmethane-d_1	Table 6.23

Corrected temperatures are recorded in degrees Centigrade, and Kelvin, and relaxation times in milliseconds to three decimal places. The half-height line widths are corrected for the field inhomogeneity, after subtraction of the applied exponential broadening. The correction was 1.5 Hz for the two *n*-octyl compounds, and 1 Hz for tricyclohexylmethane-d_1. The T_2 relaxation times are computed from the half-height line widths using the usual expression for a Lorentzian shape, and the less accurate values at small line widths are recorded to only two significant figures.

6.8 SILICON-29 T_1 RELAXATION TIME DATA

The silicon-29 relaxation times that were obtained for tri-*n*-octylsilane at 53.5977 MHz are given in Table 6.24. Corrected temperatures are recorded in degrees Centigrade, and Kelvin, and relaxation times in seconds to three decimal places. The half-height line widths of the silicon-29 resonance were only a few Hertz at every measured temperature.

REFERENCES FOR CHAPTER 6

1 For the peak height data from the FX270 spectrometer, this least squares optimization was executed using the Microsoft® Excel® 4.0a program, running on an Elonex PC-450 personal computer. The general method was that described in Section 7.1 in connexion with the analyses of the carbon-13 relaxation data, and in the reference given there: W. J. Orvis, *Excel 4 for Scientists and Engineers*, Sybex, 1993. On the GX400, the optimization was performed automatically using the spectrometer software provided by Jeol Ltd.

2 A very careful investigation of sample heating by decoupler irradiation appears in J. J. Led and S. B. Petersen, *J. Magn. Res.*, 1978, **32**, 497; see also A. L. Van Geet, *Anal. Chem.*, 1968, **40**, 2227; A. L. Van Geet, *Anal. Chem.*, 1970, **42**, 679; D. S. Raiford, C. L. Fisk, and E. D. Becker, *Anal. Chem.*, 1979, **51**, 2050

Temperature		T_1	Width	T_2
^0C	K	ms	Hz	ms
137.0	410.2	32.70	11	29
118.3	391.5	23.67	14	23
99.9	373.1	16.84	21	15
81.0	354.2	10.28	26	12
61.1	334.3	6.28	51	6.19
41.7	314.9	3.99	94	3.38
27.0	300.2	3.22	148	2.15
14.0	287.2	3.08	193	1.65
5.0	278.2	3.48	270	1.18
-4.7	268.5	4.83	377	0.84
-14.1	259.1	6.00	638	0.50

Table 6.21: Deuterium T_1 relaxation times and line widths for 9,10-di-n-octyl-n-octadecane-9d_1 at 41.4056 MHz.

Temperature		T_1	Width	T_2
^0C	K	ms	Hz	ms
118.3	391.5	71.29	4	72
99.9	373.1	51.56	6	53
81.0	354.2	34.24	10	32
61.1	334.3	20.69	14	23
41.7	314.9	12.58	25	13
27.0	300.2	8.20	29	11
14.0	287.2	5.49	58	5.48
5.0	278.2	4.34	98	3.24
-4.7	268.5	3.35	129	2.46
-14.1	259.1	3.47	160	1.98
-19.0	254.2	3.21	200	1.60

Table 6.22: Deuterium T_1 relaxation times and line widths for 9-n-octyl-n-heptadecane-9d_1 at 41.4056 MHz.

Temperature		T_1	Width	T_2
^0C	K	ms	Hz	ms
137.0	410.2	77.97	16	20
127.7	400.9	66.80	10	32
118.3	391.5	55.64	12	27
109.3	382.5	43.17	14	23
99.9	373.1	32.27	16	20
89.9	363.1	22.09	22	15
81.0	354.2	14.73	27	12
71.0	344.2	9.36	36	8.81
61.1	334.3	5.80	56	5.72

Table 6.23: Deuterium T_1 relaxation times and line widths for tricyclohexylmethane-d_1 at 41.4055 MHz.

Temperature		T_1
^0C	K	s
137.0	410.2	4.06
118.3	391.5	5.27
99.9	373.1	6.81
81.0	354.2	7.73
61.1	334.3	6.04
41.7	314.9	4.68
27.0	300.2	3.23
14.0	287.2	2.43
5.0	278.2	1.89
-4.7	268.5	1.55
-14.1	259.1	1.24
-23.9	249.3	1.08

Table 6.24: Silicon-29 T_1 relaxation times for tri-*n*-octylsilane at 53.5977 MHz.

Chapter 7

ANALYSES OF THE DATA FOR 9,10-DI-*n*-OCTYL-*n*-OCTADECANE, 9-*n*-OCTYL-*n*-HEPTADECANE, AND TRI-*n*-OCTYLSILANE

7.1 GENERAL OBSERVATIONS

The objective was to simulate the carbon-13 R_1 relaxation rates and NOE factors measured for each of the model lubricant compounds within the theoretical model of Lipari and Szabo for carbon-proton dipolar relaxation discussed in Chapter 1, and thus to determine the generalised order parameters appearing in the expressions, together with the temperature dependence of the correlation times τ_m and τ_i.

For each compound, the values of R_1 and η for each dynamically equivalent carbon atom position in the molecule are predicted by this model as functions of the two correlation times τ_m and τ_i, the resonant frequencies ω_C and ω_H, and the generalised order parameter S^2:

$$\frac{1}{T_1} = R_1 \equiv R_1(\tau_m, \tau_i, \omega_C, \omega_H, S^2) = N\frac{(DCC)^2}{4}(J(\omega_H - \omega_C) + 3J(\omega_C) + 6J(\omega_H + \omega_C)) \quad (1)$$

$$\eta \equiv \eta(\tau_m, \tau_i, \omega_C, \omega_H, S^2) = \left(\frac{\gamma_H}{\gamma_C}\right)\frac{6J(\omega_H + \omega_C) - J(\omega_H - \omega_C)}{J(\omega_H - \omega_C) + 3J(\omega_C) + 6J(\omega_H + \omega_C)} \quad (2)$$

where

$$J(\omega) = \frac{2}{5}\left(\frac{S^2\tau_m}{1+\omega^2\tau_m^2} + \frac{(1-S^2)\tau}{1+\omega^2\tau^2}\right), \quad \text{and} \quad \frac{1}{\tau} = \frac{1}{\tau_m} + \frac{1}{\tau_i} \quad (3)$$

and N is 1, 2, or 3, according to the number of directly bonded protons. The dipolar coupling constant, DCC, was taken as 143.40 kHz in this work.

The expressions for R_1 and η can be written in a more convenient form for numerical work by recognising them as functions of only the carbon-13 frequency at the applied field

$$\frac{1}{T_1} = R_1 \equiv R_1(\tau_m, \tau_i, \omega, S^2) = N\frac{(DCC)^2}{4}(J(2.977092\omega) + 3J(\omega) + 6J(4.977092\omega)) \quad (4)$$

$$\eta \equiv \eta(\tau_m, \tau_i, \omega, S^2) = \left(\frac{\gamma_H}{\gamma_C}\right) \frac{6J(4.977092\omega) - J(2.977092\omega)}{J(2.977092\omega) + 3J(\omega) + 6J(4.977092\omega)} \tag{5}$$

where there is now no need to distinguish ω by a subscript.

The data measured for any one compound consisted of values of R_1 and η, each one at some known absolute temperature T, and a known carbon-13 resonant frequency ω, $\{R_1(T,\omega), \eta(T,\omega)\}$. In the present case there were two frequencies present, so for a given temperature there would be four measured quantities, two R_1 rates and two NOE factors. In principle, by equating these measurements to the values predicted by Eqs. (3)-(5) it would be possible to obtain the values of the three unknowns τ_m, τ_i and S^2 at this temperature by obtaining the solution, or at least the closest simultaneous solution, for the resulting set of over determined equations. This approach is used in one paper of Kovalewski[1], where measurements were made at four different frequencies. Continuing in this way at different temperatures would lead to the solution of the temperature dependence of τ_m and τ_i. Assuming an Arrhenius relationship would produce corresponding activation energies E and values of τ^{298}, if the dependence was of this form. The dependence of S^2 on temperature (if any) would also be revealed. However, this work adopted a different approach used often by Gillies and Sutcliffe[2], and by Kovalewski in a previous paper[3].

The assumption was made, a priori, that the temperature dependence of the correlation times should be described by Arrhenius relationships:

$$\tau_m = \tau_m^{298} \exp\left(\frac{E_m}{R}\left(\frac{1}{T} - \frac{1}{298}\right)\right) \tag{6}$$

$$\tau_i = \tau_i^{298} \exp\left(\frac{E_i}{R}\left(\frac{1}{T} - \frac{1}{298}\right)\right) \tag{7}$$

In this way the predicted relaxation rates and NOE factors for each dynamically equivalent carbon atom position appear via Eqs. (3)-(5) as functions of the temperature, T, the frequency ω, and five unknown parameters, E_m, E_i, τ_m^{298}, τ_i^{298}, and S^2

$$R_1 \equiv R_1(T, \omega; E_m, \tau_m^{298}, E_i, \tau_i^{298}, S^2) \tag{8}$$

$$\eta \equiv \eta(T, \omega; E_m, \tau_m^{298}, E_i, \tau_i^{298}, S^2) \tag{9}$$

The unknown parameters were then determined by requiring that the values predicted by Eqs. (8) and (9) should fit the measured values, $\{R_1(T,\omega), \eta(T,\omega)\}$, as functions of

temperature, at each given frequency ω, "as well as possible". As is common, the criterion employed was that this should be the best least squares fit. A sum such as

$$F(E_m,\tau_m^{298},E_i,\tau_i^{298},S^2)=\sum_{\omega}\sum_{T}\{R_1(T,\omega)-R_1(T,\omega;E_m,\tau_m^{298},E_i,\tau_i^{298},S^2)\}^2$$

$$+\sum_{\omega}\sum_{T}\{\eta(T,\omega)-\eta(T,\omega;E_m,\tau_m^{298},E_i,\tau_i^{298},S^2)\}^2 \qquad (10)$$

was formed, using the Microsoft® Excel® 4.0a package, running on an Elonex PC-450 personal computer, where the summations were carried out in the order indicated. The function F was then minimized by the conjugate gradient search provided with the same package[4], with partial derivatives approximated by central differences. In the actual summation used an allowance was made for the differing numerical magnitudes of the T_1 and NOE data, by scaling the separate sums of squares for T_1 and NOE data at each frequency according to the squared standard deviation of the measured data[4], and in this way the contributions of both the NOE and T_1 data to F were equally weighted.

The advantage is that although individual data points might be rather inaccurate, the fitting of the temperature dependent form of the Lipari and Szabo equations effectively interpolates these without being unduly influenced by local errors at any given temperature. The disadvantage is that the functional temperature dependence of the parameters must be known, or assumed. However, it is important to note that this method is still consistent with the previous more direct approach. Assuming the fits obtained for the temperature dependent curves of T_1 and η are close to the measured individual data points, then at any given temperature the values of τ_m, τ_i given by Eqs. (6) and (7), together with the S^2 parameter, are in effect the solution that was sought before, but perturbed in this case to take account of the general trend of the data in the locality of this temperature. The assumption of the Arrhenius dependence becomes self-justified.

A similar approach was used for the corresponding deuterium relaxation data of the deuterium labelled isotopomers, where these were available. The assumption was made that the equations of Section 1.7 could be used, in which only E_m, τ_m^{298}, and a scaling parameter S^2 appear as unknown quantities:

$$\frac{1}{T_1}=R_1=\frac{\pi^2}{10}\left(1+\frac{\eta^2}{3}\right)S^2(QCC)^2(3J(\omega)+12J(2\omega)) \qquad (11)$$

$$\frac{1}{T_2}=R_2=\frac{\pi^2}{20}\left(1+\frac{\eta^2}{3}\right)S^2(QCC)^2(9J(0)+15J(\omega)+6J(2\omega)) \qquad (12)$$

where

$$J(\omega) = \frac{\tau_m}{1+\omega^2\tau_m^2} \tag{13}$$

and ω is the deuterium resonant frequency.

It turned out, as discussed below in the individual cases, that this description was satisfactory. The multiplicative factors appearing at the front of these formulae were absorbed as a single unknown parameter

$$K^2 = \left(1+\frac{\eta^2}{3}\right)S^2(QCC)^2 \tag{14}$$

to give R1 and R2 as functions of temperature T, frequency ω, and three unknown parameters, E_m, τ_m^{298} and K^2

$$R_1 \equiv R_1(T,\omega;E_m,\tau_m^{298},K^2) \tag{15}$$

$$R_2 \equiv R_2(T,\omega;E_m,\tau_m^{298},K^2) \tag{16}$$

The unknown parameters could then be determined by least squares fits of the predicted R_1 and R_2 values to the measured data as functions of frequency and temperature, in the manner described for the carbon-13 data. In the cases of 9,10-di-*n*-octyl-*n*-octadecane-9d_1 and 9-*n*-octyl-*n*-heptadecane-9d_1 these fits were extremely good, and easily determined values for E_m and τ_m^{298}, as well as K^2. The case of tricyclohexylmethane-d_1 required a more subtle analysis, but still proved informative. The use of these values in conjunction with the analyses of the carbon-13 relaxation data is discussed further in the following section.

The silicon-29 R_1 relaxation rates for tri-*n*-octylsilane were described by the equations of Section 1.8, using only the reduced form of the spectral density, and including the term for isotropic spin–rotational relaxation at extreme narrowing. Redefining $J(\omega)$ slightly, by repositioning S^2 in the main formula, the relevant equations become

$$\frac{1}{T_1} = R_1 = \frac{S^2(DCC)^2}{10}(6J(\omega_H-\omega_{Si})+3J(\omega_{Si})+J(\omega_H+\omega_{Si}))+\frac{C^2}{\tau_m} \tag{17}$$

where DCC is the appropriate dipolar coupling constant, and

$$J(\omega) = \left(\frac{\tau_m}{1+\omega^2\tau_m^2}\right) \tag{18}$$

The expression for R_1 can be written in a more convenient form for numerical work as a function of only the silicon-29 frequency at the applied field

$$\frac{1}{T_1} = R_1 = \frac{S^2(DCC)^2}{10}(6J(4.032529\omega)+3J(\omega)+J(6.032529\omega))+\frac{C^2}{\tau_m} \qquad (19)$$

Following the example of the equations for deuterium relaxation, two multiplicative factors were absorbed as a single unknown parameter

$$D^2 = S^2(DCC)^2 \qquad (20)$$

to give R_1 as a function of temperature T, the silicon-29 frequency ω, and four unknown parameters, E_m, τ_m^{298}, C^2 and D^2

$$R_1 \equiv R_1(T,\omega;E_m,\tau_m^{298},C^2,D^2) \qquad (21)$$

A least squares fit of the predicted R_1 values to the measured data as a function of temperature was very satisfactory, and determined E_m, although the remaining parameters were not individually determined by the limited amount of measured data available.

7.2 PRELIMINARY EXAMINATION OF THE DATA FOR 9-*n*-OCTYL-*n*-HEPTADECANE

The initial examination of the data for 9-*n*-octyl-*n*-heptadecane allowed five parameter fits of the temperature dependent Lipari and Szabo equations for each equivalent carbon position, as described above. These fits were quite satisfactory mathematically, but there was a serious problem from the point of view of the theoretical assumptions. Although one expected that the values of the parameters for overall molecular motion should be the same for all carbon positions, this was not the case. The values of E_m and τ_m^{298} that emerged from the optimization procedure for F differed at each carbon position of the molecule, contrary to the theory, which assumes the overall motion should be equivalent for all positions. In particular, E_m tended to decrease towards the more flexible carbon positions on the periphery of the molecule.

The idea of the correlation time τ_m originates in the work of Debye dealing with the relaxation of polarisation in a dielectric when an applied electric field is removed, or changed. The initial polarisation of the sample decays away, as random thermal motions re-orientate the dipoles. In the case of a liquid composed of "spherical" molecules in which no particular direction of angular motion is dynamically

favoured, the rate at which this occurs is described by Debye's theory in terms of a single constant D, the spherical rotational diffusion constant. Averages of physical quantities dependent on the distribution of angular directions of the dipoles at any time during the decay are simple exponentials dependent on D. The relaxation effects in NMR of liquids can be shown to depend on this same molecular re-orientation, and the τ_m that appears in theoretical formulae such as those quoted in this work can be related to D by

$$\tau_m = \frac{1}{6D} \tag{22}$$

The same idea of a rotational correlation time also occurs in the theory of Brownian Motion, due to Einstein. A small, spherical, particle suspended in a liquid is shown to have a characteristic correlation time for rotational motion given by the Stokes-Einstein-Debye equation

$$\tau_c = \frac{4\pi r^3 \eta}{3kT} \tag{23}$$

where r is its radius, and η is the viscosity of the liquid. The dynamical meaning of the τ_c in this equation is the same as that for τ_m, so one hopes that by shrinking down the particle to molecular dimensions, τ_c will be transmuted into τ_m, thus establishing a relationship between τ_m and the macrophysical observable of viscosity. Not surprisingly, this simple minded approach proves to be inadequate, and it is necessary to "adjust" Eq. (23) by introducing a scaling factor, the microviscosity factor.

Thus τ_m arises from a picture of a liquid in which the molecules are viewed from a close, but not too close, vantage point as small, hard, spheres undergoing random rotational diffusion. Since the atoms in an actual molecule are not fixed relative to each other, but undergo all manner of vibrations and rotations, such a picture does not prove adequate to explain all the physical phenomena that depend on molecular and atomic motion, including the relaxation effects in NMR measurements.

The theory of Lipari and Szabo assumes that after allowing for the motion represented by τ_m, the residual vibrations and rotations of the atoms in a molecule are limited in spatial extent, and very much faster than this. They can then be represented adequately by a single characteristic correlation time τ_i, with a similar mathematical meaning to τ_m, and a scaling factor S^2. The theory is often called "model free", but this is rather a misnomer, since the picture of molecular motion just described is a very definite one. In the case of a molecule with a more flexible geometry, such as a long chain alkane, it is easy to that this picture may cause difficulties. The reason is that co-operative motions extending over different parts of the molecule can represent intermediate correlation times that begin to blurr the distinction between τ_m and τ_i;

one can expect this to begin to occur in the low temperature region, as the liquid approaches its freezing point.

The correlation time τ_i is representative for the fast internal motions of the particular carbon position, but not unique, as several close values may be just as good as predictors of the NMR relaxation effects that arise from these. When one performs the type of least squares approximation of the experimental data used for these analyses, one doesn't know which τ_i will emerge from the available range of suitable values, and more importantly, what the effect of this ambiguity is on the value of τ_m that is determined simultaneously. In fact, from the preliminary observations for 9-*n*-octyl-*n*-heptadecane, it appears that for those positions where S^2 is low, and the molecule is rather flexible, the effect on τ_m is pronounced. The varying values of τ_m obtained are no longer the τ_m related to D, or the liquid viscosity, as required by the assumptions of the theory, but other correlation times that include the effects of the intermediate time scales of the co-operative motions on the data fits for each particular position in the structure.

In order to try to save the situation, an alternative is to substitute the "correct" value of τ_m, the one related to D and the liquid viscosity, for each carbon position, and attempt to fit the experimental data with the remaining parameters, τ_i and S^2. It turned out that this was possible, and the values of S^2 and τ_i were only slightly perturbed from the previous ones, which tends to confirm the interpretation of the difficulties regarding τ_m. Of course, the danger that this indicates is that the theory of Lipari and Szabo may be a soft theory - one that can be adapted to fit any data, without any real physical meaning - but one hopes that this is not the case.

It was therefore necessary to obtain suitable estimates of the "correct" values of τ_m, or equivalently the associated Arrhenius parameters, E_m and τ_m^{298}. In principle this can be attempted by viscosity measurements, and by ESR methods involving specially synthesized spin probes. The alternative is to determine τ_m from the NMR measurements at those positions in the molecule where intuition about the dynamics of the structure suggests that any co-operative motions have the least effect, and the τ_m that emerged from the fitting process could be relied upon.

In this way, one expects that the "correct" τ_m will emerge from solutions for the motional parameters of the carbon atoms at the centres of the alkane structures examined in this work, positions **z** and/or **a**, where the time scales of τ_m and τ_i are well separated and S^2 is large. In the case of 9-*n*-octyl-*n*-heptadecane, the initial five parameter fits gave consistent values for τ_m^{298} and E_m for these two positions, which tended to confirm this approach.

Since the corresponding isotopomer, 9-*n*-octyl-*n*-heptadecane-9d_1 was labelled at the appropriate central position, the results from the deuterium relaxation data were expected to provide the parameters for the "correct" τ_m as well. It was found that the fit of the theoretical values to the deuterium relaxation data was very good and the

values of E_m and τ_m^{298}, similar to those already found from the carbon-13 data for the central positions, appeared to be very precisely determined by the measured data. In consequence, it was decided to take these values of E_m and τ_m^{298}, and insert them as known parameters in the fits of the carbon-13 data for all positions, leaving only E_i, τ_i^{298} and S^2 to be determined. The results were satisfactory.

7.3 PRELIMINARY EXAMINATION OF THE DATA FOR 9,10-DI-*n*-OCTYL-*n*-OCTADECANE

An analysis of the measured deuterium relaxation data for the other deuterated isotopomer, 9,10-di-*n*-octyl-*n*-octadecane-9d_1, produced values of E_m and τ_m^{298}, as in the case of 9-*n*-octyl-*n*-heptadecane-9d_1. The lowest temperature data had to be removed to obtain a fit of the theoretical and measured values, as explained in the detailed analysis in Section 7.6. However, the results were still convincing, and led to the use of these values of E_m and τ_m^{298} in the fitting procedure for all the carbon-13 data, as had been done for 9-*n*-octyl-*n*-heptadecane. But in this case the results were totally negative, and it was obvious that the values predicted by the theoretical equations were completely incompatible with the measured data for most of the carbon positions in the molecule. Even allowing variation of E_m and τ_m^{298} at different carbon positions made little improvement, despite thereby introducing two extra degrees of freedom for the optimization of the fit.

If the lower temperature data were omitted, a reasonable simultaneous fit of the remaining data became possible for all the carbon positions, using E_m and τ_m^{298} from the deuterium measurements. Secondly, it was observed that some of the carbon positions could be fitted over the whole temperature range with reasonable success; these were the central carbons, **z**, and the two positions at the ends of the octyl chains, **g** and **h**. That is, the positions with the highest and lowest S^2 values, as found from 9-*n*-octyl-*n*-heptadecane. The other positions in the middle parts of the chains were those that deviated most from the theoretical predictions.

Both of these observations tended to suggest that allowing S^2 to vary with the temperature would produce a better fit of the theoretical relaxation values to the measured data. One would expect S^2 to be large for the central carbon atoms, and more or less constant at any temperature, since the molecular structure around this point would always have strongly defined positions. For the terminal carbon positions in the octyl chains, if these were similarly mobile at all reasonable temperatures in the liquid state, S^2 would be approximately constant, and small. And so in both these cases, assuming S^2 was a constant would be a good approximation. Similarly, if the major variations of S^2 occurred only as the liquid approached its freezing point for carbon positions in the intermediate regions of the molecule, then removing these data

would again enable the assumption of a constant S^2 for the other data sets, as was observed to be the case.

7.4 THE TEMPERATURE DEPENDENCE OF S^2: S^2 AS A VARIATIONAL FUNCTION

There were two possibilities to include a temperature dependent order parameter S^2 in the theoretical model. The obvious one was to return to calculating the motional parameters one temperature at a time, as in the first approach suggested in Section 7.1. The other was to propose a suitable temperature dependence for S^2 a priori, and examine the results of using this in the fitting of the theoretical predictions to the measured NMR data. It was the latter course that was chosen.

As mentioned in the previous section, the data suggested that the onset of marked change in S^2 was occurring in the more flexible parts of the molecule, as the temperature neared the freezing point of the liquid. In the case of 9,10-di-*n*-octyl-*n*-octadecane this was measured to be around -20 ^{0}C by solidifying the sample in the spectrometer probe; solidification required at least 30 minutes, but the resulting frozen compound had a fine crystalline appearance. An obvious inference was that as the temperature dropped, one was seeing the internal motions of the molecule being re-ordered in preparation for the process of crystallisation at the freezing point. The motions would become more restricted and S^2 should increase, possibly towards some limiting maximum value at around the freezing point. This might be $S^2 = 1$, for an extreme case, or in the case of a mobile methyl group some residual motion might persist into the crystalline state, as is known to occur in many crystal structures. On the other hand, at high temperatures, one might expect the approach to a lower, but essentially constant value of S^2, as indicated by the satisfactory fits of the measured data with the lower temperatures removed.

On the basis of these ideas, the following approximate temperature dependence of S^2 in such molecules was assumed:

$$S^2(T) = S_0^2 - (S_0^2 - S_\infty^2)\exp\left(\frac{-A^2}{(T-T_0)^2}\right) \qquad (24)$$

Four parameters express the general properties expected for S^2. T_0 is a temperature close to the freezing point of the compound at which S^2 becomes greatest, and the value of S^2 at this temperature is S_0^2, while S_∞^2 is the limiting value at much higher temperatures. The sharpness of the change in S^2 as the temperature drops is controlled in a crude way by the fourth parameter, A. T_0 was expected to lie below the range of temperatures actually measured, hence S^2 would always decrease with increasing temperature.

Using Eq. (24) to define S^2 at all temperatures, the carbon-13 NMR data for 9,10-di-*n*-octyl-*n*-octadecane were again fitted, with the known values of E_m and τ_m^{298} determined from the deuterium NMR measurements on 9,10-di-*n*-octyl-*n*-octadecane-9d_1. No restraints were placed on the signs or magnitudes of the parameters governing S^2 during the optimizations of the fits; the only proviso was to choose initial values that were appropriate. Usually T_0 was chosen to be some 50 ^{0}C below the freezing point of the liquid, S_0^2 and S_∞^2 were chosen to be about 1 and 0.5 respectively, and A set at around 20. Optimizations were started from several initial parameter vectors to examine the influence on the resulting solutions.

It was found that quite reasonable fits of the data sets for all carbon positions were now possible, and the temperature dependence of S^2 at each carbon position, as encompassed in Eq. (24), was surprisingly well determined, considering its ad hoc nature. The value of T_0 was almost invariant, and close to the determined freezing point, S_0^2 and S_∞^2 had meaningful values, and A varied from position to position as one expected it should.

Values of E_i and τ_i^{298} were obtained simultaneously for each carbon position, and they agreed well with those expected from the previous work on *n*-octyl compounds, whereas those from the previous fits using a constant S^2 did not. It was also possible to observe the real time progress of the optimizations of the fits of the theoretical values to the experimental data, graphically and numerically. The values of E_i and τ_i^{298} were soon determined during the optimisations, even while the fits were relatively poor, whereas the remaining refinement of the solution took place only through the variation of the parameters determining S^2. In fact, it appeared to be the case that τ_i in general converged to a maximal value at each temperature, while S^2 could be treated roughly as a variational function introduced simply to approximate the actual solution, but whose exact form was not essential to the determination of E_i and τ_i^{298}.

The analogy is with quantum mechanics, and the well known variational method in which the ground state molecular energy can be well determined, by the substitution of only an approximate ground state wave function into a variational integral:

$$E_0 \leq \frac{\int \psi^* H \psi \, d\tau}{\int \psi^* \psi \, d\tau} \qquad (24)$$

The sum of squares function, F, can be seen to be an approximation to an integral, with S^2 and $1\text{-}S^2$ then being analogous to the weightings of two parts of a probability density, ψ^2. Without a theoretical investigation, this can only be plausible speculation, but it is interesting that S^2 derives from a weighted average of the angular

directions adopted by a C–H fragment during its internal librations, as governed by some law of probability.

So it may be that it is not necessary to know the exact variation of S^2 in order to determine suitable values of E_i and τ_i^{298} using the fitting approach that was adopted in this work. In fact, several other functional forms for S^2 were tried, as well as the one given in Eq. (24), including Lorentzian and Gaussian functions, multi-step functions, and simple exponential (Arrhenius) type functions. It was found that for any S^2 that led to a reasonable fit of the measured data, the values for E_i and τ_i^{298} predicted by each fit were consistent to within about 10 % of each other, although the actual forms of S^2 might differ in detail. However, the general trend and temperature variation S^2 required was always the same for all these models, if the fits to the measured data were reasonably good, and it was not possible to fit the data using parametrized S^2 functions that could not behave in the way expected. For example, choosing an S^2 with maxima at two temperatures within the measured range, or which decreased with decreasing temperature, always failed.

The values predicted from the fits obtained using S^2 given by Eq. (24) were within the experimental error for both T_1 and NOE factors, so the end results still justify the form chosen for S^2 as a very good approximation of the "real" values. This logic depends, of course, on the assumption that the Lipari and Szabo system of equations has a unique physically acceptable solution for the given data at each temperature.

The actual significance of the required temperature dependence of S^2 is less simple, however, than that which was first envisaged, and introduced as the preliminary justification in this section. It also appears to be related to the question of the interelationship between τ_m and τ_i in this theory, as discussed in the previous section. The temperature dependence of S^2 then occurs in part as a compensatory artefact in a theory which assumes a single fast correlation time for the internal motions, when in fact intermediate time scales are probably present in these molecules which make this approximation problematical. This relationship of S^2 to the time scales of the internal motions was suggested by the results of the analyses of the deuterium relaxation data for 9,10-di-*n*-octyl-*n*-octadecane-$9d_1$ and 9-*n*-octyl-*n*-heptadecane-$9d_1$, and is discussed in more detail in Sections 7.6 and 7.7.

The variation of S^2 described by Eq. (24) was also included for the case of 9-*n*-octyl-*n*-heptadecane, and it was found that as well as improving the fits, the behaviours of S^2 that emerged were distinct from the case of 9,10-di-*n*-octyl-*n*-octadecane. The optimizations converged to solutions in which S^2 varied little over a wider range of temperature, showing that the assumption of a constant S^2 would not be inappropriate in such a case. Naturally, it was not just the variation of S^2 with temperature that differed, but also the actual magnitudes of the order parameters at corresponding positions in the molecules.

As a final remark in this section, it can be mentioned that Gillies and Sutcliffe suggested that a temperature variation of S^2 was necessary to explain some of their NMR relaxation data for tetra-*n*-octyl tin[5], tri-*n*-octylamine, and poly-α-decene[6]. They introduced a simple exponential dependence of the Arrhenius kind into their equations, apparently with satisfactory results. However, this was not found to be the case over the wider temperature ranges in the present work, which approach the freezing points of the compounds.

7.5 PRELIMINARY EXAMINATION OF THE DATA FOR TRI-*n*-OCTYLSILANE

The initial approach was to allow five parameter fits (with S^2 as a constant) of the temperature dependent Lipari and Szabo equations to the carbon-13 relaxation and NOE data. The fits were quite good, but suggested some different features from the hydrocarbon homologue, 9-*n*-octyl-*n*-heptadecane. The values of E_m were much smaller at all carbon positions, as well as decreasing towards the free ends of the octyl chains. Also the S^2 values were very much smaller, even for the a carbon position in the octyl chains, next to the central silicon atom. In the case of 9-*n*-octyl-*n*-heptadecane, the same fitting procedure for this position gave values of E_m and τ_m^{298} which were close to those derived independently from the deuterium data, and E_m was some 26 kJ mol^{-1}. The carbon-13 data for the a position in tri-*n*-octylsilane suggested a value of only 18 kJ mol^{-1}

However, it proved possible to utilize the silicon-29 R_1 relaxation rates for tri-*n*-octylsilane to deduce a better estimate of E_m. Unfortunately, the appropriate value of τ_m^{298} for tri-*n*-octylsilane could not be ascertained from the silicon-29 T_1 data alone, but had to be estimated from the carbon-13 data for the **a** carbon position, using E_m as a known parameter. Subsequently, these values of E_m and τ_m^{298} were used as known parameters in fits of the remaining carbon-13 relaxation and NOE data to the theoretical picture of Lipari and Szabo used in the cases of the two hydrocarbons, with the S^2 variational function of Eq. (24). The results were satisfactory, and values of E_i and τ_i^{298} were determined for each carbon position, together with the approximate temperature dependencies of S^2, which were distinctive for this molecule.

7.6 ANALYSES FOR 9,10-DI-*n*-OCTYL-*n*-OCTADECANE AND 9,10-DI-*n*-OCTYL-*n*-OCTADECANE-9d_1

After the removal of the two lowest temperatures from the deuterium R_1 and R_2 relaxation data for 9,10-di-*n*-octyl-*n*-octadecane-9d_1, simultaneous fits of the theoretical values predicted by Eqs. (11)-(14) to the remaining measured data determined the values of E_m, τ_m^{298}, and K recorded in Table 7.1. The optimized theoretical curves and measured data are plotted in Fig. 7.2.

If the deuterium relaxation data for the two lowest temperatures were included, it was no longer possible to obtain such a good fit between the theoretical and experimental data. The extra data points are included in the plots in Fig. 7.3, along with theoretical curves that match the selected higher temperature data. The deviation seems to be quite systematic, rather than due to random experimental error, with the values of both R_1 and R_2 being larger than predicted by extrapolating the theoretical curves from the higher temperatures. This can be rationalized by remembering that the theory uses only reduced spectral densities, without any explicit frequency dependent relaxation from the faster internal motions of the C-D vector, as discussed in Section 1.7. The increased rates observed at low temperatures can be ascribed to the appearance of this contribution to the relaxation, as the correlation times of the internal motions slow down.

Using the values of E_m and τ_m^{298} in Table 7.1, analysis of the carbon-13 relaxation and NOE data for 9,10-di-*n*-octyl-*n*-octadecane determined the values of the remaining parameters related to the internal molecular motions which are recorded in Table 7.2. The corresponding dependencies of S^2 on temperature for each carbon position are plotted in Fig. 7.4, starting at 250 K, which is a few degrees below the freezing point of the compound. Plots of the optimized theoretical curves of carbon-13 relaxation rates and NOE factors, together with the actual data, appear in Appendix 6.

The high value of E_i for the case of carbon position **z** might be erroneous, since this peak had the smallest signal to noise ratio in the NMR spectra, especially at low temperatures, and also overlapped a small part of the lock solvent peaks. However, it is interesting to notice that the high value indicates a rapid slowing down of the time scale of the internal motions at this position at lower temperatures, and this correlates with the appearance of extra relaxation noticed in connexion with the deuterium data. The similar central position in 9-*n*-octyl-*n*-heptadecane, (discussed in Section 7.7, hereafter), produced a much lower value of E_i, and the deuterium NMR relaxation data from 9-*n*-octyl-*n*-heptadecane-9d_1 could be reproduced at all temperatures using only the reduced theoretical picture.

Rearranging the equation defining K^2 (Eq. (14)) leads to an expression for the quadrupolar coupling constant:

$$QCC = \frac{\pm K}{\left(1+\eta^2/3\right)^{1/2} S} \qquad (26)$$

Assuming that it is possible to identify the S here with that which appears in the theoretical equations for the carbon-13 relaxation rates for the corresponding carbon position, one can obtain a value for the quadrupolar coupling constant in 9,10-di-*n*-octyl-*n*-octadecane-9d_1. The question, of course, is which value of S^2 to choose, and why the deuterium relaxation data is so well reproduced here (and later for 9-*n*-octyl-*n*-heptadecane-9d_1 as well) using only a constant S^2, while the carbon-13 data required a temperature dependence to obtain any kind of reasonable approximation?

One can propose an answer which ties in with the earlier discussion of the τ_m / τ_i conundrum in the data fits using the Lipari and Szabo picture of molecular motion, and also elucidates the meaning of the temperature variation of S^2 that was introduced. Consider that S^2 contains not just a dependence due to possible spatial variation of the internal motions with temperature, in line with its original theoretical significance, but also a contribution related to the presence of those co-operative internal motions on intermediate time scales which were proposed in Section 7.2.

The variation of S^2 resulting from this latter contribution would then appear as a compensatory artefact introduced at the point where the data can no longer follow a theory which assumes a single time scale, governed by an Arrhenius dependence, for the internal molecular motions. This is going to be most likely to occur as the temperature is reduced and the internal motions slow down, possibly becoming more complex, with components of significantly differing time scales. At this point it may not be possible to choose a single τ_i to adequately represent the relaxation effects of such motions. Crudely, the effect of increasing S^2 is to mix in an extra element of relaxation from the parts of the Lipari and Szabo equations related to τ_m which would not have been present otherwise, although obviously this does not "prove" the interpretation suggested here.

Thus, for position **z** in 9,10-di-*n*-octyl-*n*-octadecane, assuming most of the the variation in S^2 had this origin would explain the apparent contradiction between the results of the deuterium and carbon-13 analyses. At temperatures where the deuterium relaxation is governed by the reduced equations, as were in fact used, there is no explicit dependence on the details of correlation times describing any internal motions, and so S^2 can be taken to be a constant if their spatial dependence is roughly the same at all temperatures. The variation of S^2 in the carbon-13 case is then an artefact caused by the changes in the distribution of correlation times required to adequately describe the internal motions, which are able to influence the higher frequency dependence of the carbon-13 relaxation data in detail, but which are too fast to do so in the case of the deuterium data.

This rationale suggests that the value of S^2 at the highest temperatures will be the actual Lipari and Szabo S^2, determined only by considerations of the spatial extent of the internal motions, with a single correlation time adequately representing the relevent time scale. This should be the one to use as the S^2 that occurs in the deuterium relaxation theory. Thus, for the central carbon atom, setting K = 144 kHz, $S^2 = 0.73$, and assuming the asymmetry parameter, η, is zero, gives QCC = $\pm$169 kHz.

E_m kJ mol^{-1}	τ_m^{298} ns	K kHz
29.90	2.01	144.3

Table 7.1: The parameters for overall molecular motion and averaged quadrupolar interaction for 9,10-di-*n*-octyl-*n*-octadecane-9d_1 determined from the deuterium NMR data at 41.405 MHz.

carbon position	E_i kJ mol^{-1}	τ_i ps	S^2			
			S_0^2	S_∞^2	T_0	A
z	32.6	69.1	0.886	0.725	261	10.01
a	15.9	43.4	0.628	0.413	261	12.00
b	23.5	47.5	0.705	0.214	257	12.45
c	20.7	40.8	0.761	0.093	256	12.64
d	19.2	33.4	0.716	0.045	254	12.54
e	19.3	27.3	0.631	0.029	256	10.51
f	18.0	22.2	0.548	0.012	249	10.79
g	16.6	16.9	0.389	0.005	248	10.44
h	15.6	6.1	0.179	0.002	248	5.40

Table 7.2: The parameters for internal molecular motion for 9,10-di-*n*-octyl-*n*-octadecane determined from the carbon-13 NMR data at 67.83 and 100.53 MHz.

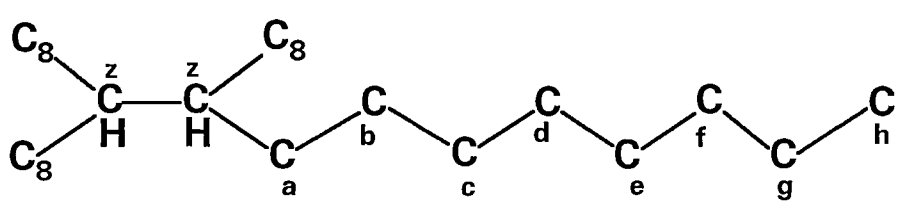

Fig 7.1: The assignments in 9,10-di-*n*-octyl-*n*-octadecane.

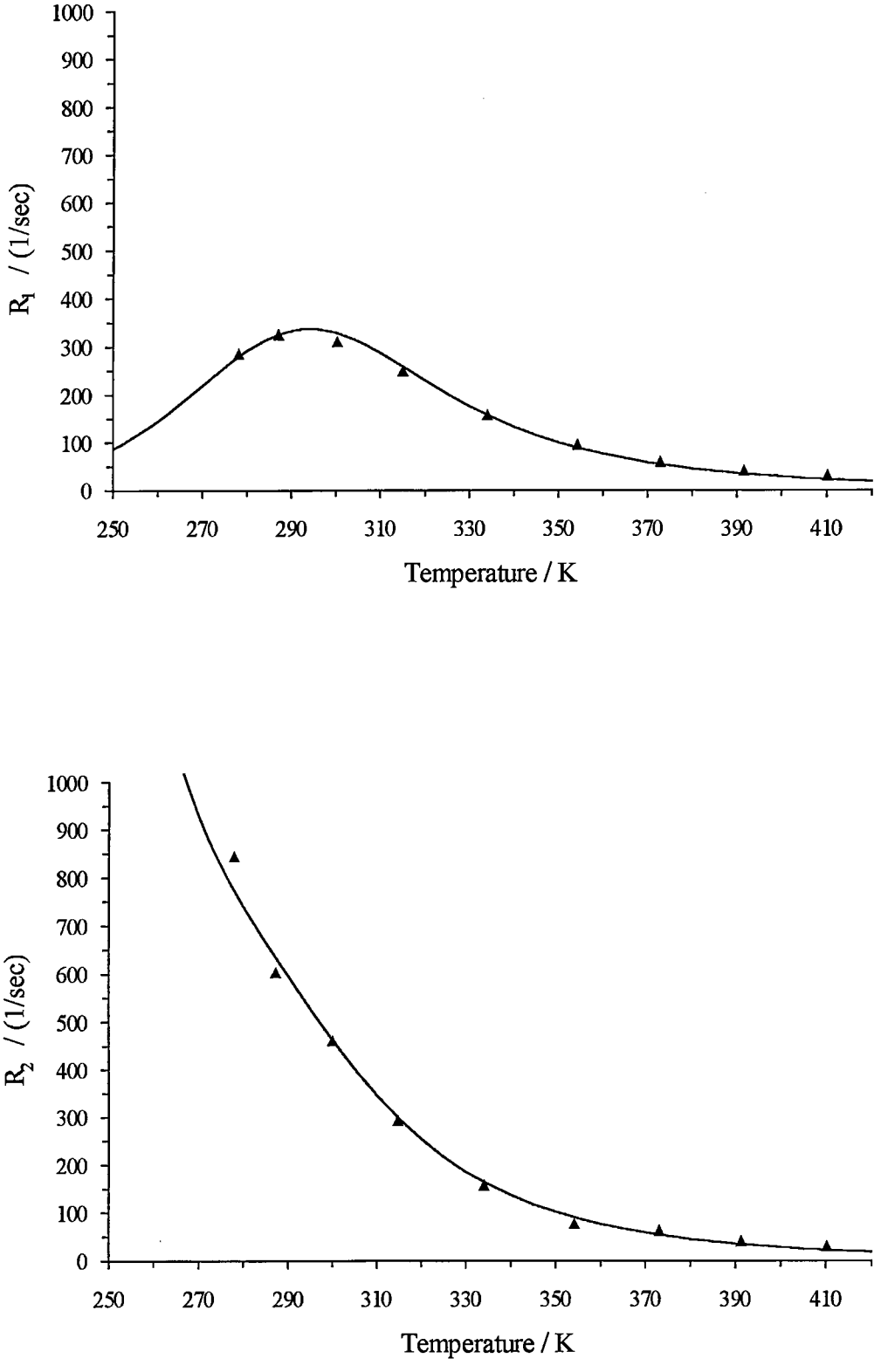

Fig. 7.2: The selected deuterium relaxation data at 41.405 MHz and the optimized simultaneous fits of the theoretical curves for 9,10-di-*n*-octyl-*n*-octadecane-9d_1.

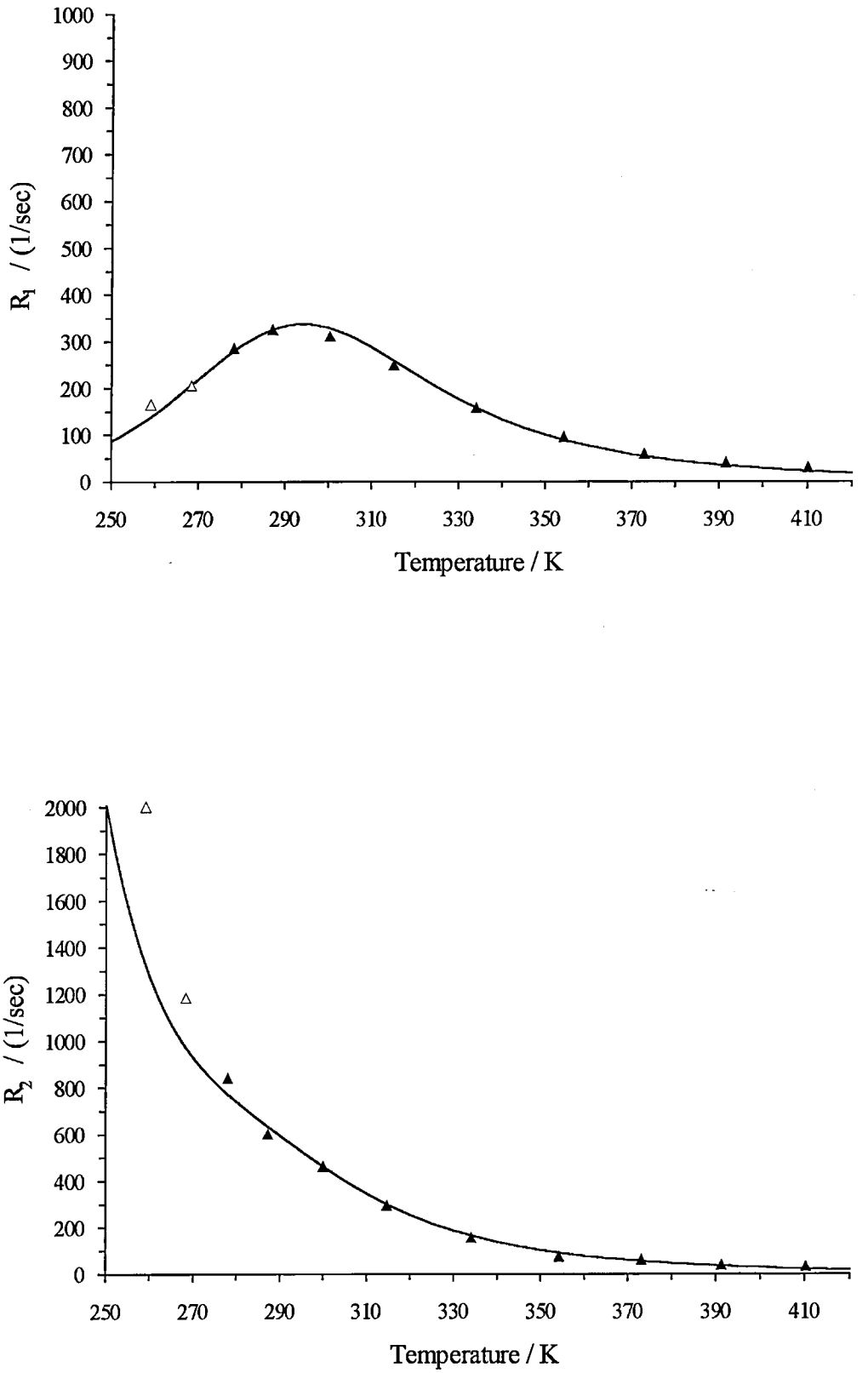

Fig. 7.3: The selected deuterium relaxation data at 41.405 MHz and the optimized simultaneous fits of the theoretical curves for 9,10-di-*n*-octyl-*n*-octadecane-9d_1, plotted together with the lower temperature relaxation data (Δ).

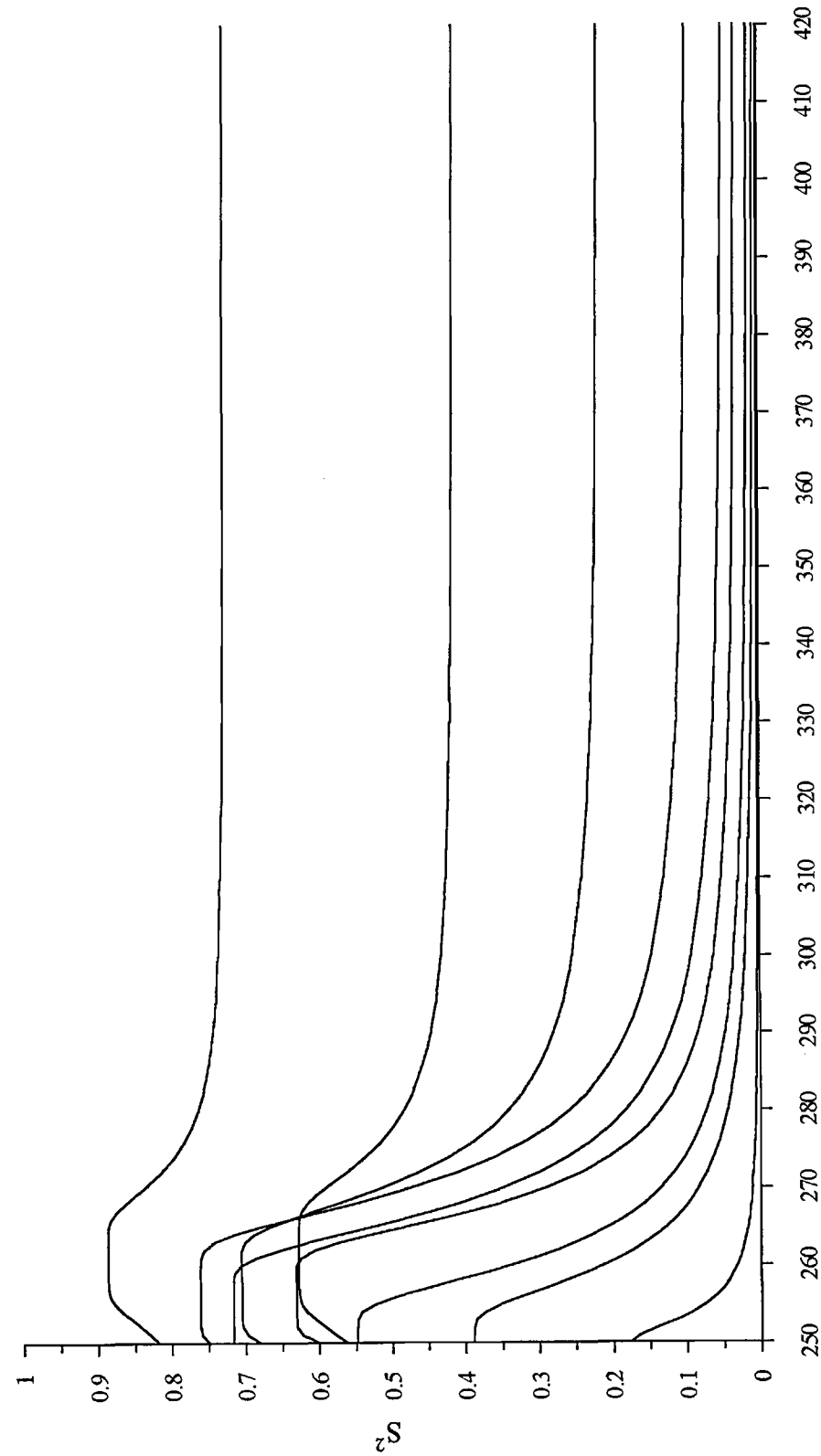

Fig. 7.4: The dependence of S^2 on temperature for each carbon position in 9,10-di-*n*-octyl-*n*-octadecane. The compound freezes between 250 and 260 K.

7.7 ANALYSES FOR 9-*n*-OCTYL-*n*-HEPTADECANE AND 9-*n*-OCTYL-*n*-HEPTADECANE-9d_1

All the deuterium relaxation data for 9-*n*-octyl-*n*-heptadecane-9d_1 were adequately reproduced using the theoretical picture of Eqs. (11)-(14), and simultaneous fits of the theoretical values to the measured data determined the values of E_m, τ_m^{298} and K recorded in Table 7.3. The optimized theoretical curves and measured data are plotted in Fig. 7.6. Unlike the case of 9,10-di-*n*-octyl-*n*-octadecane-9d_1, there was no need to omit the lower temperature data, which indicates that internal motion at the z position in this molecule is faster at these temperatures than in the larger hydrocarbon.

Using these values of E_m and τ_m^{298}, analyses of the carbon-13 relaxation and NOE data for 9-*n*-octyl-*n*-heptadecane determined the values of the remaining parameters related to the internal molecular motions which are recorded in Table 7.4. The corresponding dependencies of S^2 on temperature for each carbon position are plotted in Fig. 7.7, starting at 245 K, which is a few degrees below the freezing point of the compound. Plots of the optimized theoretical curves of carbon-13 relaxation rates and NOE factors, together with the actual data, appear in Appendix 7. The low value of E_i for the case of carbon **z**, if accurate, would indicate the presence of faster internal motion at this position in 9-*n*-octyl-*n*-heptadecane at low temperatures than at the corresponding position in 9,10-di-*n*-octyl-*n*-octadecane.

Making the same assumptions as were made in the case of 9,10-di-*n*-octyl-*n*-octadecane-9d_1, it is possible to determine a value of the quadrupolar coupling constant for 9-*n*-octyl-*n*-heptadecane-9d_1. For the central carbon atom in this case, setting K = 138.3 kHz, S^2 = 0.60, and assuming again that the asymmetry parameter is zero, gives QCC = ±179 kHz.

E_m	τ_m^{298}	K
kJ mol^{-1}	ns	kHz
27.70	0.48	138.3

Table 7.3: The parameters for overall molecular motion and averaged quadrupolar interaction for 9-*n*-octyl-*n*-heptadecane-9d_1 determined from the deuterium NMR data at 41.405 MHz.

carbon	E_i	τ_i	S^2			
position	kJ mol^{-1}	ps	S_0^2	S_∞^2	T_0	A
z	10.0	70.7	0.810	0.603	238	12.50
a	12.9	46.3	0.667	0.357	247	3.80
b	16.1	30.0	0.468	0.259	247	4.30
c	19.6	19.5	0.560	0.192	247	3.18
d	17.8	18.6	0.579	0.125	244	4.65
e	17.9	15.4	0.567	0.093	243	4.87
f	15.5	16.1	0.388	0.040	242	5.75
g	14.8	13.3	0.302	0.019	240	6.69
h	13.0	6.3	0.267	0.001	234	4.12

Table 7.4: The parameters for internal molecular motion for 9-*n*-octyl-*n*-heptadecane determined from the carbon-13 NMR data at 67.83 and 100.53 MHz.

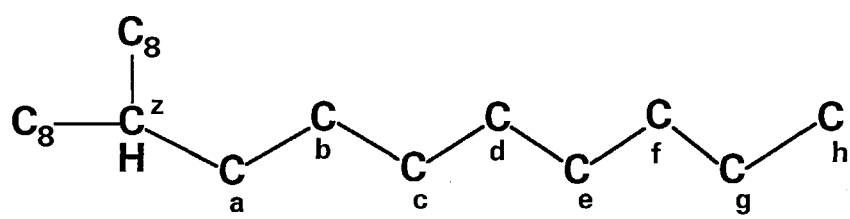

Fig 7.5: The assignments in 9-*n*-octyl-*n*-heptadecane.

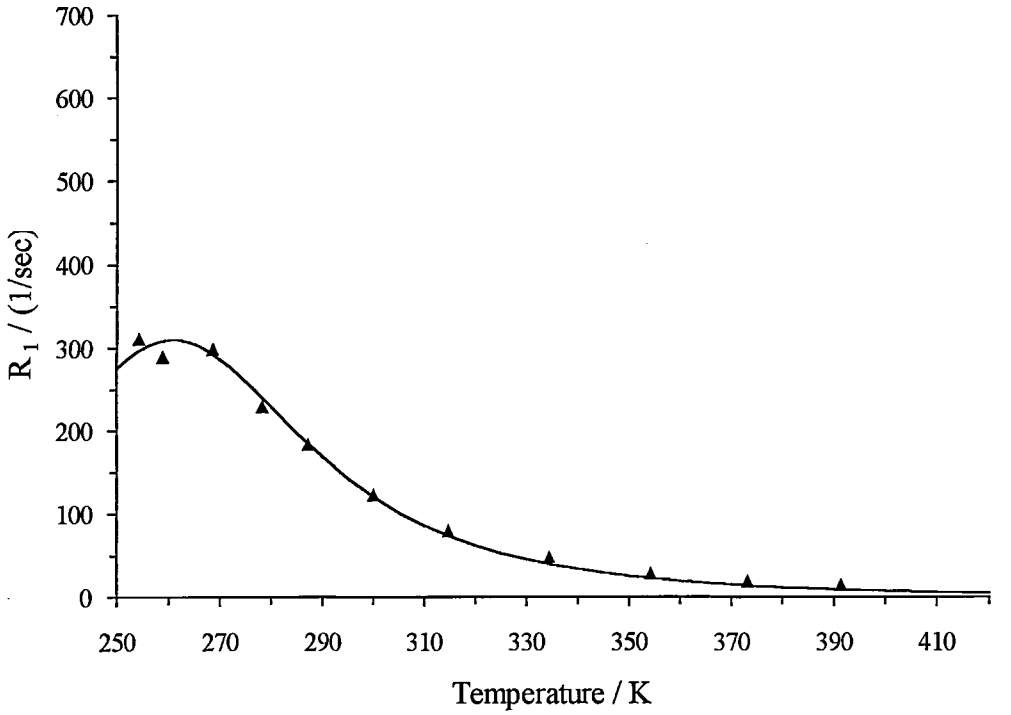

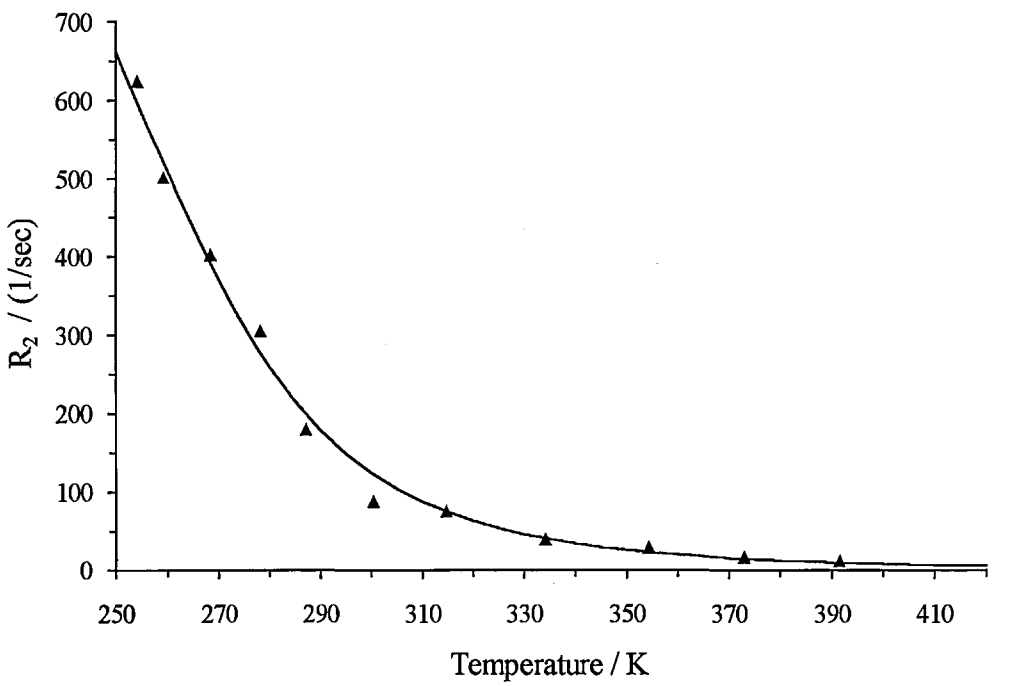

Fig. 7.6: The deuterium relaxation data at 41.405 MHz and the optimized simultaneous fits of the theoretical curves for 9-*n*-octyl-*n*-heptadecane-9d_1.

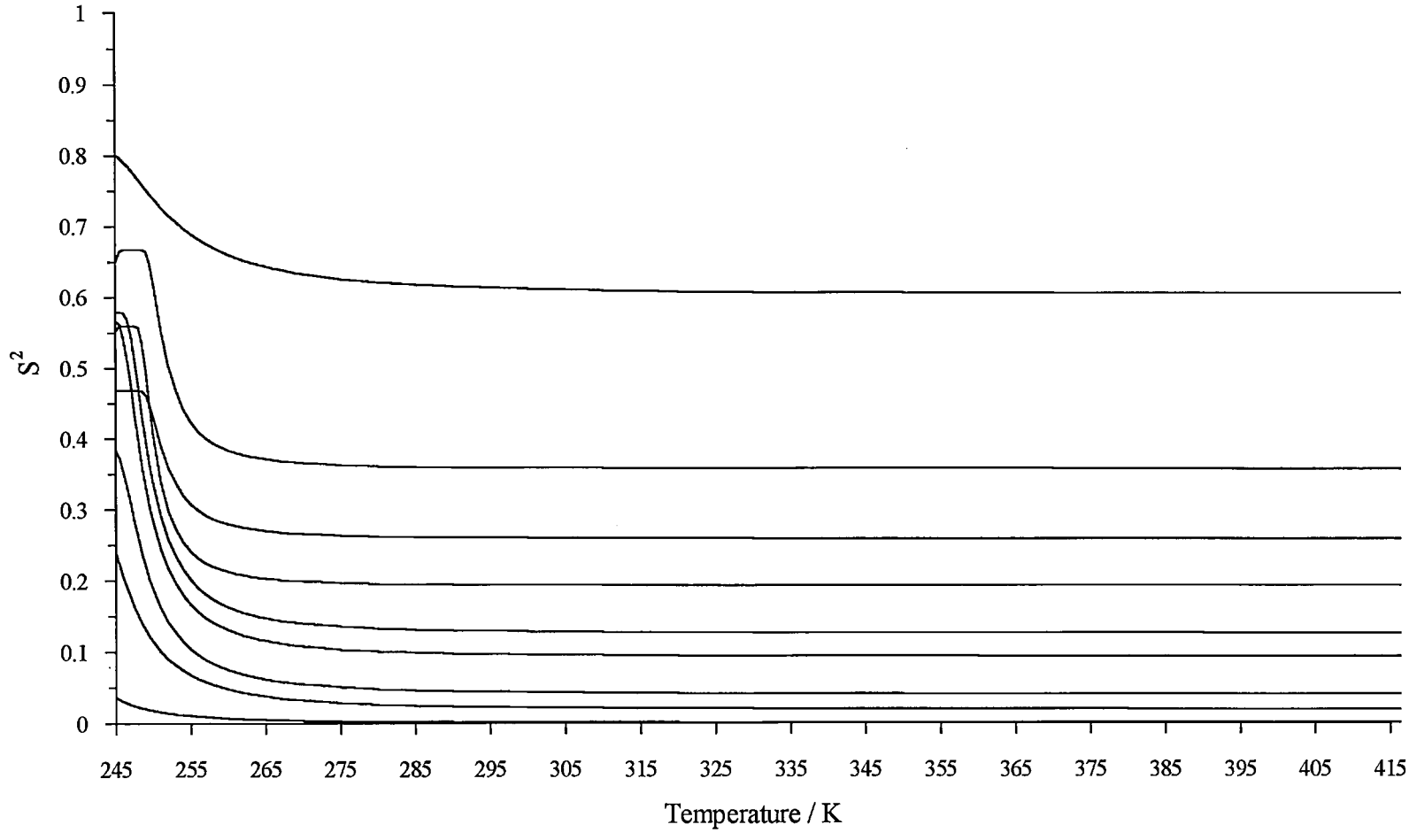

Fig. 7.7: The dependence of S^2 on temperature for each carbon position in 9-*n*-octyl-*n*-heptadecane. The compound freezes between 245 and 255 K.

7.8 ANALYSES FOR TRI-*n*-OCTYLSILANE

The silicon-29 relaxation data for tri-*n*-octylsilane were examined in the hope of obtaining independent values of E_m and τ_m^{298}, as had been done for the two hydrocarbons through the deuterium relaxation data. Since the line widths measured were only 2 - 3 Hz at all temperatures, T_2 relaxation data were not available in the same way as in the case of the deuterated *n*-octyl compounds. The most noticeable feature of the silicon-29 T_1 data for tri-*n*-octylsilane (Table 6.23) is the decrease at higher temperatures, which indicated that the relaxation could not be accounted for by assuming a dipolar mechanism alone. The only possibility is a predominant contribution from spin-rotational relaxation at higher temperatures.

The silicon-29 R_1 data are plotted in Fig. 7.9, and also in Fig. 7.10 as $\ln(R_1)$ against (1000/T). The increase in the rate at higher temperatures can be seen, but the rest of the data appear to approximate a more linear function, which suggests an approach to dipolar relaxation in the condition of extreme narrowing. (From Eqs. (7) and (11), in Section 1.4, one easily shows that a $\ln(R_1)$ against 1000/T plot is linear in this case, with slope equal to $E_m/1000R$). A least squares fit of the theoretical equations, Eqs. (19) and (20), for combined silicon-29 dipolar and spin rotational R_1 relaxation produced the curves shown superimposed on the data in Figs. 7.9 and 7.10. As can be seen, the fit is very good, and determined E_m as 22.73 kJ mol^{-1}. The slope of the theoretical curve in Fig. 7.10 is essentially $\pm E_m/1000R$ on either side of the minimum, which is why E_m is determined by this T_1 data alone.

However, the corresponding values of C^2, D^2, and τ_m^{298} were not well determined from these data, since in the case of extreme narrowing these parameters enter essentially as C^2/τ_m^{298} and $D^2\tau_m^{298}$. This problem did not arise with the deuterium data in Sections 7.6 and 7.7, where the availability of the T_2 data separated the functional contributions of K^2 and τ_m^{298} at the lower temperatures, outside the region of extreme narrowing. If T_2 measurements had been made in the present case, using the CPMG method for example, the same determination of the parameters might have been possible. Measurements of the silicon-29 NOE effects due to proton decoupling would also have aided this determination.

Substitution of the value of E_m determined in this way as a known parameter in the analysis of the carbon-13 relaxation time and NOE data for carbon position a in tri-*n*-octylsilane determined a value for τ_m^{298}, as well as the remaining parameters for internal motion for this carbon atom. The values of E_m and τ_m^{298} are recorded in Table 7.5.

Using these values of E_m and τ_m^{298}, analyses of the remaining carbon-13 relaxation and NOE data for tri-*n*-octylsilane determined the values of the parameters in Table 7.6 related to internal molecular motion for the other carbon positions. Plots of the optimized theoretical curves of carbon-13 relaxation rates and NOE factors, together with the actual data, appear in Appendix 8. The corresponding dependencies

of S^2 on temperature for each carbon position are plotted in Fig. 7.11, starting at 245 K, which is a few degrees below the freezing point of the compound.

Although the values for S_0^2 exceed 1, the values of S^2 itself over the measured temperature range were well determined, between the theoretical limits of 0 and 1, and the fits of the theoretical relaxation rates and NOE factors to the measured data were at least as good as in the cases of 9,10-di-*n*-octyl-*n*-octadecane and 9-*n*-octyl-*n*-heptadecane. This example therefore indicates the caution needed in any attempt to interpret the S^2 parameters, beyond their role as variational optimizers; they give the values of S^2, as determined by the data, but may not have any great significance themselves. If one knew the exact theoretical functional form of S^2, then such parameters might have definite interpretations.

The methyl groups showed a contribution from spin-rotational relaxation at higher temperatures, where the relaxation rate began to increase again. However, the presence of these data did not seem to affect the optimization procedure unduly, so they were retained. The presence of spin-rotational relaxation was also noticeable to a smaller extent in the data for the methyl groups in 9,10-di-*n*-octyl-*n*-octadecane and 9-*n*-octyl-*n*-heptadecane.

Since it appears that the internal motions of the Si-H bond can be ignored in the silicon R_1 data at low temperatures, they must be faster than those of the corresponding C-H bond in the hydrocarbon, and this agrees with the faster values of the internal correlation times in tri-*n*-octylsilane found from the analyses of the carbon-13 NMR data for the other positions in the molecule. The reversal of the order of the weighting factors of the spectral densities in the equations describing silicon-29 relaxation, as compared with those for carbon-13 relaxation, also decreases the contributions of faster motions.

In the carbon-13 NMR case, the influence of the faster internal motions becomes more apparent at lower temperatures in the measured relaxation data, and the corresponding parameters can therefore be determined. The NOE factors appear to be especially influenced by the smaller contributions due to the fast internal motions, and this is probably related to the theoretical expression as a quotient of sums and differences of spectral densities, whereas the relaxation rates are simple linear combinations of these. (This same observation applies to all the *n*-octyl compounds). If a set of multi-frequency relaxation rate and NOE data had been measured for the silicon-29 resonance, a full analysis for the faster motions of the Si-H bond could probably be carried out, just as for the corresponding carbon position in 9-*n*-octyl-*n*-heptadecane.

E_m kJ mol^{-1}	τ_m^{298} ns
22.73	0.91

Table 7.5: The parameters derived from a combination of the silicon-29 and carbon-13 NMR data for the overall molecular motion of tri-*n*-octylsilane.

carbon position	E_i kJ mol^{-1}	τ_i ps	S^2			
			S_0^2	S_∞^2	T_0	A
a	14.2	33.7	1.319	0.055	229	9.97
b	13.5	28.8	1.161	0.035	230	8.89
c	14.1	26.7	1.282	0.034	232	7.51
d	12.4	18.4	1.175	0.013	226	11.09
e	13.1	17.8	1.205	0.011	225	11.20
f	13.9	15.8	1.110	0.008	235	4.67
g	13.4	13.0	1.009	0.003	235	3.90
h	15.4	4.7	0.866	0.002	240	0.85

Table 7.6: The parameters for internal molecular motion for tri-*n*-octylsilane determined from the carbon-13 NMR data at 67.83 and 100.53 MHz.

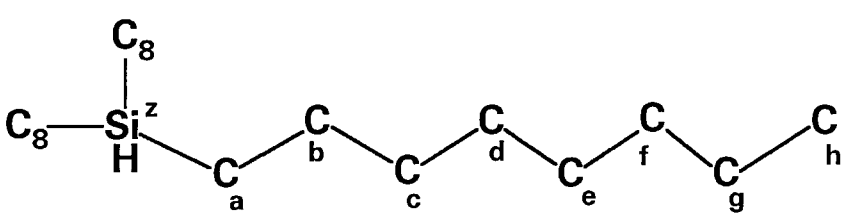

Fig 7.8: The assignments in tri-*n*-octylsilane.

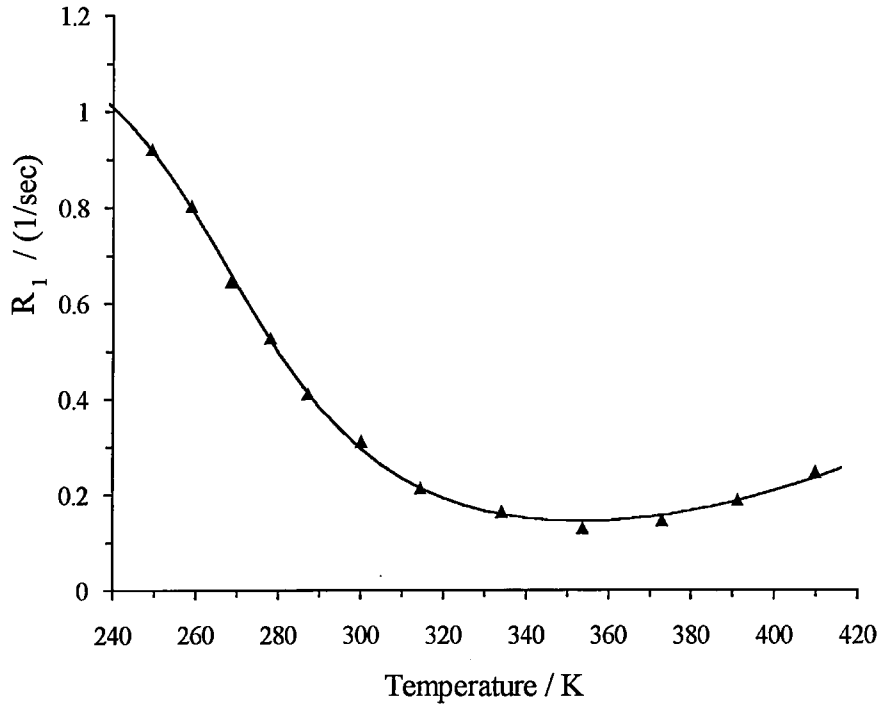

Fig. 7.9: The silicon-29 R_1 relaxation rates measured for tri-*n*-octylsilane at 53.5977 MHz and the optimized theoretical curve.

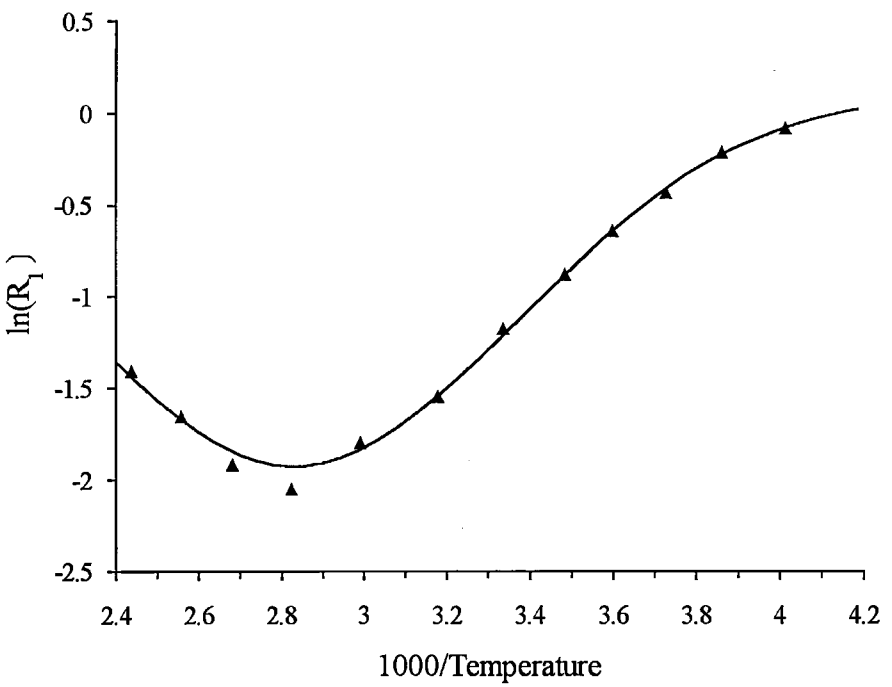

Fig. 7.10: The silicon-29 R_1 relaxation rates measured for tri-*n*-octylsilane at 53.5977 MHz and the optimized theoretical curve, plotted as $\ln(R_1)$ against 1000/T.

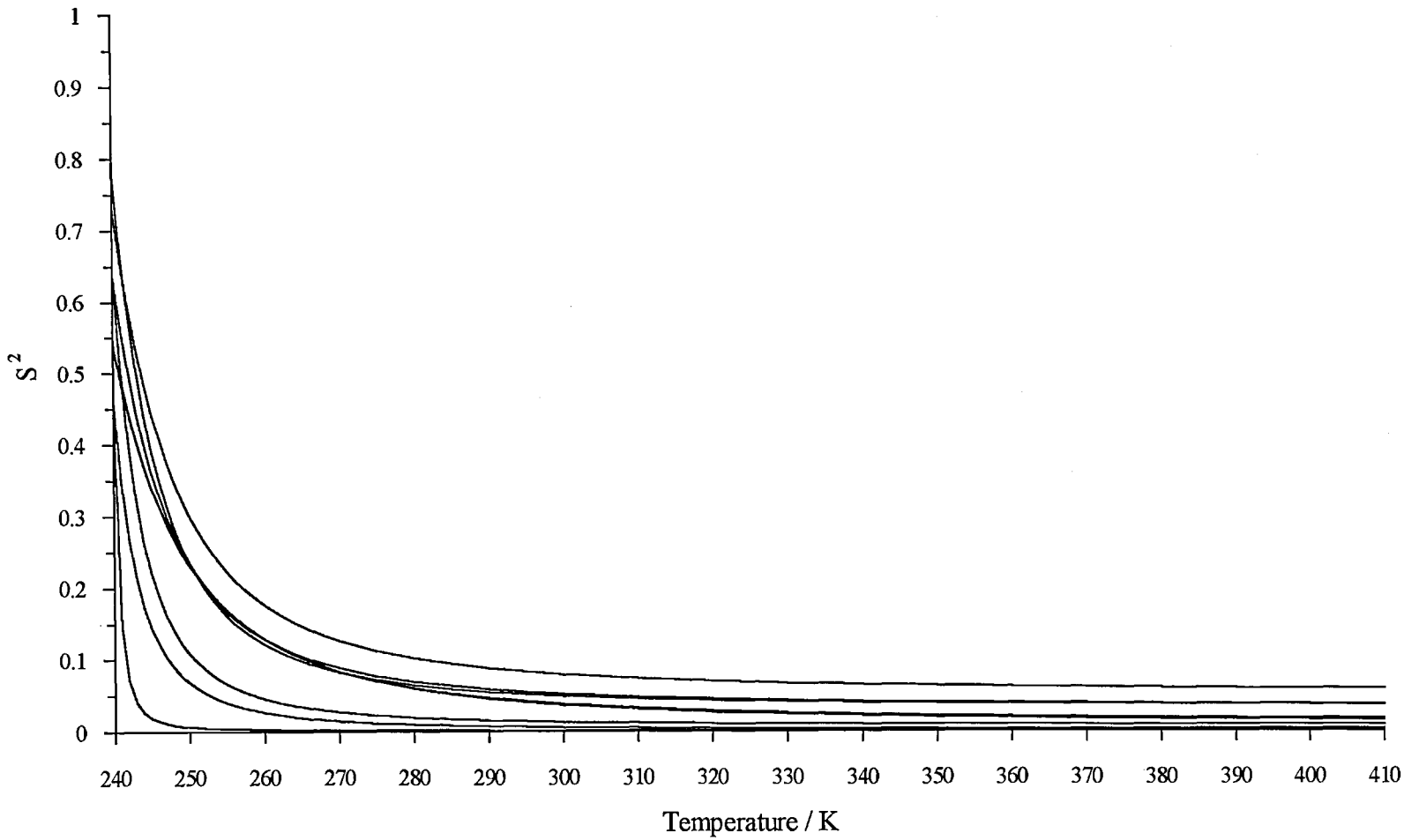

Fig. 7.11: The dependence of S^2 on temperature for each carbon position in tri-*n*-octylsilane. The compound freezes between 240 and 250 K.

7.9 ACCURACY OF THE MOTIONAL PARAMETERS

It has become the habit in papers using the Lipari and Szabo model for authors to quote error bounds for the values of the motional parameters derived from the equation fitting process, with no discussion of how they were arrived at. This is not surprising, considering that one is optimizing a real valued function (the sum of squared differences, F) of at least five real variables, which is non-linear and described in terms of coefficients (the measured NMR data) which are subject to error, and in the case of NOE values, considerable error. Obviously, to attempt a detailed theoretical analysis of the propagation of measurement errors in such an optimization, and their influence on the final parameter vector will be no easy task. It can of course be done in the case of the fitting of linear models to data sets, and standard formulae and statistical functions exist to express the relationships. However, a simple approach can be used to assess the accuracy of the solution vectors in the present circumstances.

The idea is to take the fitting process itself as a kind of experiment, and by performing many repeated fits starting from arbitrary (but reasonable) initial parameter vectors, analyze the resulting sets of optimized parameters statistically in the normal way. This is related to the well known Monte-Carlo method. In the present case, one can also introduce a random controlled variation into the primary NMR data to simulate the effect of experimental error.

In an analysis involving least squares optimizations, there is a further indicator available which points to how well defined the parameter values are by the measured data; the time rate at which the solution vector converges to the optimum. This is to some extent rather subjective, but it was usually very obvious in the cases analyzed in this work, where a rapid convergence showed a strong determination of the required parameters by the measurements, and a slow convergence the opposite, including the extreme example of parameters that wander without determination. This occurred in the analyses of the carbon-13 relaxation data for tricyclohexylmethane in the next chapter. Obviously, these behaviours can all be related to the geometry of a surface representing F, but failing a visualization of spaces of five or more dimensions, the observation of the rate of optimization factor is informative.

In this work it was not possible to perform many repeated fits of the data and obtain statistics for the optimized parameter vectors due to time limitations, but from a few repeated optimizations, together with observations of their rate of convergence, estimates of the likely accuracy of the resulting parameter values could be made in terms of the ranges of values expected around a typical quoted figure.

The values of E_m and τ_m^{298} obtained from the deuterium NMR data were very strongly determined; E_m was estimated to be accurate to within ± 0.5 kJ mol^{-1}, and τ_m^{298} to within ± 0.05 ns. The values of E_m and τ_m^{298} obtained in the case of tri-*n*-octylsilane from a combination of the silicon-29 and carbon-13 data were less

accurate; E_m to within ±1 kJ mol^{-1}, and τ_m^{298} to within ±0.05 ns. The values of E_i were estimated to be accurate to within ±1.5 kJ mol^{-1}, and τ_i^{298} to within ±10 %.

Of the S^2 parameters, T_0 was usually surprisingly well defined and often emerged as almost a constant across several carbon positions in the molecule, although there was no restriction placed on the optimization of this parameter. Although S_∞^2 was always well determined, there was some interdependence of the remaining S^2 parameters. However, the resulting overall curve of S^2 was always well determined over the temperature range considered to within ±0.05, whatever the final optimized parameter values. The values of E_i and τ_i^{298} were indifferent to small differences in the temperature dependence of S^2, as long as the fit was a good one.

7.10 DISCUSSION

Examining the three sets of results, each compound shows characteristic features, with the differing patterns of S^2 behaviour being the most noticeable. Even 9-*n*-octyl-*n*-heptadecane and tri-*n*-octylsilane are sharply distinguished by this means, although one might have expected there to be little difference between them. It is perhaps easier to examine the S^2 patterns plotted on a logarithmic scale, since this spreads out the closely spaced curves for the terminal carbon positions in the octyl chains, and this is done in Figs. 7.12 - 7.14.

Taking the two hydrocarbons first, the obvious difference is that the S^2 curves tend towards their constant high temperature value more slowly for 9,10-di-*n*-octyl-*n*-octadecane than for 9-*n*-octyl-*n*-heptadecane. This is characterized by typical values for A of around 11 in the case of 9,10-di-*n*-octyl-*n*-octadecane, and only 5 in the case of 9-*n*-octyl-*n*-heptadecane. However, except for positions **z** and **a** , the final values of S^2 are less for the larger hydrocarbon. The reverse is true as the freezing points are approached, S^2 in 9,10-di-*n*-octyl-*n*-octadecane quickly becomes maximized, even before the compound freezes within the limits of the approximate form of S^2 used, while this occurs in 9-*n*-octyl-*n*-heptadecane only over the last ten degrees. One feature is common to both sets of curves; the clustering of the order parameters of chain positions **a** - **e** as the temperature is lowered, with the terminal positions remaining more mobile.

The logarithmic plots of S^2 also show a rather regular linear spacing between the curves at higher temperatures, which indicates that the S^2 values decrease in geometric progression along the chain, at least until the last two or three positions. For 9,10-di-*n*-octyl-*n*-octadecane, the factor is 0.7, surprisingly consistently, while for 9-*n*-octyl-*n*-heptadecane it is about 0.5, and slightly less well defined. This observation might be quite fortuitous, since the same is not true for tri-*n*-octylsilane, but one cannot overlook it.

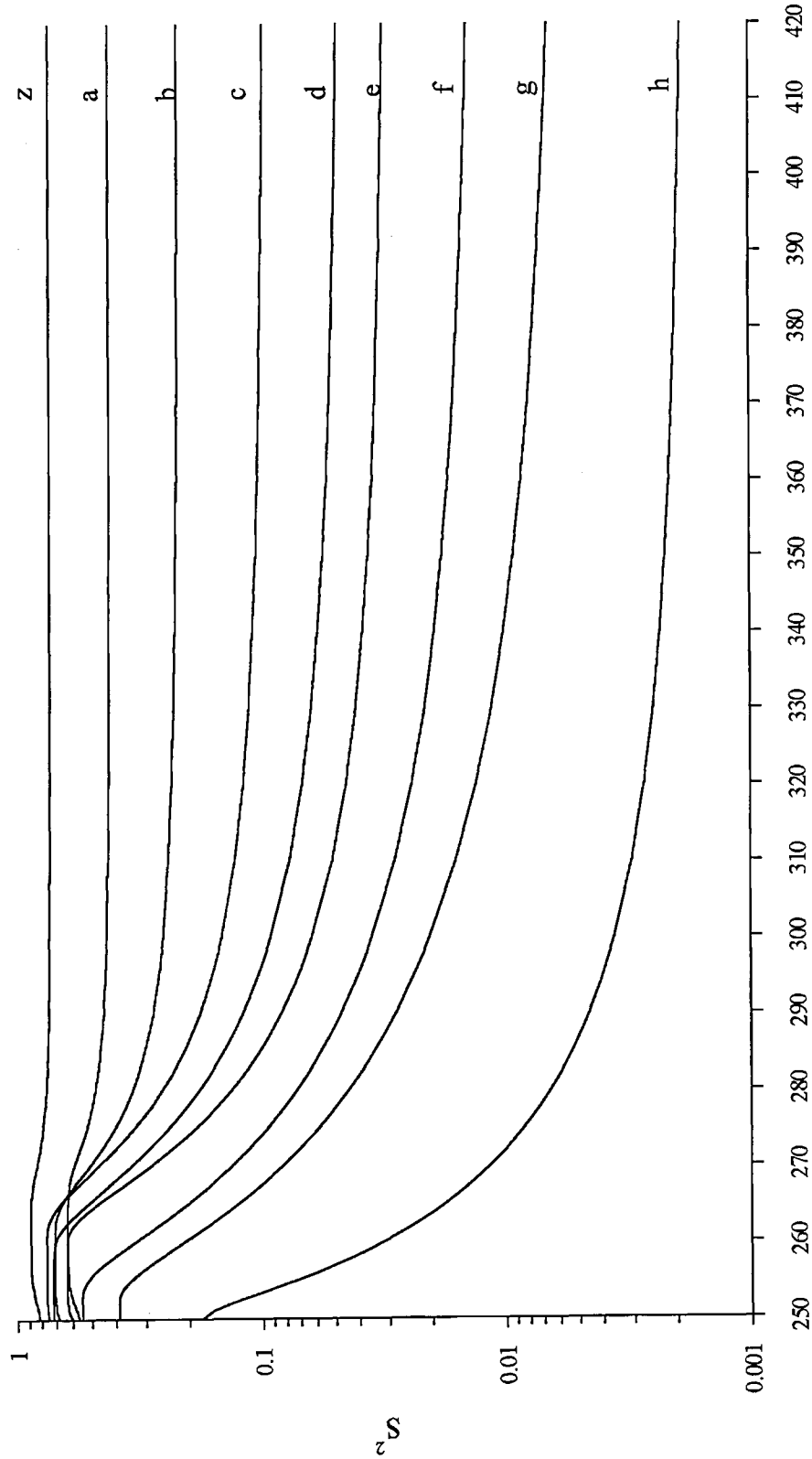

Fig 7.12: The dependence of S^2 on temperature for each carbon position in 9,10-di-*n*-octyl-*n*-octadecane. The compound freezes between 250 and 260 K.

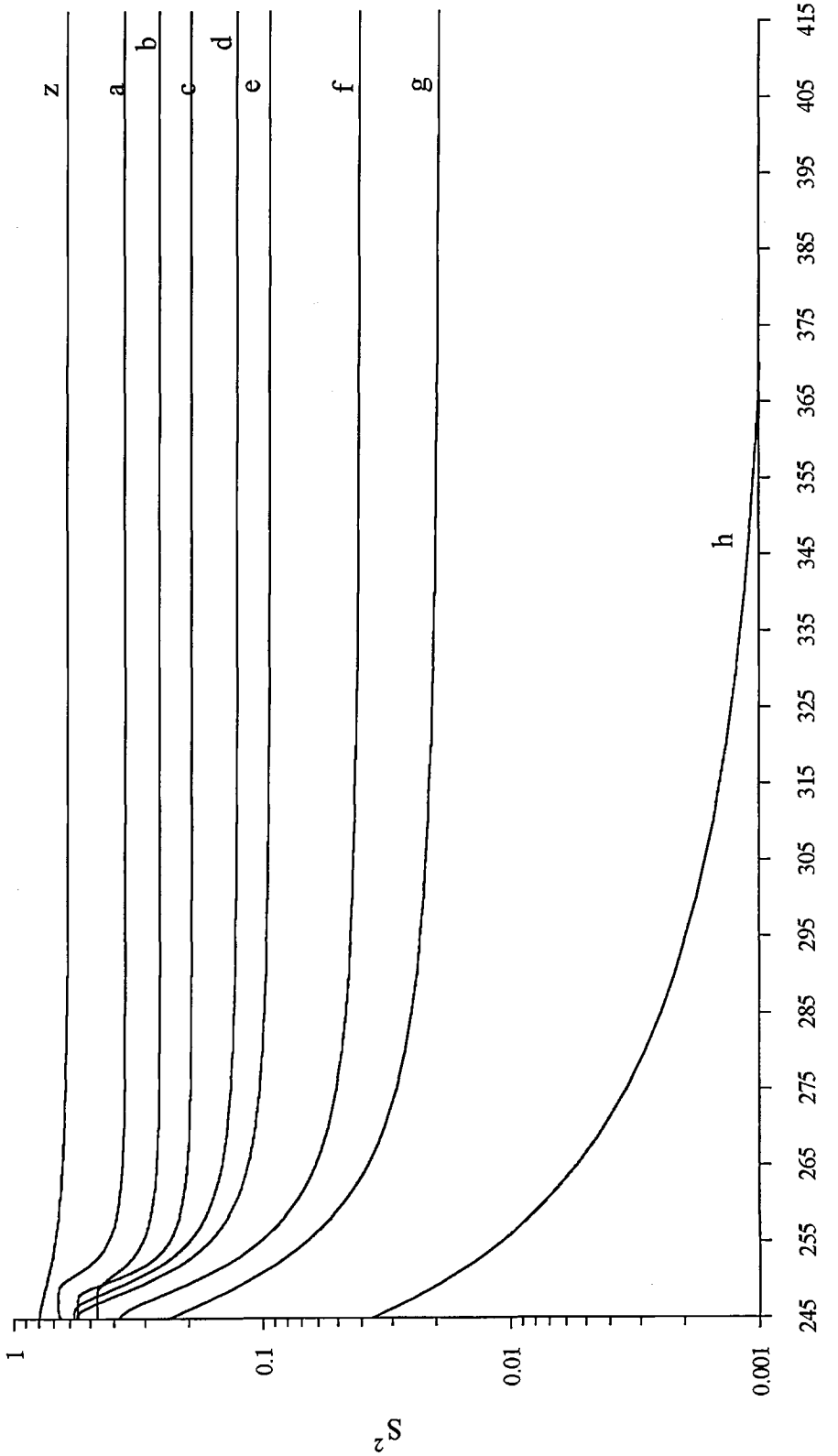

Fig 7.13: The dependence of S^2 on temperature for each carbon position in 9-*n*-octyl-*n*-heptadecane The compound freezes between 245 and 255 K.

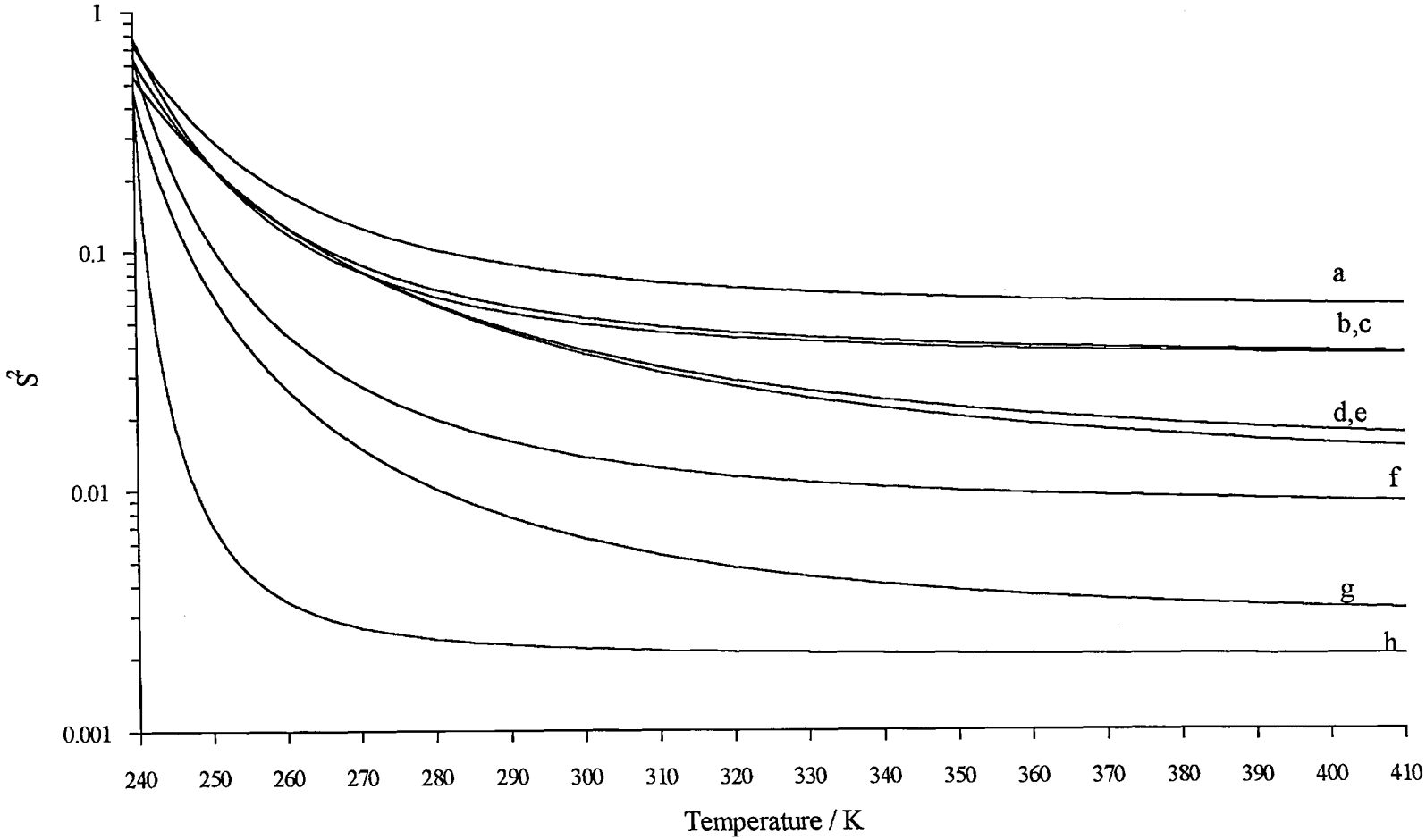

Fig 7.14: The dependence of S^2 on temperature for each carbon position in tri-*n*-octylsilane. The compound freezes between 240 and 250 K.

Since the previous work of Gillies and Sutcliffe has suggested the values of S^2 are correlated to the lubricating properties of a liquid, the differences noticed here may be of significance. Their work has linked lubricants with high traction coefficients[7] to large values of S^2, while lubricants of the *n*-octyl type[5,6] with low traction coefficients, were linked to generally low values of S^2. However, the observations of the S^2 behaviour found here for 9,10-di-*n*-octyl-*n*-octadecane and 9-*n*-octyl-*n*-heptadecane are evidently of a more subtle kind, since they seem to distinguish between two lubricants expected to both be of the low traction variety, i.e. normal lubricants.

Unfortunately, without appropriate mechanical experimental data, one cannot be sure of the significance of the differing S^2 behaviours for the relative effectiveness of these two oils as engineering lubricants. Certainly, 9,10-di-*n*-octyl-*n*-octadecane is the molecule which approximates the structures found in poly-α-decene lubricants most closely, and it may be that the special S^2 features found for this molecule are those which indicate a superior performance. The low values of S_∞^2 at the periphery of the molecule may be significant, when one might not have expected them to differ very much from those in 9-*n*-octyl-*n*-heptadecane. Or else the very regular geometric decay in the values along the chain, and the size of the factor involved, may be the result of types of internal motion that are well suited to providing good lubricating potential in a molecule. Any of these might be individually significant, or they may be simply aspects of some larger picture, to be assembled only from further evidence.

The correlation times and activation energies for internal motion, τ_i and E_i, are rather larger for 9,10-di-*n*-octyl-*n*-octadecane than for 9-*n*-octyl-*n*-heptadecane, as one might have expected for a bulkier molecule, and the values of E_i also show a small maximum around position **b**, which agrees with the findings of the previous work of Gillies and Sutcliffe on *n*-octyl compounds. There appears to be a large difference in E_i at the central carbon position, which may be because the arrangements of the molecules differ most strongly around this point. The types of internal motion that occur in the two cases appear to be different, leading to the differing activation energies.

The S^2 plots of tri-*n*-octylsilane differ noticeably from those of 9-*n*-octyl-*n*-heptadecane, with very much smaller values of S_∞^2 and an irregular spacing of the curves. The somewhat surprising conclusion is that the internal motions that predominate for carbon-13 relaxation in the silane are very different from those in the hydrocarbon. Together with this, the values of τ_i^{298} for positions **a** and **b** are much smaller, and the internal activation energies, E_i, appear almost constant all along the octyl chain. One can propose a simple rationalization of this, which would require further experimental confirmation.

If one considers the larger diameter of the silicon atom, compared with a covalently sp^3 bonded carbon atom, the steric interactions of the proximal methylene

groups of the three *n*-octyl chains, positions **a**, will be rather less for the silane. Therefore, one can hypothesize that each *n*-octyl chain can rotate about this point of attachment with much less resistance in the silane, and this rotary motion would be superimposed on the "usual" internal motions present in the hydrocarbon octyl chain. This would explain the reduced and more uniform τ_i^{298} and E_i values for the silane *n*-octyl groups, and probably also the spin-rotational relaxation observed in the terminal methyl groups. The presence of the longer Si-C bond alone might also give extra flexibility in the silane molecule, and should be taken into account.

In all three cases, of course, the general decrease in S^2 and τ_i towards the ends of the *n*-octyl chains coincides with the expectation of increasing segmental mobility, at least in the high temperature regime. The assumption of this correlation confirms the actual assignments of the middle positions of the *n*-octyl chains, given previously for these compounds only on the basis of the measured T_1 values[8], and places them on a more satisfying theoretical basis.

The overall rotational reorientation of the three molecules presents a simpler picture, following more or less what one would expect. The larger activation energy and slower motion of 9,10-di-*n*-octyl-*n*-octadecane, compared to 9-*n*-octyl-*n*-heptadecane, follow on from the increased molecular volume, and special interactions related to the more branched structure. Comparison of tri-*n*-octylsilane with 9-*n*-octyl-*n*-heptadecane presents more interest, since the value of E_m is considerably less for the silane. This could be related to the flexible linkage of the *n*-octyl chains in the silane, or to a marked departure from covalent tetrahedral bonding, which would also alter the dynamics of the molecule in the liquid state. The latter is a strong possibility, considering the reactivity of the tertiary proton, which was exploited in the synthesis of labelled compounds in this work. The Si-H grouping can be thought to be polar, and also represented by the structure $Si^{\delta+}$-$H^{\delta-}$.

Finally, one should keep in mind that the actual physical significance of the apparent temperature dependence of S^2, that is needed to correctly model the experimental data, is somewhat obscur. However, the differences in the parameters obtained for the three molecules are real enough, and apparently characteristic for particular molecular structures. There is some rational basis to them, which is probably close to the general picture adopted in this work, and may well indicate interesting details of the nature of molecular motion, and its relationship to the macroscopic physical properties displayed by the liquids, in particular as lubricants.

7.11 SUGGESTIONS FOR FURTHER WORK

The most important task would be a thorough theoretical examination of the applicability of the Lipari and Szabo model to flexible molecules of the kind examined here, in order to place the whole analytical procedure on a firmer footing. Even if a

more suitable adaptation of the theory was required, the results obtained here might at least be re-interpreted in a new light, to some benefit. It would be interesting to see if further measurements of relaxation times at one or two other frequencies gave the values which can be predicted by the theory and results of the present work.

Together with this, one should examine the possibility of developing computational methods of predicting the internal motions in *n*-alkyl structures of these kinds in ways which generate motional parameters of relevance to NMR relaxational behaviour. One would not require exact real time molecular dynamics simulations, but rather general predictions of quantities such as S^2, and this might be within the capabilities of present day computation.

Of more particular relevance to the work done on the three *n*-octyl compounds here, the measurement of engineering properties, such as temperature and pressure dependence of viscosities, would be helpful in trying to correlate the results of the analyses to the lubricating properties of the compounds. Measurements of NMR relaxation rates and NOE factors under high applied pressures would complement these, and could be performed using the type of equipment used already by Benedek[9], and by Gillies and Sutcliffe[10].

Measurements of deuterium relaxation rates on 9,10-di-*n*-octyl-*n*-octadecane-$9d_1$ and 9-*n*-octyl-*n*-heptadecane-$9d_1$ at other frequencies, and extra measurements in the low temperature region, would help to confirm the accuracy of the overall motional parameters obtained in this work. Together with this, theoretical work is needed to confirm the validity of the equations used, and perhaps also extend them to include the internal motions in the molecule, so that the lowest temperature measurements can also be included adequately. Line shape analyses of the deuterium resonances may well reveal whether the molecular motion is isotropic, or not, at low temperatures. One would hope that the determination of deuteron quadrupolar coupling constants suggested in this work can be shown to be justified theoretically.

The silicon-29 T_1 measurements on tri-*n*-octylsilane at 53.5977 MHz could be extended up to, say, 170 ^{0}C, which would confirm the theoretical curve (Fig. 7.9) found using the present data. A more detailed analysis of the motion of the silicon-proton bond could be attempted, as mentioned already in Section 7.8, if multifrequency silicon-29 measurements were made, including NOE and T_2 values. Of these, the experience of the deuterium relaxation measurements indicates that accurate T_2 values would be most immediately profitable, even at only the same frequency.

It appeared from this work that any temperature variation required of S^2 reveals itself most strongly in the behaviour of the low temperature NOE factors. The theoretical curves shown in Appendix 6 for NOE factors show small undulations in the low temperature region, and the correspondence with the general trends of the data points tends to suggest that what is at first sight random scatter in the measured NOE factors may be a real effect. If more numerous and accurate NOE factors were

determined in this region, it would be possible to interpolate a precise NOE curve, and use this to solve for the actual temperature variation of S^2. Conversely, the same consideration makes it appear unwise to try a simple minded smoothing out of the NOE data, in the expectation that one is averaging away experimental error.

REFERENCES FOR CHAPTER 7

[1] J. Kowalewski and G. Widmalm, *J. Phys. Chem.*, 1994, **98**, 28

[2] See the references to work by these authors in Chapter1.

[3] S. Bagley, H. Kovacs, J. Kowalewski, and G. Widmalm, *Magn. Reson. Chem.*, 1992, **30**, 733

[4] The procedure for least squares approximation employed here is described in detail in several examples in: W. J. Orvis, *Excel 4 for Scientists & Engineers*, Sybex, 1993. The Excel® conjugate gradient search uses the GRG2 non-linear optimization code developed by L. Lasdon, University of Texas at Austin, and A. Warren, Cleveland State University, which is the copyright of Frontline Systems, Inc., P. O. Box 4288, Incline Village, Nevada, 89450-4288, U. S. A.

[5] D. G. Gillies, S. J. Matthews, and L. H. Sutcliffe, *Magn. Reson. Chem.*, 1991, **29**, 1221

[6] L. M. Bull, D. G. Gillies, S. J. Matthews, L. H. Sutcliffe, and A. J. Williams, *Magn. Reson. Chem.*, 1991, **29**, 273; D. G. Gillies, S. J. Matthews, L. H. Sutcliffe, and A. J. Williams, *J. Magn. Reson.*, 1990, **86**, 371

[7] D. G. Gillies, S. J. Matthews, and L. H. Sutcliffe, *Magn. Reson. Chem.*, 1990, **28**, 171; D. G. Gillies, S. J. Matthews, and L. H. Sutcliffe, *Magn. Reson. Chem.*, 1991, **29**, 777 and 823; D. G. Gillies, S. J. Matthews, and L. H. Sutcliffe, *Magn. Reson. Chem.*, 1992, **30**, 259; D. G. Gillies, S. J. Matthews, L. H. Sutcliffe, and A. J. Williams, *J. Magn. Reson.*, 1990, **86**, 371

[8] E. Bengsch, B. Perly, C. Deleuze, and A.Valero, *J. Mag. Res.*, 1986, **68**, 1

[9] G. B. Benedek, *Magnetic Resonance at High Pressures*, Interscience Publishers, 1963

[10] D. G. Gillies, S. J. Matthews, and L. H. Sutcliffe, *Mag. Reson. Chem.*, 1991, **29**, 823

Chapter 8

ANALYSES OF THE DATA FOR TRICYCLOHEXYLMETHANE AND 1,1,2-TRICYCLOHEXYLETHANE

8.1 GENERAL OBSERVATIONS

The objective was to simulate the measured carbon-13 R_1 relaxation rates and NOE factors as functions of temperature and frequency within the theoretical description of Lipari and Szabo, in the manner described in the Chapter 7, and in particular in Section 7.1, to obtain the relevant parameters describing the molecular motion.

8.2 PRELIMINARY EXAMINATION OF THE DATA

As was done for the *n*-octyl compounds previously, the carbon-13 data for tricyclohexylmethane were firstly examined using the description in which S^2 was assumed to be a constant for each individual carbon position, with four remaining unknown parameters, E_m, τ_m^{298}, E_i, and τ_i^{298} also to be determined. However, as each optimization progressed, it was clear the values of E_i and τ_i^{298} were not determined by the data, and the values of τ_i quickly converged to zero under any starting conditions, while E_m and τ_m were determined, and were essentially the same for each carbon position. This did not mean that there were no internal motions present in this molecule, but simply that they their detailed influence on the relaxation rate and NOE data across the range of temperatures that was examined was not measurable. The description required was only that of the reduced Lipari and Szabo equations, where the internal motions are accounted for by averaging down the dipolar interaction using the scaling factor S^2.

Since the values of E_m and τ_m^{298} that emerged were fairly consistent across the molecule, it was apparent that this was the type of example in which the Lipari and Szabo theory could be expected to apply well, within its original conception. The steric interactions of the cyclohexyl rings crowded around the central carbon position create a molecule without the flexibility present in *n*-alkyl structures that was discussed in the previous chapter. (Section 7.2)

It would have been helpful to have also determined values for E_m and τ_m^{298} independently using the deuterium NMR data for tricyclohexylmethane-d_1, following the examples of 9,10-di-*n*-octyl-*n*-octadecane-9d_1 and 9-*n*-octyl-*n*-heptadecane-9d_1, but in this case a simultaneous fit of the R_1 and R_2 data proved impossible within the theoretical description used in Chapter 7. The line widths were always small, so the R_2

data were probably rather inaccurate, but it appeared that the widths began to increase at the higher temperatures, instead of continuing to decrease as expected. Whatever the cause of this, the standard equations for quadrupolar relaxation presented in Section 7.1 do not allow for such behaviour.

However, the results from the data analyses in Chapter 7 had demonstrated the likelihood of the approximate identity of the S^2 scaling factor in the carbon-13 relaxation theory, and the S^2 factor appearing in the expressions used for quadrupolar relaxation of a deuteron bonded at the same location in a monodeuterated isotopomer. The use of this assumption enabled a simultaneous fit of the carbon-13 relaxation data for the carbon atom in position **z** in tricyclohexylmethane, and the deuterium R_1 relaxation data for tricyclohexyl methane-d_1. The values of E_m and τ_m^{298} that emerged were close to those obtained from the carbon-13 data alone. The quadrupole coupling constant could also be included as a parameter to be determined by the optimization.

These values of E_m and τ_m^{298} were then used, together with the reduced Lipari and Szabo equations, to analyze the remaining carbon-13 data for tricyclohexylmethane, with only S^2 remaining to be determined at each position. The resulting fits to the measured data were adequate. An attempt was made to invoke a temperature variation of S^2, using the function applied in the cases of the *n*-octyl compounds, but the S^2 parameters were not defined by the optimization procedure, and any combination was possible, just so long as it made S^2 effectively constant over the range of temperatures considered. Therefore, there was no loss in assuming that S^2 was in fact temperature independent; if there is a variation it must be small.

The case of 1,1,2-tricyclohexylethane turned out to be rather different. The same initial analyses were carried out as for tricyclohexylmethane, but this time it was clear that the data did in fact determine values of E_i and τ_i^{298} at every carbon position. The apparent reason for this was that it was possible to make the measurements from 40 ^{0}C, where the dependence of the relaxation effects on the internal motions was increased, whereas in the case of tricyclohexylmethane measurements were limited by the crystallization of the compound at 58.5 ^{0}C. Otherwise, one would not have expected to encounter any difference in the analyses of the data from such similar molecules. As for tricyclohexylmethane, the values of E_m and τ_m^{298} were quite consistent, showing only a small drop in E_m towards the periphery of the molecule.

Since there were no comparable deuterium data available for 1,1,2-tricyclohexylmethane, there was no independent way of checking the correct values of E_m and τ_m^{298}. However, the results for tricyclohexylmethane showed that it would be sufficient to take the values that had emerged from the initial analysis for the most central carbon position, in this case position **2z**. The optimizations for the remaining carbon positions were carried out by assuming these same values of E_m and τ_m^{298}, and the results were satisfactory. There was no need to assume any variation of S^2 with temperature.

8.3 ANALYSES FOR TRICYCLOHEXYLMETHANE AND TRICYCLOHEXYLMETHANE-d_1

An attempt to obtain simultaneous fits of the measured R_1 and R_2 relaxation rates to the values predicted by the theoretical description used previously for 9,10-di-*n*-octyl-*n*-octadecane-9d_1 and 9-*n*-octyl-*n*-heptadecane-9d_1 was negative, although a reasonable result was obtained if the four highest temperature measurements were removed from the R_2 data. Instead, it was assumed that the S^2 factors in both the Lipari and Szabo equations for carbon-13 relaxation and the standard equations for deuteron quadrupolar relaxation could be identified. In this way a simultaneous fit became possible for the carbon-13 relaxation and NOE data for the **z** carbon in tricyclohexylmethane, and the deuterium R_1 relaxation data for tricyclohexylmethane-d_1. Assuming equal weighting of the sets of deuterium and carbon-13 data gave the values of E_m and τ_m^{333} in Table 8.2. The quadrupolar coupling constant was also included as a parameter to be optimized, and the value predicted was ±175 kHz. The table quotes τ_m^{333} as a more appropriate Arrhenius frequency factor, since the compound crytallizes just below 333 K. The optimized theoretical curve and measured deuterium relaxation data are plotted in Fig. 8.2, while the plots of the carbon-13 data and corresponding optimized theoretical curves appear in Fig. 8.4. Fig 8.3 shows the same curve and data as Fig. 8.2, plotted as $\ln(R_1)$ against 1000/T.

The linear plot of the theoretical curve in Fig. 8.3 indicates relaxation in the region of extreme narrowing, but there is obviously a small systematic deviation from the actual data, which was not explained. It could be a consequence of experimental error, possibly in the measured temperatures, but the good results obtained for the other deuterium measurements in Chapter 7 suggest that the discrepancy has some real physical origin. The increase of the line widths at higher temperatures is probably not unconnected with this.

One possible cause may be exchange between the liquid and gas phases in the sample tube. Some fine crystals of the compound were found to have sublimed into the upper portions of the tube after the experiments, and the boiling point under high vacuum would be around 145 ^{0}C. Another more interesting possibility is that strong changes in some concerted motion of the three cyclohexyl rings around the central carbon atom may lead to a temperature dependent value of the quadrupolar coupling constant, through their influence on the average bond angles and the field gradients at the deuteron. The most obvious candidate would be an umbrella-like opening and closing motion, which would have a strong effect concentrated at the molecular apex.

A more mundane explanation might be that E_m is not a constant, as assumed, but actually decreases at higher temperature. This would give the observed curvature in Fig. 8.3. Engineering measurements of viscosity have been reported on tricyclohexylmethane which confirm the high value for E_m, but also suggest just this kind of temperature dependence for the activation energy. If true, this indicates that

the usual Arrhenius formula may not be a wholely satisfactory description. The values at 1 bar were quoted as[1]:

Temperature / ^{0}C	75	85	95	105	115
E_m / kJ mol^{-1}	48.7	46.9	43.3	39.1	33.7

Table 8.1 : The reported values of E_m for tricyclohexylmethane, from 75 to 115 ^{0}C.

Using the values of E_m and τ_m^{333} given in Table 8.2, analyses of the remaining carbon-13 relaxation and NOE data for tricyclohexylmethane determined the values of S^2 for the other carbon positions recorded in Table 8.3. Plots of the optimized theoretical curves of carbon-13 relaxation rates and NOE factors, together with the actual data, appear in Appendix 9. One notes that a certain systematic deviation appears in the higher temperature regions, with slightly higher relaxation rates, and lower NOE factors than expected, especially in the 100.5 MHz data. This suggests that it may be necessary to include an element of spin-rotational relaxation into the theoretical equations to fully analyze this data, as was done for silicon-29 relaxation in tri-*n*-octylsilane; the rather short overall rotational correlation time τ_m at higher temperatures would explain this.

E_m kJ mol^{-1}	τ_m^{333} ns	QCC kHz
43.11	0.56	±175

Table 8.2: The parameters for overall molecular motion of tricyclohexylmethane-d_1 determined from combined deuterium R_1 relaxation rate and carbon-13 NMR data, and the determined quadrupolar coupling constant.

carbon position	S^2
z	0.73
a	0.71
b	0.60
c	0.59
d	0.67

Table 8.3: The constant generalized order parameters for internal motion in tricyclohexylmethane determined from the carbon-13 NMR data.

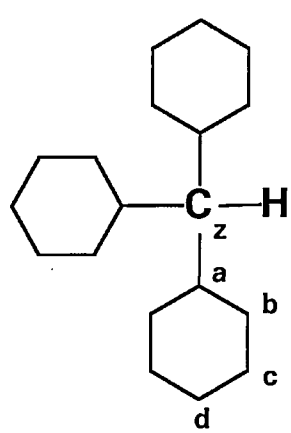

Fig 8.1: The assignments in tricyclohexylmethane.

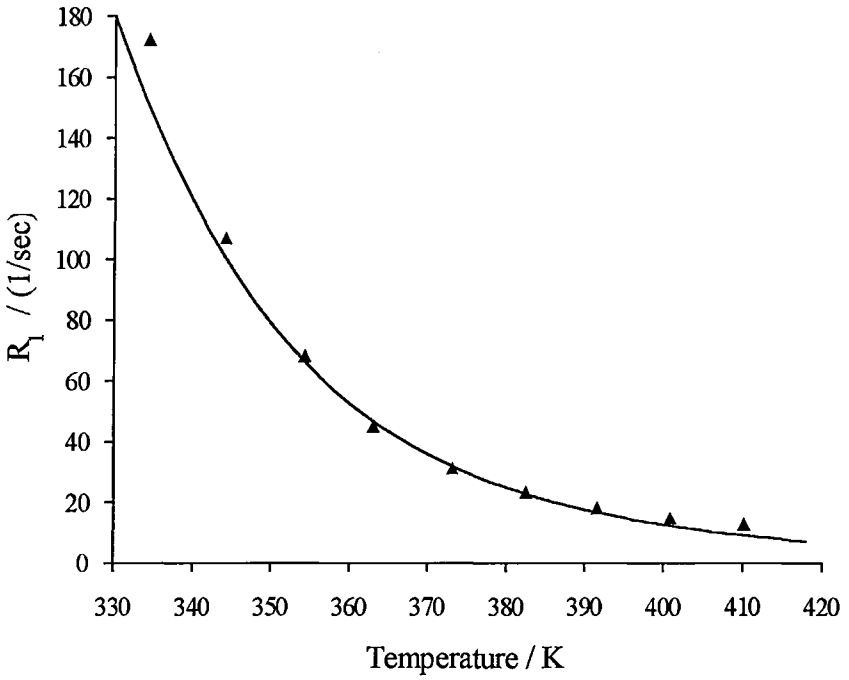

Fig 8.2: The deuterium R_1 NMR relaxation data at 41.405 MHz and the optimized theoretical curve for tricyclohexylmethane-d_1, as determined in combination with the corresponding carbon-13 NMR data.

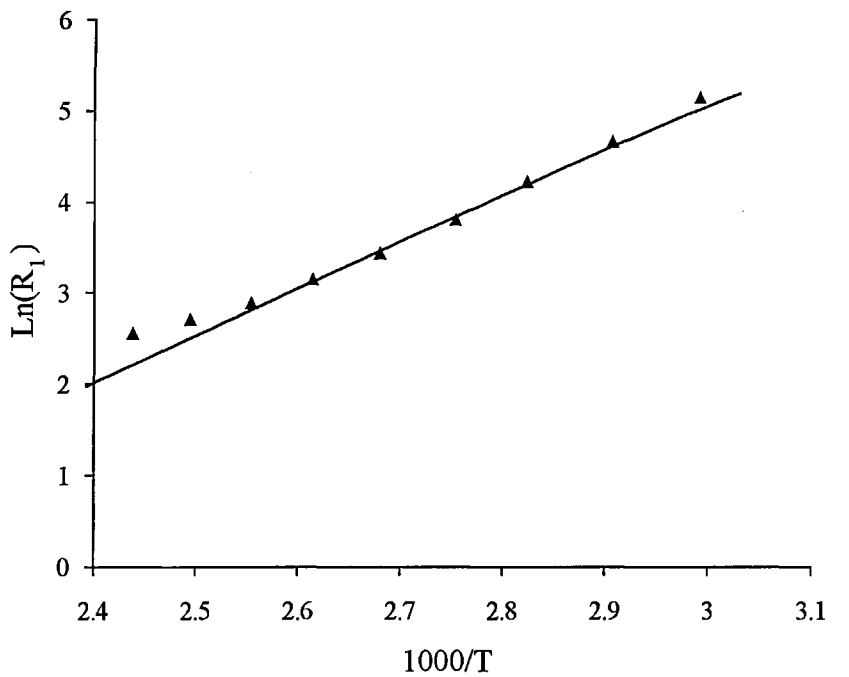

Fig 8.3: The same data and optimized theoretical curve as in Fig. 8.2 plotted as $Ln(R_1)$ against 1000/T.

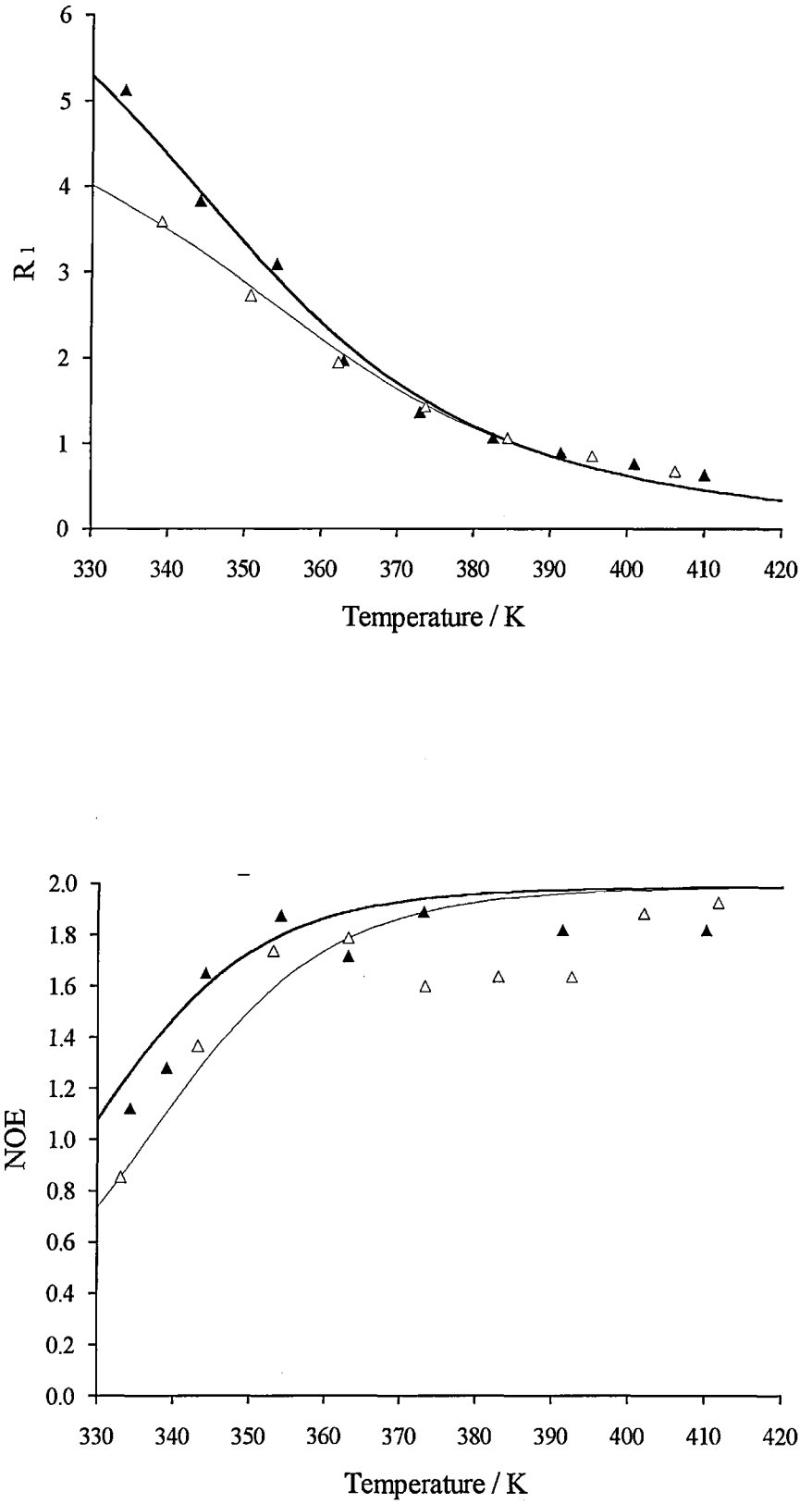

Fig 8.4: The carbon-13 relaxation data for position **z** in tricyclohexylmethane and the optimized theoretical curves at 67.83 MHz (—) and 100.5 MHz (–), as determined in combination with the corresponding deuterium R_1 data for tricyclohexylmethane-d_1.

8.4 ANALYSES FOR 1,1,2-TRICYCLOHEXYLETHANE

The values of E_m and τ_m^{333} are given in Table 8.4, and are those which were obtained from the analysis of the carbon-13 data for position **2z**. Using these values, analyses of the remaining carbon-13 relaxation and NOE data for 1,1,2-tricyclohexylethane determined the values of E_i, τ_i^{333}, and S^2 for the other carbon positions recorded in Table 8.5. Plots of the optimized theoretical curves of carbon-13 relaxation rates and NOE factors, together with the actual data, appear in Appendix 10. Since the resonances for all three **d** positions overlapped, the parameters for these are some average over the three rings.

The same comments regarding the possible inclusion of spin-rotational relaxation in the theoretical equations apply here, as for tricyclohexylmethane in Section 3.

E_m kJ mol^{-1}	τ_m^{333} ns
41.28	0.64

Table 8.4: The parameters for the overall molecular motion of 1,1,2-tricyclohexylethane as determined from the carbon-13 data for position 2z.

carbon position	E_i kJ mol^{-1}	τ_i^{333} ps	S^2
1z	22.1	40.3	0.57
2z	21.6	8.6	0.76
1a	55.4	15.3	0.56
2a/3a	43.4	35.0	0.59
1b/1b'	33.4	33.1	0.43
2b/3b	29.8	42.4	0.48
2b'/3b'	26.9	48.2	0.47
1c/1c'	30.3	37.4	0.42
2c/3c	23.7	43.6	0.47
2c'/3c'	26.7	42.2	0.48
1d/2d/3d	7.8	25.3	0.57

Table 8.5: The parameters for internal motion in 1,1,2-tricyclohexylethane determined from the carbon-13 NMR data.

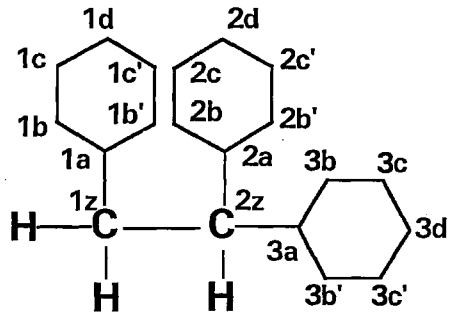

Fig. 8.5: The assignments in 1,1,2-tricyclohexylethane.

8.5 ACCURACY OF THE MOTIONAL PARAMETERS

The same comments apply here as for the cases of the *n*-octyl compounds in Chapter 7, with the obvious simplifications brought about by the use of the Lipari and Szabo equations in their original form, with S^2 as a constant. In view of the method of analysis required for the deuterium relaxation measurements for tricyclohexylmethane-d_1, the values obtained for E_m and τ_m^{333} were less accurate than the corresponding values for 9,10-di-*n*-octyl-*n*-octadecane-9d_1 and 9-*n*-octyl-*n*-heptadecane-9d_1 in Chapter 7. The estimates were that E_m was correct to within ±1 kJ mol^{-1}, and τ_m^{298} to ±0.05 ns. The accuracies of the corresponding parameters for 1,1,2-tricyclohexylethane are probably about the same. The values of E_i were estimated to be accurate to within ±1.5 kJ mol^{-1}, and τ_i^{298} to within ±10 % in both cases, and it appeared that S^2 was determined to within ±0.03.

8.6 DISCUSSION

The parameters obtained from the analyses for these less flexible molecules can be expected to have the meaning attached to them by the original theory of Lipari and Szabo, and the discussion is therefore on a different footing from that of the *n*-octyl structures in the Chapter 7. It is possible, and more profitable, to discuss both tricyclohexylmethane and 1,1,2-tricyclohexylethane simultaneously, and also necessary to use the information about their structures obtained from the proton and carbon-13 spectra of the liquid state in Chapter 4, and the X-ray crystallographic and ESR studies related to tricyclohexylmethane in Chapter 5.

Examining the tables of S^2 values, it is interesting to notice the regular pattern in the rings, where S^2 is similar, and larger, for positions **a** and **d**, and smaller at positions **b/b'** and **c/c'**. From the studies related to tricyclohexylmethane in Chapter 5, and the proton NMR spectra, one can assume the rings are in chair type conformations, with equatorial attachment to the **z** carbons. The difference in the S^2 values among these positions could then be explained by the chairs twisting to and fro around an axis through positions **a-d**, which would leave positions **a** and **d** less mobile than **b/b'** and **c/c'**. Of course, this does not exclude an actual bodily oscillation of each ring about this axis from being present, as well as the more limited internal twisting of the rings.

The internal motion of the C-H vectors in positions **a** would be expected to correspond to this kind of oscillation, and it is interesting to note the very high values of E_i for just these positions in 1,1,2-tricyclohexylethane, reflecting, as one might hope, the high barrier to rotation of the rings as a whole due to steric conflict. Careful consideration of the proton and carbon-13 NMR spectra of tricyclohexylmethane in Chapter 4 also demonstrates the existenace of this torsional motion, and elucidates its nature.

The small effective vicinal coupling constant of 4 Hz between the **z** and **a** protons in this molecule shows that the rotational diffusion of the cyclohexyl rings around the **z-a** axis is not isotropic, and the distribution of torsional angles over time is not completely uniform. On the other hand, the extra equivalences present in the chemical shifts of the carbon-13 spectrum of this molecule have to be reconciled with this. Assuming a simple Karplus type dependence of the coupling constant on the usual dihedral angle between proton **z** and a representative **a** proton, of the form $J = J_0\cos^2\theta \approx 12\cos^2\theta$ Hz, suggests an oscillation of each ring between two symmetrically orientated gauche arrangements of the C-H vectors at the **z** and **a** positions; such that the carbon atoms at positions **b** in the attached ring experience, on average, similar environments. A relatively fixed symmetric conformation, with $\theta = 0^0$, or 180^0, is made impossible by the observed coupling constant of only 4 Hz. An asymmetric arrangement, to give the correct coupling constant, would lead to an expected inequivalence between two **b** and **b'** carbon positions in each ring, which is not observed in this example.

Presumably, closely analogous internal torsional reorientation of the cyclohexyl rings is also present in tricyclohexylmethanol, tricyclohexylmethylchloride, and the other related structures, to give the carbon-13 equivalences observed in their respective solution spectra.

In the case of 1,1,2-tricyclohexylethane, the inequivalences between the primed and unprimed positions in rings **2** and **3** arise inherently from the three different substituents on carbon **2z**, regardless of any motional averaging, and do not necessarily lead to any deductions concerning the angular motions of the two rings about the **2z-2a** and **2z-3a** axes. However, the situation of ring **1** is different, and allows the generation of the observed equivalences through a suitable torsional motion, with respect to the rest of the molecule; and, apparently, this does occur. The argument parallels that of the **b** carbons in tricyclohexylmethane, with the two **1z** protons taking the rôles of the other two cyclohexyl rings in that case.

The activation energies and correlation times deduced for the torsional motions of the cyclohexyl rings in 1,1,2-tricyclohexylethane, from the relaxation data for carbons **1a**, **2a**, and **3a**, can be assumed to be representative of the relevant parameters in the other molecules, and this confirms that the motion is fast enough on the carbon-13 NMR time scale to allow the generation of the observed extra equivalences through motional averaging.

The torsional motions about the **z-a** axes present some complications from the theoretical viewpoint for positions **d**. The reason is that the angular motions of the two C-H vectors at this positions will not be equivalent, since one will coincide more or less with the rotational axis of the ring, and the other will be more perpendicular to it, and more mobile. This might explain the anomalies in the values of E_i and τ_i^{333} at these positions in 1,1,2-tricyclohexylethane.

The values of S^2 and τ_i for ring **1** in 1,1,2-tricyclohexylethane are definitely smaller than the corresponding ones in rings **2** and **3**, which are generally similar. This correlates nicely with the expectation that ring **1** should be rather more mobile in this molecule, with extra freedom given by its attachment "at a distance" along the **1z-2z** axis. On the basis of this assumption, the analysis therefore appears to be sensitive enough to have been used to assign the carbon-13 resonances correctly to the different rings, thus lending support to the theoretical picture of the Lipari and Szabo equations in this example. Of course, the assignments have already been deduced unambiguously by standard methods in Chapter 4, chiefly using the 2D-INADEQUATE spectrum.

In summary, the overall picture that emerges for these various polycyclohexyl alkanes is of molecules with very subtle and involved internal dynamics.

8.7 SUGGESTIONS FOR FURTHER WORK

The suggestions made in Section 7.11 concerning further NMR and related work on the *n*-octyl lubricant compounds also apply in general here. NMR and engineering measurements at high pressures are particularly important for the present case, since the special behaviours of high traction lubricants manifest themselves under these conditions. It would also be interesting to see if computational studies on these two molecules are able to confirm the nature of the internal motions, that the NMR measurements have suggested.

Investigation of 1,1,2-tricyclohexylethane is especially indicated. The reason is that the existing engineering data on tricyclohexylmethane[1,2] indicate that the compound displays a strong increase in viscosity with applied pressure, and thus potential as a traction fluid lubricant; at least if it did not solidify at high pressures, which was found to be the case[1]. One can expect that 1,1,2-tricyclohexylethane will prove to have very similar characteristics as far as its viscosity/pressure dependence is concerned, but without the undesirable solidification under applied pressure. The fact that it is still liquid at room temperature suggests this. The lack of symmetry in 1,1,2-tricyclohexylethane appears to hinder crystallization, and the compound passes instead into a very viscous supercooled phase.

Further deuterium NMR measurements on tricyclohexylmethane-d_1 could possibly lead to an explanation of the relaxation effects observed so far, and the inclusion of spin-rotational relaxation in the theoretical equations should also be investigated, as was done for the silicon-29 data from tri-*n*-octylsilane.

Finally, the synthesis of tricyclohexylmethylamine remains to be accomplished.

REFERENCES FOR CHAPTER 8

[1] E. Kuss, *Ber. Bunsenges. Phys. Chem.*, 1983, **87**, 33.

[2] K.-H. Hentschel, *J. Synthetic Lubrication*, 1985, **2**, 143 and 239.

Appendix 1

PROCEDURES FOR FRACTIONAL AND SHORT PATH DISTILLATION

Fractional distillations under reduced pressure were made through a 35 cm x 1.7 cm internal diameter glass column, filled with glass Raschig rings, of average size 3.5 mm in each dimension. The column was surrounded by an air jacket constructed from two concentric glass tubes, heated internally by turns of electrical resistance wire. The low voltage supply was obtained via an isolating transformer and Simmerstat controller from mains ac current, and was capable of heating the column to 200 ^{0}C. The power settings were calibrated before use by measuring the internal column temperatures, and the jacket was also equipped with a thermometer during distillation.

The distillation pot was a 150 ml round bottom flask, equipped with magnetic stirring and electric heating mantle. The column was equipped with a simple take off, short air cooled condenser, and vacuum receiver adaptor for three fractions. Reduced pressure was provided by a reliable rotary pump. This simple arrangement was all that was required for the separations described in this work. The take off ratio could be adjusted by judicious insulation of the unheated few centimeters at the top of the column. The column temperature and boil-up rate were adjusted in the usual way, and the column was allowed to equilibrate for at least 30 minutes before collecting any fractions. The fractions to be expected were identified by GC analysis before commencing distillation. Usually only one was of interest, and represented the major portion of the distilland; other components could be combined. The boiling points quoted are only approximate, since the vacuum was measured using an electric gauge attached close to the pump itself, but they were in close agreement with those reported by Challenger and Pantony for 9-*n*-octyl-*n*-heptadecane and related structures.

For short-path distillations, a simple apparatus was assembled using standard Quickfit glassware. A 250 ml round bottom flask was fitted with a vacuum take-off adaptor, and into this was placed a standard size water cooled cold finger, to which was attached a small bucket hanging just below its tip, a few centimeters above the bottom of the flask. This allowed some 30 ml of distilland to be placed into the flask, together with a magnetic stirrer bar. To commence distillation, a high vacuum was carefully established, and the flask stirred and heated in an electric mantle. The temperature was measured simply by placing a thermometer in the mantle, close to the flask, which was always surrounded with glass wool to ensure uniform heating. The condensation of the volatile components could be easily observed on the cold finger,

whence they gradually collected in the bucket provided. When desired, the flask was allowed to cool under vacuum, opened, and cold finger and bucket containing the distillate carefully removed. The method was easily adapted to smaller quantities, by using a smaller flask.

Appendix 2

GAS CHROMATOGRAPHIC ANALYSES

Gas-liquid phase chromatographic analyses of reaction intermediates and products were carried out on a DB5 (SE 54) glass capillary column, with 1 ml min^{-1} flow of hydrogen as carrier gas, and detection by flame ionization. The column is a 15m glass capillary containing a substituted siloxane copolymer film. It was installed in a Carlo Erba Fractovap FTV 2150 programmable gas chromatography machine for most of the work, and latterly in a Pye-Unicam machine, which offered improved performance. Peak areas were calculated automatically using a Milton-Roy electronic integrator/plotter directly connected to the amplified FID signal.

Since very precise quantitative work was not involved, calibrations involving response factors were not made. All the compounds were very similar chemically, and direct determinations of percentages of components based on peak areas were considered sufficiently accurate indicators of the relative masses of compounds present. There was some indication that lower molecular weight components gave a slightly higher response, but this was not important in qualitative analysis of crude reaction products, and only served to validate the purities quoted for the final products.

Various temperature conditions were used during the work in analyses of the different compounds, including temperature programming. In final analyses for purity the product was tested under several different sets of conditions, in order to try to separate out any unseen overlapping components, and the shape of the actual peak was carefully observed for symmetry under these changing conditions. This GC work, together with carbon-13 NMR analyses, provided a powerful combination to assure product purity, and eliminate the possibility of the presence of isomers or close homologues in the alkane products that were required.

Typical injector and column temperatures used for the various compounds on the Carlo-Erba machine, and corresponding approximate retention times under these conditions, are given in Table A2.1. On the rather old Carlo-Erba machine, the temperature settings were not very accurate, and similar analyses on the Pye-Unicam machine could be carried out at some 30 ^{0}C less for both injector and column, to give similar retention times and resolution.

The retention times are only approximate, and tended to vary somewhat for these large molecules, depending on the presence of other components in the sample and how well conditioned the column was. Suitable mixtures were used for positive identification when necessary.

Compound	Injector Temperature / ^{0}C	Column temperature / ^{0}C	Retention Time / minutes
9-heptadecanone	250	160	8
9,10-di-*n*-octyl-*n*-octadec-9-ene	350	230	25
9,10-di-*n*-octyl-*n*-octadecane	350	230	26
9-*n*-octyl-*n*-heptadecan-9-ol	275	200	28
9-*n*-octyl-*n*-heptadecane	275	190	18
Tricyclohexylmethanol	275	170	22
Tricyclohexylmethane	275	170	10
1,1,2-tricyclohexylethane	275	170	16
Cycohexanol	175	55-4 minutes/8 ^{0}C min^{-1}/160	2.5
Diphenylether	175	55-4 minutes/8 ^{0}C min^{-1}/160	14
Dicyclohexylether	175	55-4 minutes/8 ^{0}C min^{-1}/160	13

Table A2.1: Typical GC conditions for compounds mentioned in this work.

Appendix 3

X-RAY CRYSTALLOGRAPHIC DATA FOR TRICYCLOHEXYLMETHANE

The full X-ray crystallographic data for the structure of tricyclohexylmethane were published in the paper which is reproduced on the following pages.

Journal of Molecular Structure, 318 (1994) 113–121

The structure of tricyclohexylmethane

D.G. Gillies, S. Luff, G.W. Smith, L.H. Sutcliffe*

Chemistry Department, University of Surrey, Guildford GU2 5XH, U.K.

(Received 23 August 1993)

Abstract

Tricyclohexylmethane has a melting point close to ambient temperature. Nevertheless the X-ray structure has been determined. The crystal is chiral but its chirality could not be established. The solid is unusual in that the atomic volume per carbon atom is 22.2 Å^3 which is substantially greater than is usual for a hydrocarbon. Since there is little data in the literature on the compound we have reported the solution-state proton and proton-decoupled NMR spectra.

Introduction

We are studying model traction fluids with the aim of linking molecular structure with engineering performance, thus eventually leading to new practical fluids [1–3]. There are three stages in our investigations, (i) molecular modelling, (ii) synthesis, and (iii) magnetic resonance measurements at ambient temperatures and high pressures. Generally, traction fluids are hydrocarbons containing cyclohexyl rings. It has been shown [4,5] that the highest traction is attained by the tricyclic derivatives and we have synthesized several such compounds for evaluation. Among the latter is tricyclohexylmethane (1, 1′, 1″-methylidyne-tris-cyclohexane). The compound has a melting point near to room temperature but nevertheless, we have obtained some good quality single crystals which were subjected to X-ray examination.

Experimental

Tricyclohexylmethane was prepared as follows. Triphenylmethane (10 g, 41 mmol; Aldrich) was dissolved in a mixture of cyclohexane (95 cm^3) plus toluene (5 cm^3). The solution was placed in a 500 cm^3 capacity Parr pressure vessel (S and M Products, Shirley Institute, Didsbury, Manchester) along with a slurry of activated Raney nickel catalyst (Sigma). Hydrogenation was then carried out at 400 psi and 100°C [6]. The crude product was obtained in 90% yield: it was recrystallized from ethanol (m.p. 57.5/58.5°C). Complete hydrogenation was proved by 300 MHz proton and 75 MHz carbon-13 NMR spectroscopy using a Bruker AC300 NMR spectrometer. As the spectra have not been reported before they are reproduced in Figs. 1 and 2. Without a more detailed examination, the proton spectra cannot be analysed fully; however, the group of lines centred at about 1.6 ppm can be assigned to the equatorial protons and the lines centred at about 1.2 ppm arise from the axial protons. The low intensity multiplet at 0.75 ppm is due to the proton attached to the central carbon atom, C1. No signals were observed in the aromatic region at about 7 ppm. The proton-decoupled carbon-13 spectrum is simple to assign, the carbon nuclei having the following chemical

* Corresponding author.

SSDI 0022-2860(93)07915-J

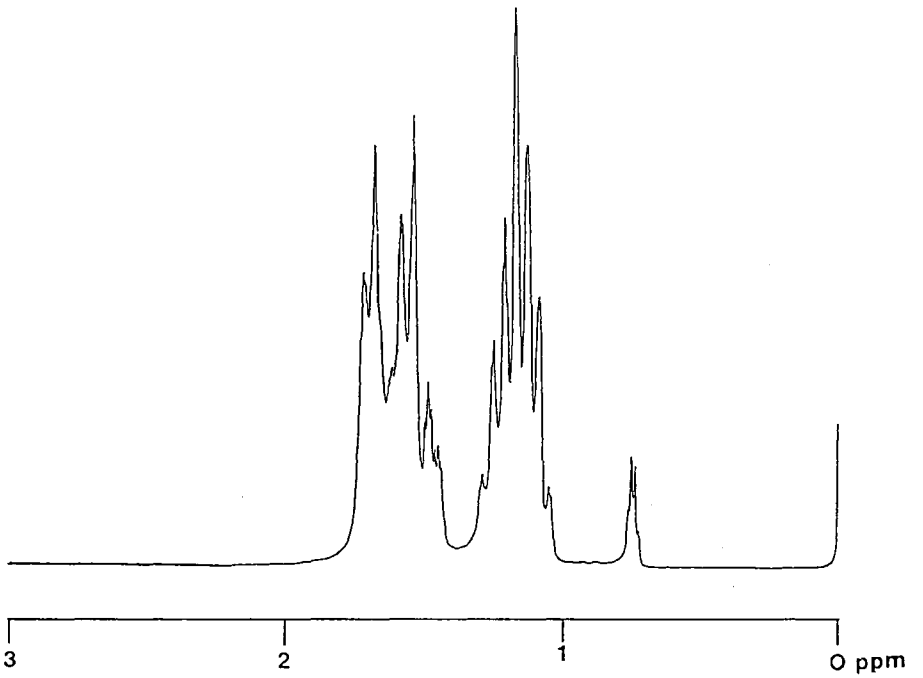

Fig. 1. The 300.1 MHz proton NMR spectrum of tricyclohexylmethane in deuteriochloroform with tetramethylsilane as internal reference.

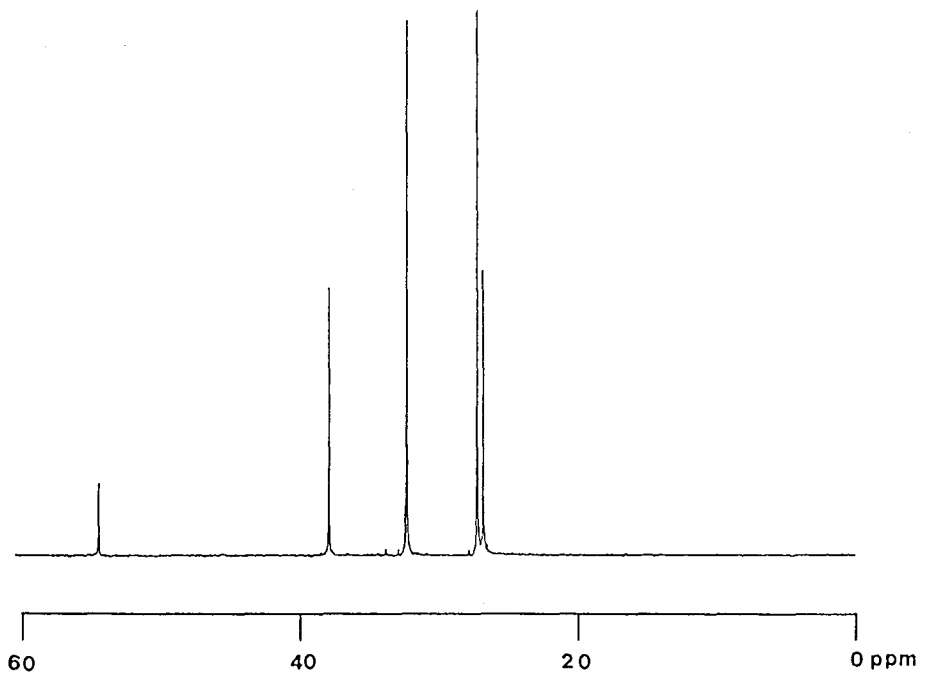

Fig. 2. The proton-decoupled 75.47 MHz carbon-13 NMR spectrum of tricyclohexylmethane in deuteriochloroform with tetramethylsilane as internal reference.

Table 1
Physical properties and parameters for data collection and refinement

Formula	$C_{19}H_{34}$
Mol. wt. (g)	262.48
Crystal system	Orthorhombic
Space group $P2_12_12_1$ (19)	
a (Å)	6.380 (8)
b (Å)	14.289 (4)
c (Å)	18.335 (4)
V (Å^3)	1687.9 (2.9)
Z	4
ρ (g cm^{-3}) calc.	1.033
μ (Mo Kα) (cm^{-1})	0.53
λ (Å)	0.71073
F (000)	592

Table 2
Positional parameters and their estimated standard deviations

Atom	x	y	z	B(Å2)
C1	0.4339(3)	0.0683(1)	0.30393(9)	2.97(3)
C11	0.2370(3)	0.1231(1)	0.32881(9)	3.14(3)
C12	0.2509(4)	0.1473(1)	0.4103(1)	4.32(4)
C13	0.0554(4)	0.1975(2)	0.4374(1)	5.11(5)
C14	0.0150(4)	0.2852(2)	0.3944(1)	5.63(5)
C15	0.0032(4)	0.2642(1)	0.3139(1)	5.37(5)
C16	0.1973(4)	0.2124(1)	0.2863(1)	4.37(4)
C21	0.4641(3)	0.0675(1)	0.22027(9)	3.07(3)
C22	0.6840(3)	0.0356(1)	0.1971(1)	3.84(3)
C23	0.7144(3)	0.0433(2)	0.1152(1)	4.17(4)
C24	0.5442(3)	−0.0083(2)	0.0738(1)	4.38(4)
C25	0.3266(3)	0.0227(2)	0.0968(1)	4.10(4)
C26	0.2970(3)	0.0131(1)	0.17891(9)	3.47(3)
C31	0.4537(3)	−0.0316(1)	0.33583(9)	3.17(3)
C32	0.2503(3)	−0.0795(1)	0.3596(1)	3.88(3)
C33	0.2931(4)	−0.1802(1)	0.3809(1)	4.95(4)
C34	0.4604(4)	−0.1877(2)	0.4393(1)	5.27(5)
C35	0.6608(4)	−0.1392(2)	0.4171(1)	4.93(4)
C36	0.6196(3)	−0.0392(2)	0.3958(1)	4.39(4)
H1	0.5550	0.1038	0.3238	3*
H11	0.1126	0.0818	0.3218	3*
H12A	0.3745	0.1866	0.4192	5*
H12B	0.2701	0.0892	0.4390	5*
H13A	0.0713	0.2114	0.4899	5*
H13B	−0.0690	0.1545	0.4325	5*
H14A	0.1295	0.3304	0.4041	6*
H14B	−0.1216	0.3131	0.4109	6*
H15A	−0.0119	0.3238	0.2858	5*
H15B	−0.1255	0.2272	0.3029	5*
H16A	0.3225	0.2533	0.2896	4*
H16B	0.1793	0.1971	0.2333	4*
H21	0.4502	0.1336	0.2035	3*
H22A	0.7926	0.0730	0.2223	4*
H22B	0.7049	−0.0305	0.2118	4*
H23A	0.8548	0.0173	0.1011	4*
H23B	0.7121	0.1102	0.1003	4*
H24A	0.5614	0.0006	0.0204	5*
H24B	0.5586	−0.0766	0.0831	5*
H25A	0.3054	0.0883	0.0818	4*
H25B	0.2196	−0.0159	0.0703	4*
H26A	0.3048	−0.0543	0.1929	4*
H26B	0.1533	0.0363	0.1925	4*
H31	0.5100	−0.0701	0.2951	3*
H32A	0.1890	−0.0462	0.4025	4*
H32B	0.1475	−0.0780	0.3184	4*
H33A	0.3402	−0.2154	0.3363	5*
H33B	0.1629	−0.2101	0.3983	5*
H34A	0.4911	−0.2542	0.4487	5*
H34B	0.4074	−0.1603	0.4851	5*
H35A	0.7612	−0.1412	0.4588	5*
H35B	0.7258	−0.1727	0.3751	5*
H36A	0.7524	−0.0101	0.3791	5*
H36B	0.5715	−0.0040	0.4397	5*

Starred atoms were refined isotropically.
Anisotropically refined atoms are given in the form of the isotropic equivalent thermal parameter defined as: $(4/3)\text{-}[a2 \times B(1,1) + b2 \times B(2,2) + c2 \times B(3,3) + ab(\cos\gamma) \times B(1,2) + ac(\cos\beta) \times B(1,3) + bc(\cos\alpha) \times B(2,3)]$

shifts:

C1	54.39 p.p.m.
C11, C21, C31	37.84 p.p.m.
C12, C16, C22, C26, C32, C36	32.25 p.p.m.
C13, C15, C23, C25, C33, C35	27.19 p.p.m.
C14, C24, C34	26.76 p.p.m.

The compound crystallizes as long needles. A suitable specimen of approximate dimensions 0.4 × 0.35 × 0.6 mm was mounted on a CADA diffractometer and its orthorhombic cell determined from 25 accurately centred reflections in the θ range 10–12°. The radiation used was monochromatized Mo Kα. Intensity data were collected from two octants of reciprocal space, $1° \leq \theta \leq 26°$ covering the index range $0 \leq h \leq 7$, $0 \leq k \leq 17$

Table 3
General temperature factor expressions

Name	$U(1,1)$	$U(2,2)$	$U(3,3)$	$U(1,2)$	$U(1,3)$	$U(2,3)$
Cl	0.0293(7)	0.0405(7)	0.0428(8)	−0.0023(6)	−0.0021(7)	−0.0028(6)
C11	0.0357(8)	0.0386(7)	0.0450(8)	0.0002(7)	0.0003(7)	−0.0013(7)
C12	0.064(1)	0.0509(9)	0.0490(9)	0.0085(9)	0.0007(9)	−0.0064(8)
C13	0.077(1)	0.058(1)	0.060(1)	0.012(1)	0.017(1)	−0.0078(9)
C14	0.075(1)	0.050(1)	0.089(1)	0.015(1)	0.020(1)	−0.009(1)
C15	0.071(1)	0.0517(9)	0.081(1)	0.023(1)	0.010(1)	0.011(1)
C16	0.058(1)	0.0505(9)	0.057(1)	0.0112(8)	0.0106(9)	0.0071(8)
C21	0.0275(7)	0.0456(8)	0.0434(8)	−0.0007(7)	0.0013(6)	0.0006(7)
C22	0.0250(7)	0.067(1)	0.0534(9)	−0.0013(8)	0.0009(7)	−0.0039(8)
C23	0.0329(8)	0.068(1)	0.057(1)	−0.0027(8)	0.0110(8)	−0.0039(9)
C24	0.0471(9)	0.073(1)	0.0463(9)	−0.0008(9)	0.0070(8)	−0.0084(9)
C25	0.0380(8)	0.073(1)	0.0443(9)	−0.0036(9)	−0.0027(8)	−0.0018(8)
C26	0.0263(6)	0.0616(9)	0.0441(8)	−0.0020(7)	0.0003(7)	−0.0022(7)
C31	0.0324(7)	0.0442(8)	0.0440(7)	0.0035(7)	−0.0010(7)	0.0000(7)
C32	0.0378(8)	0.0455(8)	0.064(1)	−0.0017(8)	0.0017(8)	0.0059(8)
C33	0.058(1)	0.0462(9)	0.085(1)	−0.0010(9)	0.005(1)	0.008(1)
C34	0.085(1)	0.053(1)	0.062(1)	0.016(1)	0.006(1)	0.0128(9)
C35	0.062(1)	0.066(1)	0.059(1)	0.018(1)	−0.0159(9)	0.0033(9)
C36	0.0446(9)	0.062(1)	0.061(1)	0.0032(9)	−0.0136(8)	0.0051(9)

The form of the anisotropic thermal parameter is: $\exp\{-2PI2[h2a2U(1,1) + k2b2U(2,2) + l2c2U(3,3) + 2hkabU(1,2) + 2hlacU(1,3) + 2klbcU(2,3)]\}$ where a, b, and c are reciprocal lattice constants.

Table 4
Bond distances (Å)

Atom 1	Atom 2	Distance	Atom 1	Atom 2	Distance	Atom 1	Atom 2	Distance
Cl	C11	1.553(2)	C16	H16A	0.996(2)	C31	C32	1.534(2)
Cl	C21	1.546(2)	C16	H16B	1.002(2)	C31	C36	1.530(3)
Cl	C31	1.560(2)	C21	C22	1.537(2)	C31	H31	0.998(2)
Cl	H1	0.997(2)	C21	C26	1.526(2)	C32	C33	1.529(3)
C11	C12	1.536(2)	C21	H21	1.007(2)	C32	H32A	1.002(2)
C11	C16	1.527(2)	C22	C23	1.518(3)	C32	H32B	1.000(2)
C11	H11	1.000(2)	C22	H22A	0.994(2)	C33	C34	1.517(3)
C12	C13	1.526(3)	C22	H22B	1.001(2)	C33	H33A	1.008(2)
C12	H12A	0.986(2)	C23	C24	1.519(3)	C33	H33B	0.989(2)
C12	H12B	0.997(2)	C23	H23A	1.004(2)	C34	C35	1.513(3)
C13	C14	1.513(3)	C23	H23B	1.004(2)	C34	H34A	0.995(2)
C13	H13A	0.989(2)	C24	C25	1.518(3)	C34	H34B	0.987(2)
C13	H13B	1.012(2)	C24	H24A	0.993(2)	C35	C36	1.518(3)
C14	C15	1.508(4)	C24	H24B	1.004(2)	C35	H35A	0.998(2)
C14	H14A	0.996(2)	C25	C26	1.524(2)	C35	H35B	0.999(2)
C14	H14B	1.008(3)	C25	H25A	0.995(2)	C36	H36A	0.993(2)
C15	C16	1.533(3)	C25	H25B	1.006(2)	C36	H36B	1.001(2)
C15	H15A	1.008(2)	C26	H26A	1.007(2)			
C15	H15B	1.000(2)	C26	H26B	1.007(2)			

Numbers in parentheses are estimated standard deviations in the least significant digits.

Table 5
Bond angles (deg)

Atom 1	Atom 2	Atom 3	Angle	Atom 1	Atom 2	Atom 3	Angle	Atom 1	Atom 2	Atom 3	Angle
C11	C1	C21	113.3(1)	C11	C16	H16B	109.2(2)	C25	C26	H26B	109.2(2)
C11	C1	C31	115.2(1)	C15	C16	H16A	109.7(2)	H26A	C26	H26B	107.6(2)
C11	C1	H1	104.9(1)	C15	C16	H16B	109.6(2)	C1	C31	C32	117.0(1)
C21	C1	C31	110.8(1)	H16A	C16	H16B	106.3(2)	C1	C31	C36	113.0(1)
C21	C1	H1	105.7(1)	C1	C21	C22	113.0(1)	C1	C31	H31	105.3(1)
C31	C1	H1	106.0(1)	C1	C21	C26	114.2(1)	C32	C31	C36	110.4(2)
C1	C11	C12	110.8(1)	C1	C21	H21	106.5(1)	C32	C31	H31	105.4(2)
C1	C11	C16	114.5(1)	C22	C21	C26	110.2(1)	C36	C31	H31	104.4(2)
C1	C11	H11	107.6(1)	C22	C21	H21	106.3(1)	C31	C32	C33	110.5(2)
C12	C11	C16	108.3(1)	C26	C21	H21	106.0(1)	C31	C32	H32A	109.7(2)
C12	C11	H11	107.8(2)	C21	C22	C23	111.6(1)	C31	C32	H32B	109.3(2)
C16	C11	H11	107.7(2)	C21	C22	H22A	110.2(2)	C33	C32	H32A	109.0(2)
C11	C12	C13	112.2(2)	C21	C22	H22B	109.4(2)	C33	C32	H32B	109.3(2)
C11	C12	H12A	109.9(2)	C23	C22	H22A	109.4(2)	H32A	C32	H32B	109.1(2)
C11	C12	H12B	109.3(2)	C23	C22	H22B	108.7(2)	C32	C33	C34	111.9(2)
C13	C12	H12A	109.0(2)	H22A	C22	H22B	107.4(2)	C32	C33	H33A	109.0(2)
C13	C12	H12B	109.1(2)	C22	C23	C24	111.5(2)	C32	C33	H33B	110.3(2)
H12A	C12	H12B	107.2(2)	C22	C23	H23A	109.8(2)	C34	C33	H33A	109.0(2)
C12	C13	C14	111.5(2)	C22	C23	H23B	109.6(2)	C34	C33	H33B	109.3(2)
C12	C13	H13A	109.3(2)	C24	C23	H23A	109.1(2)	H33A	C33	H33B	107.1(2)
C12	C13	H13B	108.7(2)	C24	C23	H23B	109.1(2)	C33	C34	C35	111.8(2)
C14	C13	H13A	110.8(2)	H23A	C23	H23B	107.6(2)	C33	C34	H34A	109.3(2)
C14	C13	H13B	109.5(2)	C23	C24	C25	111.7(2)	C33	C34	H34B	109.3(2)
H13A	C13	H13B	107.0(2)	C23	C24	H24A	110.4(2)	C35	C34	H34A	109.1(2)
C13	C14	C15	110.6(2)	C23	C24	H24B	109.3(2)	C35	C34	H34B	109.5(2)
C13	C14	H14A	109.2(2)	C25	C24	H24A	109.6(2)	H34A	C34	H34B	107.8(2)
C13	C14	H14B	108.9(2)	C25	C24	H24B	109.0(2)	C34	C35	C36	111.3(2)
C15	C14	H14A	110.1(2)	H24A	C24	H24B	106.6(2)	C34	C35	H35A	108.8(2)
C15	C14	H14B	109.4(2)	C24	C25	C26	111.2(2)	C34	C35	H35B	109.5(2)
C14	C13	H13A	110.8(2)	H23A	C23	H23B	107.6(2)	C33	C34	H34A	109.3(2)
C14	C13	H13B	109.5(2)	C23	C24	C25	111.7(2)	C33	C34	H34B	109.3(2)
H13A	C13	H13B	107.0(2)	C23	C24	H24A	110.4(2)	C35	C34	H34A	109.1(2)
C13	C14	C15	110.6(2)	C23	C24	H24B	109.3(2)	C35	C34	H34B	109.5(2)
C13	C14	H14A	109.2(2)	C25	C24	H24A	109.6(2)	H34A	C34	H34B	107.8(2)
C13	C14	H14B	108.9(2)	C25	C24	H24B	109.0(2)	C34	C35	C36	111.3(2)
C15	C14	H14A	110.1(2)	H24A	C24	H24B	106.6(2)	C34	C35	H35A	108.8(2)
C15	C14	H14B	109.4(2)	C24	C25	C26	111.2(2)	C34	C35	H35B	109.5(2)
H14A	C14	H14B	108.6(2)	C24	C25	H25A	109.2(2)	C36	C35	H35A	109.6(2)
C14	C15	C16	112.4(2)	C24	C25	H25B	108.9(2)	C36	C35	H35B	109.5(2)
C14	C15	H15A	109.5(2)	C26	C25	H25A	110.0(2)	H35A	C35	H35B	108.0(2)
C14	C15	H15B	110.2(2)	C26	C25	H25B	110.0(2)	C31	C36	C35	111.9(2)
C16	C15	H15A	109.0(2)	H25A	C25	H25B	107.6(2)	C31	C36	H36A	109.8(2)
C16	C15	H15B	109.7(2)	C21	C26	C25	111.0(1)	C31	C36	H36B	109.3(2)
H15A	C15	H15B	105.9(2)	C21	C26	H26A	109.6(1)	C35	C36	H36A	109.4(2)
C11	C16	C15	112.2(2)	C21	C26	H26B	109.9(2)	C35	C36	H36B	109.1(2)
C11	C16	H16A	109.7(2)	C25	C26	H26A	109.6(2)	H36A	C36	H36B	107.2(2)

Numbers in parentheses are estimated standard deviations in the least significant digits.

Table 6
Torsional angles (deg)

Atom 1	Atom 2	Atom 3	Atom 4	Angle	Atom 1	Atom 2	Atom 3	Atom 4	Angle
C21	C1	C11	C12	−162.4	C22	C21	C26	H26B	−177.4
C21	C1	C11	C16	−39.7	H21	C21	C26	C25	58.1
C21	C1	C11	H11	80.0	H21	C21	C26	H26A	179.2
C31	C1	C11	C12	68.5	H21	C21	C26	H26B	−62.8
C31	C1	C11	C16	−168.7	C21	C22	C23	C24	−54.5
C31	C1	C11	H11	−49.1	C21	C22	C23	H23A	−175.6
H1	C1	C11	C12	−47.6	C21	C22	C23	H23B	66.4
H1	C1	C11	C16	75.1	H22A	C22	C23	C24	−176.7
H1	C1	C11	H11	−165.2	H22A	C22	C23	H23A	62.3
C11	C1	C21	C22	165.4	H22A	C22	C23	H23B	−55.8
C11	C1	C21	C26	−67.6	H22B	C22	C23	C24	66.3
C11	C1	C21	H21	49.1	H22B	C22	C23	H23A	−54.8
C31	C1	C21	C22	−63.4	H22B	C22	C23	H23B	−172.8
C31	C1	C21	C26	63.7	C22	C23	C24	C25	54.2
C31	C1	C21	H21	−179.6	C22	C23	C24	H24A	176.5
H1	C1	C21	C22	51.0	C22	C23	C24	H24B	−66.5
H1	C1	C21	C26	178.0	H23A	C23	C24	C25	175.7
H1	C1	C21	H21	−65.3	H23A	C23	C24	H24A	−62.0
C11	C1	C31	C32	24.8	H23A	C23	C24	H24B	55.0
C11	C1	C31	C36	−105.2	H23B	C23	C24	C25	−67.0
C11	C1	C31	H31	141.5	H23B	C23	C24	H24A	55.3
C21	C1	C31	C32	−105.5	H23B	C23	C24	H24B	172.3
C21	C1	C31	C36	124.5	C23	C24	C25	C26	−55.3
C21	C1	C31	H31	11.2	C23	C24	C25	H25A	66.2
H1	C1	C31	C32	140.3	C23	C24	C25	H25B	−176.6
H1	C1	C31	C36	10.3	H24A	C24	C25	C26	−178.0
H1	C1	C31	H31	−103.0	H24A	C24	C25	H25A	−56.5
C1	C11	C12	C13	−177.5	H24A	C24	C25	H25B	60.7
C1	C11	C12	H12A	61.1	H24B	C24	C25	C26	65.6
C1	C11	C12	H12B	−56.3	H24B	C24	C25	H25A	−172.9
C16	C11	C12	C13	56.2	H24B	C24	C25	H25B	−55.7
C16	C11	C12	H12A	−65.2	C24	C25	C26	C21	56.7
C16	C11	C12	H12B	177.4	C24	C25	C26	H26A	−64.4
H11	C11	C12	C13	−60.1	C24	C25	C26	H25B	178.0
H11	C11	C12	H12A	178.5	H25A	C25	C26	C21	−64.3
H11	C11	C12	H12B	61.1	H25A	C25	C26	H26A	174.6
C1	C11	C16	C15	−179.1	H25A	C25	C26	H26B	56.9
C1	C11	C16	H16A	−56.9	H25B	C25	C26	C21	177.3
C1	C11	C16	H16B	59.2	H25B	C25	C26	H26A	56.2
C12	C11	C16	C15	−55.0	H25B	C25	C26	H26B	−61.4
C12	C11	C16	H16A	67.2	C1	C31	C32	C33	173.3
C12	C11	C16	H16B	−176.7	C1	C31	C32	H32A	−66.6
H11	C11	C16	C15	61.3	C1	C31	C32	H32B	53.0
H11	C11	C16	H16A	−176.5	C36	C31	C32	C33	−55.5
H11	C11	C16	H16B	−60.4	C36	C31	C32	H32A	64.6
C11	C12	C13	C14	−57.3	C36	C31	C32	H32B	−175.8
C11	C12	C13	H13A	179.9	H31	C31	C32	C33	56.6
C11	C12	C13	H13B	63.4	H31	C31	C32	H32A	176.8
H12A	C12	C13	C14	64.6	H31	C31	C32	H32B	−63.7
H12A	C12	C13	H13A	−58.2	C1	C31	C36	C35	−170.7

Table 6 (continued)

Atom 1	Atom 2	Atom 3	Atom 4	Angle	Atom 1	Atom 2	Atom 3	Atom 4	Angle
H12A	C12	C13	H13B	−174.6	C1	C31	C36	H36A	−49.0
H12B	C12	C13	C14	−178.6	C1	C31	C36	H36B	68.3
H12B	C12	C13	H13A	58.6	C32	C31	C36	C35	56.1
H12B	C12	C13	H13B	−57.8	C32	C31	C36	H36A	177.7
C12	C13	C14	C15	54.8	C32	C31	C36	H36B	−64.9
C12	C13	C14	H14A	−66.6	H31	C31	C36	C35	−56.8
C12	C13	C14	H14B	175.0	H31	C31	C36	H36A	64.9
H13A	C13	C14	C15	176.7	H31	C31	C36	H36B	−177.7
H13A	C13	C14	H14A	55.4	C31	C32	C33	C34	55.4
H13A	C13	C14	H14B	−63.0	C31	C32	C33	H33A	−65.3
H13B	C13	C14	C15	−65.5	C31	C32	C33	H33B	177.3
H13B	C13	C14	H14A	173.2	H32A	C32	C33	C34	−65.2
H13B	C13	C14	H14B	54.8	H32A	C32	C33	H33A	174.1
C13	C14	C15	C16	−54.1	H32A	C32	C33	H33B	56.7
C13	C14	C15	H15A	−175.4	H32B	C32	C33	C34	175.7
C13	C14	C15	H15B	68.5	H32B	C32	C33	H33A	55.0
H14A	C14	C15	C16	66.7	H32B	C32	C33	H33B	−62.3
H14A	C14	C15	H15A	−54.6	C32	C33	C34	C35	−54.8
H14A	C14	C15	H15B	−170.7	C32	C33	C34	H34A	−175.7
H14B	C14	C15	C16	−174.1	C32	C33	C34	H34B	66.6
H14B	C14	C15	H15A	64.6	H33A	C33	C34	C35	65.9
H14B	C14	C15	H15B	−51.4	H33A	C33	C34	H34A	−55.0
C14	C15	C16	C11	55.8	H33A	C33	C34	H34B	−172.7
C14	C15	C16	H16A	−66.4	H33B	C33	C34	C35	−177.4
C14	C15	C16	H16B	177.2	H33B	C33	C34	H34A	61.8
H15A	C15	C16	C11	177.3	H33B	C33	C34	H34B	−55.9
H15A	C15	C16	H16A	55.1	C33	C34	C35	C36	54.2
H15A	C15	C16	H16B	−61.2	C33	C34	C35	H35A	175.1
H15B	C15	C16	C11	−67.2	C33	C34	C35	H35B	−67.0
H15B	C15	C16	H16A	170.7	H34A	C34	C35	C36	175.2
H15B	C15	C16	H16B	54.3	H34A	C34	C35	H35A	−64.0
C1	C21	C22	C23	−175.2	H34A	C34	C35	H35B	53.9
C1	C21	C22	H22A	−53.5	H34B	C34	C35	C36	−67.1
C1	C21	C22	H22B	64.4	H34B	C34	C35	H35A	53.8
C26	C21	C22	C23	55.7	H34B	C34	C35	H35B	171.6
C26	C21	C22	H22A	177.4	C34	C35	C36	C31	−55.3
C26	C21	C22	H22B	−64.7	C34	C35	C36	H36A	−177.2
H21	C21	C22	C23	−58.8	C34	C35	C36	H36B	65.8
H21	C21	C22	H22A	62.9	H35A	C35	C36	C31	−175.7
H21	C21	C22	H22B	−179.2	H35A	C35	C36	H36A	62.4
C1	C21	C26	C25	175.0	H35A	C35	C36	H36B	−54.6
C1	C21	C26	H26A	−63.9	H35B	C35	C36	C31	66.0
C1	C21	C26	H26B	54.2	H35B	C35	C36	H36A	−55.9
C22	C21	C26	C25	−56.5	H35B	C35	C36	H36B	−172.9
C22	C21	C26	H26A	64.6					

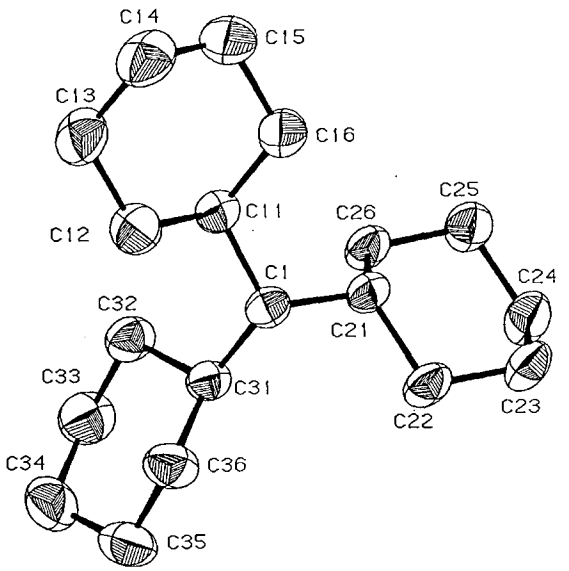

Fig. 3. A perspective view of tricyclohexylmethane.

and $-22 \leq l \leq 22$, with the 004 reflection to be the intensity standard, measured hourly.

After the usual Lp correction, from a total of 3750 reflections 3188 have $I > 3\alpha(I)$ with 421 having zero intensity. Analysis of the intensity of the standard reflection showed negligible decay. Inspection of the three principal zones showed the space group to be uniquely determined as $P2_12_12_1(19)$. The data were averaged, based upon the point group 222, which yielded 2890 unique data, 653 observed averaged data with agreement factors for the intensity of all reflections of 0.021. The relevant crystal data are given in Table 1.

Structure solution and refinement

Routine application of the Direct Methods program MULTAN produced 18 atoms of the molecule, and subsequent structure factor/Fourier calculation revealed the remaining carbon atom. Isotropic full-matrix refinement, with hydrogen atoms in fixed calculated position, $d = 1.0$ Å, converged at $R = 0.094$.

Anisotropic refinement of non-hydrogen atoms converged smoothly to $R = 0.049$, $wR = 0.064$

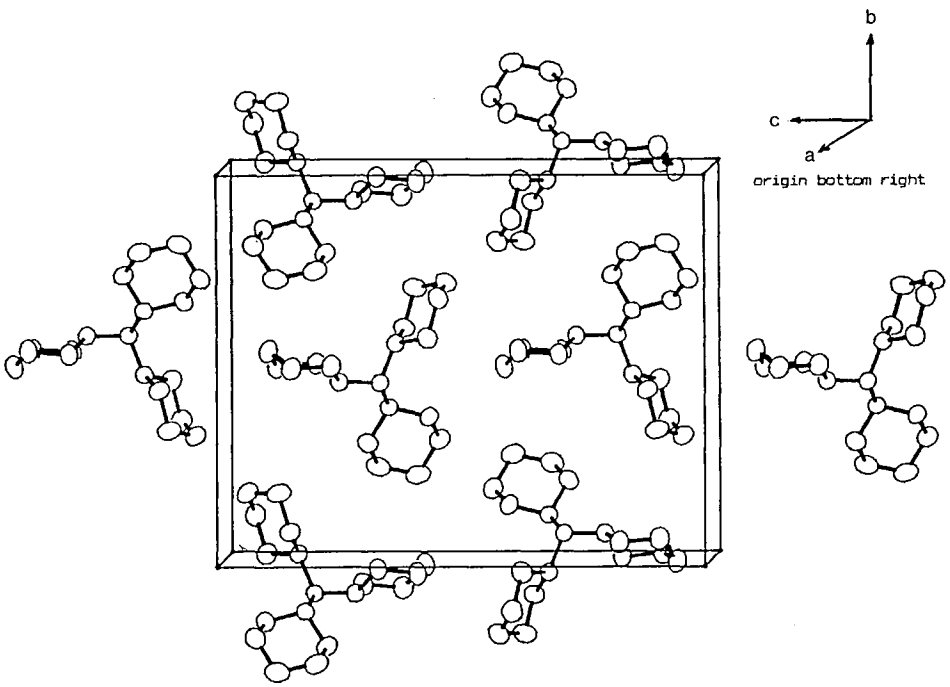

Fig. 4. The packing of tricyclohexylmethane in the unit cell.

and $S = 1.049$ using a weighting scheme:

$$w^{-1} = [\sigma(F^2) + (0.042)^2 + 4.2]$$

The highest residual peak in a difference Fourier map was 0.3 electrons.

A refinement based upon the enantiomorphic coordinates produced the same R, wR and S values, so that the chirality of the crystal could not be established.

Description of the structure

Tables 2 and 3 give the positional coordinates and thermal vibration parameters, and in Tables 4–6 are listed selected bond distances and angles. Figure 3 is an ORTEP diagram of the molecule. All bond and angle geometries are within normal limits for a hydrocarbon but it is worthy of note that the atomic volume per carbon atom is 22.2 Å^3 which is substantially greater than would be expected for a hydrocarbon. Thus the molecules pack quite loosely in the unit cell as may be seen from the packing diagram shown in Fig. 4, and as a result, all intermolecular contacts exceed 3.92 Å except for C13–C24 $(1/2 - x, \bar{y}, 1/2 + z)$ where the distance is 3.76 Å.

The angles around C1 show only a small increase from the tetrahedral value due to a slight strain caused by the bulky cyclohexane groups. It is interesting to note that these rings arrange themselves irregularly: the angles between their mean planes are:

(C11–C16)–(C21–C26) = 119°
(C11–C16)–(C31–C36) = 83°
(C21–C26)–(C31–C36) = 107°

From our data it can be seen that the crystal is chiral but, of course, the individual molecules are not chiral.

Acknowledgements

One of us (S.L.) wishes to thank S.E.R.C. and BP International for a CASE Studentship.

References

1 D.G. Gillies, S.J. Matthews and L.H. Sutcliffe, Magn. Reson. Chem., 29 (1991) 777.
2 D.G. Gillies, S.J. Matthews and L.H. Sutcliffe, Magn. Reson. Chem., 29 (1991) 823.
3 D.G. Gillies, S.J. Matthews and L.H. Sutcliffe, J. Mol. Struct., 54 (1992) 205.
4 K.-H. Hentschel, J. Synth. Lubr., 2 (1985) 143.
5 M. Muraki, Tribol. Int., 20 (1987) 347.
6 S. Luff, submitted for publication.

Appendix 4

X-RAY CRYSTALLOGRAPHIC DATA FOR TRICYCLOHEXYLMETHYLCHLORIDE

The full tables of X-ray crystallographic data for the structure of tricyclohexylmethylchloride are reproduced on the following pages.

Table A4.1: Physical properties and parameters for data collection and refinement

Formula	$C_{19}H_{33}Cl$
Mol. wt. (g)	296.93
Crystal system	Orhorhombic
Space group	Pnma
a (Å)	10.725(3)
b (Å)	15.670(3)
c (Å)	10.168(3)
V (Å^3)	1708.8(1.3)
Z	4
ρ (g cm^{-3}) calc.	1.154
μ (Mo Kα) (cm^{-1})	0.53
λ (Å)	0.71073
F (000)	

Table A4.2: Positional parameters and their estimated standard deviations

Atom	x	y	z	B(A2)	Atom	x	y	z	B(A2)
Cl	0.36354(6)	0.250	0.55636(7)	3.32(1)	H13B	0.6405	0.1687	0.1581	4*
C	0.5358(2)	0.250	0.5321(2)	2.29(4)	H14A	0.4110	0.250	0.0916	4*
C11	0.5571(2)	0.250	0.3801(2)	2.48(4)	H14B	0.5277	0.250	0.0044	4*
C12	0.5094(2)	0.1704(1)	0.3082(2)	3.36(4)	H21	0.5206	0.1250	0.5472	4*
C13	0.5474(2)	0.1706(1)	0.1641(2)	4.05(4)	H22A	0.7735	0.1774	0.6122	4*
C14	0.5007(4)	0.250	0.0945(3)	4.56(7)	H22B	0.7310	0.1468	0.4654	4*
C21	0.5799(2)	0.1641(1)	0.5935(2)	2.41(3)	H23A	0.8293	0.0329	0.5820	4*
C22	0.7157(2)	0.1395(1)	0.5619(2)	3.35(4)	H23B	0.6852	0.0090	0.5455	4*
C23	0.7399(2)	0.0467(1)	0.6000(2)	4.05(4)	H24A	0.7741	0.0622	0.7992	4*
C24	0.7130(2)	0.0299(1)	0.7442(2)	3.89(4)	H24B	0.7215	-0.0325	0.7621	4*
C25	0.5822(2)	0.0582(1)	0.7791(2)	3.65(4)	H25A	0.5697	0.0514	0.8760	4*
C26	0.5600(2)	0.1514(1)	0.7416(2)	3.05(3)	H25B	0.5211	0.0214	0.7310	4*
H11	0.6495	0.250	0.3676	4*	H26A	0.6195	0.1884	0.7911	4*
H12A	0.4163	0.1688	0.3139	4*	H26B	0.4724	0.1675	0.7648	4*
H12B	0.5448	0.1185	0.3515	4*	C15	0.5474	0.3293	0.1640	4*
H13A	0.5116	0.1191	0.1201	4*	C16	0.5094	0.3295	0.3082	4*

Starred atoms were refined isotropically.
Anisotropically refined atoms are given in the form of the isotropic equivalent thermal parameter defined as:
$(4/3)[a^2B(1,1) + b^2B(2,2) + c^2B(3,3) + ab(\cos(\gamma))B(1,2) + ac(\cos(\beta))B(1,3) + bc(\cos(\alpha))B(2,3)]$

Table A4.3: General temperature factor expressions

Name	U(1,1)	U(2,2)	U(3,3)	U(1,2)	U(1,3)	U(2,3)
Cl	0.0279(3)	0.0478(3)	0.0503(3)	0	0.0006(3)	0
C	0.025(1)	0.031(1)	0.031(1)	0	0.0010(9)	0
C11	0.038(1)	0.027(1)	0.029(1)	0	-0.003(1)	0
C12	0.061(1)	0.0318(8)	0.0351(8)	-0.0068(8)	-0.0073(9)	-0.0036(7)
C13	0.080(1)	0.040(1)	0.0341(9)	-0.000(1)	-0.005(1)	-0.0055(9)
C14	0.090(1)	0.052(2)	0.031(1)	0	-0.014(1)	0
C21	0.0322(7)	0.0279(7)	0.0316(7)	-0.0003(7)	0.0000(7)	0.0006(6)
C22	0.0392(9)	0.046(1)	0.0420(9)	0.0103(8)	0.0051(8)	0.0098(8)
C23	0.057(1)	0.047(1)	0.050(1)	0.0203(8)	0.003(1)	0.0044(9)
C24	0.062(1)	0.0374(9)	0.048(1)	0.0099(9)	-0.006(1)	0.0096(6)
C25	0.062(1)	0.0361(9)	0.041(1)	-0.0011(9)	0.0035(9)	0.0097(8)
C26	0.048(1)	0.0342(8)	0.0340(8)	0.0034	0.0051(8)	0.0044(8)

The form of the anisotropic thermal parameter is:
$\exp\{-2\pi^2[h^2a^2U(1,1)+k^2b^2U(2,2)+l^2c^2U(3,3)+2hkabU(1,2)+2hlacU(1,3)+2klbcU(2,3)]\}$,
where a,b, and c are reciprocal lattice constants.
Numbers in parentheses are estimated standard deviations in the least significant digits.

Table A4.4: Bond distances (Å)

Atom 1	Atom 2	Distance	Atom 1	Atom 2	Distance	Atom 1	Atom 2	Distance
Cl	C	1.864(2)	C24	C25	1.513(3)	C22	H22A	1.001(2)
C	C11	1.562(3)	C25	C26	1.528(3)	C22	H22B	1.001(2)
C	C21	1.557(2)	C11	H11	1.000(3)	C23	H23A	1.000(2)
C11	C12	1.533(2)	C12	H12A	1.000(2)	C23	H23B	0.999(2)
C12	C13	1.521(2)	C12	H12B	1.000(2)	C24	H24A	1.000(2)
C13	C14	1.516(3)	C13	H13A	0.999(2)	C24	H24B	1.000(2)
C21	C22	1.541(3)	C13	H13B	1.001(3)	C25	H25A	1.000(2)
C21	C26	1.534(2)	C14	H14A	0.961(4)	C25	H25B	1.000(2)
C22	C23	1.528(3)	C14	H14B	0.961(3)	C26	H26A	1.000(2)
C23	C24	1.517(3)	C21	H21	1.000(2)	C26	H26B	1.000(2)

Numbers in parentheses are estimated standard deviations in the least significant digits.

Table A4.5: Bond angles (deg)

Atom 1	Atom 2	Atom 3	Angle	Atom 1	Atom 2	Atom 3	Angle	Atom 1	Atom 2	Atom 3	Angle
Cl	C	C11	106.0(2)	C11	C12	H12A	108.9(2)	C22	C23	H23A	108.8(2)
Cl	C	C21	104.3(1)	C11	C12	H12B	108.9(2)	C22	C23	H23B	108.8(2)
C11	C	C21	110.6(1)	C13	C12	H12A	108.9(2)	C24	C23	H23A	108.7(2)
C21	C	C21	119.6(2)	C13	C12	H12B	108.9(2)	C24	C23	H23B	108.8(2)
C	C11	C12	115.0(1)	H12A	C12	H12B	109.5(2)	H23A	C23	H23B	109.6(2)
C12	C11	C12	108.8(2)	C12	C13	H13A	109.0(2)	C23	C24	H24A	109.2(2)
C11	C12	C13	111.6(2)	C12	C13	H13B	109.0(2)	C23	C24	H24B	109.1(2)
C12	C13	C14	111.3(2)	C14	C13	H13A	109.1(2)	C25	C24	H24A	109.2(2)
C13	C14	C13	110.2(2)	C14	C13	H13B	109.0(2)	C25	C24	H24B	109.2(2)
C	C21	C22	114.8(2)	H13A	C13	H13B	109.4(2)	H24A	C24	H24B	109.5(2)
C	C21	C26	117.7(2)	C13	C14	H14A	110.2(2)	C24	C25	H25A	108.9(2)
C22	C21	C26	107.7(2)	C13	C14	H14B	110.2(2)	C24	C25	H25B	108.9(2)
C21	C22	C23	110.2(2)	H14A	C14	H14B	105.9(3)	C26	C25	H25A	109.0(2)
C22	C23	C24	112.2(2)	C	C21	H21	98.5(1)	C26	C25	H25B	109.0(2)
C23	C24	C25	110.6(2)	C22	C21	H21	110.4(2)	H25A	C25	H25B	109.5(2)
C24	C25	C26	111.4(2)	C26	C21	H21	107.0(2)	C21	C26	H26A	109.2(2)
C21	C26	C25	110.4(2)	C21	C22	H22A	109.3(2)	C21	C26	H26B	109.2(2)
C11	C	C21	110.6(1)	C21	C22	H22B	109.3(2)	C25	C26	H26A	109.3(2)
C21	C	C21	119.6(2)	C23	C22	H22A	109.3(2)	C25	C26	H26B	109.2(2)
C	C11	H11	105.7(2)	C23	C22	H22B	109.3(2)	H26A	C26	H26B	109.5(2)
C12	C11	H11	105.7(2)	H22A	C22	H22B	109.4(2)				

Numbers in parentheses are the estimated standard deviations in the least significant digits.

Table A4.6: Torsion angles (deg)

Atom 1	Atom 2	Atom 3	Atom 4	Angle	Atom 1	Atom 2	Atom 3	Atom 4	Angle
Cl	C	C11	C12	-63.9	C26	C21	C22	H22B	179.6
Cl	C	C11	H11	180.0	H21	C21	C22	C23	-57.1
Cl	C	C11	C16	63.9	H21	C21	C22	H22A	-177.3
C21	C	C11	C12	48.7	H21	C21	C22	H22B	63.0
C21	C	C11	H11	-67.5	C	C21	C26	C25	167.9
C21	C	C11	C16	176.4	C	C21	C26	H26A	-71.9
Cl	C	C21	C22	168.2	C	C21	C26	H26B	47.8
Cl	C	C21	C26	-63.5	C22	C21	C26	C25	-60.5
Cl	C	C21	H21	50.9	C22	C21	C26	H26A	59.8
C11	C	C21	C22	54.6	C22	C21	C26	H26B	179.4
C11	C	C21	C26	-177.1	H21	C21	C26	C25	58.3
C11	C	C21	H21	-62.7	H21	C21	C26	H26A	178.5
C	C11	C12	C13	-173.2	H21	C21	C26	H26B	-61.8
C	C11	C12	H12A	66.6	C21	C22	C23	C24	-57.4
C	C11	C12	H12B	-52.8	C21	C22	C23	H23A	-177.7
H11	C11	C12	C13	-57.0	C21	C22	C23	H23B	63.0
H11	C11	C12	H12A	-177.3	H22A	C22	C23	C24	62.8
H11	C11	C12	H12B	63.3	H22A	C22	C23	H23A	-57.5
C16	C11	C12	C13	56.1	H22A	C22	C23	H23B	-176.8
C16	C11	C12	H12A	-64.2	H22B	C22	C23	C24	-177.5
C16	C11	C12	H12B	176.4	H22B	C22	C23	H23A	62.2
C	C11	C16	C15	173.2	H22B	C22	C23	H23B	-57.1
C12	C11	C16	C15	-56.1	C22	C23	C24	C25	54.0
H11	C11	C16	C15	57.0	C22	C23	C24	H24A	-66.2

Table A4.6 (continued)

Atom 1	Atom 2	Atom 3	Atom 4	Angle	Atom 1	Atom 2	Atom 3	Atom 4	Angle
C11	C12	C13	C14	-57.3	C22	C23	C24	H24B	174.2
C11	C12	C13	H13A	-177.7	H23A	C24	C25	C25	174.3
C11	C12	C13	H13B	62.9	H23A	C24	C25	H24A	54.2
H12A	C12	C13	C14	63.0	H23A	C24	C25	H24B	-65.5
H12A	C12	C13	H13A	-57.3	H23B	C24	C25	C25	-66.4
H12A	C12	C13	H13B	-176.7	H23B	C24	C25	H24A	173.5
H12B	C12	C13	C14	-177.6	H23B	C24	C25	H24B	53.8
H12B	C12	C13	H13A	62.0	C23	C24	C25	C26	-54.5
H12B	C12	C13	H13B	-57.4	C23	C24	C25	H25A	-174.8
C12	C13	C14	H14A	-65.4	C23	C24	C25	H25B	65.8
C12	C13	C14	H14B	178.1	H24A	C24	C25	C26	65.7
C12	C13	C14	C15	56.3	H24A	C24	C25	H25A	-54.6
H13A	C13	C14	H14A	54.9	H24A	C24	C25	H25B	-174.0
H13A	C13	C14	H14B	-61.5	H24B	C24	C25	C26	-174.7
H13A	C13	C14	C15	176.7	H24B	C24	C25	H25A	65.1
H13B	C13	C14	H14A	174.4	H24B	C24	C25	H25B	-54.4
H13B	C13	C14	H14B	57.9	C24	C25	C26	C21	59.1
H13B	C13	C14	C15	-63.9	C24	C25	C26	H26A	-61.1
C13	C14	C15	C16	-56.3	C24	C25	C26	H26B	179.2
H14A	C14	C15	C16	65.4	H25A	C25	C26	C21	179.3
H14B	C14	C15	C16	-178.1	H25A	C25	C26	H26A	59.1
C	C21	C22	C23	-167.4	H25A	C25	C26	H26B	-60.1
C	C21	C22	H22A	72.4	H25B	C25	C26	C21	-61.2
C	C21	C22	H22B	-47.3	H25B	C25	C26	H26A	178.6
C26	C21	C22	C23	59.4	H25B	C25	C26	H26B	58.9
C26	C21	C22	H22A	-60.8	C14	C15	C16	C11	57.3

Appendix 5

ESR STUDY OF THE TRICYCLOHEXYLMETHYL RADICAL

The results of a study of the tricyclohexylmethyl radical using a combination of ESR spectroscopy and structure determination by computational methods were published in the paper which is reproduced on the following pages.

MATERIAL REDACTED AT REQUEST OF UNIVERSITY

Appendix 6

CARBON-13 DATA PLOTS AND OPTIMIZED THEORETICAL CURVES FOR 9,10-DI-*n*-OCTYL-*n*-OCTADECANE

The carbon-13 R_1 relaxation rate and NOE data for 9,10-di-*n*-octyl-*n*-octadecane are shown in the plots on the following pages, together with the optimized theoretical curves corresponding to the tables of parameters in Section 7.6.

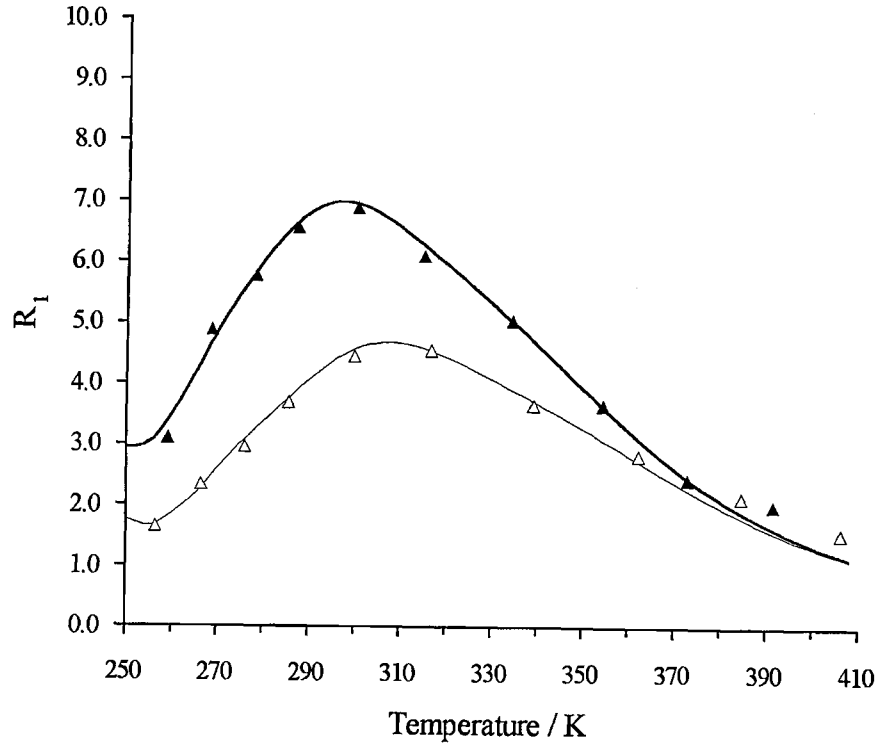

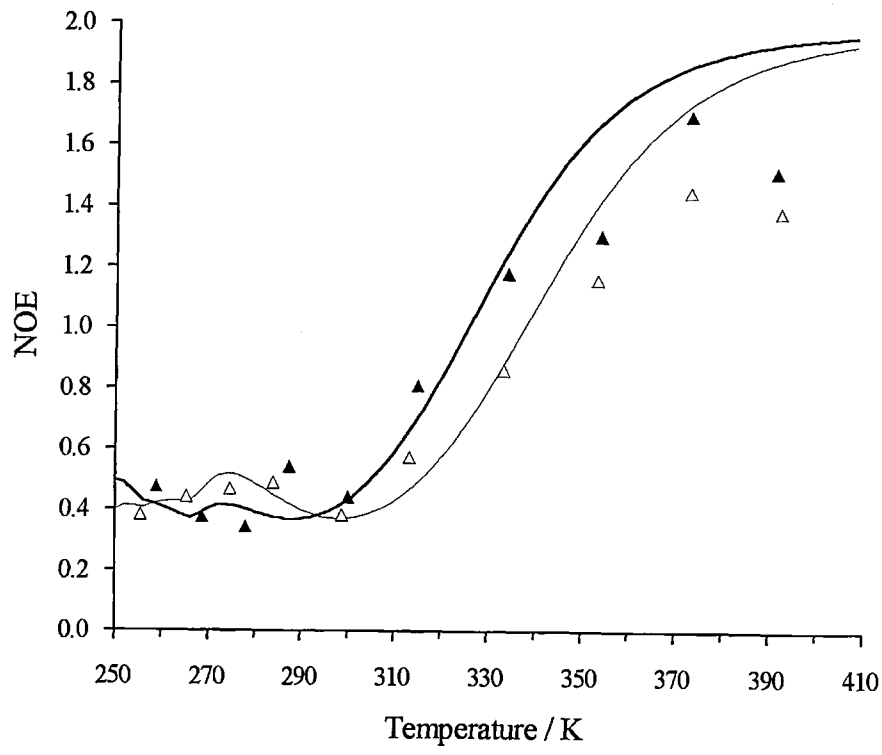

Fig A6.1: 9,10-di-*n*-octyl-*n*-octadecane - position z; carbon-13 data and optimized theoretical curves at 67.83 MHz (—) and 100.53 MHz (–).

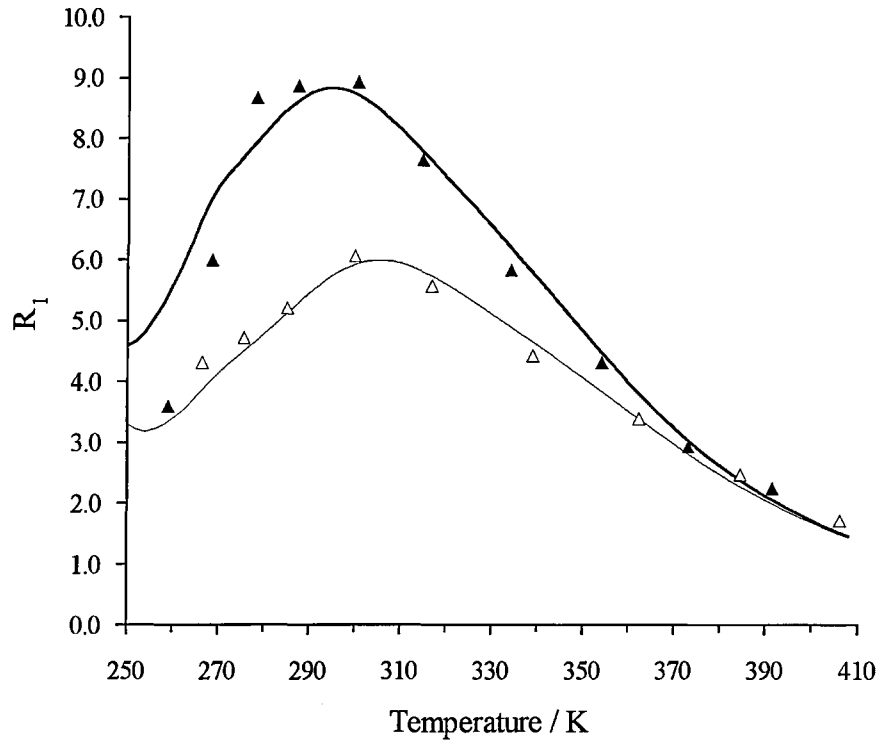

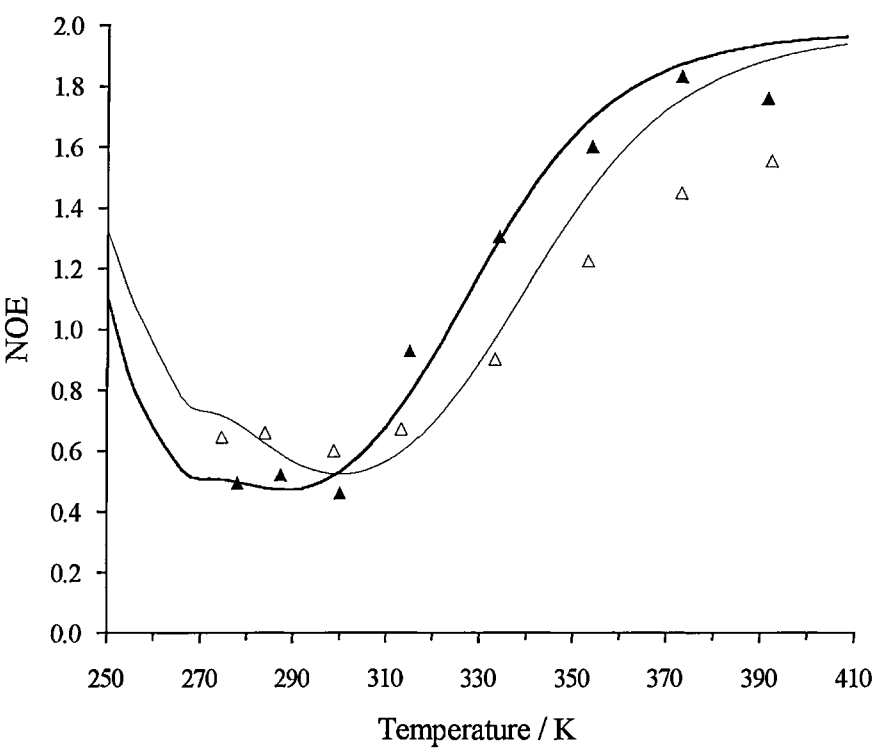

Fig A6.2: 9,10-di-*n*-octyl-*n*-octadecane - position **a**; carbon-13 data and optimized theoretical curves at 67.83 MHz (—) and 100.53 MHz (–).

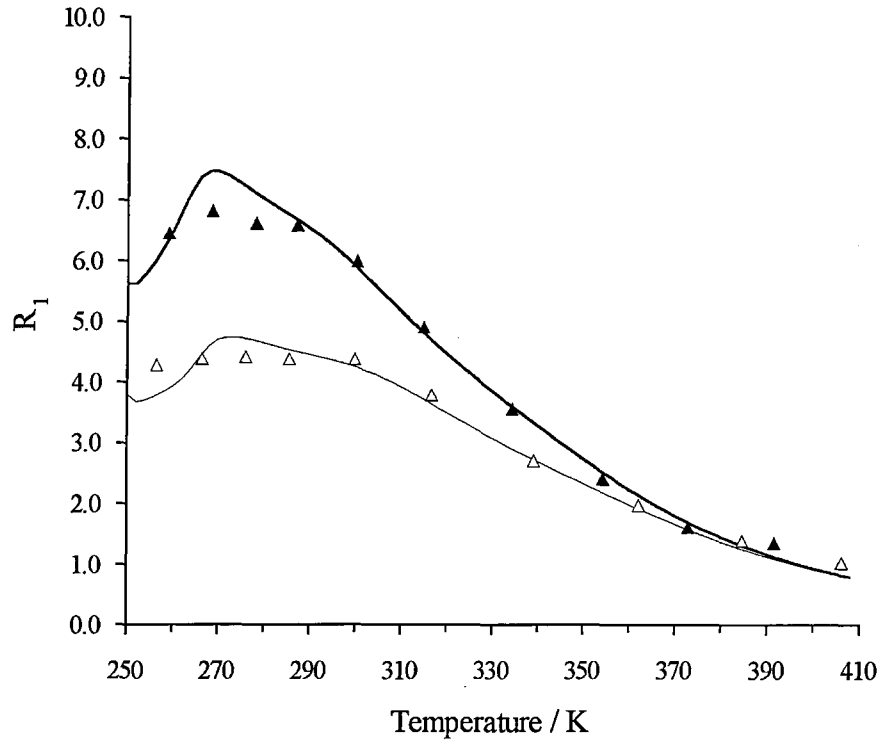

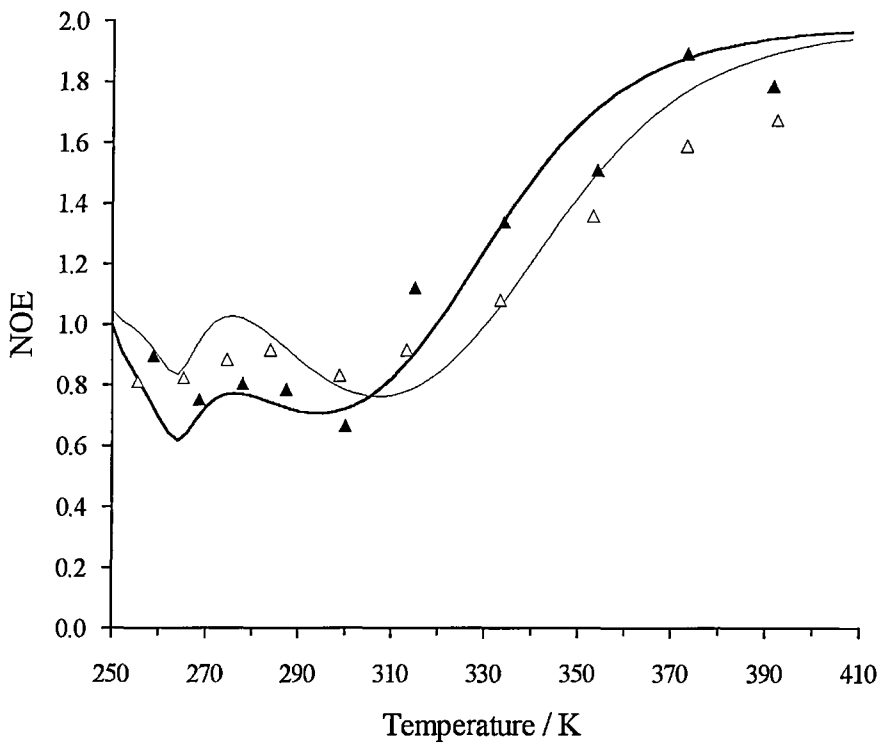

Fig A6.3: 9,10-di-*n*-octyl-*n*-octadecane - position **b**; carbon-13 data and optimized theoretical curves at 67.83 MHz (—) and 100.53 MHz (–).

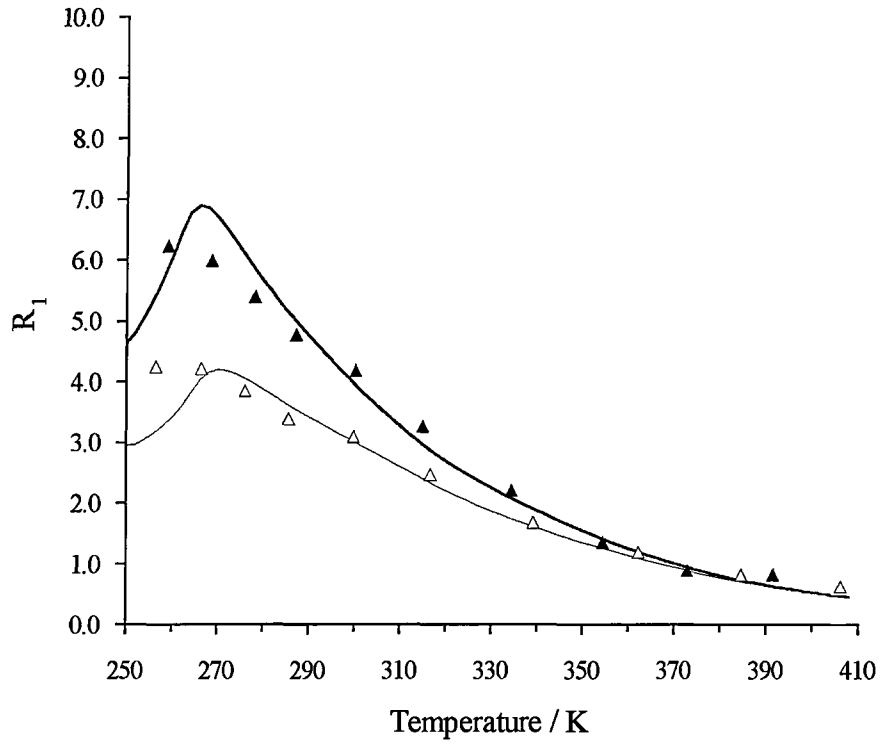

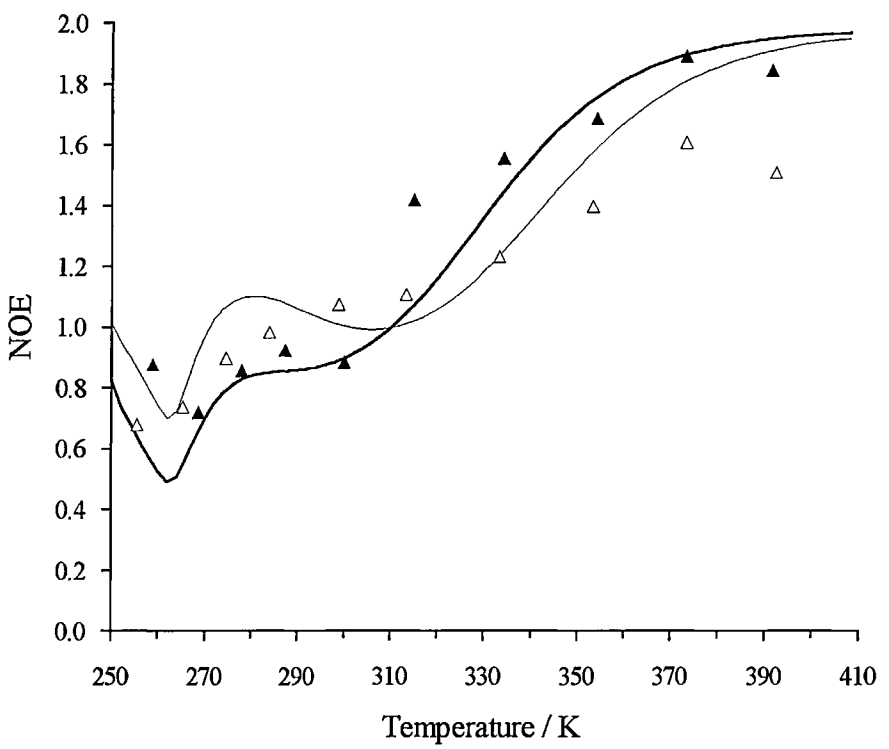

Fig A6.4: 9,10-di-*n*-octyl-*n*-octadecane - position **c**; carbon-13 data and optimized theoretical curves at 67.83 MHz (—) and 100.53 MHz (–).

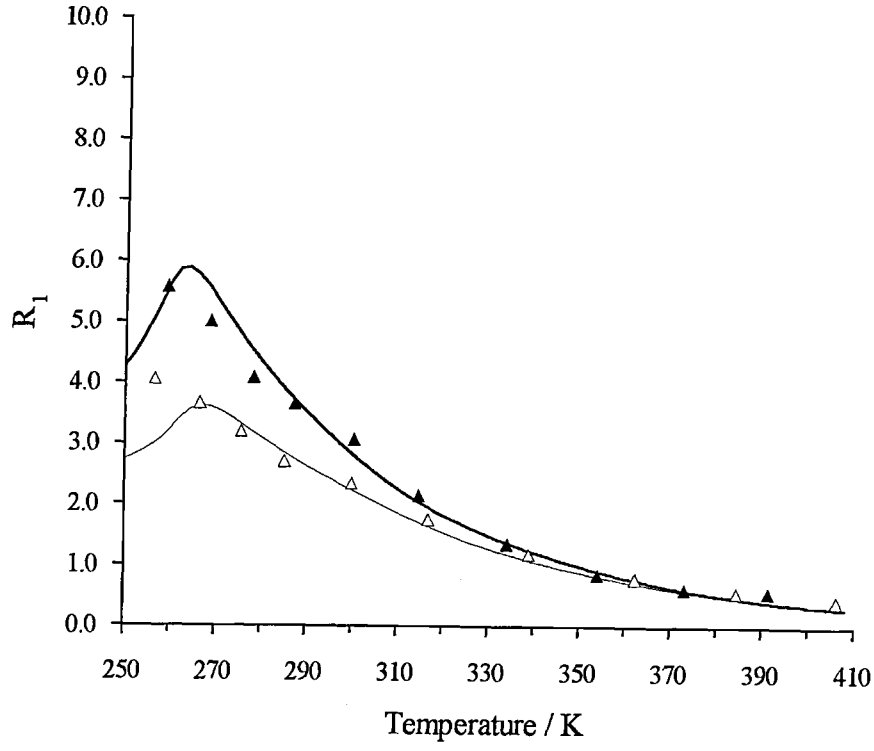

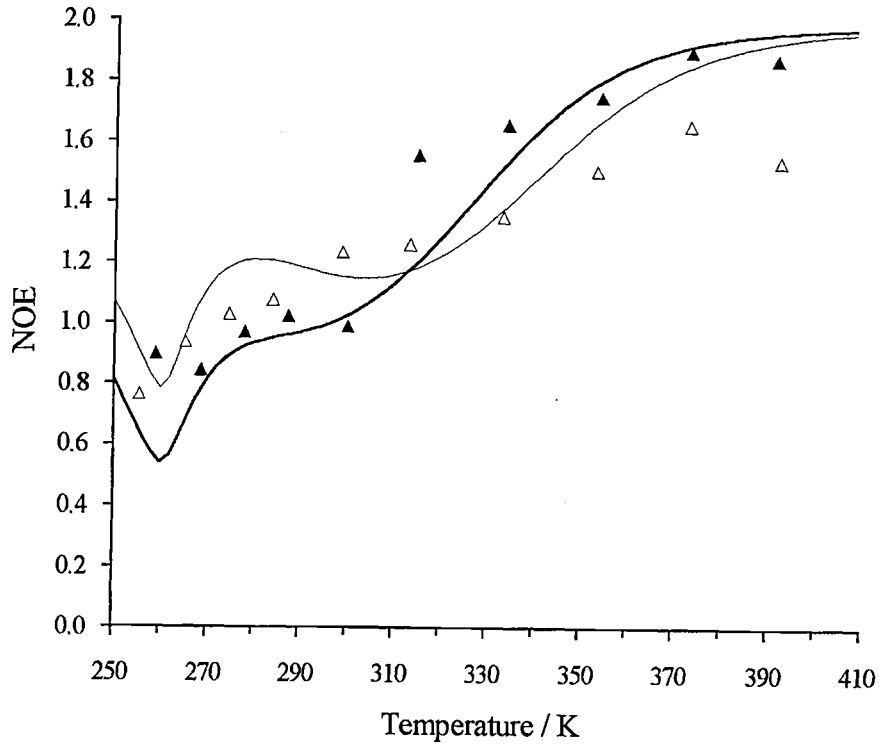

Fig A6.5: 9,10-di-*n*-octyl-*n*-octadecane - position **d**; carbon-13 data and optimized theoretical curves at 67.83 MHz (—) and 100.53 MHz (–).

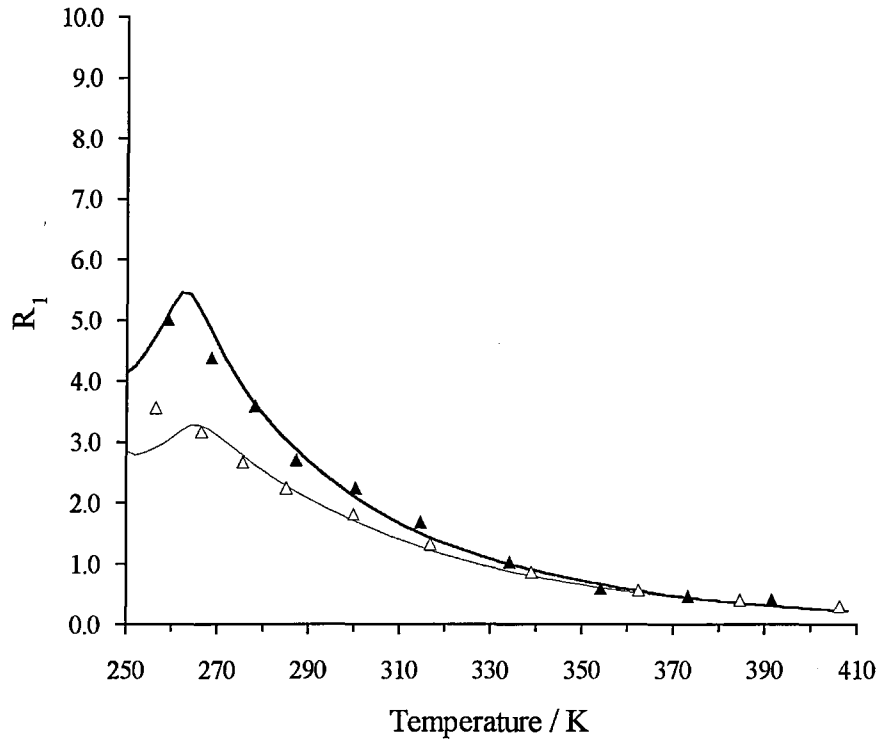

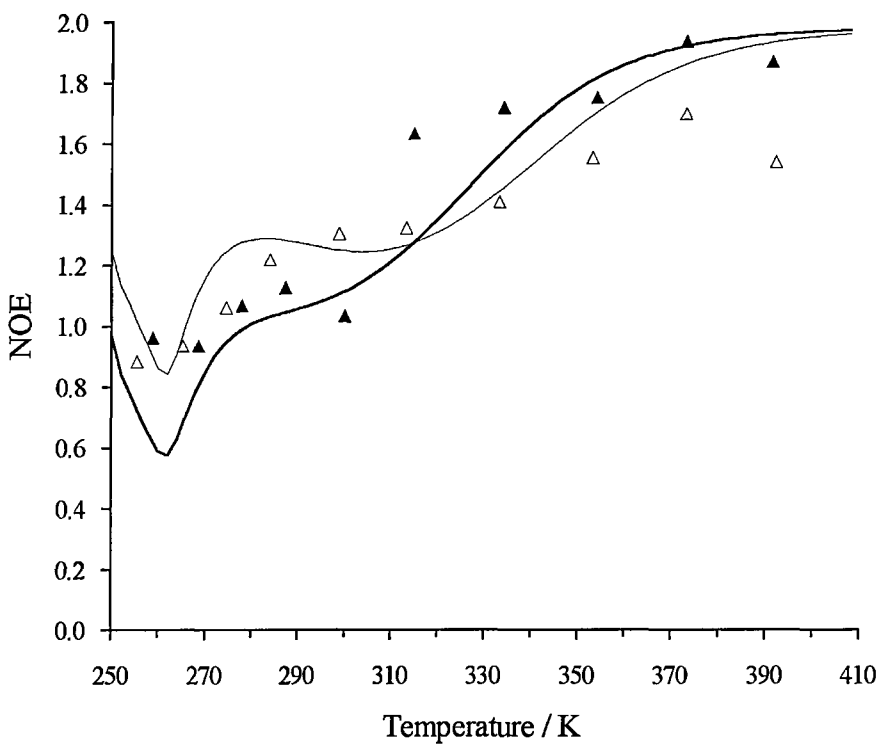

Fig A6.6: 9,10-di-*n*-octyl-*n*-octadecane - position **e**; carbon-13 data and optimized theoretical curves at 67.83 MHz (—) and 100.53 MHz (–).

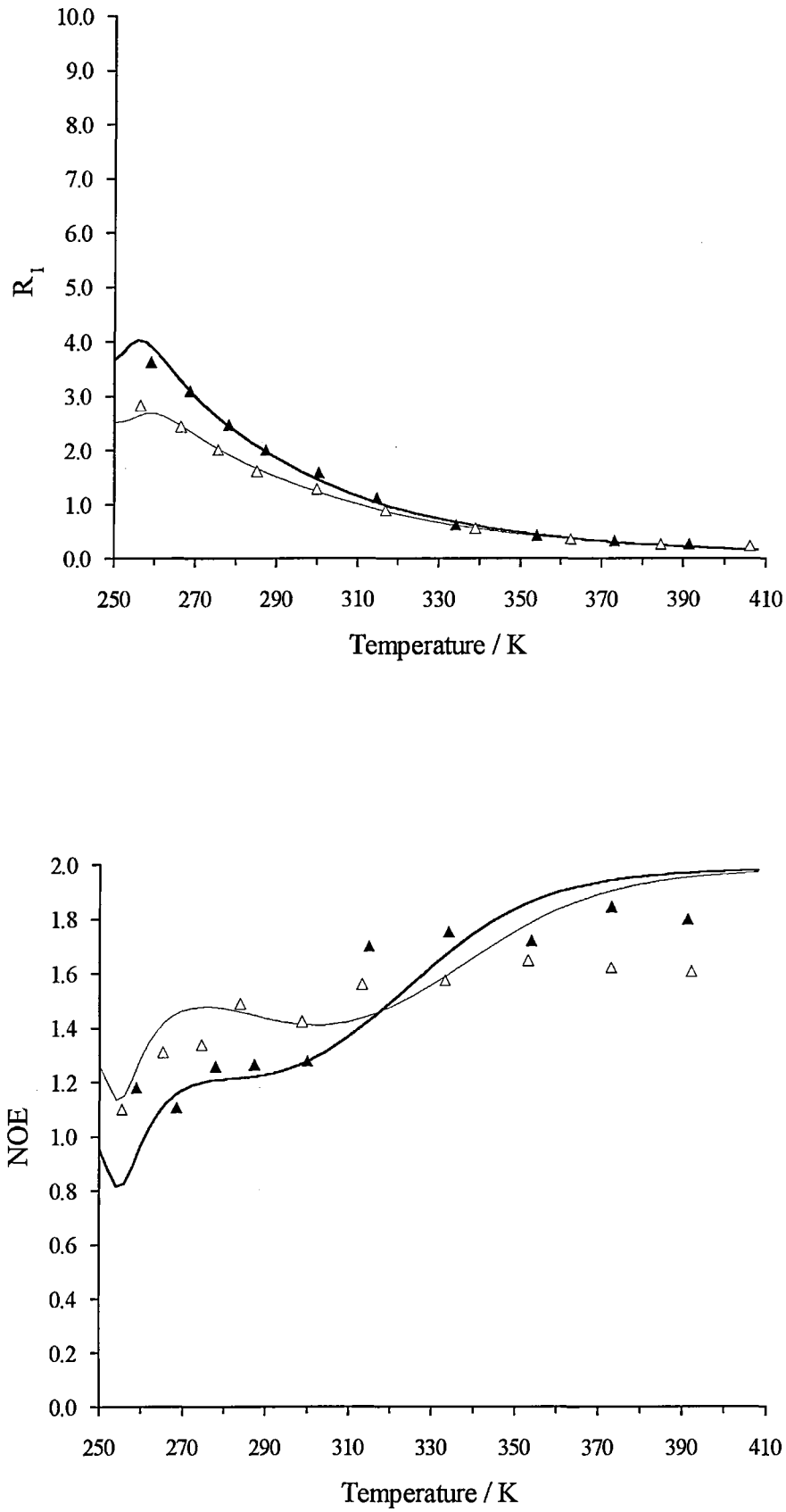

Fig A6.7: 9,10-di-*n*-octyl-*n*-octadecane - position **f**; carbon-13 data and optimized theoretical curves at 67.83 MHz (—) and 100.53 MHz (–).

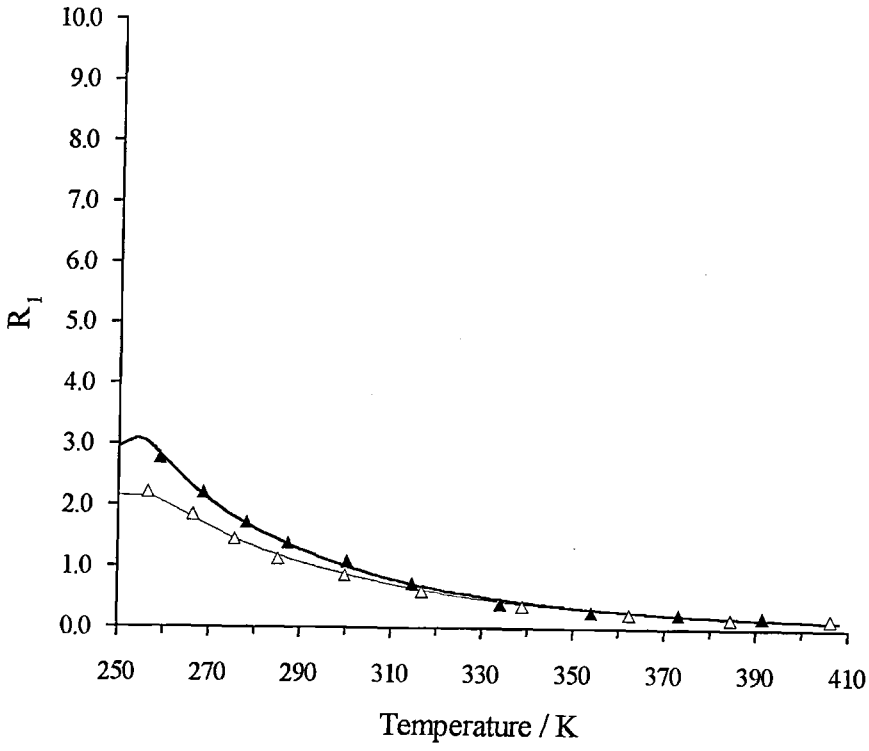

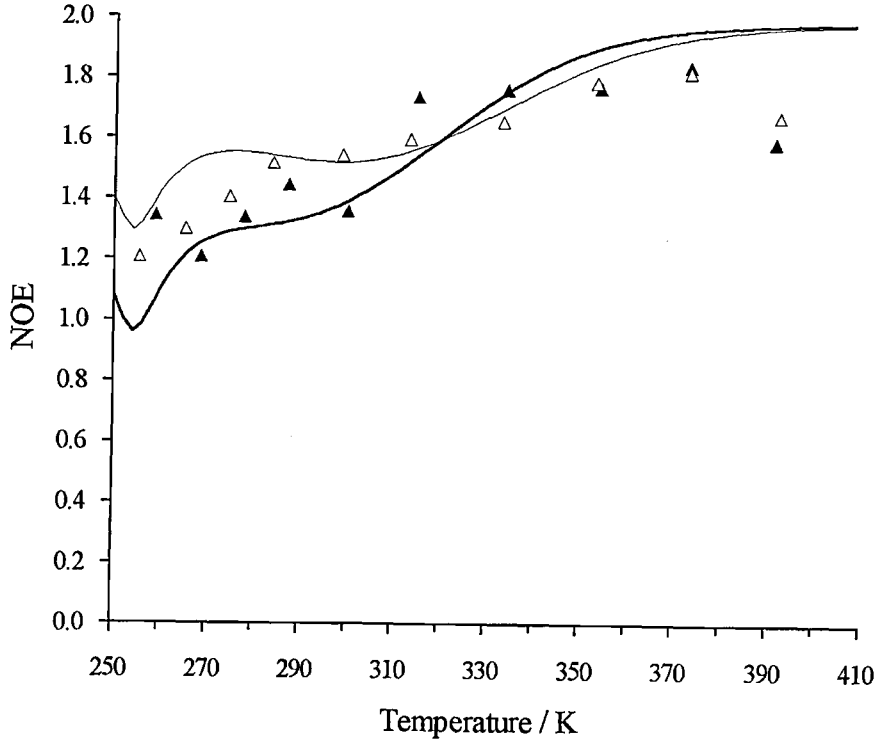

Fig A6.8: 9,10-di-*n*-octyl-*n*-octadecane - position g; carbon-13 data and optimized theoretical curves at 67.83 MHz (—) and 100.53 MHz (–).

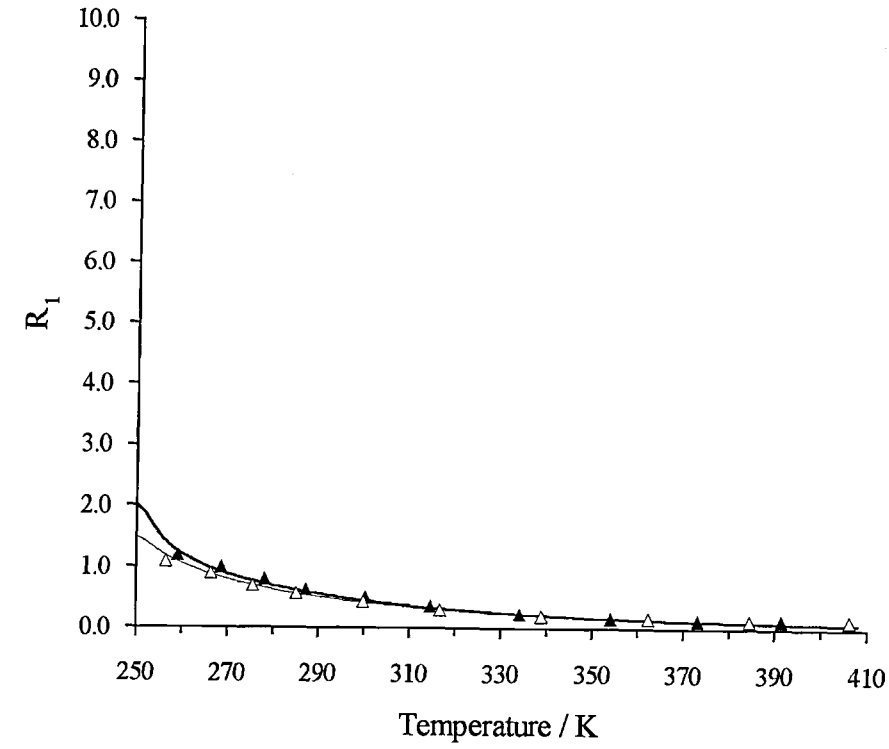

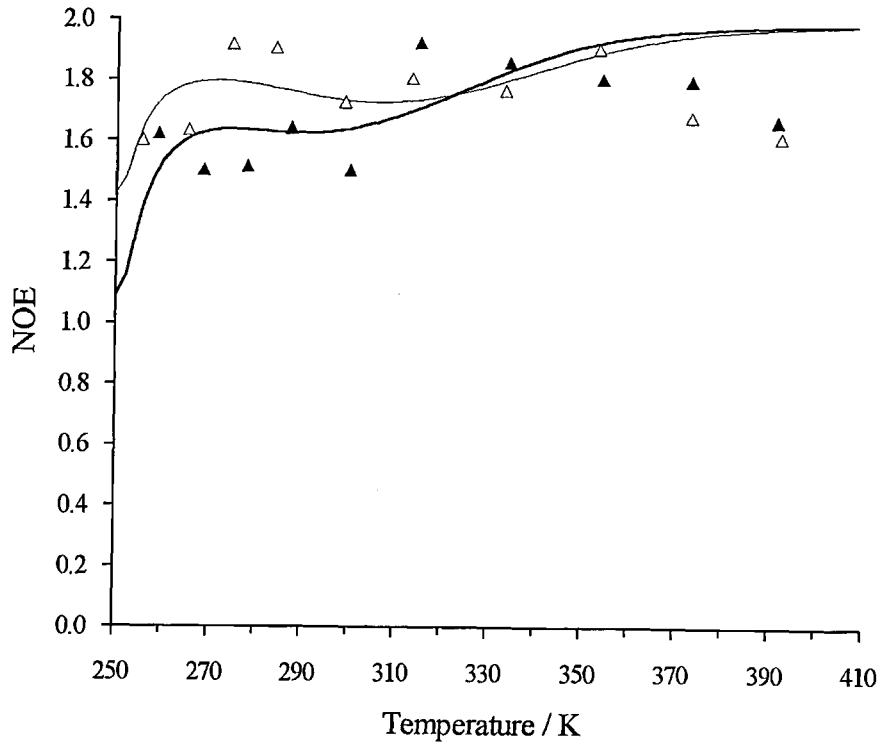

Fig A6.9: 9,10-di-*n*-octyl-*n*-octadecane - position **h**; carbon-13 data and optimized theoretical curves at 67.83 MHz (—) and 100.53 MHz (–).

Appendix 7

CARBON-13 DATA PLOTS AND OPTIMIZED THEORETICAL CURVES FOR 9-*n*-OCTYL-*n*-HEPTADECANE

The carbon-13 R_1 relaxation rate and NOE data for 9-*n*-octyl-*n*-heptadecane are shown in the plots on the following pages, together with the optimized theoretical curves corresponding to the tables of parameters in Section 7.7.

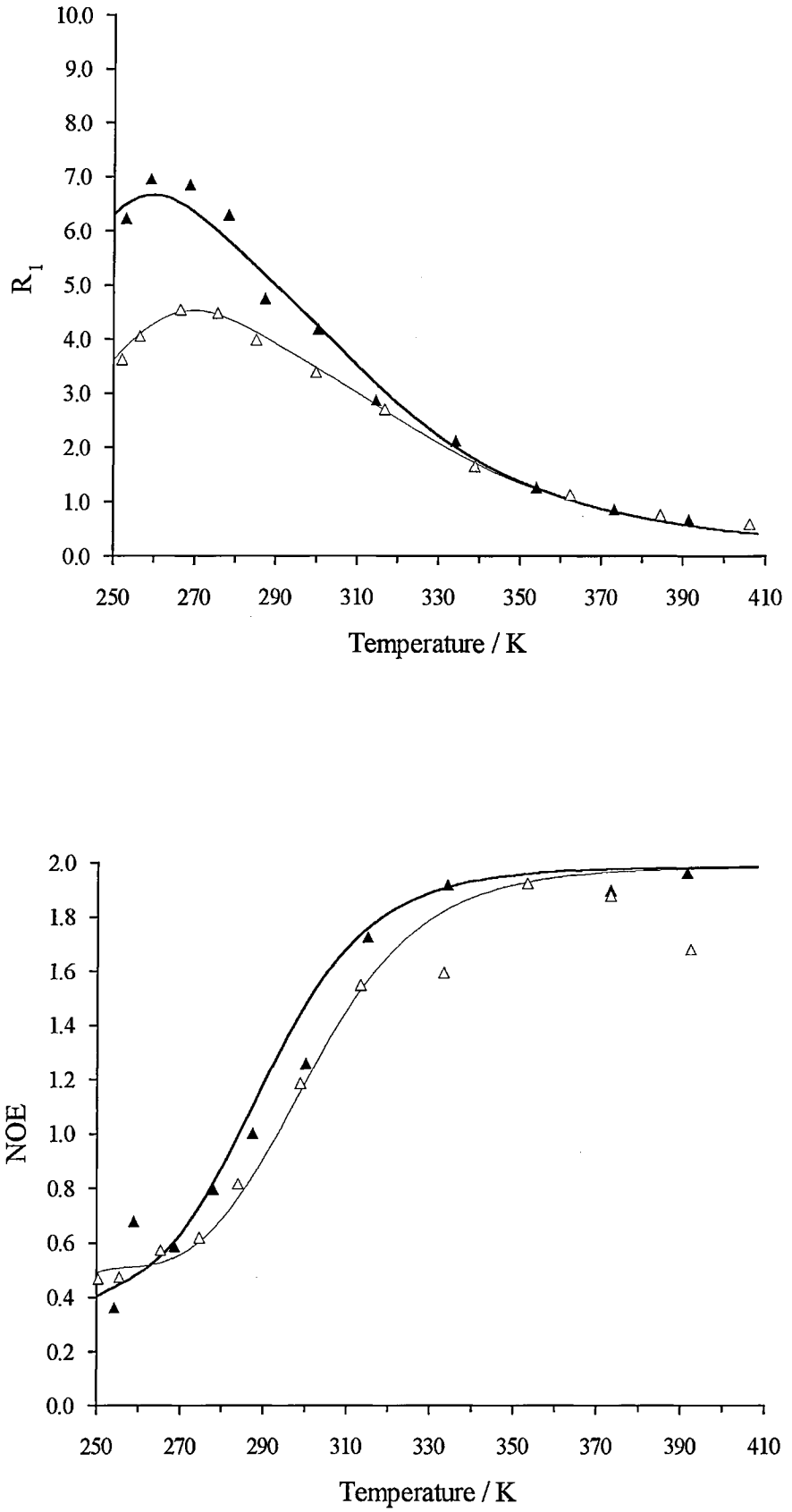

Fig A7.1: 9-*n*-octyl-*n*-heptadecane - position **z**; carbon-13 data and optimized theoretical curves at 67.83 MHz (—) and 100.53 MHz (–).

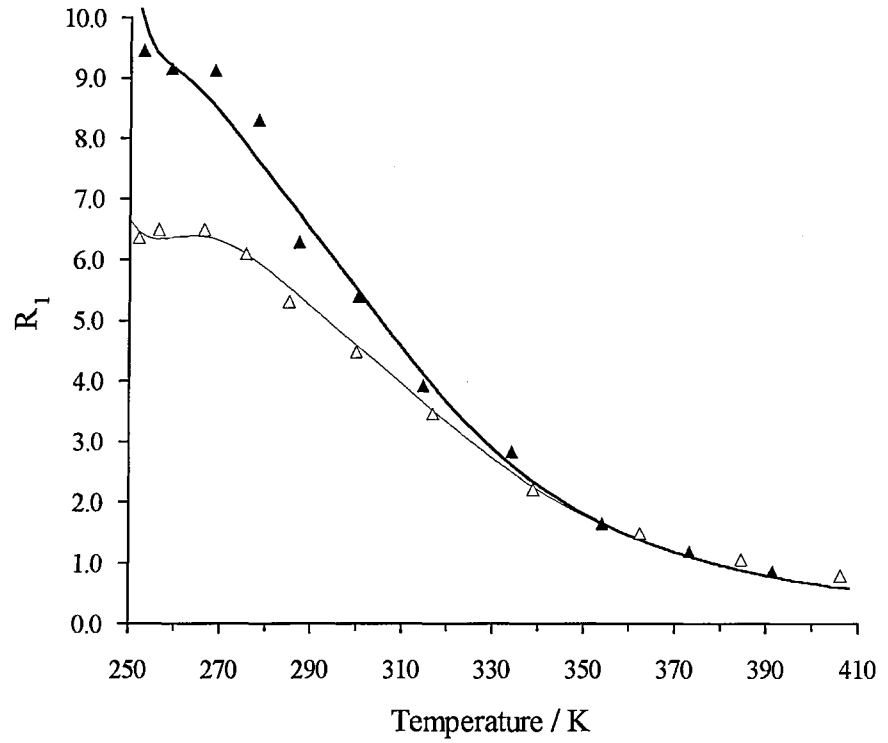

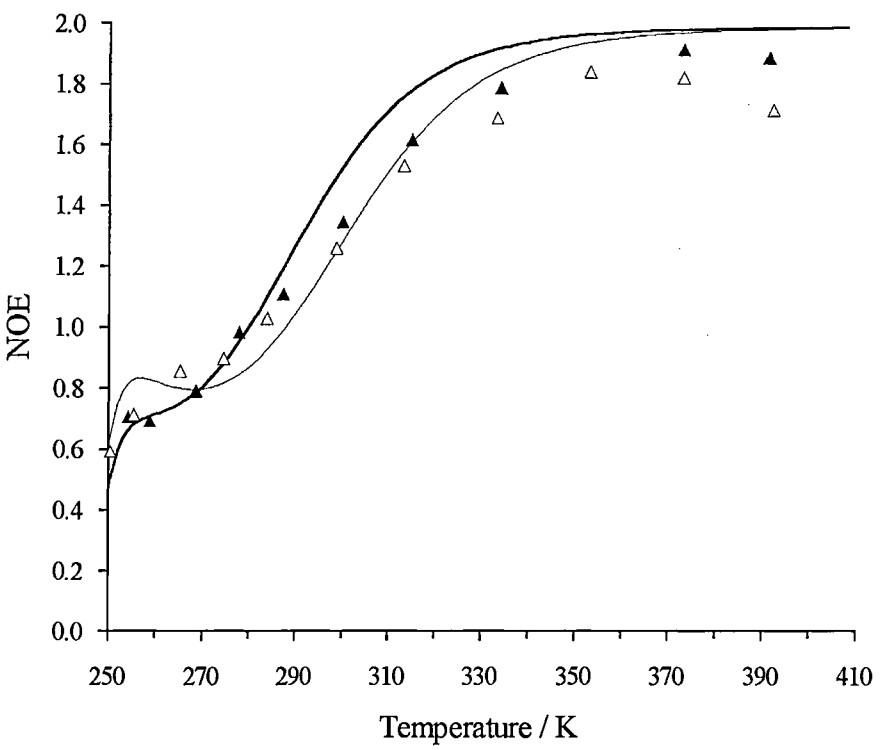

Fig A7.2: 9-*n*-octyl-*n*-heptadecane - position **a**; carbon-13 data and optimized theoretical curves at 67.83 MHz (—) and 100.53 MHz (–).

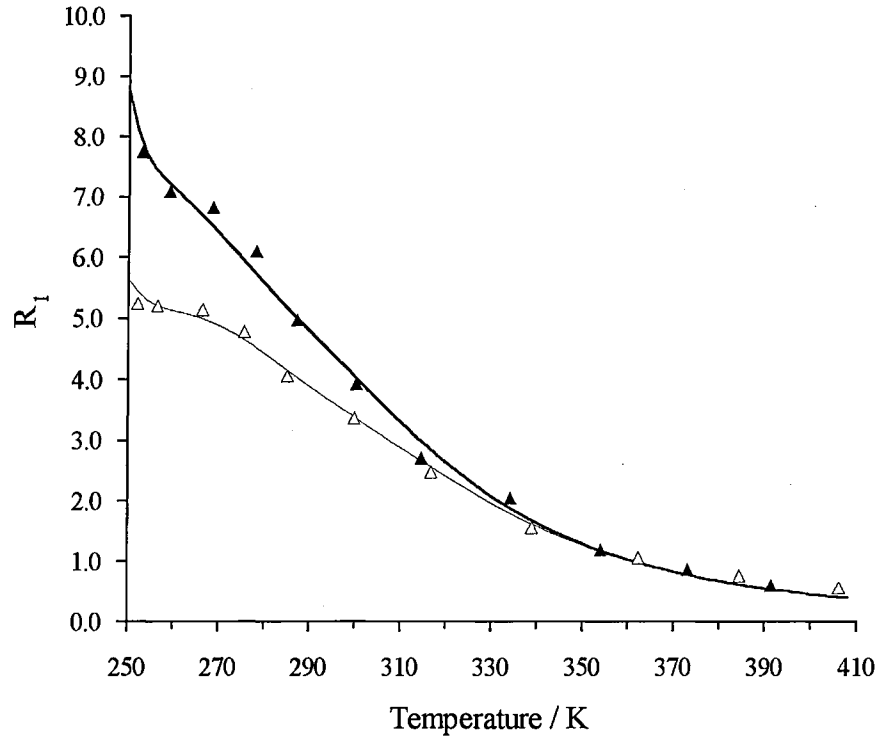

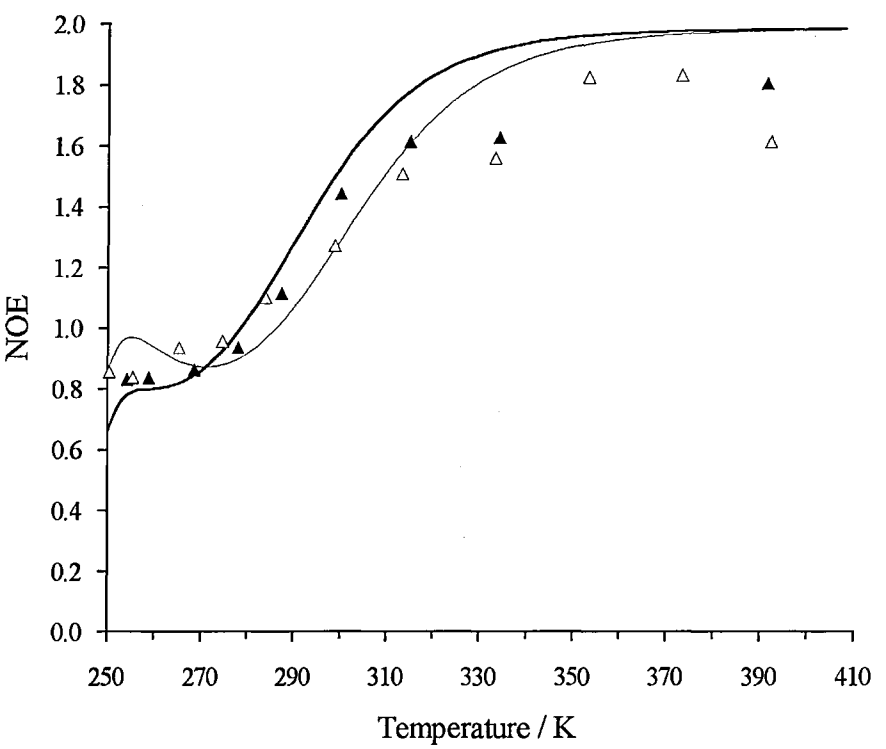

Fig A7.3: 9-*n*-octyl-*n*-heptadecane - position **b**; carbon-13 data and optimized theoretical curves at 67.83 MHz (—) and 100.53 MHz (–).

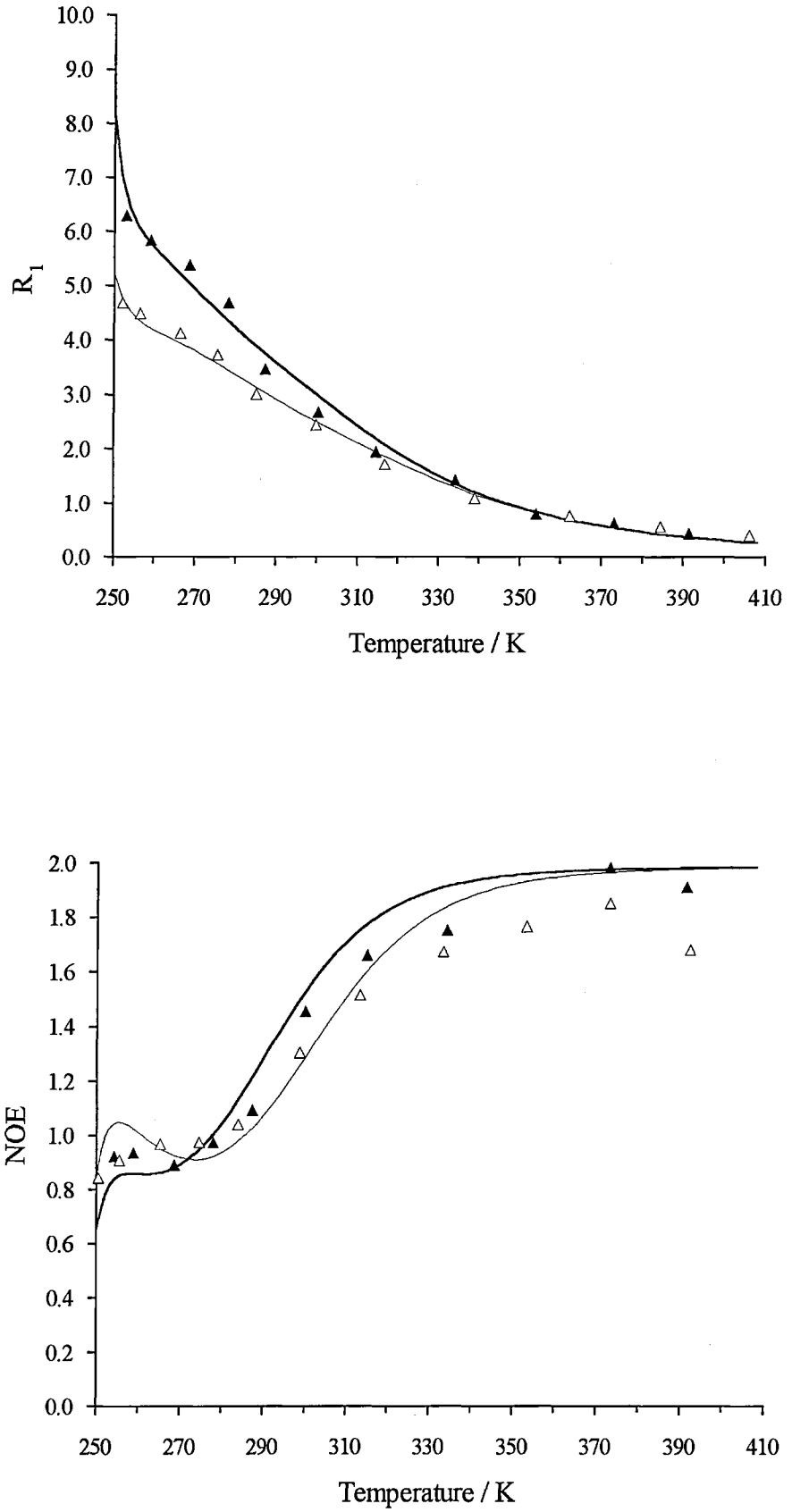

Fig A7.4: 9-*n*-octyl-*n*-heptadecane - position **c**; carbon-13 data and optimized theoretical curves at 67.83 MHz (—) and 100.53 MHz (–).

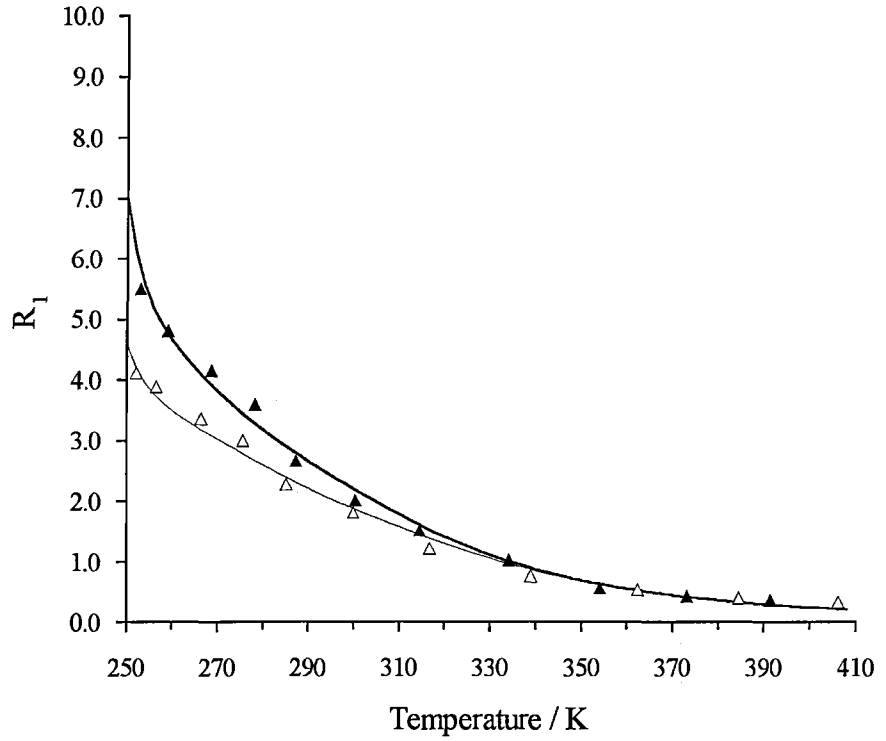

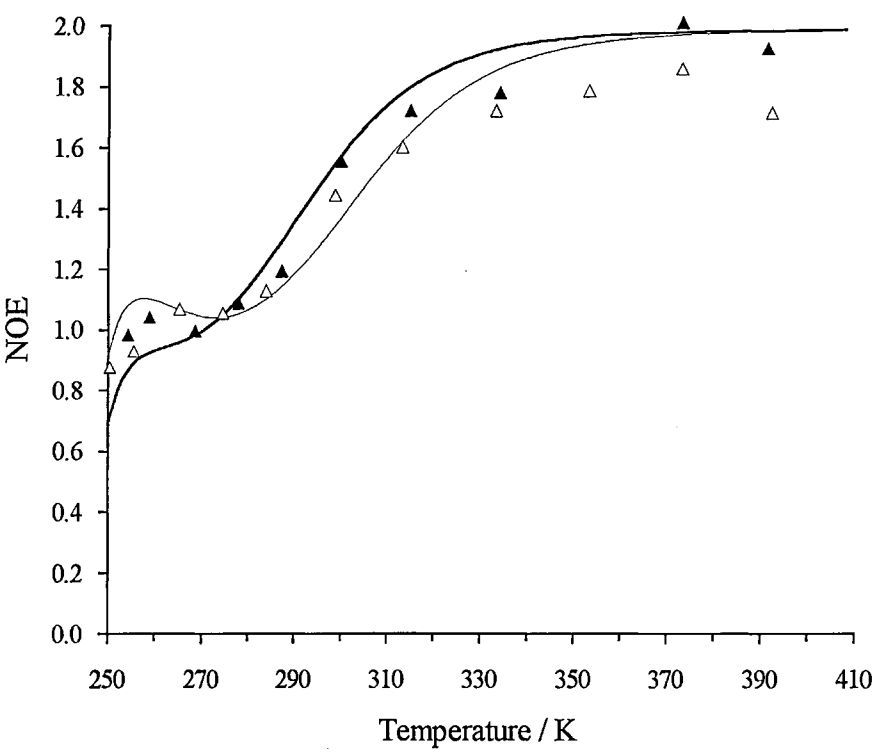

Fig A7.5: 9-*n*-octyl-*n*-heptadecane - position **d**; carbon-13 data and optimized theoretical curves at 67.83 MHz (—) and 100.53 MHz (–).

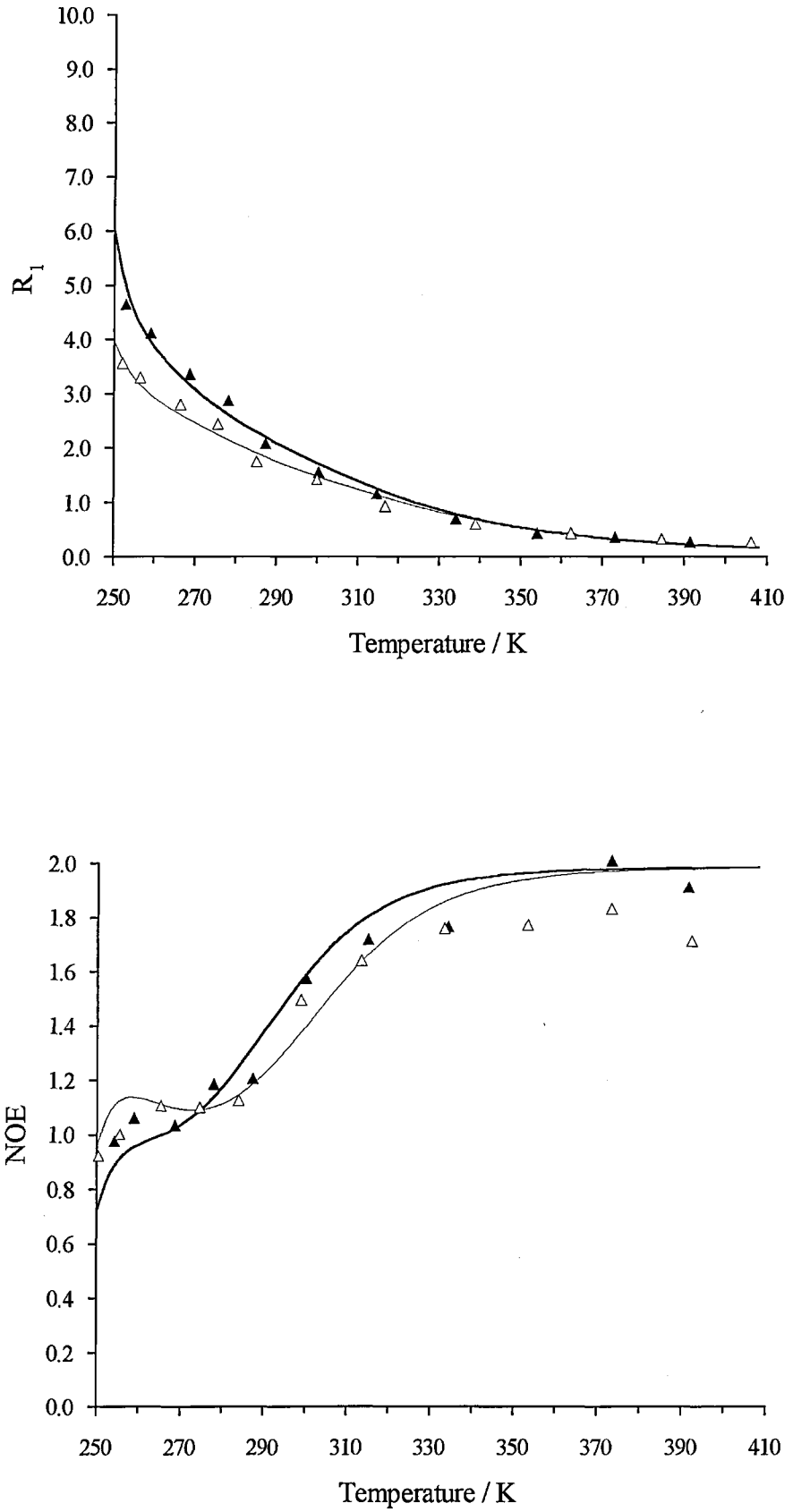

Fig A7.6: 9-*n*-octyl-*n*-heptadecane - position **e**; carbon-13 data and optimized theoretical curves at 67.83 MHz (—) and 100.53 MHz (–).

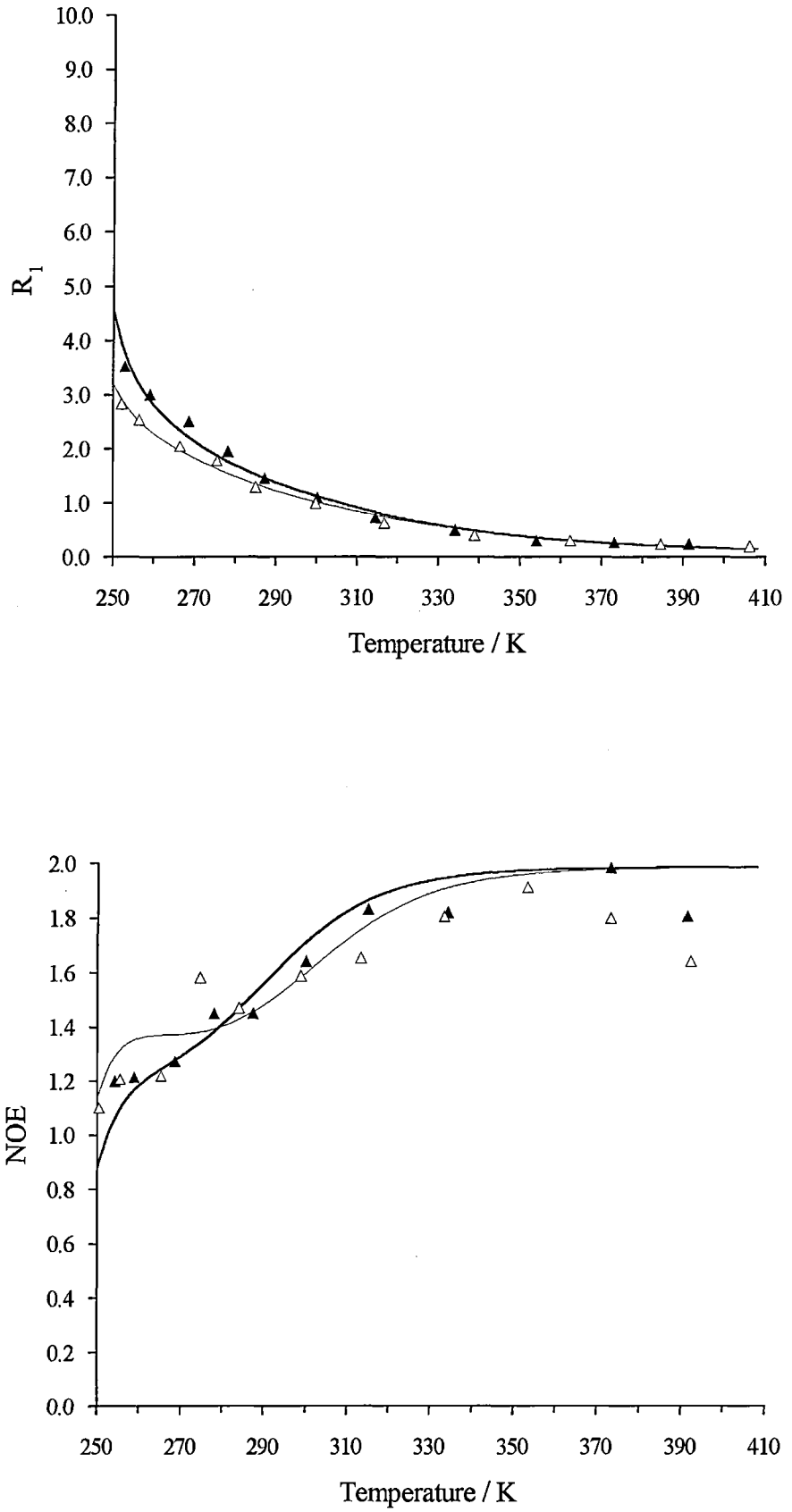

Fig A7.7: 9-*n*-octyl-*n*-heptadecane - position **f**; carbon-13 data and optimized theoretical curves at 67.83 MHz (—) and 100.53 MHz (–).

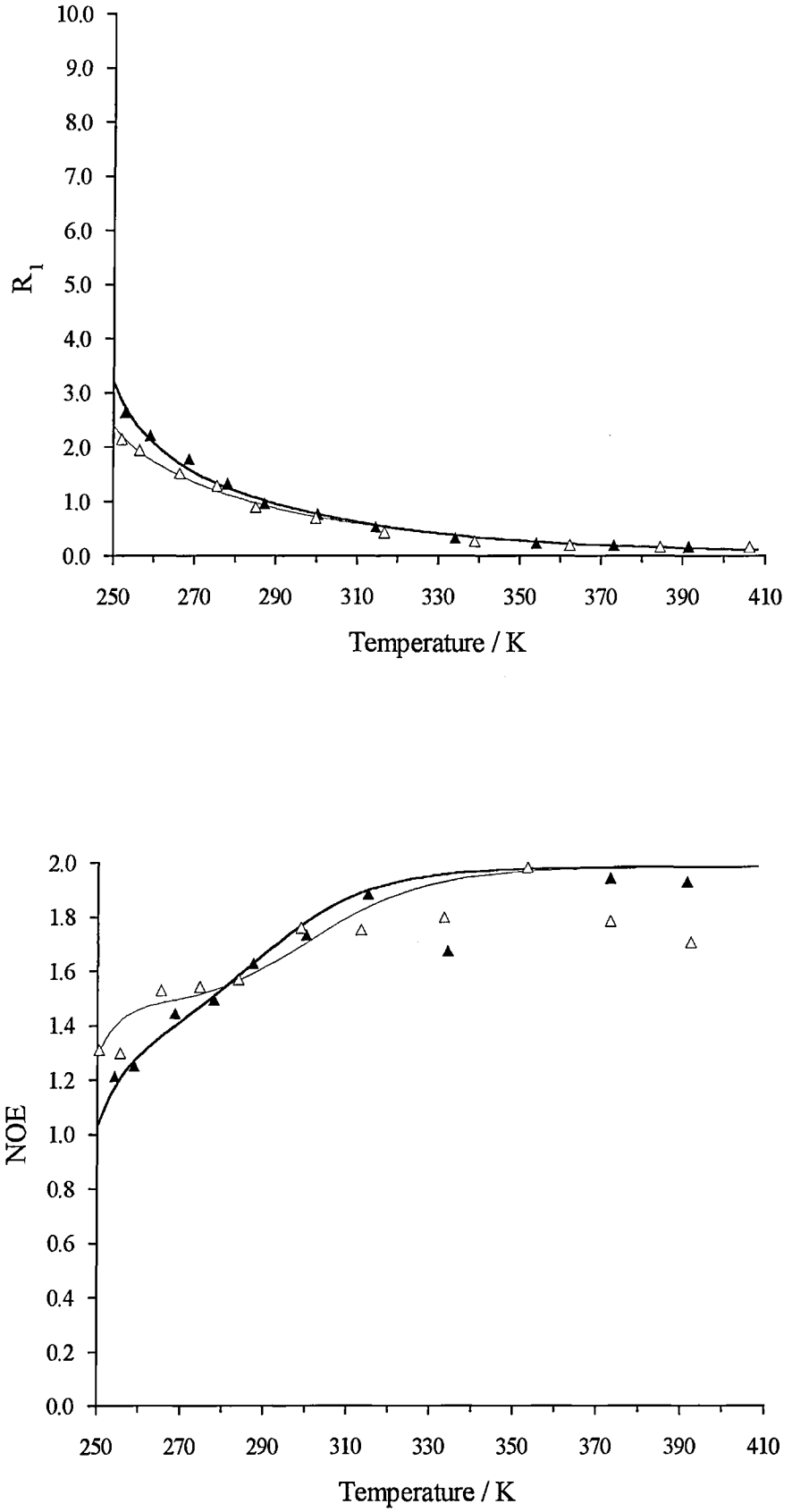

Fig A7.8: 9-*n*-octyl-*n*-heptadecane - position **g**; carbon-13 data and optimized theoretical curves at 67.83 MHz (—) and 100.53 MHz (–).

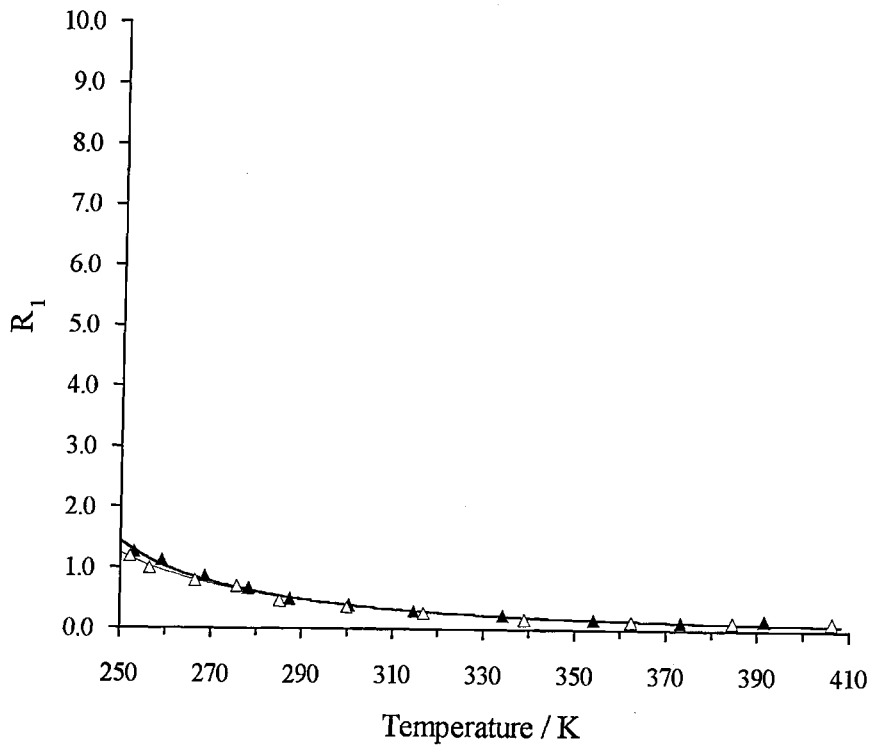

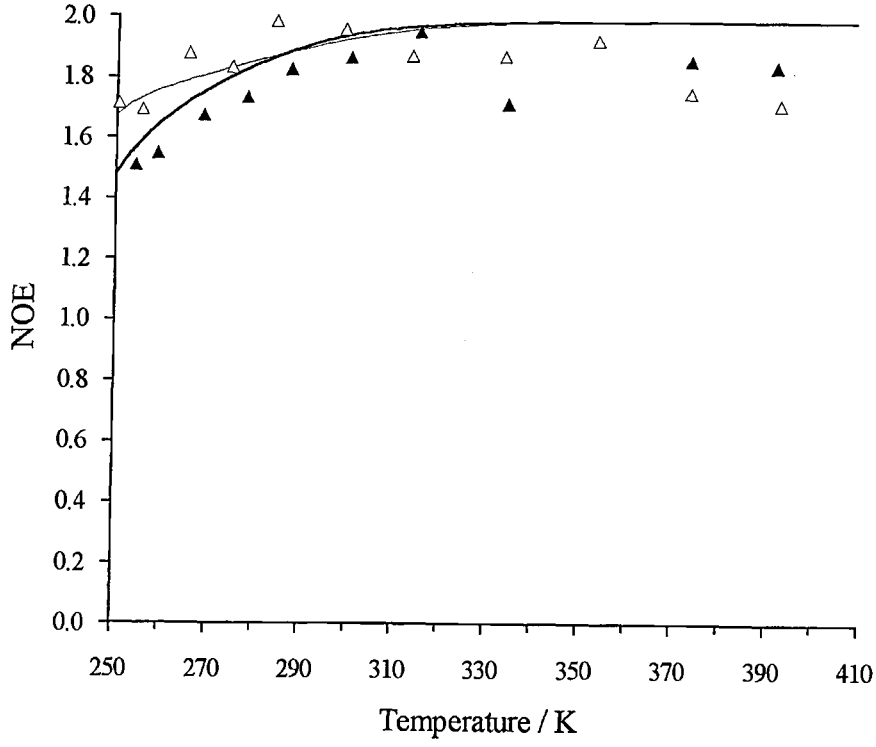

Fig A7.9: 9-*n*-octyl-*n*-heptadecane - position **h**; carbon-13 data and optimized theoretical curves at 67.83 MHz (—) and 100.53 MHz (–).

Appendix 8

CARBON-13 DATA PLOTS AND OPTIMIZED THEORETICAL CURVES FOR TRI-*n*-OCTYLSILANE

The carbon-13 R_1 relaxation rate and NOE data for tri-*n*-octylsilane are shown in the plots on the following pages, together with the optimized theoretical curves corresponding to the tables of parameters in Section 7.8.

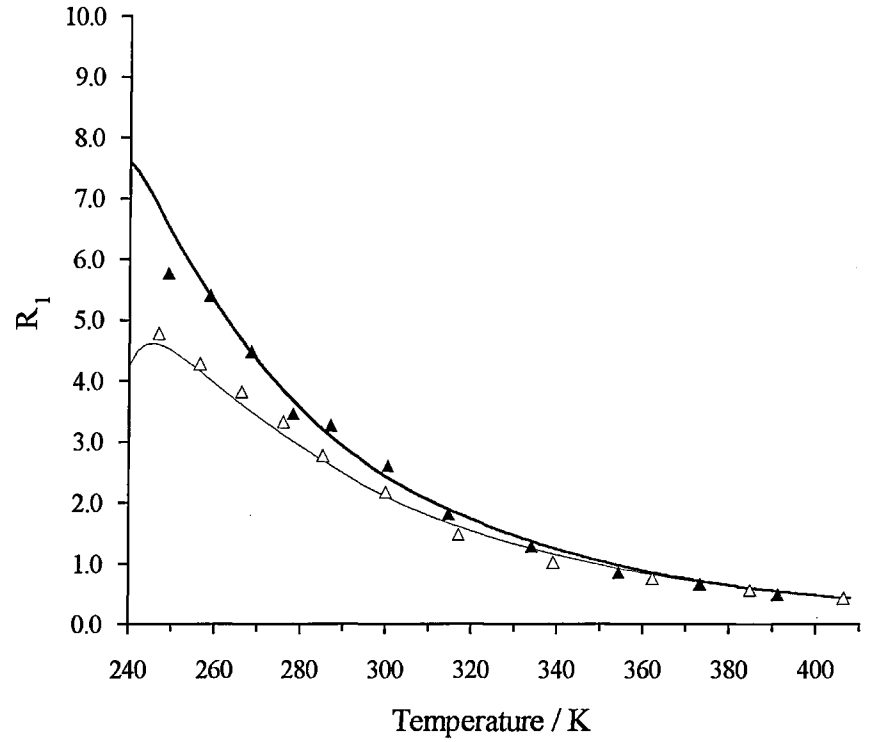

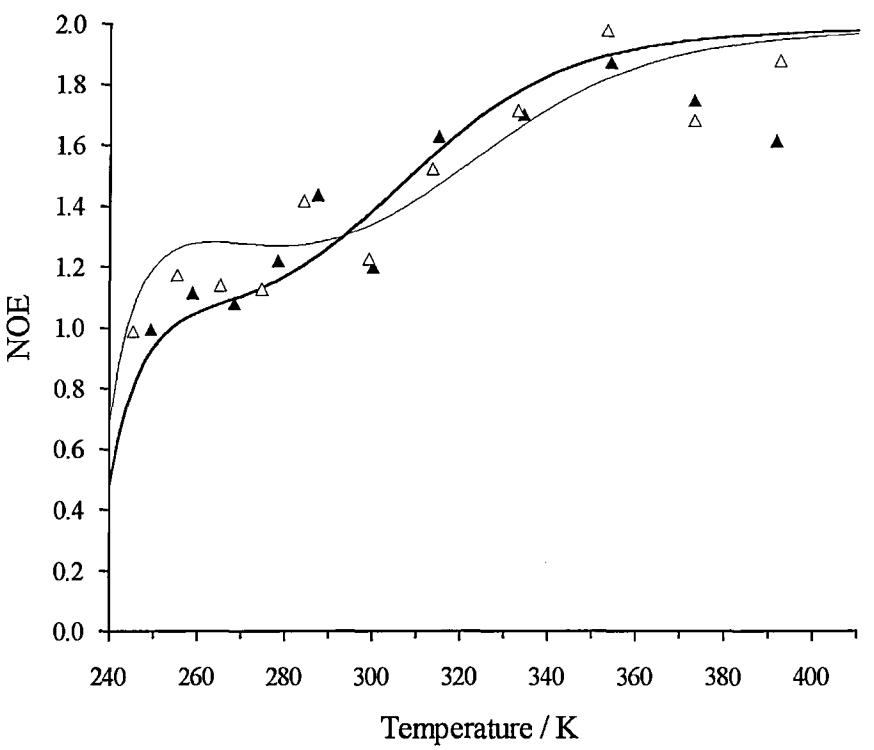

Fig A8.1: Tri-*n*-octylsilane - position **a**; carbon-13 data and optimized theoretical curves at 67.83 MHz (—) and 100.53 MHz (–).

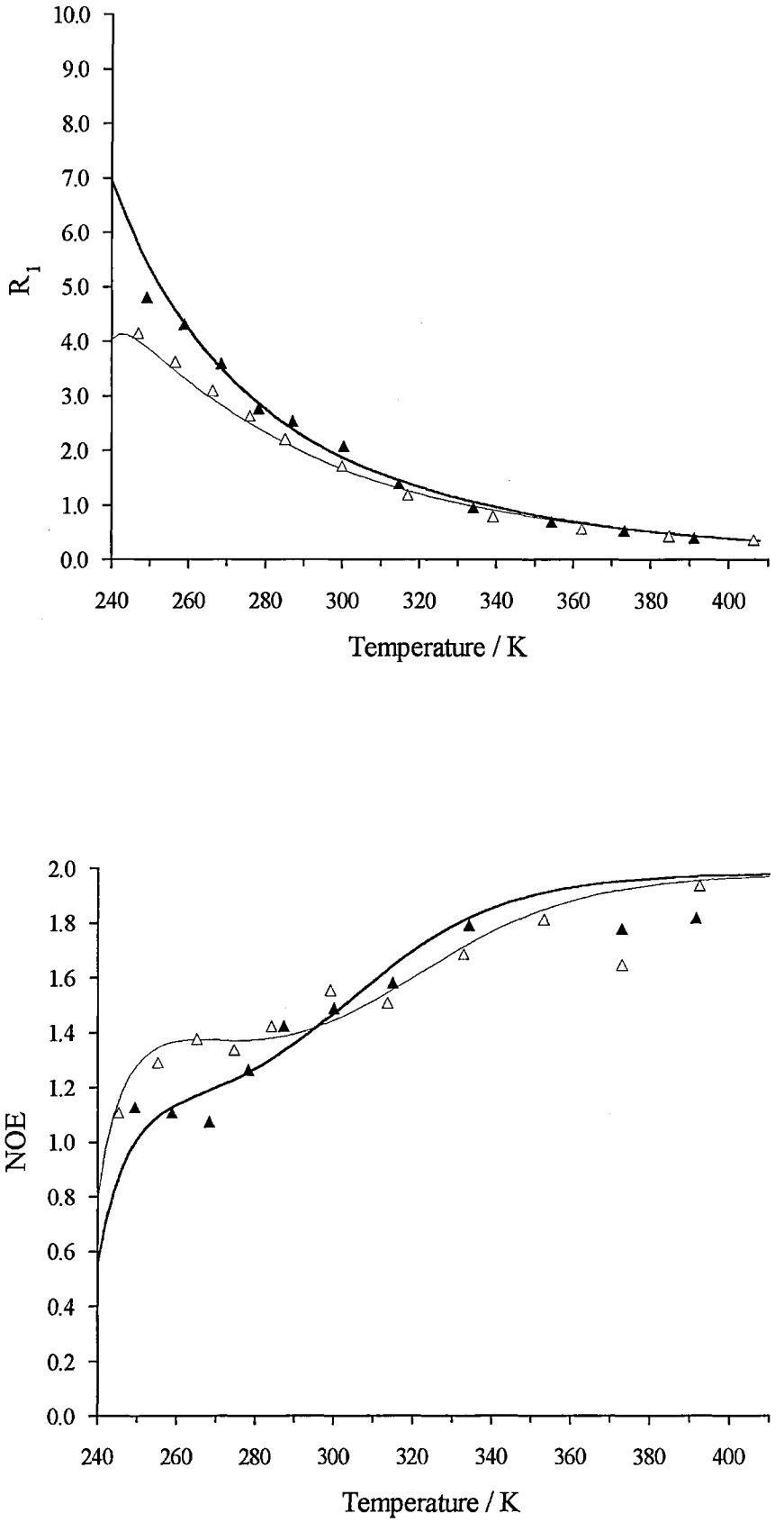

Fig A8.2: Tri-*n*-octylsilane - position **b**; carbon-13 data and optimized theoretical curves at 67.83 MHz (—) and 100.53 MHz (–).

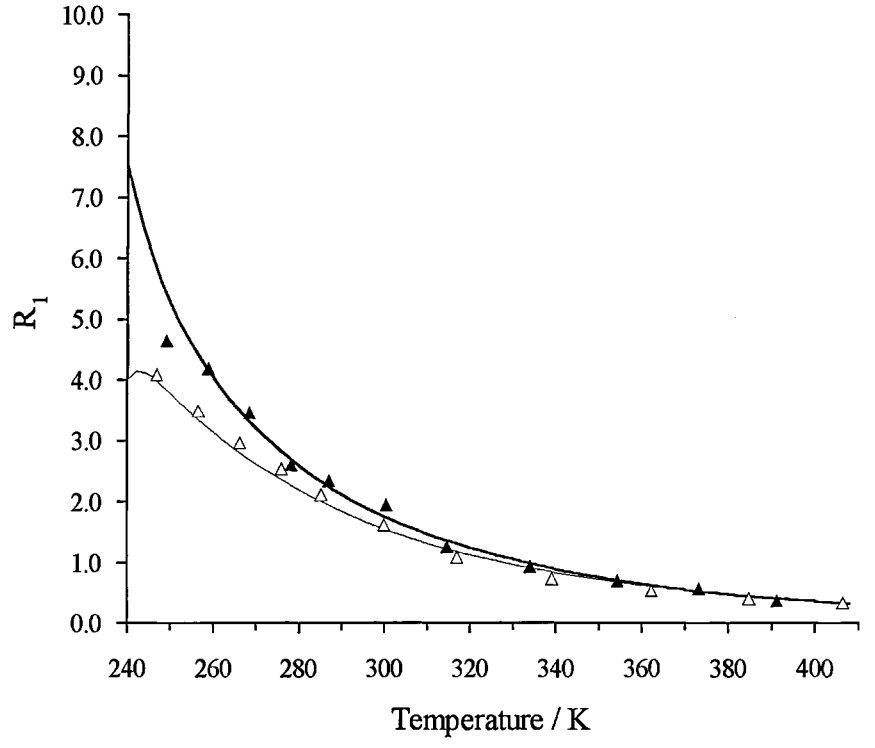

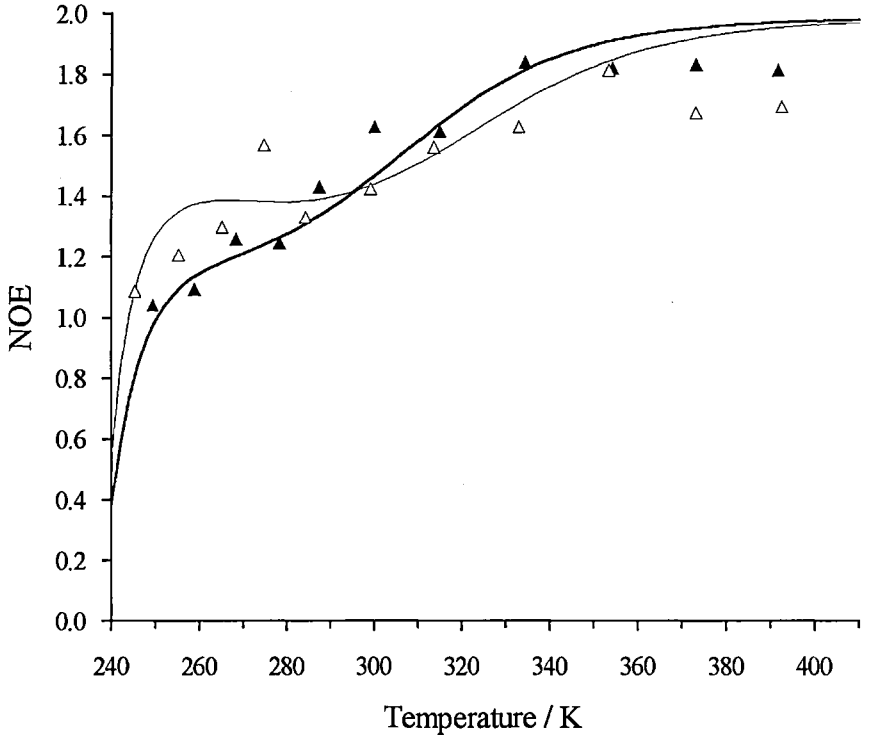

Fig A8.3: Tri-*n*-octylsilane - position **c**; carbon-13 data and optimized theoretical curves at 67.83 MHz (—) and 100.53 MHz (–).

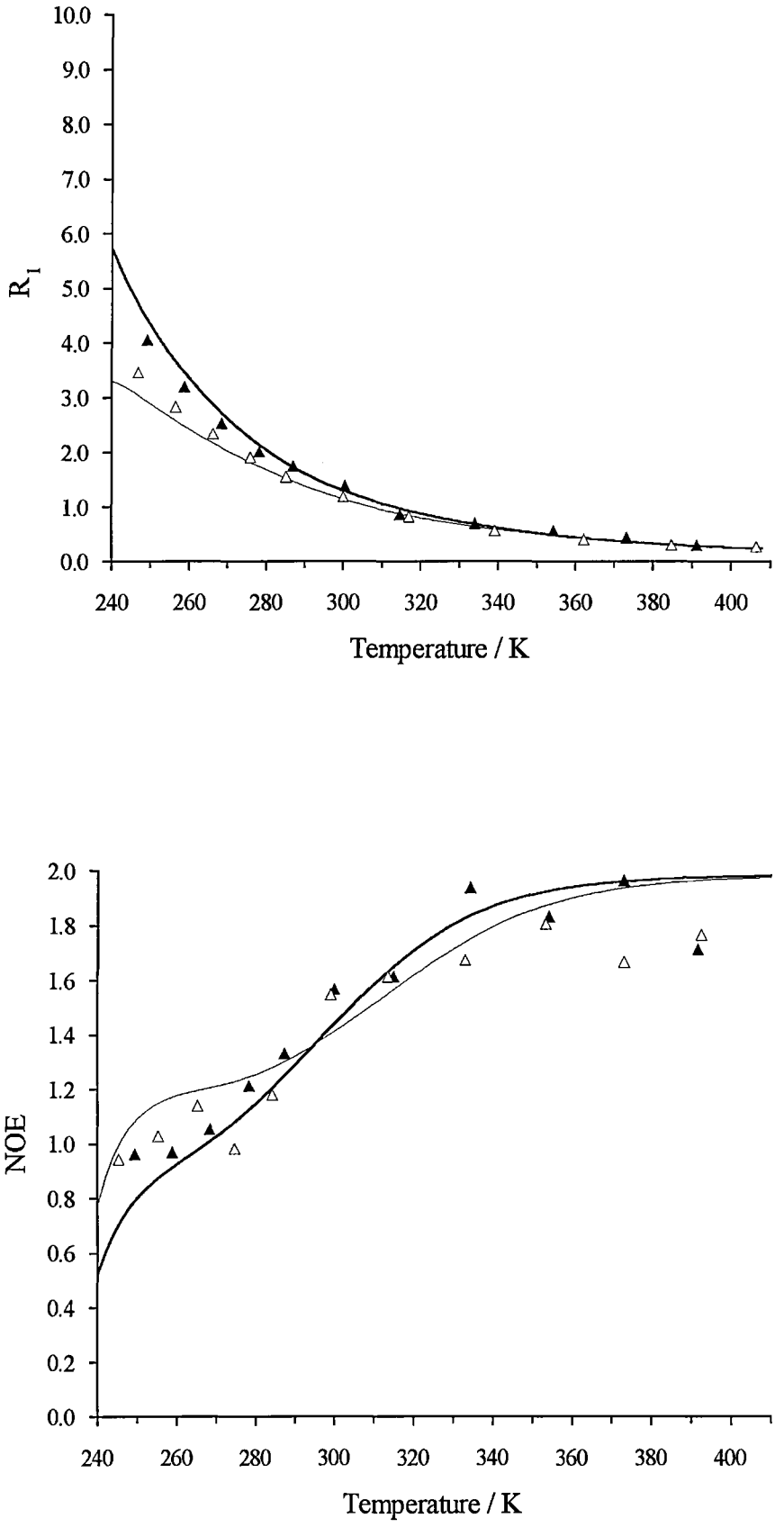

Fig A8.4: Tri-*n*-octylsilane - position **d**; carbon-13 data and optimized theoretical curves at 67.83 MHz (—) and 100.53 MHz (–).

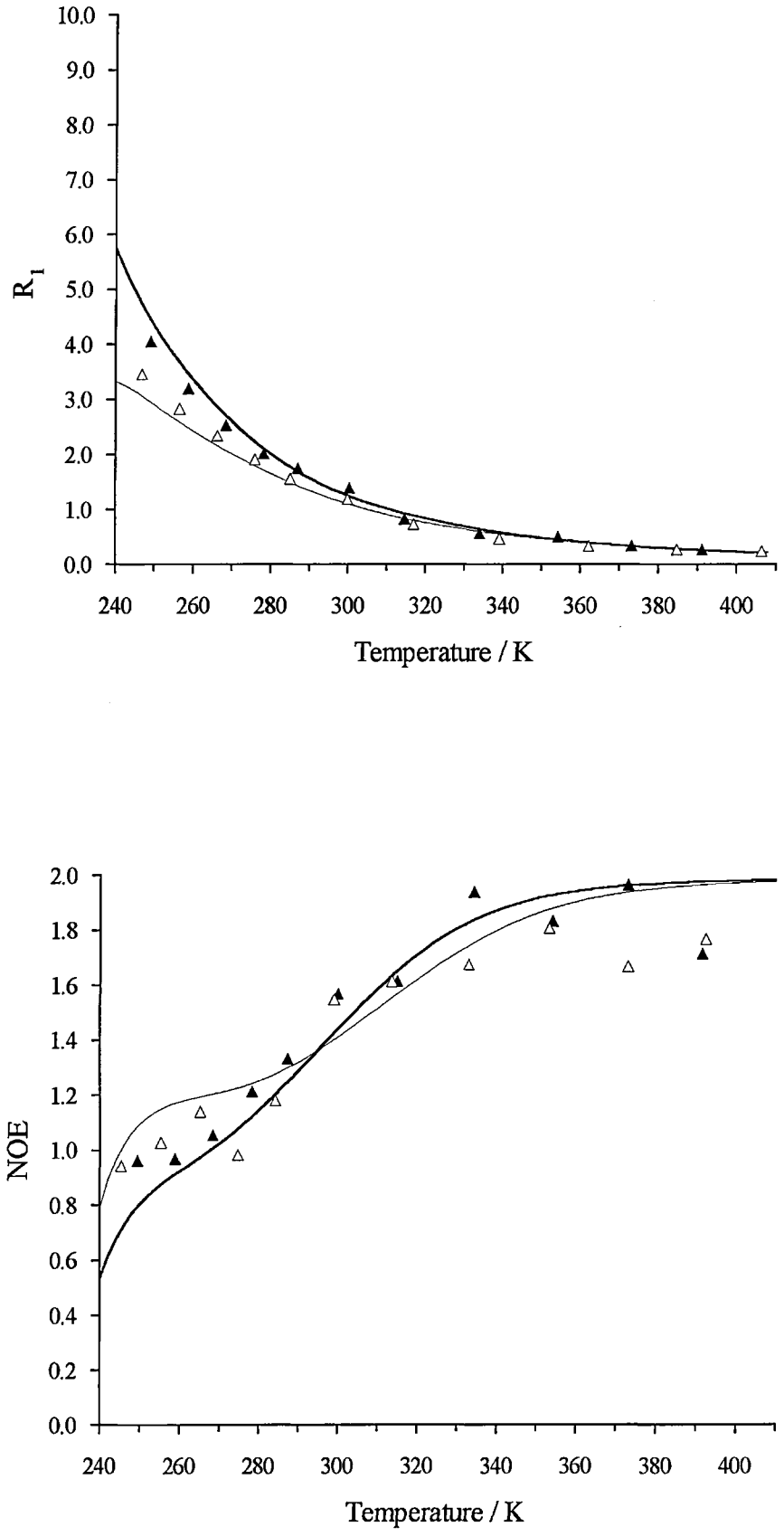

Fig A8.5: Tri-*n*-octylsilane - position **e**; carbon-13 data and optimized theoretical curves at 67.83 MHz (—) and 100.53 MHz (–).

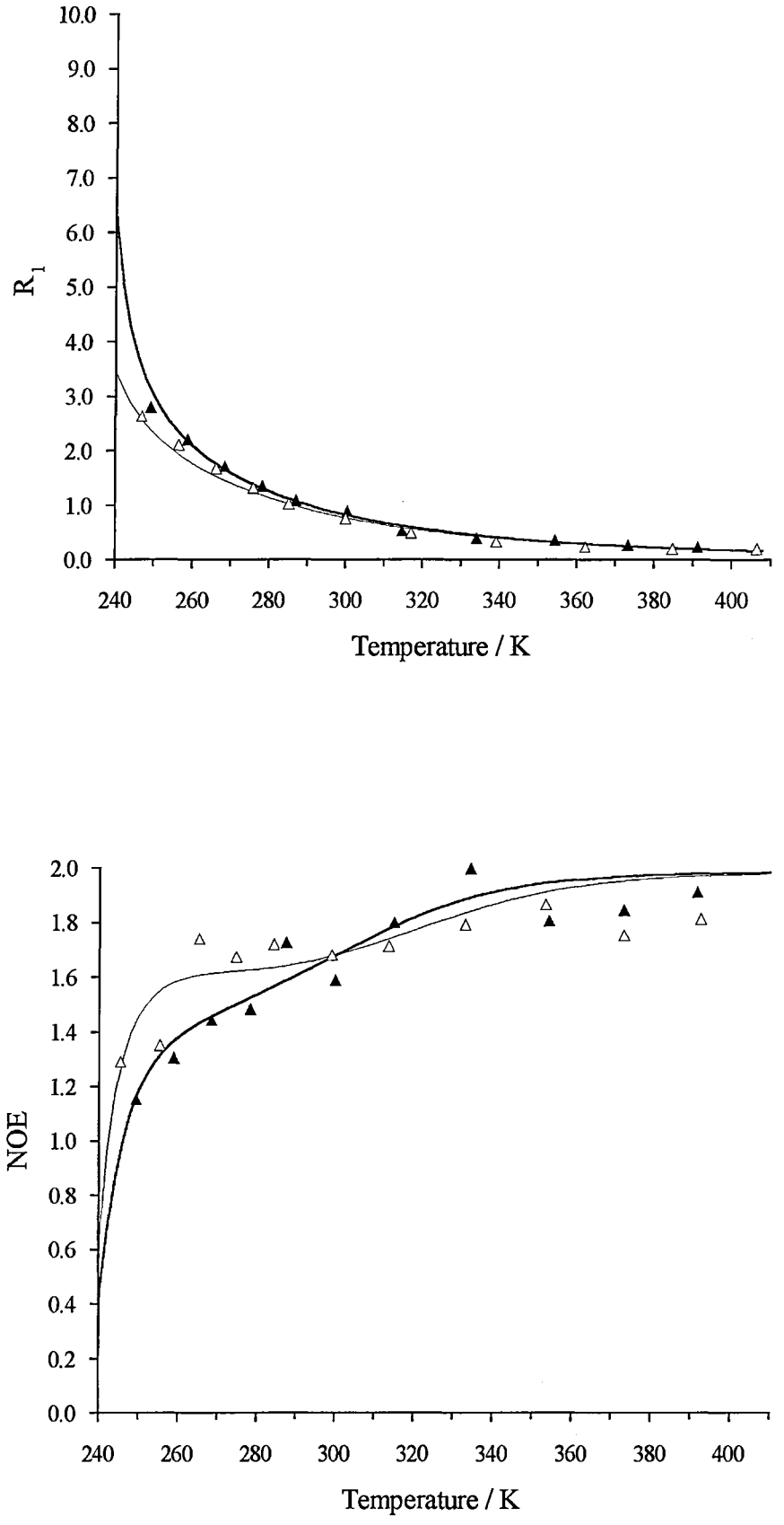

Fig A8.6: Tri-*n*-octylsilane - position **f**; carbon-13 data and optimized theoretical curves at 67.83 MHz (—) and 100.53 MHz (–).

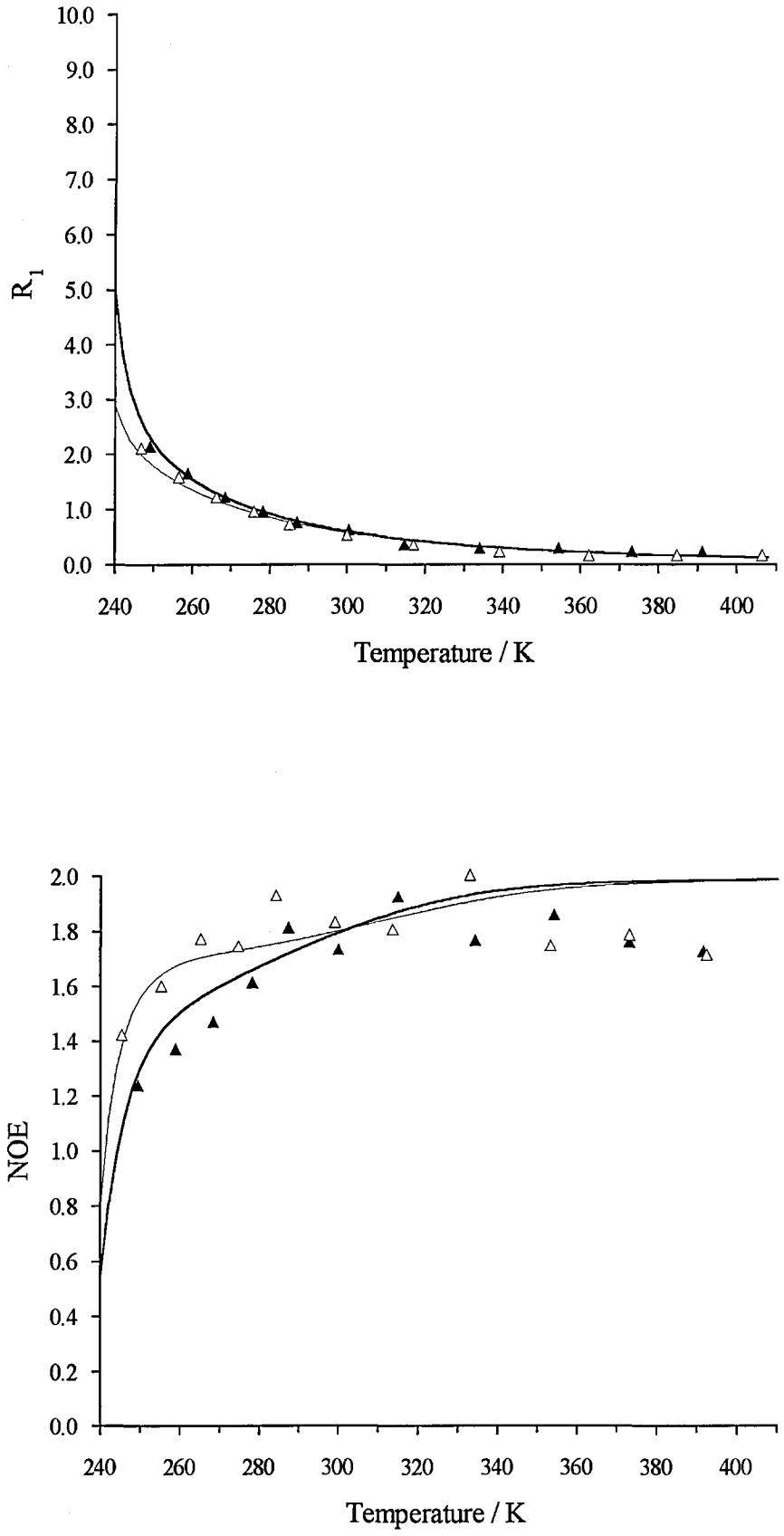

Fig A8.7: Tri-*n*-octylsilane - position **g**; carbon-13 data and optimized theoretical curves at 67.83 MHz (—) and 100.53 MHz (–).

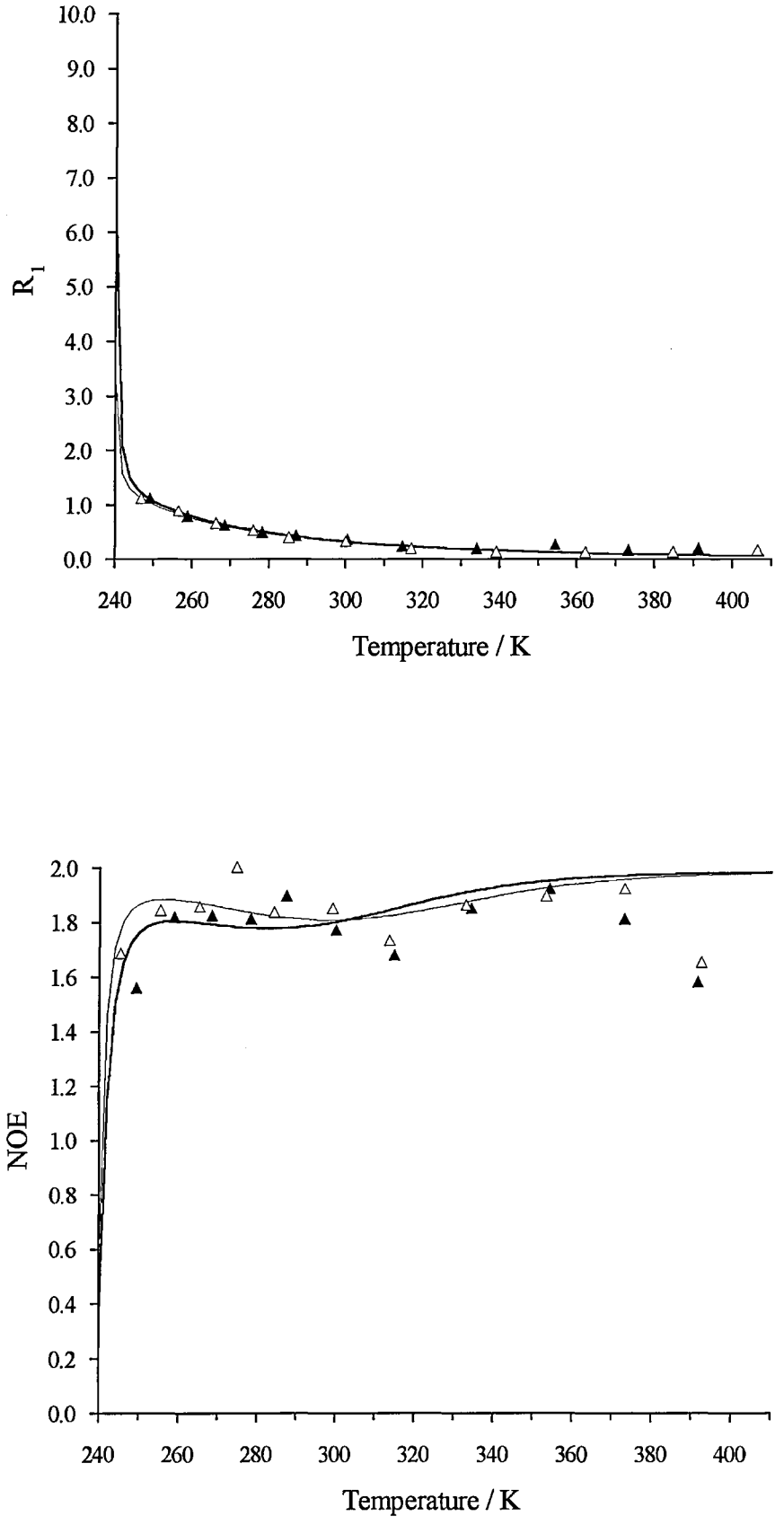

Fig A8.8: Tri-*n*-octylsilane - position **h**; carbon-13 data and optimized theoretical curves at 67.83 MHz (—) and 100.53 MHz (–).

Appendix 9

CARBON-13 DATA PLOTS AND OPTIMIZED THEORETICAL CURVES FOR TRICYCLOHEXYLMETHANE

The carbon-13 R_1 relaxation rate and NOE data for tricyclohexylmethane are shown in the plots on the following pages, together with the optimized theoretical curves corresponding to the tables of parameters in Section 8.3.

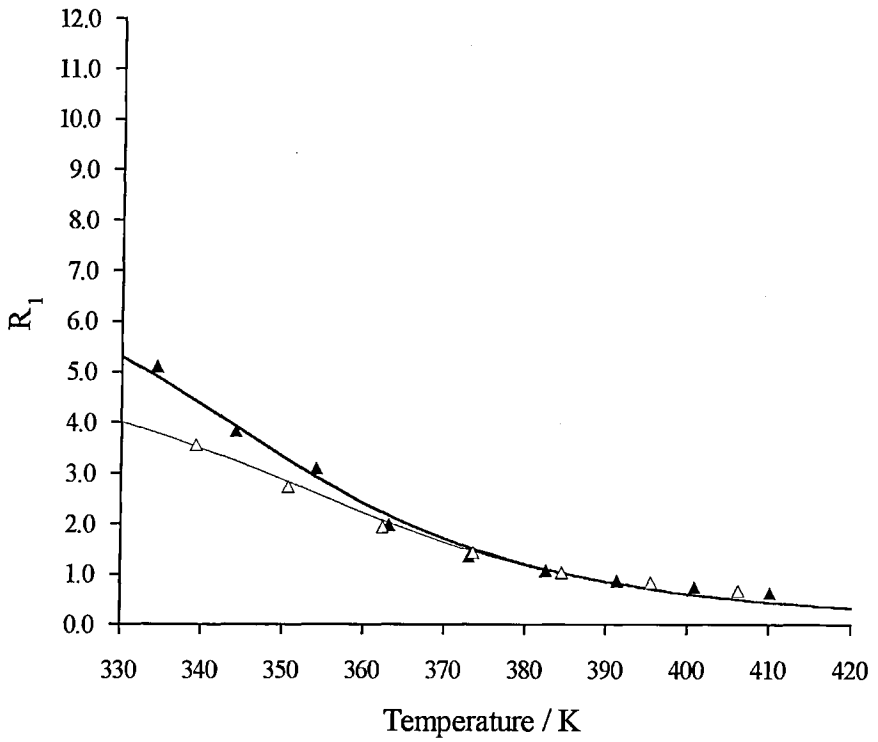

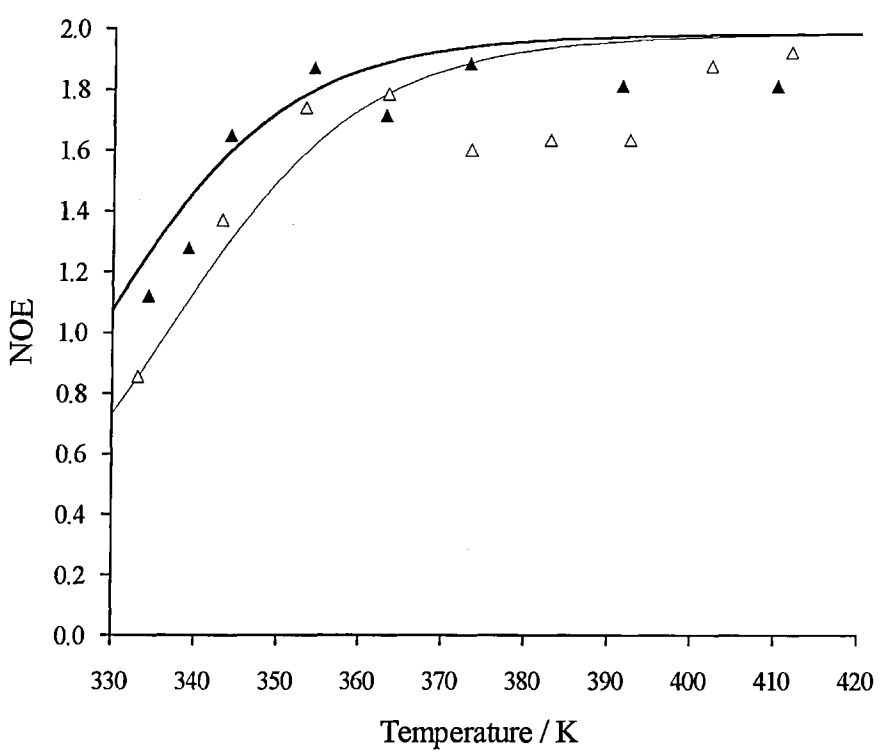

Fig A9.1: Tricyclohexylmethane - position z; carbon-13 data and optimized theoretical curves at 67.83 MHz (—) and 100.53 MHz (–).

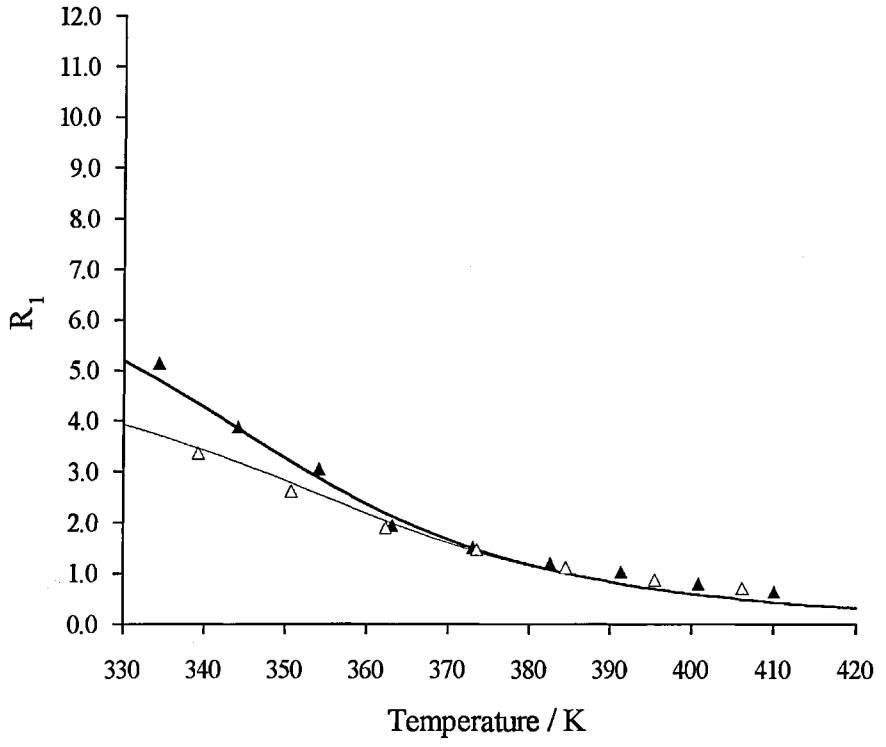

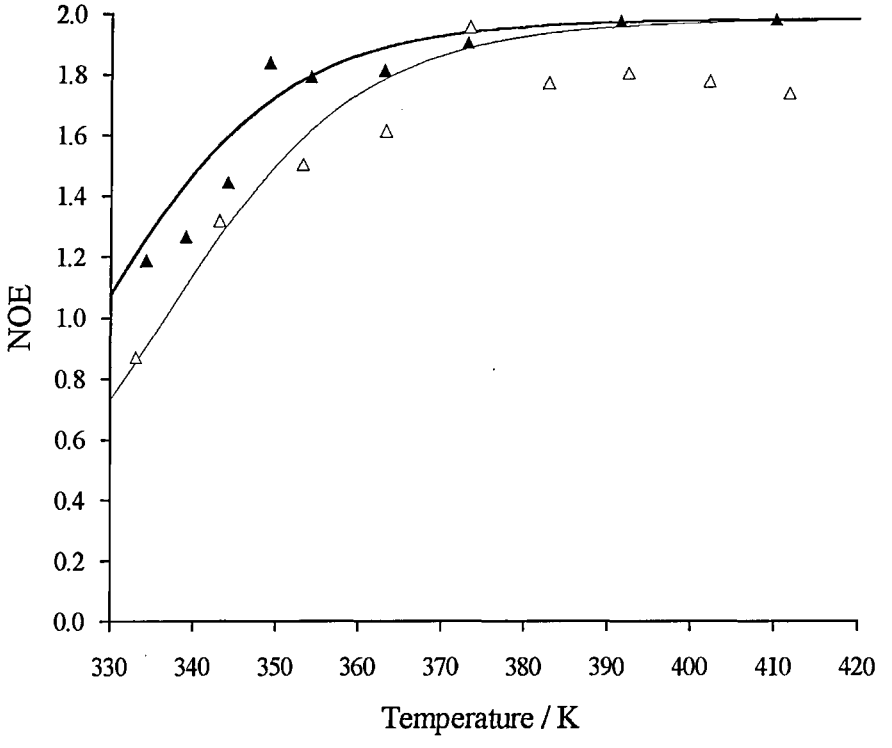

Fig A9.2: Tricyclohexylmethane - position **a**; carbon-13 data and optimized theoretical curves at 67.83 MHz (—) and 100.53 MHz (–).

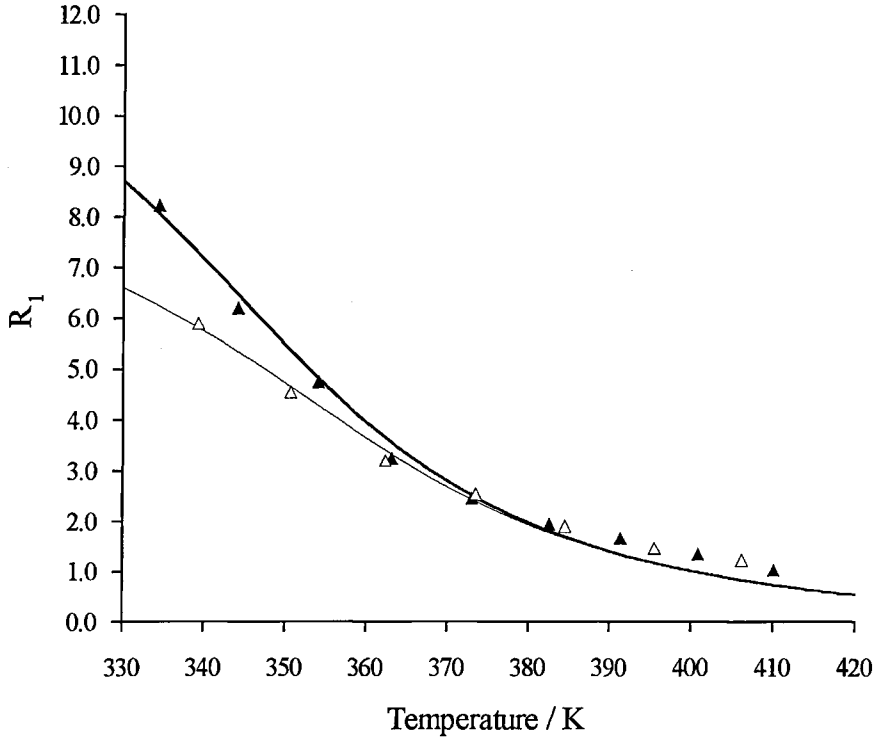

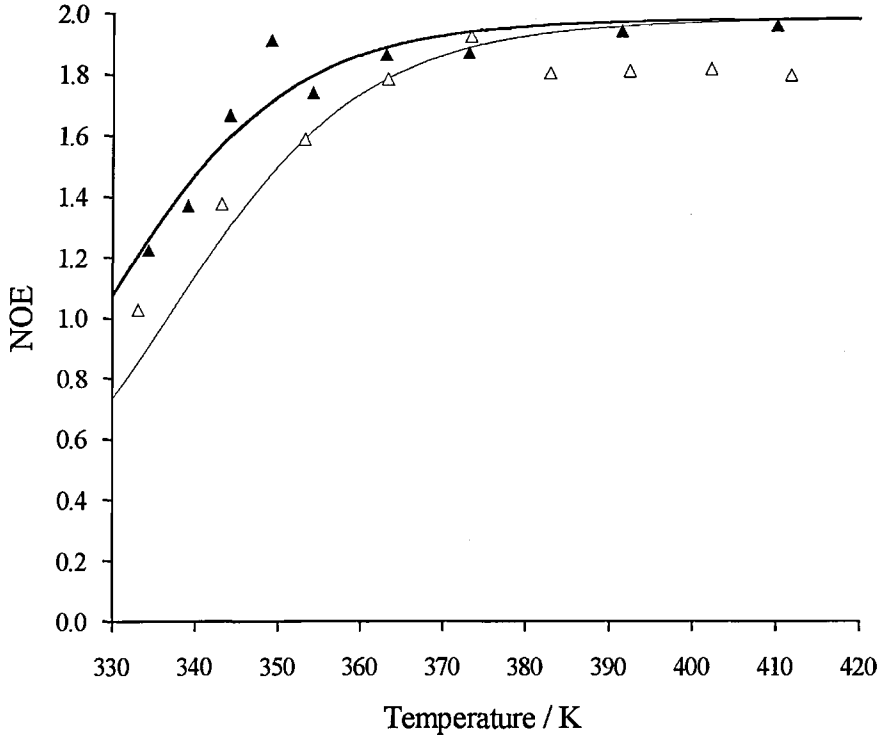

Fig A9.3: Tricyclohexylmethane - position **b**; carbon-13 data and optimized theoretical curves at 67.83 MHz (—) and 100.53 MHz (–).

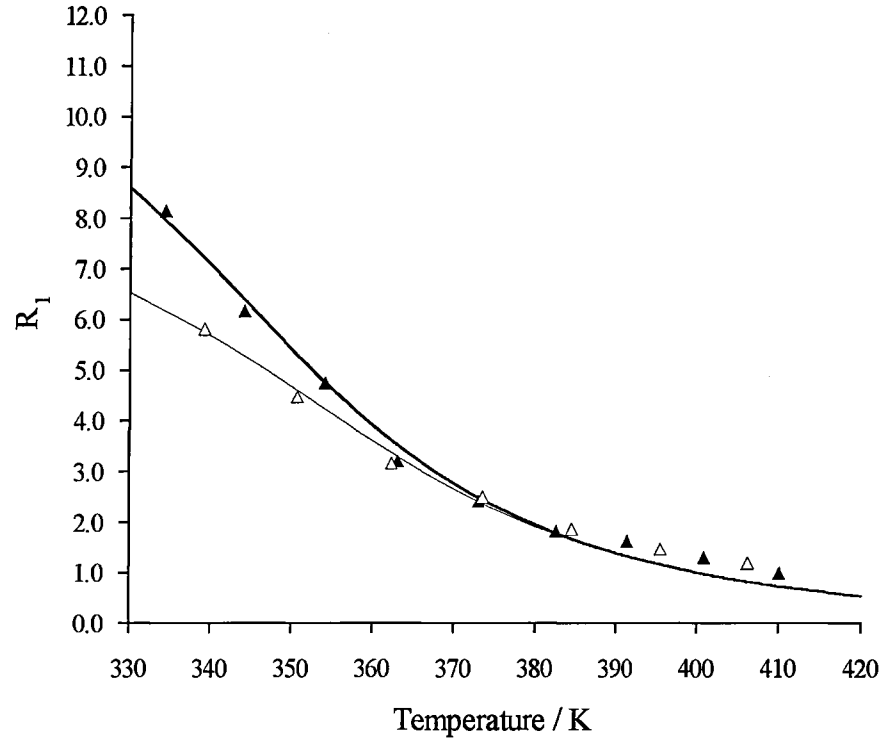

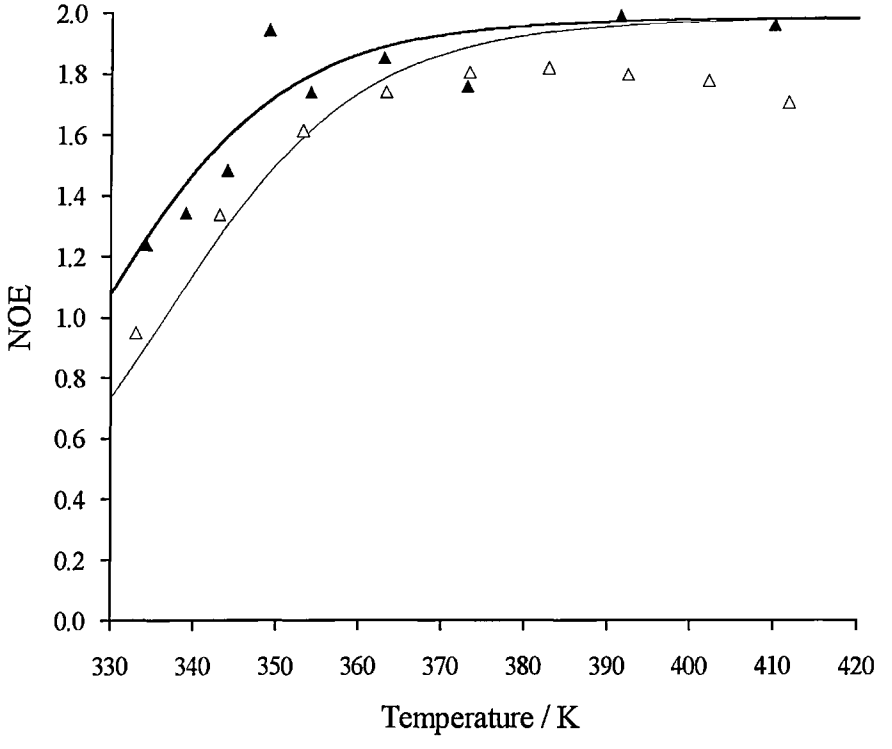

Fig A9.4: Tricyclohexylmethane - position **c**; carbon-13 data and optimized theoretical curves at 67.83 MHz (—) and 100.53 MHz (–).

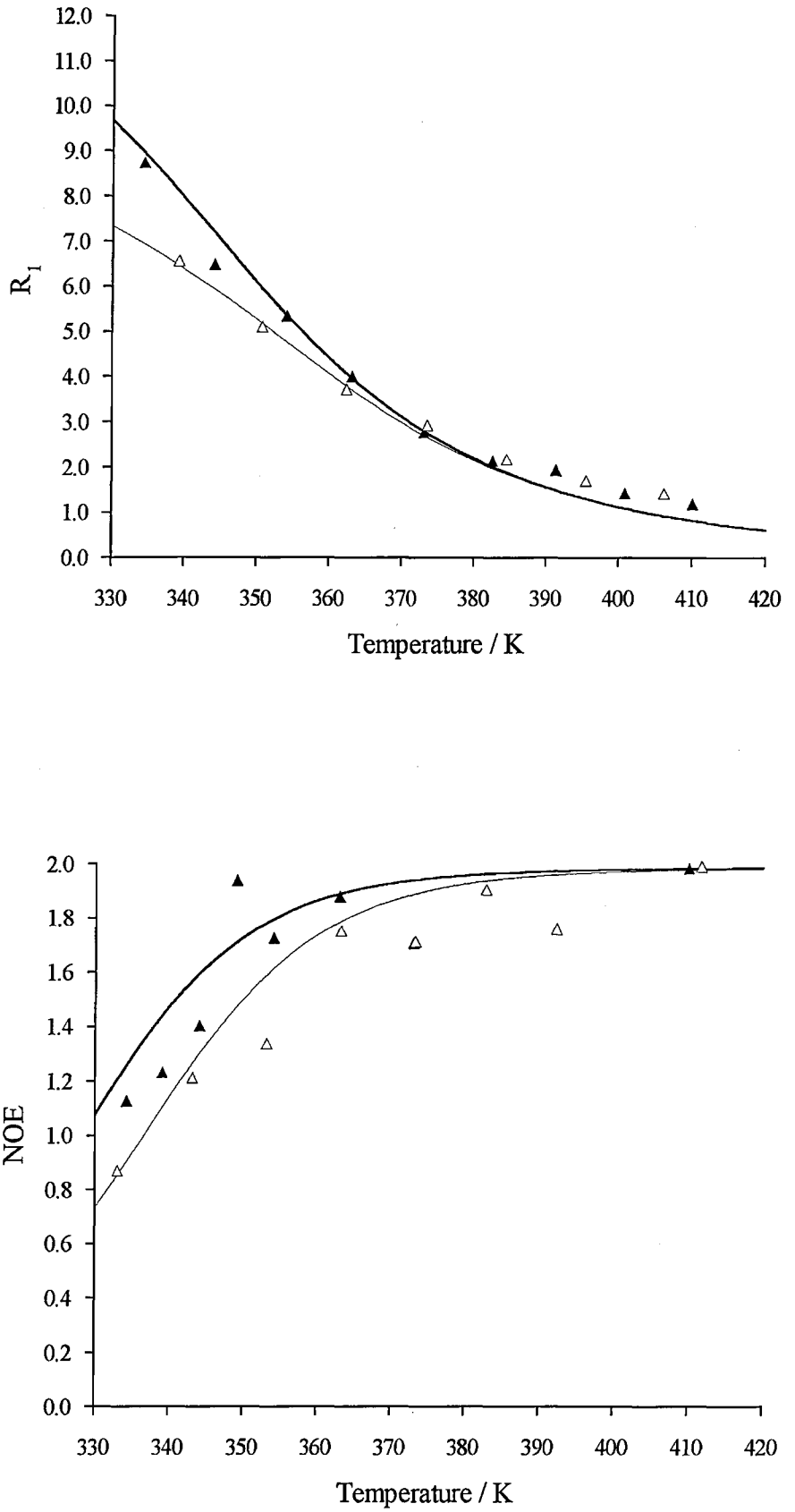

Fig A9.5: Tricyclohexylmethane - position **d**; carbon-13 data and optimized theoretical curves at 67.83 MHz (—) and 100.53 MHz (–).

Appendix 10

CARBON-13 DATA PLOTS AND OPTIMIZED THEORETICAL CURVES FOR 1,1,2-TRICYCLOHEXYLETHANE

The carbon-13 R_1 relaxation rate and NOE data for 1,1,2-tricyclohexylethane are shown in the plots on the following pages, together with the optimized theoretical curves corresponding to the tables of parameters in Section 8.4.

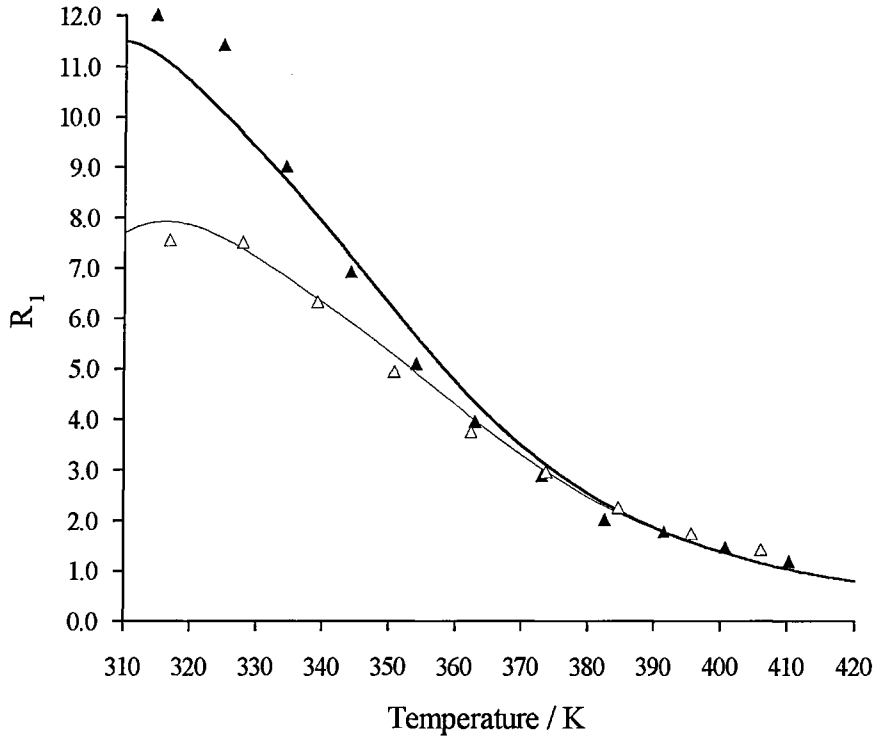

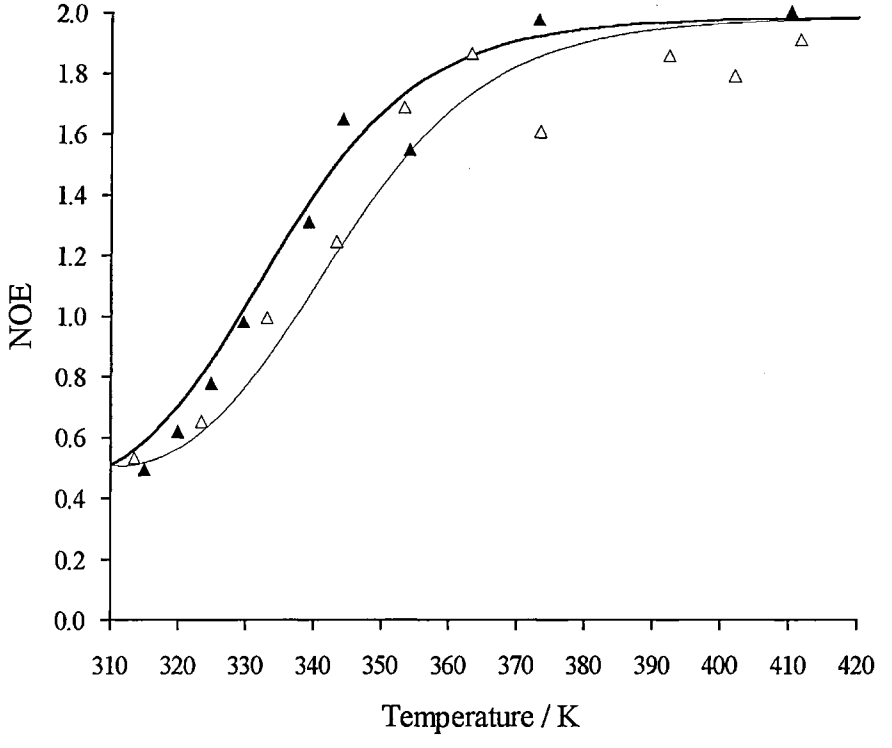

Fig A10.1: 1,1,2-tricyclohexylethane - position **1z**; carbon-13 data and optimized theoretical curves at 67.83 MHz (—) and 100.53 MHz (–).

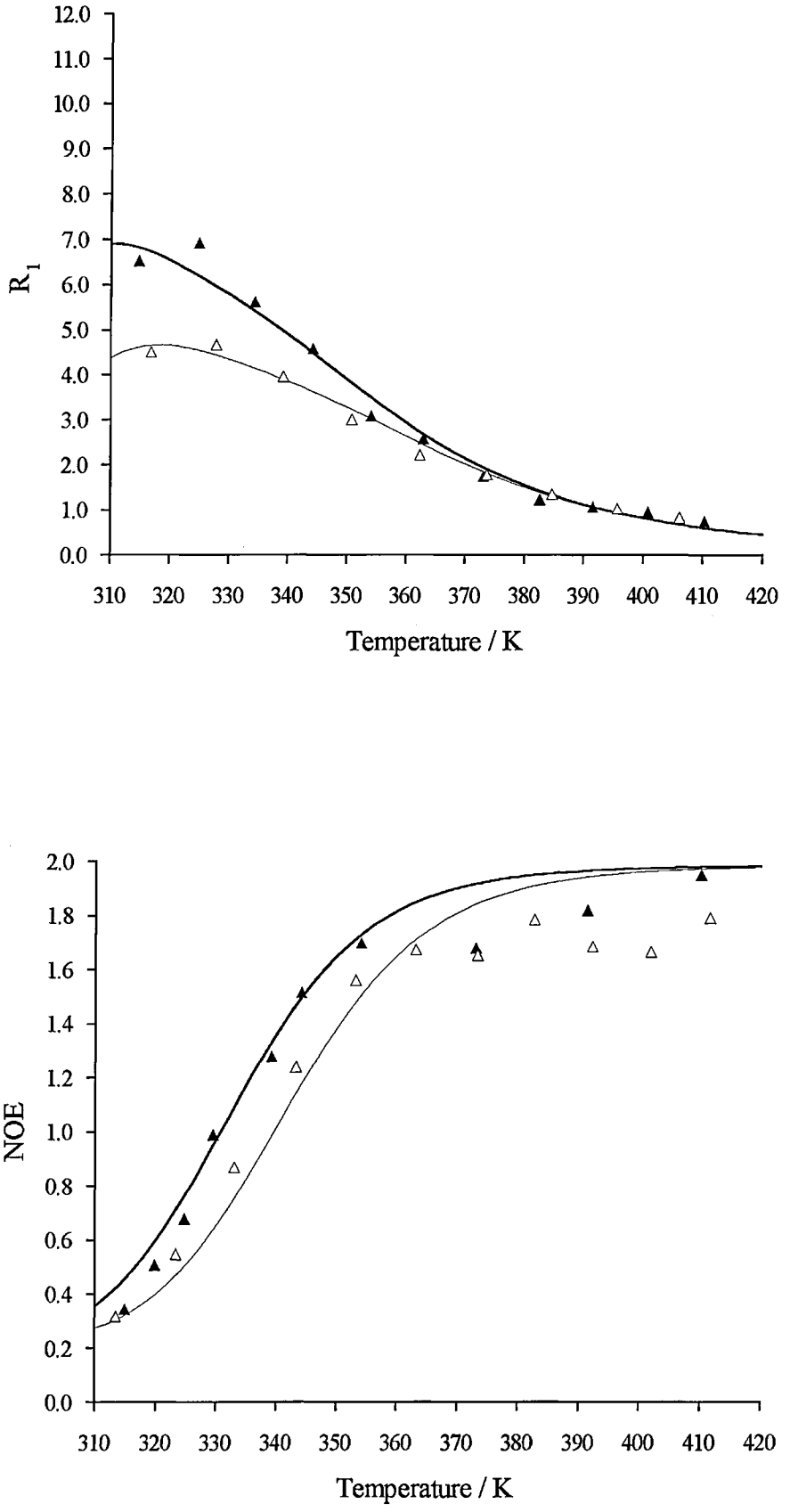

Fig A10.2: 1,1,2-tricyclohexylethane - position **2z**; carbon-13 data and optimized theoretical curves at 67.83 MHz (—) and 100.53 MHz (–).

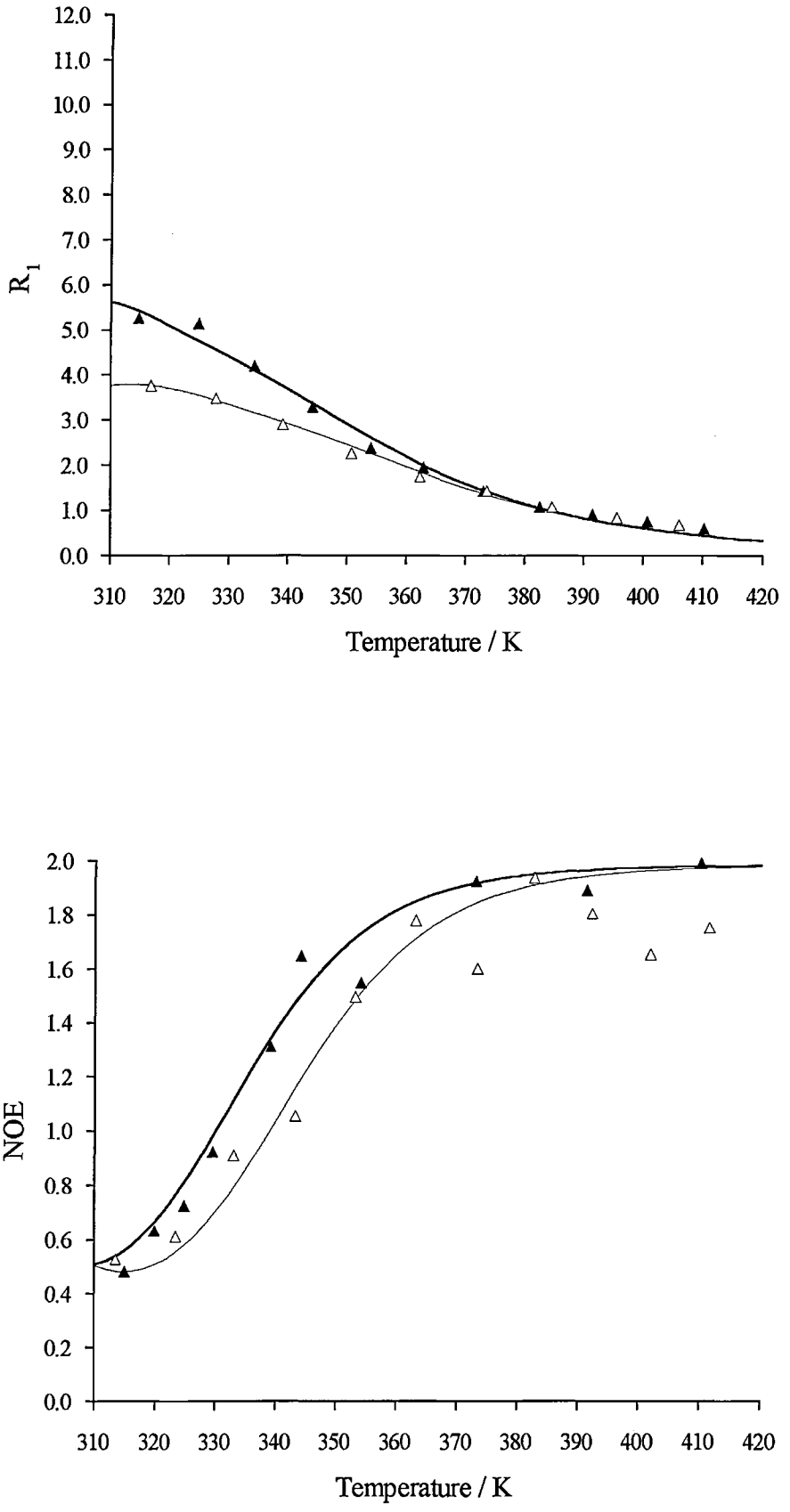

Fig A10.3: 1,1,2-tricyclohexylethane - position **1a**; carbon-13 data and optimized theoretical curves at 67.83 MHz (—) and 100.53 MHz (–).

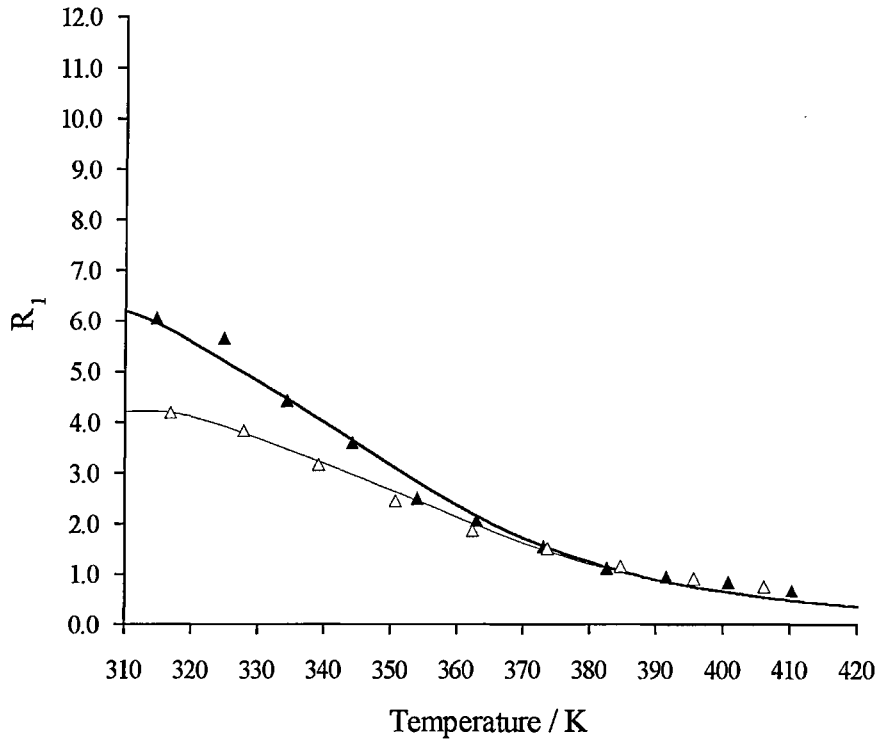

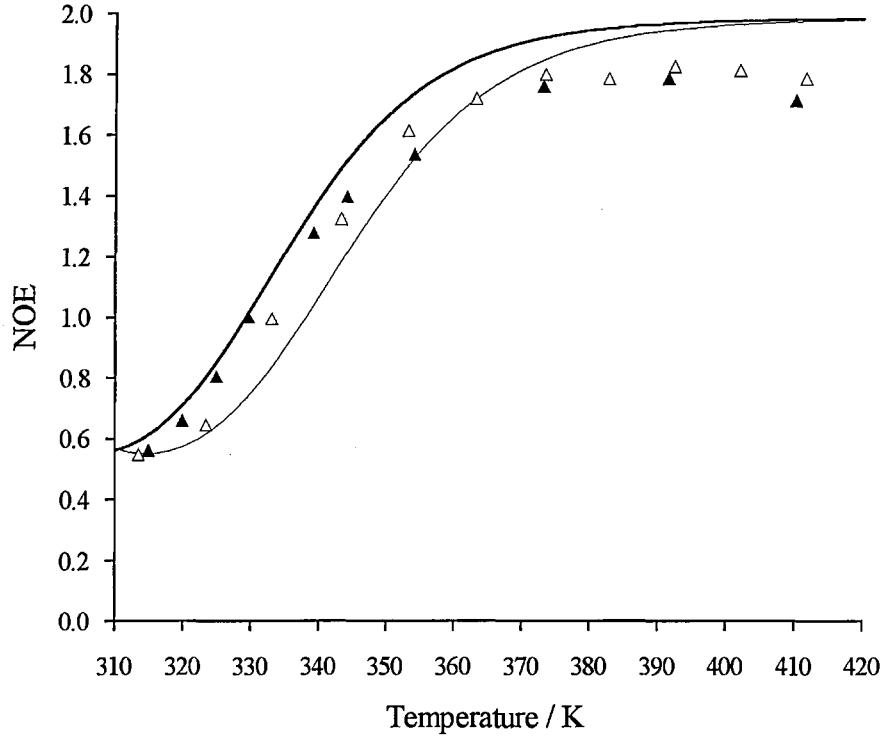

Fig A10.4: 1,1,2-tricyclohexylethane - position **2a/3a**; carbon-13 data and optimized theoretical curves at 67.83 MHz (—) and 100.53 MHz (–).

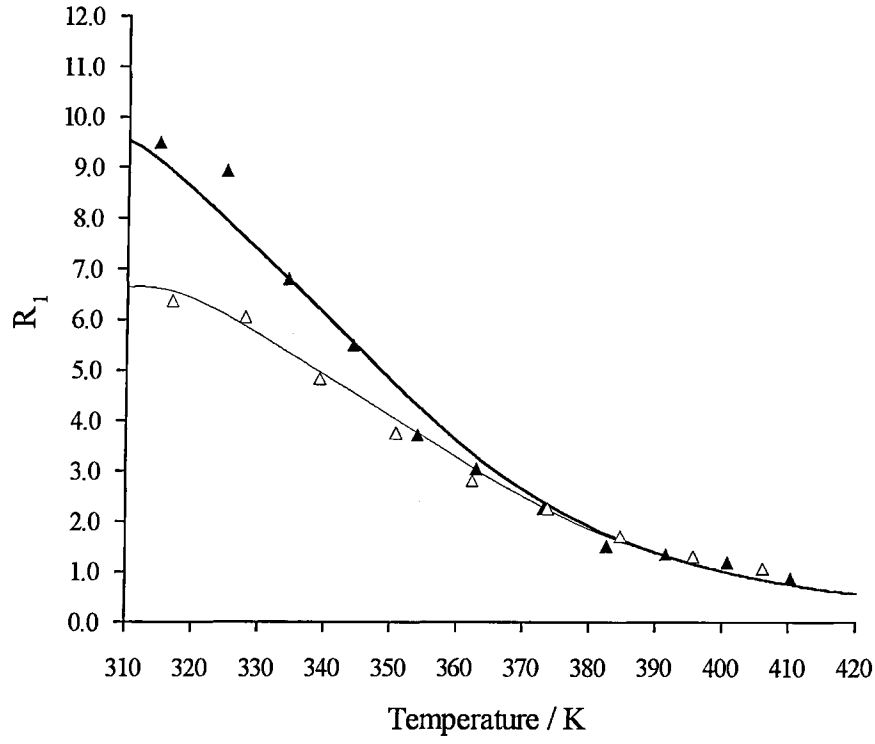

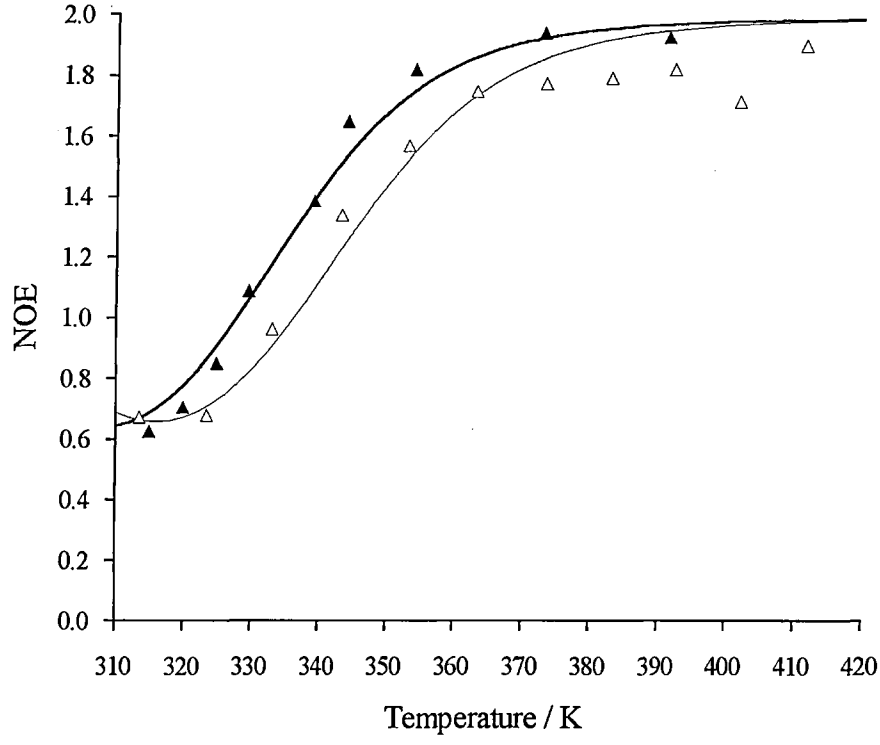

Fig A10.5: 1,1,2-tricyclohexylethane-position **1b/1b'**; carbon-13 data and optimized theoretical curves at 67.83 MHz (—) and 100.53 MHz (–).

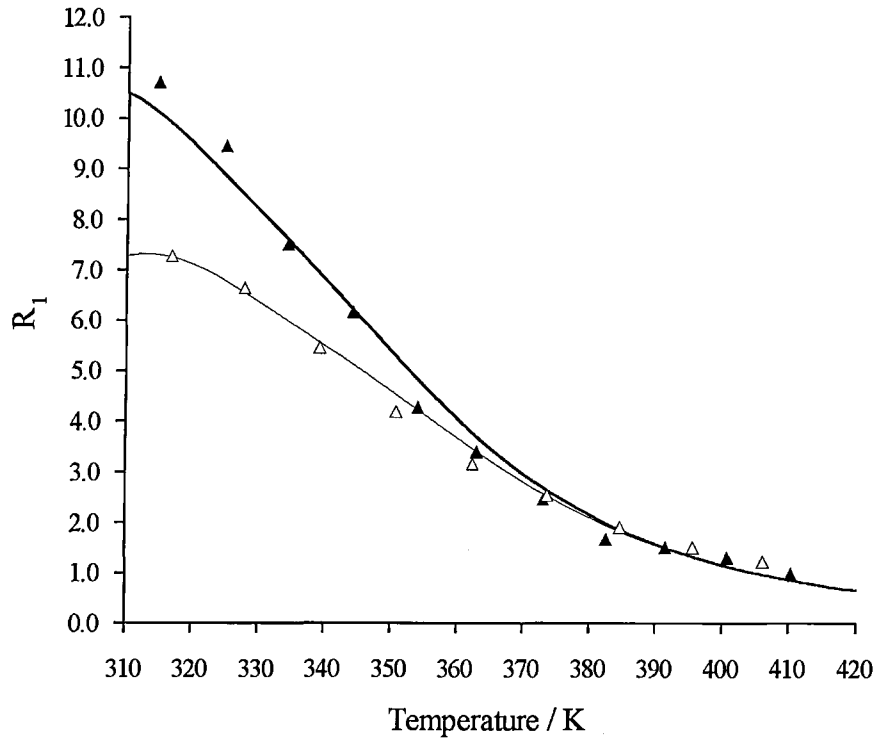

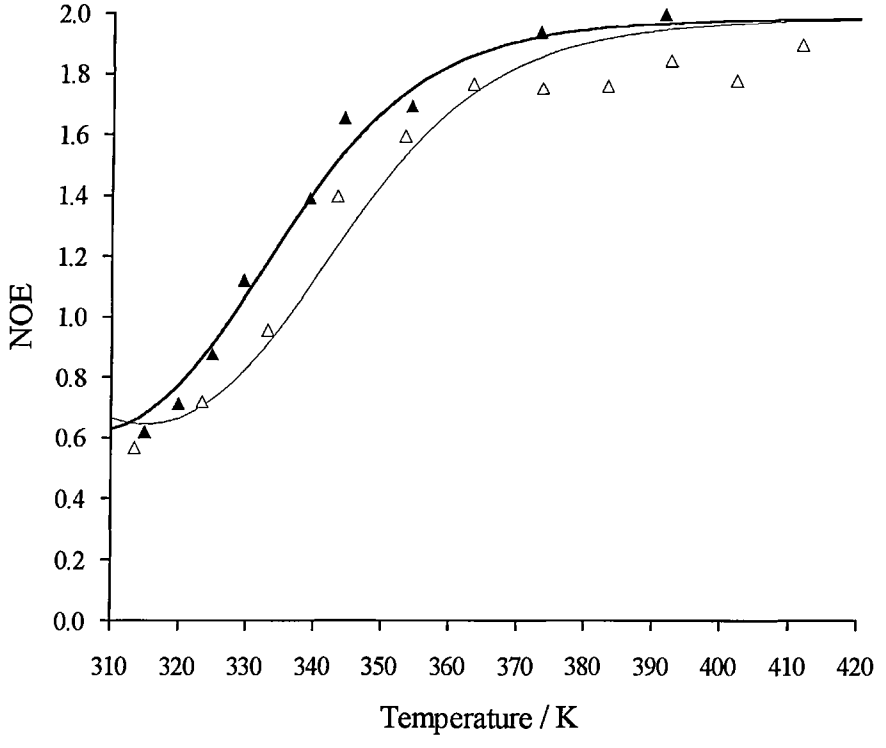

Fig A10.6: 1,1,2-tricyclohexylethane -position **2b/3b**; carbon-13 data and optimized theoretical curves at 67.83 MHz (—) and 100.53 MHz (–).

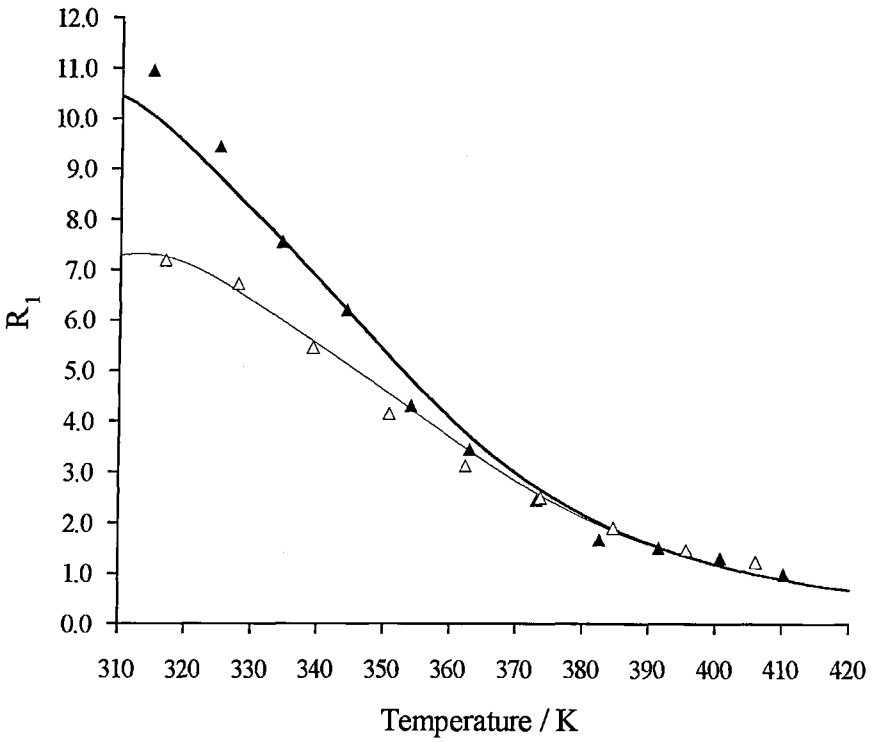

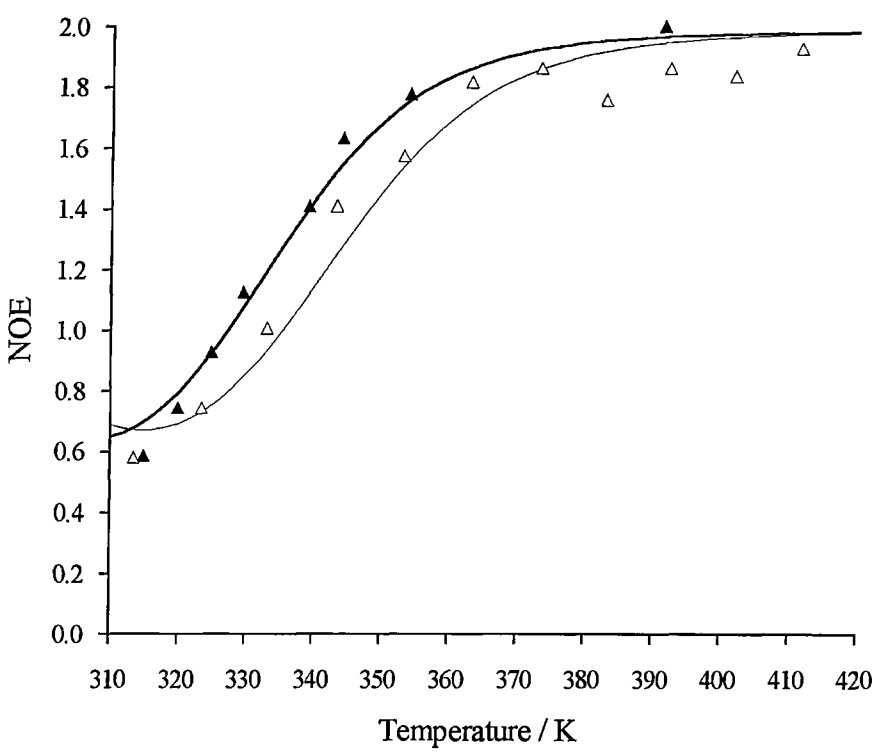

Fig A10.7: 1,1,2-tricyclohexylethane-position **2b'**/**3b'**;carbon-13 data and optimized theoretical curves at 67.83 MHz (—) and 100.53 MHz (–).

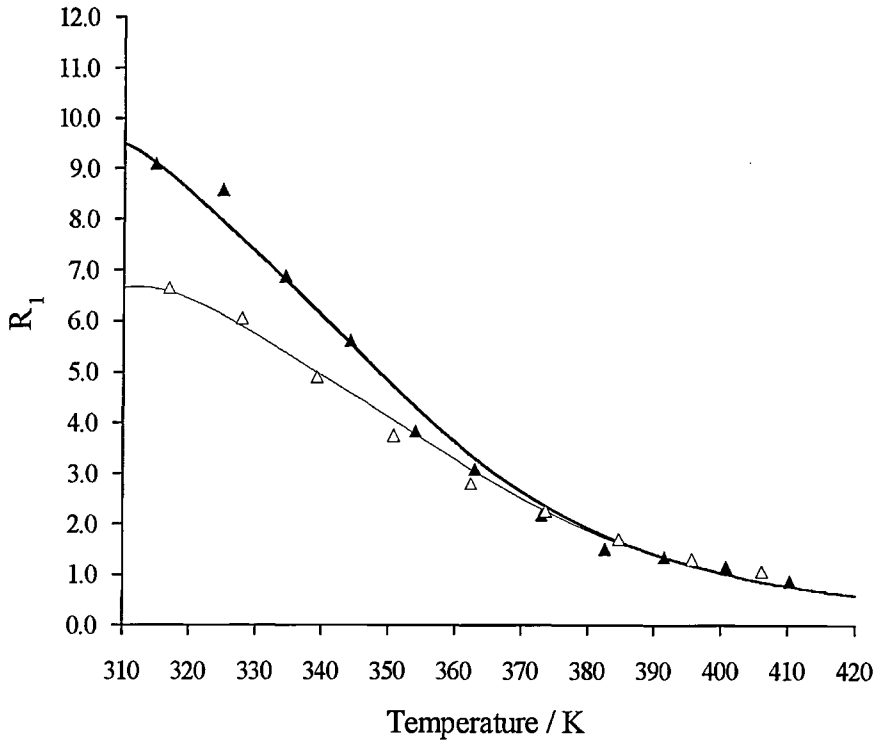

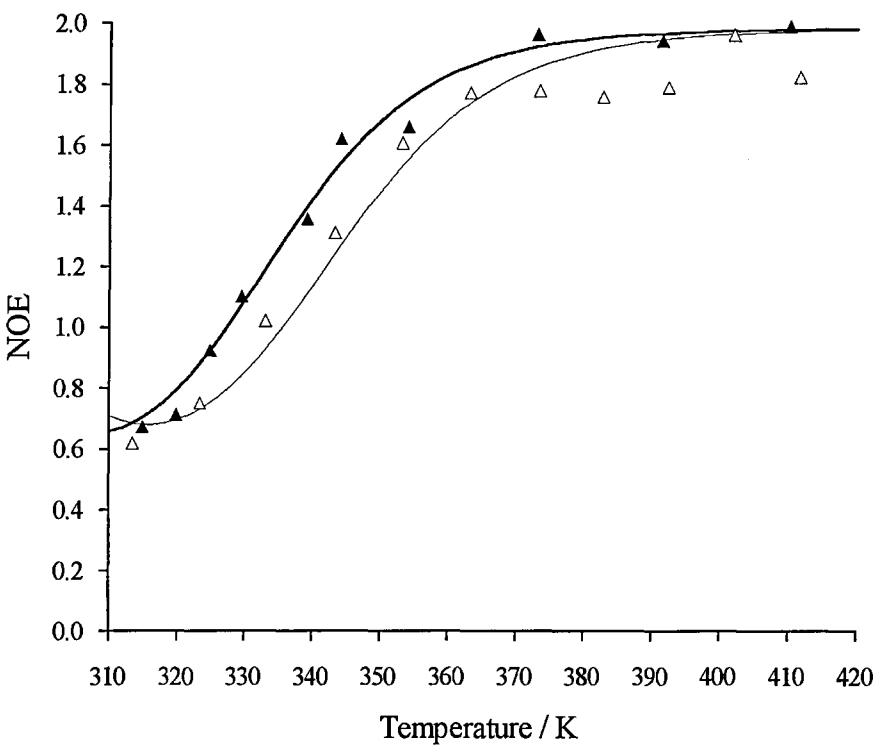

Fig A10.8: 1,1,2-tricyclohexylethane -position **1c/1c'**; carbon-13 data and optimized theoretical curves at 67.83 MHz (—) and 100.53 MHz (–).

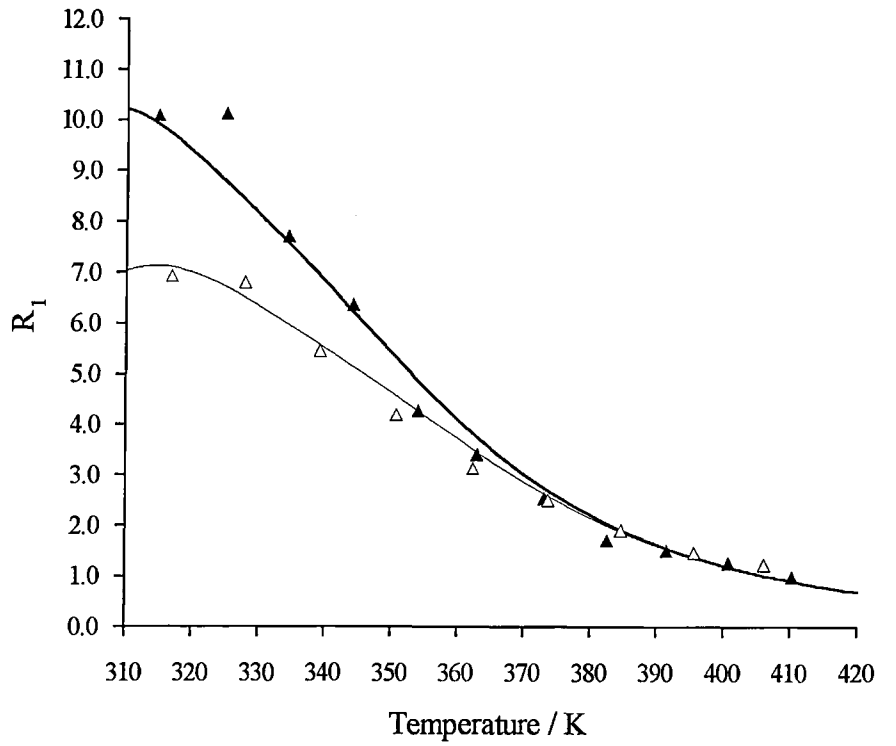

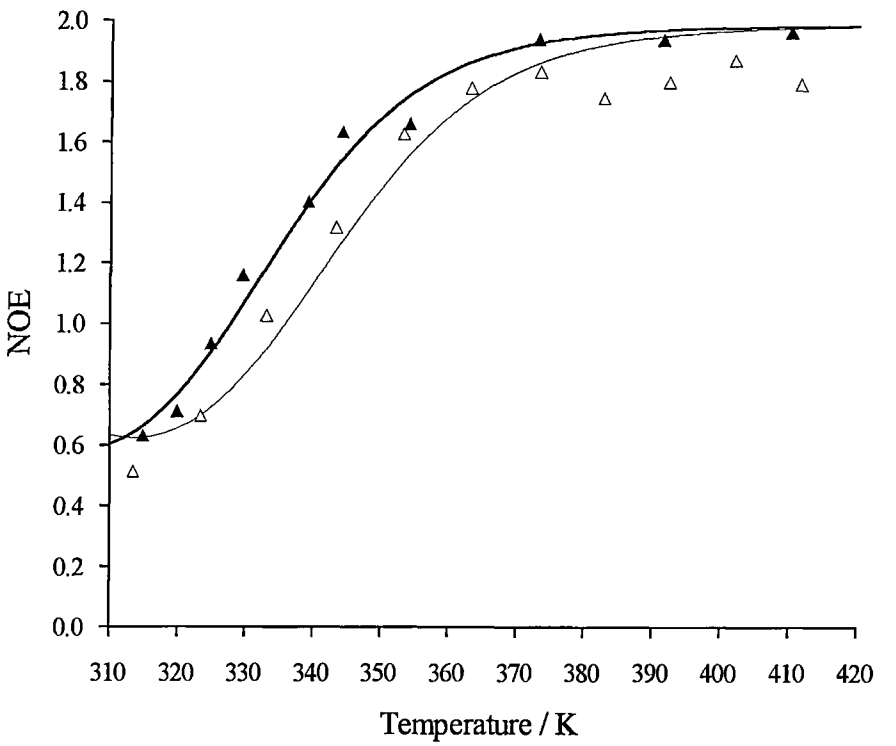

Fig A10.9: 1,1,2-tricyclohexylethane -position **2c/3c**; carbon-13 data and optimized theoretical curves at 67.83 MHz (—) and 100.53 MHz (–).

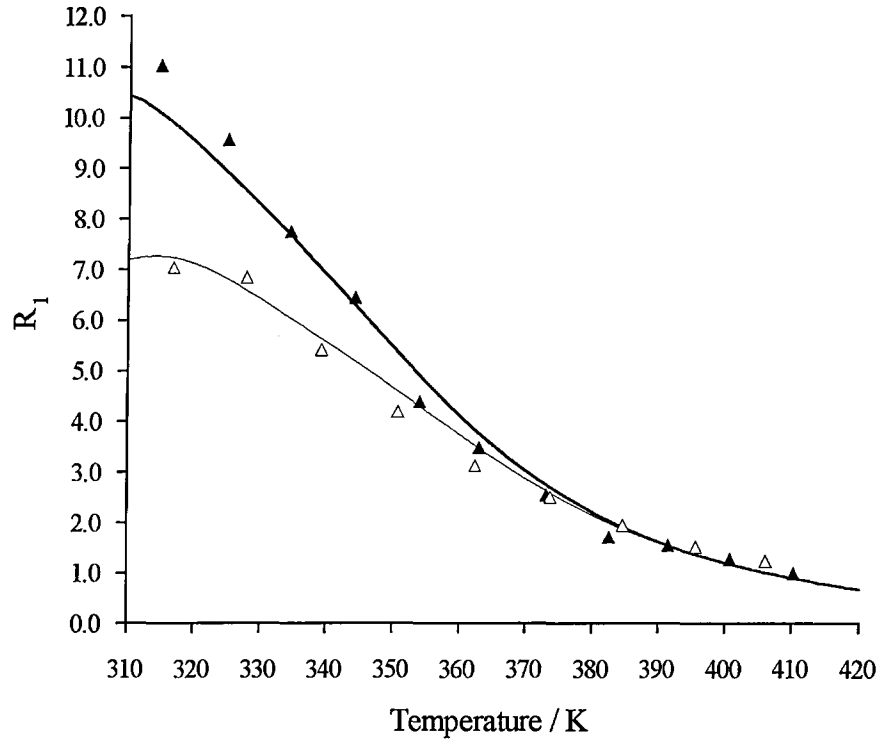

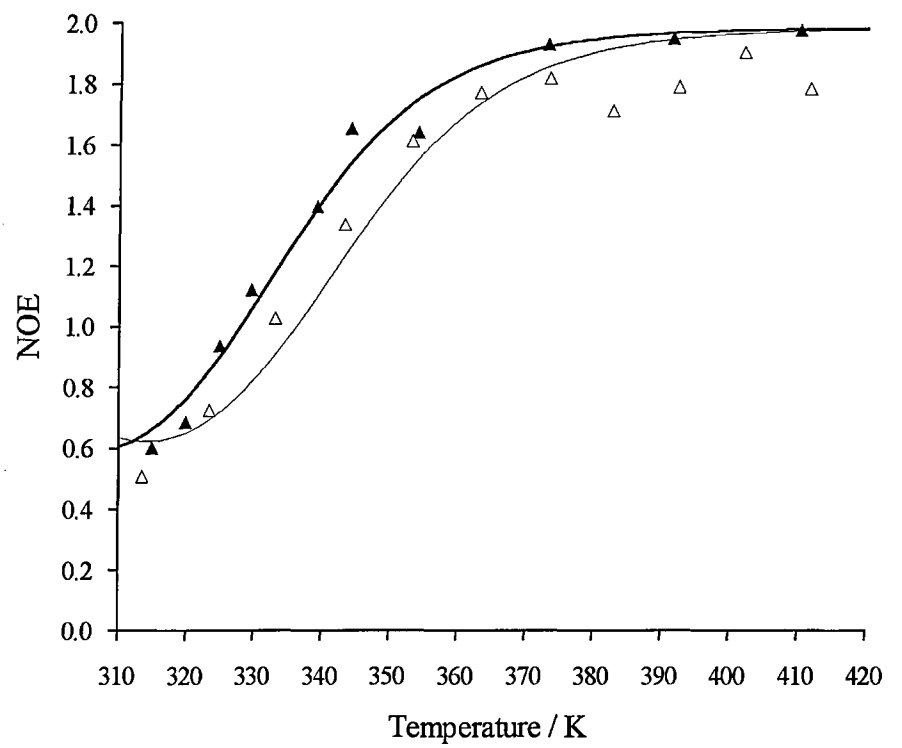

Fig A10.10: 1,1,2-tricyclohexylethane-position **2c'/3c'** carbon-13 data and optimized theoretical curves at 67.83 MHz (—) and 100.53 MHz (–).

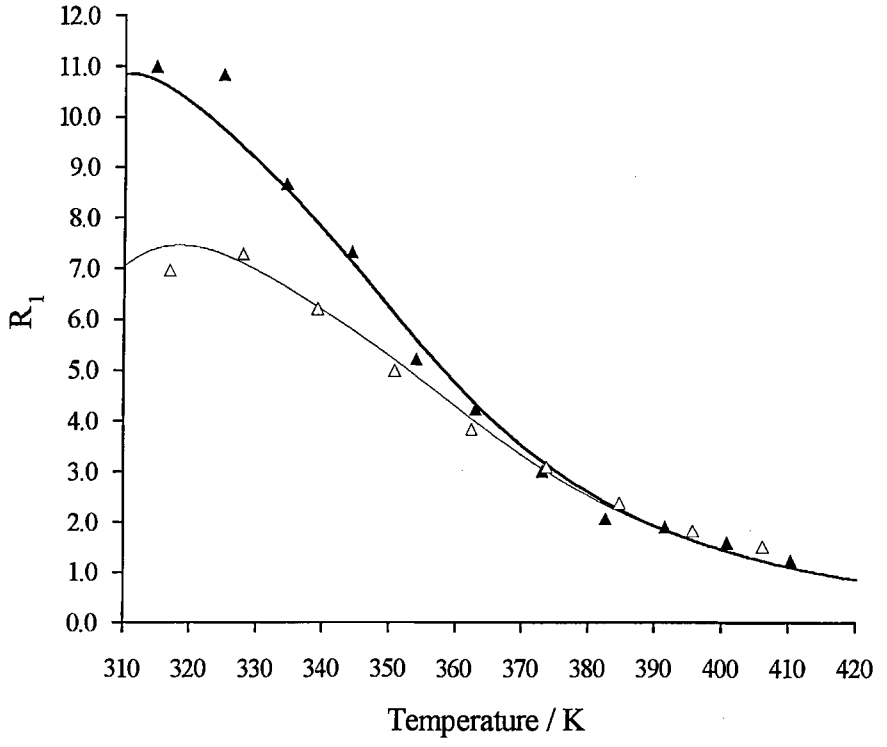

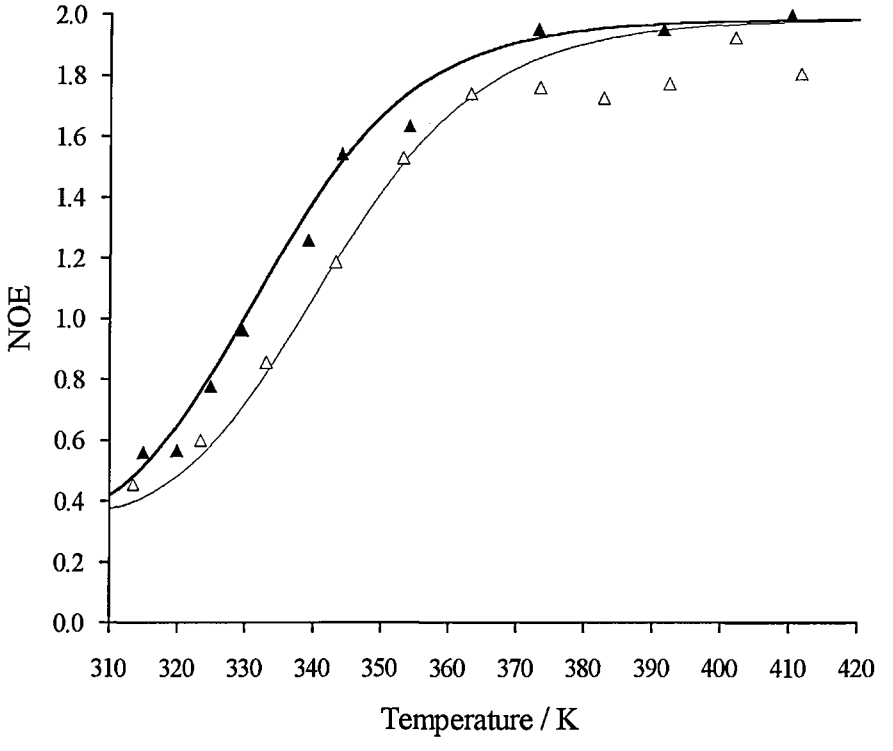

Fig A10.11: 1,1,2-tricyclohexylethane - position **1d/2d/3d**; carbon-13 data and optimized theoretical curves at 67.83 MHz (—) and 100.53 MHz (–).

Addenda